Mesoscopic phenomena driven by parallel magnetic fields

Inaugural-Dissertation

zur

Erlangung des Doktorgrades

der Mathematisch-Naturwissenschaftlichen Fakultät

der Universität zu Köln

vorgelegt von

Julia S. Meyer

aus Stuttgart

Köln 2001

Berichterstatter: Prof. Dr. A. Altland
Prof. Dr. M. R. Zirnbauer

Tag der mündlichen Prüfung: 3. Juli 2001

Contents

1. Introduction

The subject of *mesoscopic physics*, an expression coined by van Kampen [1] and of common use after a work of Imry [2], are quantum interference effects of electrons moving in a random medium. The fascinating feature of this subject is the possibility of observing these quantum effects on macroscopic objects. Therefore, a main prerequisite is the phase coherence over long time scales or large distances. To achieve this, low temperatures and reasonably clean samples are required. Over the last decades, 'mesoscopics' has been a very active area, and rapid technological progress made possible the observation of many new phenomena.

The interference effects manifest themselves in anomalously strong fluctuations of both thermodynamic and transport observables and in the spatial localisation of quantum mechanical wave functions [3–6]. E.g. in 'mesoscopic' regimes, the conductance of a diffusive metal – classically a self-veraging observable – displays pronounced quantum fluctuations. Upon increasing the size of the system, a crossover to Anderson-localised regimes takes place and the fluctuations of the conductance become even stronger (for review see [7]). Similarly, various thermodynamic coefficients of mesoscopic systems, e.g. the spectral density of states, thermal and magnetic susceptibilities, etc. exhibit quantum stochastic behaviour, too. All these fluctuation phenomena find their common origin in a conspiracy of the classical non-integrability of the charge carrier dynamics and quantum mechanical wave interference.

Superconductivity is a very interesting subject on its own right – last but not least for its technical relevance. Still novel superconducting materials are discovered,and a satisfactory theoretical description for these 'high temperature superconductors' is not yet available. Here we are only concerned with those aspects of superconductivity which are related to mesoscopic physics. To be more specific, consider a superconductor subject to a weak impurity potential. Taking a conventional (s-wave) bulk superconductor, this would not be something very promising to study. In fact, the thermodynamic properties of such a system are largely unaffected by weak non-magnetic disorder [8]. This changes drastically when allowing for a) unconventional pairing symmetry (e.g. d-wave), b) small samples – possibly in contact with a normal metal, c) additional perturbations which break time-reversal invariance, d) inhomogeneities of the order parameter, and/or e) Coulomb interaction.

The present work consists of two parts: The first part is concerned with transport properties of two-dimensional electron systems while the second part investigates the suppression of the superconducting gap due to different perturbations. As we will see later, the two parts are related by the role of in-plane magnetic fields which lead to interesting phenomena in two-dimensional 'normal' systems as well as in superconducting films.

1.1. Two-dimensional electron systems

A specific class of mesoscopic systems are so-called two-dimensional electron gases (2DEGs) realised in semiconductor heterostructures [9]. To date, these 2DEGs are the systems of choice

for studying a variety of transport phenomena because they show a rich phenomenology and are easily manageable experimentally. In fact, it has become possible to tailor make more and more sophisticated structures. In addition to extended single layer systems more complex setups are feasible, e.g. by further confining the electron gas and, thus, creating one-dimensional *quantum wires* or zero-dimensional *quantum dots*, or by building layered structures.

1.1.1. Tunnelling spectroscopy

A wide class of experiments is based on double-layer systems or so-called double quantum wells (DQWs) which consist of two parallel 2DEGs separated by a potential barrier. The first experimental realisations of DQWs only allowed one to study the influence of tunnelling on the in-plane transport [10–13] by simultaneously contacting both layers. New techniques for creating independent contacts [14–17] opened the possibility for novel experiments, in particular the direct observation of the tunnelling current between 2DEGs [18].

Measurements of the tunnelling current/conductance provide information about the *intra*layer transport complementary to what can be found from in-plane measurements. This concept has been discussed in various works, e.g. [19–23] (furthermore cf. [24] for $1d$-$2d$ tunnelling). The dependence of the tunnelling current on macroscopic system parameters can be used to reconstruct the microscopic details encoded in the Green function.

In chapter 4, we investigate an approach to experimentally observing mesoscopic correlation functions

$$F(\mathbf{x}_1,\mathbf{x}_2,\mathbf{x}_3,\mathbf{x}_4;\omega,\Delta\alpha) \equiv \langle G^-(\mathbf{x}_1,\mathbf{x}_2;\epsilon,\alpha)G^+(\mathbf{x}_3,\mathbf{x}_4;\epsilon+\omega,\alpha+\Delta\alpha)\rangle,$$

where $G^\pm$ is the retarded/advanced single-particle Green function. Here $\langle\dots\rangle$ stands for some kind of averaging, e.g. averaging over realisations of disorder, and the parameter α symbolically represents an optional dependence of the Green function on external control parameters like magnetic fields, gate voltages or others. In contrast to the averaged Green function $\langle G^\pm\rangle$ which vanishes on a scale $l_{\min}$ (typically the mean free path), the correlator F becomes long-ranged whenever two of its coordinates are close to each other pairwise. Correlation functions of this type appear as the 'most microscopic' building block in the analysis of the majority of fluctuating mesoscopic observables. Many *theoretical* investigations in mesoscopic physics concentrate on an analysis of these objects. Experimentally, however, it has proven difficult to access the correlation functions directly: Ideally, one would like to *continuously* measure the dependence of the correlators F over a range of at least the parameters $r = |\mathbf{x}_i - \mathbf{x}_j|$ and ω. Irritatingly, this cannot be achieved within experimental setups based on a standard device-contact-electron system architecture. In fact, the mere presence of local contacts introduces an entire spectrum of difficulties obstructing the continuous experimental spectroscopy of transport and spectral correlation functions.

Now the idea is to monitor the mesoscopic fluctuations of a tunnelling current flowing between the two layers of a semiconductor DQW structure, i.e. one electron system with essentially known properties is used as an *extended* tunnelling spectroscope [25, 26]. The setup is shown schematically in Fig. 1.1. From the dependence of the fluctuations on external parameters, such as in-plane or perpendicular magnetic fields, external bias voltages,etc., the temporal and spatial dependence of various prominent correlation functions of mesoscopic physics can be determined. Due to the absence of spatially localised external probes, the method provides a way to explore the interplay of interaction and localisation effects in two-dimensional systems within a relatively unperturbed environment.

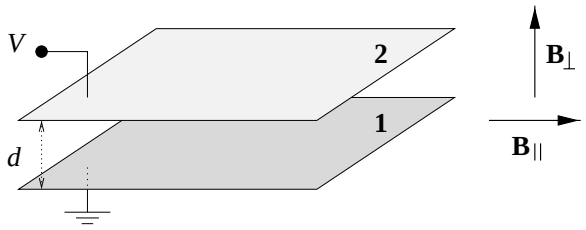

Figure 1.1.: Schematic setup of the approach: two parallel two-dimensional electron systems are subject to a bias voltage and external magnetic fields. A tunnelling current flowing between the layers is recorded as a function of the external control parameters.

Two prototypical system classes will be considered. First, we study extended systems for which the phase coherence length L_ϕ as well as the system size L are much larger than the microscopic length $l_{\min}$ and a crossover or transition from diffusive motion to Anderson localisation may take place. For such systems, a parallel magnetic field $\mathbf{B}_\parallel$ can be employed as an instrument for resolving the long-range behaviour of the correlation functions. Importantly, the field alignment parallel to the two-dimensional planes implies that the charge carrier dynamics is not affected by $\mathbf{B}_\parallel$. While in the diffusive regime explicit expressions for the correlation functions are known, no quantitative expressions for regimes with strong (non-perturbative) localisation and interaction effects are available. However, in a regime of localisation-delocalisation crossover or transition, scaling behaviour is expected to restrict the functional form of F. This opens the possibility to extract the relevant critical indices from tunnelling conductance measurements.

Second, we study a geometry, where one of the layers forms a ballistic quantum dot ($L < l_{\min}$) in the ergodic regime. The other, extended, layer serves as the spectrometer. For the quantum dot, the parametric correlations with respect to a perpendicular magnetic field, present in the correlators $F^{[d;D;C]}$, can be obtained from the current fluctuations. A similar setup has already been realised experimentally by Sivan et al. [27]. In that work, a single level (in contrast to our extended system) was used as a spectrometer to study a quantum dot device. This experiment led to results for the functional form of the density-density correlator $F^{[d]}$, compatible with theoretical predictions from random matrix theory. However, one would expect that the data obtained from single-level spectroscopy is still weighted with non-universal wave function amplitudes specific to the isolated 'monitor level'. In contrast, for the two-dimensional layer/quantum dot setup considered here, the current flow is extended and spatially uniform. As a consequence, the tunnelling current fluctuations are microscopically related to the purely spectral content of parametric correlations. Below, the quantitative connection between the field and voltage dependence of the tunnelling current fluctuations and a number of correlation functions that have been analysed in the recent theoretical literature [28] will be established. Moreover, we will try to assess to what extent these connections, obtained for the chaotic non-interacting electron gas, may be susceptible to interaction mechanisms such as Coulomb drag [29, 30] or Coulomb blockade effects [31].

1.1.2. Magnetoresistance and the Berry-Robnik phenomenon

Weak localisation (WL) corrections to the conductivity [32] and magnetoresistance of two-dimensional systems in perpendicular magnetic fields [33] have been studied extensively for many years (for review see e.g. [3–6]). These phenomena originate in the constructive interfer-

ence of time-reversed electron trajectories. As a consequence the return probability is enhanced above its classical value, leading to an increase in resistance. The magnetic field breaks time-reversal invariance and, therefore, suppresses the interference. Considerably less attention has been directed to the effect of an *in-plane* magnetic field on WL phenomena. In fact, truly two-dimensional systems do not feel the orbital effect of an in-plane field at all – the paths within the plane enclose no flux. However, this is not the case for real systems due to their finite width. There, an effect exists, and it is determined by the *microscopic* structure of the wave functions in z-direction (perpendicular to the plane). Early works focused on disordered metallic films [34, 35] in the limit of negligible size quantisation, and two-dimensional electrons subject to *short-range* disorder [36, 37]. Furthermore, a recent paper [38] considers systems with rough interfaces, as e.g. Si MOSFETs are believed to be [39, 40].

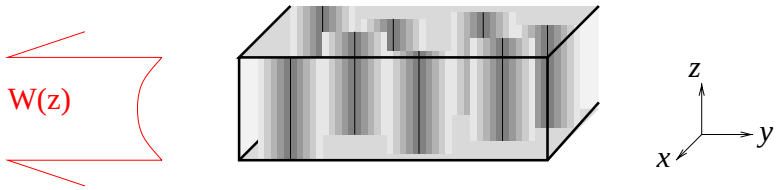

Figure 1.2.: Schematic picture of a finite quantum well with z-independent disorder.

In chapter 5, we analyse the case when motion of the carriers in z-direction is not completely stochastic. Such a situation can take place for, e.g., a gas of electrons or holes on a GaAs/AlGaAs interface. The mobility in these systems is limited by a *long-range* random potential, $V(x, y, z)$, created by charged impurities located far from the interface. The z-dependence of this potential is probably weak. In the approximation that neglects this dependence, $V = V(x, y)$, the in-plane electron motion can be separated from the motion in z-direction. Under these conditions, WL effects acquire non-universal features, depending on the structure of the confining potential $W(z)$. Thus, monitoring WL signals one can reveal information on the microscopic structure of the confining potential well. We show that the temperature and in-plane magnetic field dependence of the conductivity is sensitive to the symmetry of the confining potential under reflection, $\mathcal{P}_z : z \to -z$, and depends on the number of occupied subbands of size quantisation, M. The $M = 1$ case turns out to be special and is characterised by quite unusual magnetoresistance. Here virtual processes are necessary in order that the system feels the presence of the magnetic field. Thus, only a residual effect remains.

The dependence of the WL effects on $\mathcal{P}_z$-symmetry is a realisation of the Berry-Robnik symmetry phenomenon: even though the magnetic field breaks time-reversal ($\mathcal{T}$), the presence of an additional discrete symmetry may compensate for this effect. In fact, if in the absence of the magnetic field not only $\mathcal{T}\mathcal{H}(H=0) = \mathcal{H}(H=0)$ holds, but also $\mathcal{P}_z\mathcal{H}(H=0) = \mathcal{H}(H=0)$, in the presence of the magnetic field the Hamiltonian remains invariant under the combined symmetry, $(\mathcal{P}_z\mathcal{T})\mathcal{H} = \mathcal{H}$. Thus, pairs of distinct paths which interfere constructively can still be found, and, therefore, the WL corrections are not (completely) destroyed by the magnetic field.

1.2. Gapless superconductivity

The theory of superconductivity still used today dates back to Bardeen, Cooper and Schrieffer (BCS) in 1957 [41]. This theory describes the so-called conventional superconductors – which

we will be concerned with in this work – remarkably well.

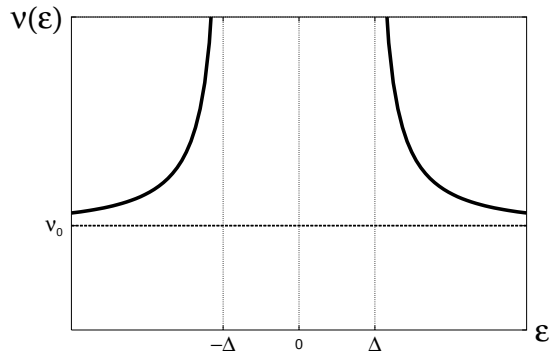

Figure 1.3.: BCS density of states of a conventional s-wave superconductor. Here ν_0 is the DoS in the normal state.

A characteristic feature of the conventional s-wave superconductor is its quasi-particle energy gap in the density of states (DoS) and the singularity at the gap edge as depicted in Fig. 1.3. Due to the Anderson theorem [8] one knows that the superconducting properties are robust with respect to 'normal' (i.e. non-magnetic) disorder. However, magnetic impurities, e.g., break time-reversal symmetry and, therefore, drastically change these properties [42]: The pair breaking effect of the magnetic impurities leads to a gradual destruction of superconductivity. More surprising is the fact that the energy gap in the quasi-particle spectrum gets suppressed more rapidly than the order parameter Δ. Thus, a gapless phase, where the system is still superconducting, but has a finite density of states down to zero energy, exists. This phase displays the characteristic features of superconductivity, namely the vanishing of the electrical resistance below a critical temperature T_c and the Meissner effect. However, the thermodynamic properties (e.g. the heat capacity) – which are determined by the energy gap rather than the order parameter – are clearly distinct from the 'usual' superconductor. A transition from the gapped to the gapless phase occurs at a critical concentration of magnetic impurities, corresponding to a scattering rate $1/\tau_s$ of order of the energy gap. It turns out that this critical concentration amounts to 91% of the value where superconductivity is completely destroyed.

1.2.1. Superconducting films

The general theory which describes the suppression of the energy gap and the occurrence of a gapless phase is due to Abrikosov and Gor'kov [42]. Although the Abrikosov-Gor'kov (AG) theory has been formulated in the context of magnetic impurities, it applies to various other perturbations, e.g. parallel magnetic fields in thin films [43]. In each case, the mechanism by which the quasi-particle energy gap is suppressed follows a similar scheme and is described by the same phenomenology: at the mean-field level, the perturbation leads to a suppression of the quasi-particle gap edge. The phenomenology of this suppression is contained within the AG theory [42] which describes the rearrangement of the ground state under the constraints imposed by the self-consistency equation. While the physical mechanisms of gap suppression differ, the mean-field equations depend on a single dimensionless parameter characterising the strength of the external perturbation (see below). Even at the mean-field level, it is found that if the perturbation is strong enough, the system is driven into a homogeneous gapless phase before the superconductivity is ultimately destroyed. Since the pioneering work of Abrikosov and Gor'kov,

it was realised that the integrity of the gapped phase is compromised even if the perturbation is weak. Optimal fluctuations of the random impurity potentials can conspire to create quasi-particle states localised on the length scale of the coherence length ξ at energies below the mean-field gap, i.e. in the presence of disorder, the system fragments into an inhomogeneous phase in which 'droplets' of localised sub-gap states are embedded in the superconducting background. Recently, it has been shown [44, 45] that, close to the mean-field energy gap edge E_{gap}, the nature of the quasi-particle states (their structure, and spectral density) are universal, depending only on the relative separation from the edge, the dimensionality, and the single dimensionless parameter characterising the strength of the perturbation.

Although in principle a time-reversal symmetry breaking perturbation, a weak magnetic field leaves the bulk properties of a superconductor unchanged due to the Meissner effect [46]: the field is expelled and only penetrates a thin surface layer. The situation drastically changes when the dimensions of the superconductor are diminished down to the London penetration depth. Then, the penetration of the field is almost complete, and significant deviations from the properties of the unperturbed system can be observed, in particular, gapless superconductivity may arise. Here two different setups are studied, namely thin films in parallel magnetic fields with a) δ-correlated disorder and b) columnar defects, i.e. an impurity potential which does not depend on the coordinate perpendicular to the plane.

In the 'diffusive' case a), after showing that the mean-field solution of the system follows the AG theory, we study sub-gap states or gap fluctuations within the gapped phase. (As in the magnetic impurity problem [44, 45],) using a supersymmetric field theory approach, the exponentially small tails of the density of states can be associated with inhomogeneous bounce or instanton solutions of the mean-field equations. Although in $2d$, this solution cannot be determined analytically, dimensional analysis admits for extracting the parameter dependence.

As in the normal case one can ask the question about symmetry effects. On the mean-field level, the choice of disorder does not affect the result qualitatively. However, within the gapless phase, the low-energy physics sensitively depends on the presence or absence of inversion symmetry. In general, the low-energy characteristics of a system in the *ergodic* regime are universal and governed by the underlying symmetries only. A complete classification scheme of symmetry classes is known [47]. Possible symmetries are time-reversal, spin-rotation, particle-hole and chiral symmetry. Now superconductors possess particle-hole symmetry. Furthermore, they may or may not possess time-reversal and/or spin-rotation symmetry. Here one finds that the diffusive film belongs to symmetry class C (according to Cartan's notation) which corresponds to spin-rotation symmetry, but broken time-reversal symmetry – as expected. By contrast, the film with columnar defects is described by the higher symmetry class CI (which usually means that the system possesses time-reversal invariance). The distinct symmetry classes manifest themselves in the energy dependence of the density of states for $\epsilon \to 0$. Thus, although superficially the suppression of superconductivity does not respond to geometrical symmetries, manifestations of the Berry-Robnik symmetry effect can be observed in the gapless phase. The distinct low-energy behaviour is confirmed by numerics.

1.2.2. Inhomogeneous superconductors

A more direct way of influencing the spectral properties of a superconductor are quenched spatial fluctuations of the coupling constant. Physically, such inhomogeneities can be induced by dislocations, twin or grain boundaries, or compositional heterogeneity as found in superconducting alloys [48]. The fluctuations of the coupling constant are reflected in inhomogeneities

of the order parameter which, in turn, induce a softening of the quasi-particle energy gap. The response of the system depends sensitively on the scale of the inhomogeneities. For large scale inhomogeneities which exceed the superconducting coherence length, the order parameter follows smoothly the variations of the coupling constant. If, however, the coupling constant fluctuates on smaller scales, one expects the faster variations to be smoothed out. In this second limit, quasi-classical phase coherence phenomena start to play an important role. To be more specific, consider a superconductor whose coupling constant displays small rapid fluctuations around a large average value. Again, the mean-field results follow the Abrikosov-Gor'kov theory. Considering only small fluctuations of the coupling constant, such that the order parameter remains positive everywhere, only the gapped regime is accessible, i.e. the parameter governing the suppression of the energy gap is always small. As Larkin and Ovchinnikov [49] pointed out, in addition to a suppression of the energy gap, even weak inhomogeneities destroy the integrity of the gap. The gap fluctuates and, therefore, does not possess a hard edge anymore, but the spectrum develops low-energy tails. Crucially, in the present problem, variations of the order parameter have to be obtained self-consistently which rules out the use of the supersymmetry method. As an alternative, a replica field theory can be used instead. Again the sub-gap states can be associated with (replica symmetry broken) instanton solutions. The tails of the density of states are described by the same universal result found in systems with time-reversal symmetry breaking perturbations. As discussed in Ref. [45], the only prerequisite for such a behaviour is the square-root singularity at the gap edge, found in all these systems.

Although the present work is broadly similar to the analysis in Ref. [49], there is a discrepancy in the energy dependence of the sub-gap tails. This can be traced back to the application of a Lifshitz type argument in Ref. [49]. In the study of band tail states in semiconductors, the bound states below the band edge can be ascribed to optimal fluctuations of the disorder potential [50–52]. Rare configurations of the disorder potential may develop exceptionally deep minima in which electrons can be trapped. This leads to an exponentially small probability of finding states within the band-gap. Crucially, the occurrence of these tails depends on details of the impurity distribution, and the states are described by slowly varying wave functions (without nodes). Lifshitz arguments have been applied successfully to the description of Landau-band tails as well [53–55]. Here the situation is somewhat different. Before deriving the mean-field equations, all disorder averages are taken. Then, details of the distribution are not relevant anymore. Furthermore, one is dealing with a superposition of rapidly oscillating wavefunctions and the optimal solution describes only the slow modulation of the envelope. Thus, instead of single bound states, in the present case, the inhomogeneous solution generates many states, confined to 'droplets', i.e. the tails are of quasi-classical origin.

1.3. Outline

The present work is organised as follows: In chapter 2, first the relevant length and energy scales are introduced (section 2.1), and then the theoretical methods used later are presented. In section 2.2 the perturbative diagrammatic method is introduced. Section 2.3 covers the field theoretic method and the derivation of a low-energy effective action, the so-called non-linear σ-model (NLσM). Two different approaches, namely supersymmetry and the replica trick (necessary when studying interacting systems), are presented. A brief introduction to random matrix theory (RMT) and symmetry classes is given in section 2.4.

The main chapters of this work belong to two larger parts as discussed in the introduction. In **part I** mesoscopic correlation functions in 2DEGs are discussed. First, in chapter 3, important concepts in mesoscopics – already mentioned in the introduction – are discussed in more detail. In section 3.1, we briefly outline the experimental realisation of two-dimensional systems. Section 3.2 develops a qualitative picture of weak localisation and negative magnetoresistance. A (very) short introduction to quantum dots can be found in section 3.3. Spectral statistics are introduced in section 3.4. Finally, interaction effects are discussed in section 3.5.

In chapter 4, an approach to observing certain correlation functions – which are commonly studied theoretically – by tunnelling spectroscopy is presented. In section 4.1, the general theory of tunnelling currents in double-layer structures is reviewed, and the main concept of the approach is introduced. The setup allows one to study transport correlations in extended systems, section 4.2, as well as spectral and parametric correlations in quantum dots, section 4.3. In the latter case, interaction effects have to be taken into account, as done in section 4.3.3. The chapter finishes with a discussion of the results in section 4.4.

In chapter 5, the influence of parallel magnetic fields on the single layer is studied in more detail. After deriving an effective action for the quasi-2d system with a subband structure in section 5.1, the role of symmetries is investigated in section 5.2, starting with the fully symmetric case before studying different perturbations. The case of one occupied subband – which shows quite unusual magnetoresistance – is presented in section 5.3. Finally, in section 5.4, we discuss our findings.

The subject of **part II** is the suppression of the quasi-particle energy gap in superconductors. As an introduction some basics of superconductivity are presented in chapter 6. While section 6.1 introduces general concepts, in section 6.2 the derivation of the Usadel equation for the quasi-classical, dirty limit is shown. In particular, the Abrikosov-Gor'kov theory of gapless superconductivity is discussed in section 6.3. To contrast the sub-gap tail states which become important in the subsequent chapters, a short introduction to Lifshitz band-tails in semiconductors is given in section 6.4. Furthermore, a brief review on the construction of a NLσM for the superconducting system can be found in section 6.5.

The influence of parallel magnetic fields on superconducting films is studied in chapter 7. In section 7.1, it will be shown that the diffusive film is well described by the Abrikosov-Gor'kov theory (section 7.1.1). However, going beyond the mean-field solution, tail states within the energy gap can be identified (section 7.1.2). Furthermore, in section 7.2, thin films with columnar defects are shown to obey the same mean-field phenomenology. The symmetry effect, discussed earlier, is visible on the level of soft fluctuations in the gapless phase, section 7.3. The results are confirmed by numerics. Section 7.4 contains the concluding discussion.

In chapter 8 inhomogeneous superconductors are studied. Within a mean-field analysis, section 8.1, one can show that inhomogeneities of the BCS coupling constant suppress the quasi-particle energy gap while preserving the integrity of the gap edge. Subsequently, in section 8.2,

taking into account instanton configurations of the NLσM action, we show that integrity of the gap edge is compromised. An analysis of the fluctuations in the vicinity of the instanton configurations shows that optimal fluctuations of the impurity potential induce sub-gap states localised on the length scale of the superconducting coherence length. A discussion of the results follows in section 8.3.

Finally, a summary is given in chapter 9.

In order to preserve a more transparent structure in the main text, some technical tools as well as details of the calculations can be found in the appendices A−D.

2. Concepts and methods

The full microscopic information characterising a mesoscopic system is contained in the single-particle Green function, $G^{\pm}(\mathbf{r}_1, \mathbf{r}_2; \epsilon)$. (For completeness, definitions are summarised in appendix A.1.) However, for one given disordered system, the Green function generally is a highly complicated object which, furthermore, does only have comparatively little predictive power. Much more interesting (and accessible) is the study of a statistical ensemble of systems. Relying on the *ergodicity hypothesis* that the statistical average of an individual system over some control parameter is equivalent to the average over an ensemble of systems[1], the quantities of interest are the average Green functions, $\langle G^{\pm} \rangle$, as well as correlation functions, $F_{n|m} = \langle (G^{+})^n (G^{-})^m \rangle$, where $\langle \dots \rangle$ stands for some kind of ensemble averaging. Before discussing how to obtain the functions $\langle G^{\pm} \rangle$ and $F_{1|1}$, in Sec. 2.1 the relevant length and energy scales in mesoscopic physics are summarised. There are a number of different methods for calculating correlators of Green functions in disordered systems – valid in different regimes. The most widely applicable is functional field integration which will be used in the main parts of this work. In the perturbative regime, the simpler and more intuitive diagrammatic method is an important tool, and a short introduction will be given in Sec. 2.2, a more complete discussion can be found in e.g. [25, 56, 57]. In Sec. 2.3 functional field integration and the non-linear σ-model – which one obtains as a low-energy, long-wavelength effective theory – are introduced. In the zero-dimensional limit random matrix theory has proven to be a powerful method; a brief review is given in Sec. 2.4.

2.1. Characteristic scales of mesoscopic systems

Some characteristics of mesoscopics have been introduced in chapter 1. To further classify mesoscopic systems, the relevant length and energy scales are summarised here.

The smallest length scale is the wavelength of the particles, i.e. at low temperatures the **Fermi wavelength** λ_{F}. Physics on scales larger than λ_{F} is in the *quasi-classical* limit. The associated energy scale is the **Fermi energy** ϵ_{F}.

The strength of the disorder potential determines the **elastic mean free path** ℓ. The corresponding energy scale[2] is the **elastic scattering rate** $1/\tau$, where $\ell = v_{\mathrm{F}}\tau$ (v_{F} Fermi velocity). Note that in two dimensions, the product $\epsilon_{\mathrm{F}}\tau \sim k_{\mathrm{F}}\ell$ (k_{F} Fermi momentum) is proportional to the dimensionless conductance g of the system (see below). On length scales smaller than ℓ transport is *ballistic* while on larger length scales one enters the *diffusive* regime.

[1] I.e. one usually calculates averages over different realisations of an impurity potential while, in *practice*, averaging will mostly be done over external control parameters, e.g. perpendicular magnetic fields, the chemical potential, or the system geometry. (For sufficiently strong variations of the control parameter) these different procedures are believed to produce equivalent results.

[2] For convenience, units where $\hbar = c = k_{\mathrm{B}} = e = 1$ are used throughout this work.

Associated with the **system size** L is the **Thouless energy** $E_{\mathrm{Th}} = 2\pi D/L^2$, where D is the diffusion constant. At low energies, $\epsilon < E_{\mathrm{Th}}$, the system is *ergodic*, i.e. the particle is given long enough time to explore the whole system. In this regime the dynamics becomes universal: the properties of ergodic systems are determined by symmetries while geometrical details of the system are irrelevant. This admits for a description by random matrix theory (cf. Sec. 2.4).

The smallest energy scale is the **mean level spacing** $\delta = 1/(\nu L^d)$, where ν is the mean density of states (DoS) and d the dimensionality of the system. The ratio $g = E_{\mathrm{Th}}/\delta$ defines the dimensionless conductance.

Finally, quantum interference is observable as long as phase coherence is not destroyed by inelastic processes. Coherent transport through the entire system is possible, if the **phase coherence length** L_ϕ exceeds L. Then quantum interference effects play an essential role and one can measure 'finger prints' of the microscopic details of the sample.

A finite **temperature** T leads to dephasing as well, introducing a length scale $L_T = \sqrt{D/T}$.

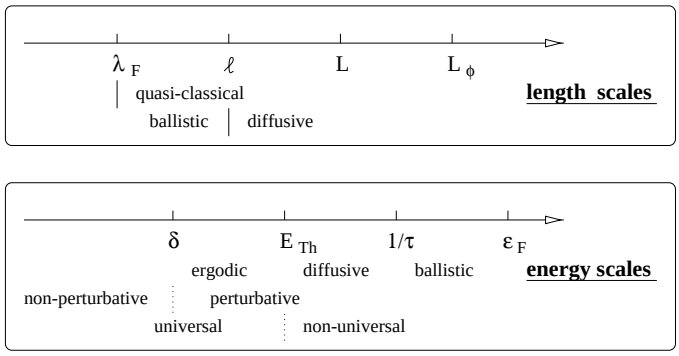

Figure 2.1.: Length and energy scales in mesoscopic physics.

In a superconductor, in addition to the length scales introduced above, the **order parameter** Δ sets a further length scale, namely the **coherence length** ξ. In a 'clean' system $\xi_0 = v_{\mathrm{F}}/\Delta$ whereas in the dirty limit, $\ell < \xi_0$, the coherence length is reduced[3] to $\xi = \sqrt{D/(2\Delta)}$.

The following sections are dedicated to an introduction of the theoretical methods used in this work. As the presentation of the results in the main chapters 3–8 attempts to be self-contained (except for some details of the methods – which are presented here), the reader who is already familiar with the methods or not interested in technical details may skip the remainder of this chapter and go straight to the beginning of part I on page 25.

2.2. Diagrammatics

Diagrammatics is a perturbative method which allows one to (a) classify different contributions to the perturbation series and (b) sum up the relevant terms. In the absence of interaction or magnetic fields, the diagrammatic representation of the problem involves (see e.g. [56])

[3]Note that these relations between scales are characteristic for the two regimes. In a ballistic system, lengths (l) and energies or times ($t \sim 1/E$) are connected via the velocity of the particles, i.e. the Fermi velocity: $l_{\mathrm{ballistic}} = v_{\mathrm{F}} t$. By contrast, diffusive dynamics leads to the connection $l_{\mathrm{diffusive}} \sim (Dt)^{1/2}$.

- the full Green functions, $G(\mathbf{p}, \mathbf{p}'; \epsilon)$,

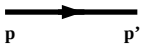

- the unperturbed (or 'bare') Green functions, $G_0(\mathbf{p}; \epsilon)$, and

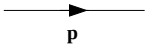

- the disorder potential, V.

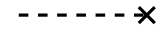

To be specific, here – for simplicity – we choose the random potential V to be drawn from a Gaussian white noise distribution:

$$\langle V(\mathbf{r})\rangle = 0, \qquad \langle V(\mathbf{r})V(\mathbf{r}')\rangle = \gamma_{\mathrm{V}}\delta(\mathbf{r}-\mathbf{r}'), \tag{2.1}$$

where γ_{V} measures the strength of the potential; its connection to system parameters will become clear below. Note that after averaging over disorder, the system is homogeneous, and, thus, the average Green function becomes translationally invariant: $\langle G(\mathbf{p}, \mathbf{p}')\rangle \equiv \langle G\rangle(\mathbf{p})\,\delta(\mathbf{p}-\mathbf{p}')$.

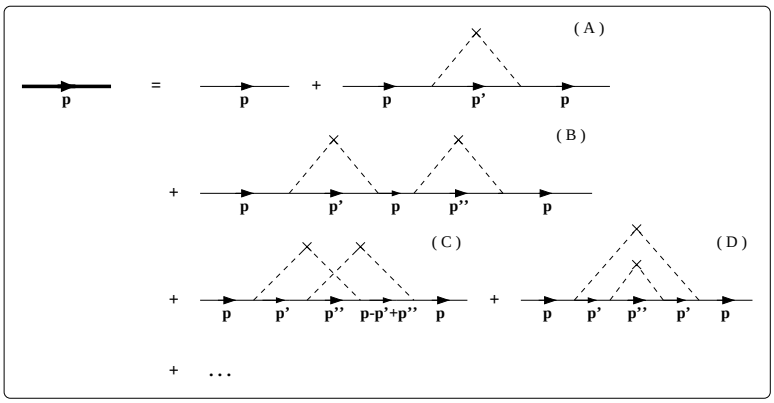

Figure 2.2.: Expansion of the average Green function.

2.2.1. The average Green function

The starting point of the perturbative approach is the representation of the Green function as a series in powers of V, i.e. $G = G_0 + G_0 \sum_n (VG_0)^n$. Under averaging, diagrams with single impurity lines vanish (due to $\langle V\rangle = 0$). Thus, the diagrammatic expansion involves only diagrams with paired impurity lines, see[4] Fig. 2.2. The average Green function is then given by a Dyson equation, depicted schematically in Fig. 2.3:

$$\langle G\rangle = G_0 + G_0 \sum_{n=1}^{\infty} (\Sigma G_0)^n = G_0 + G_0 \Sigma \langle G\rangle \quad \Longleftrightarrow \quad \langle G\rangle = \frac{G_0}{1-\Sigma G_0},$$

where the self-energy Σ contains all *irreducible* diagrams, i.e. diagrams that cannot be split into two by cutting one G_0-line (e.g. all but diagram B in Fig. 2.2).

[4] All pictures in this subsection are taken from Ref. [25].

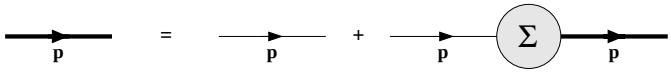

Figure 2.3.: Diagrammatic representation of the Dyson equation.

The dominant contribution to the self-energy, given by diagram A in Fig. 2.2, reads

$$\Sigma_0^{\pm}(\mathbf{p}) = \left\langle \int d\mathbf{q}\, V(\mathbf{q}) G_0^{\pm}(\mathbf{p}-\mathbf{q};\epsilon) V(-\mathbf{q}) \right\rangle, \tag{2.2}$$

where the shorthand notation $d\mathbf{q} = d^d q/(2\pi)^d$ has been introduced. Since the potential is δ-correlated in real space, its Fourier transform does not depend on momentum. Hence, $\Sigma_0^{\pm} = \gamma_{\mathrm{V}} \int d\mathbf{p}\, G_0^{\pm}(\mathbf{p};\epsilon)$. The real part of Σ, leading to a shift in energy, can be absorbed in the ground state energy. Using that the unperturbed Green function reads $G_0^{\pm}(\mathbf{p};\epsilon) = (\epsilon \pm i0 + \xi_{\mathbf{p}})^{-1}$, where $\xi_{\mathbf{p}} = \epsilon_{\mathrm{F}} - p^2/(2m)$, and the definition of the density of states, $\nu(\epsilon) = L^{-d} \sum_{\mathbf{p}} \delta(\epsilon + \xi_{\mathbf{p}})$, the imaginary part of Σ obtains

$$\Im\, \Sigma_0^{\pm} = \mp \gamma_{\mathrm{V}} \pi \int d\mathbf{p}\, \delta(\epsilon + \xi_{\mathbf{p}}) = \mp \gamma_{\mathrm{V}} \pi \nu \equiv \mp \frac{1}{2\tau}, \tag{2.3}$$

thus defining the mean free time τ. The associated length scale ℓ is the decay length of the average Green function as we will see shortly. In the case of weak disorder, $\tau^{-1} \ll \epsilon_{\mathrm{F}}$, all other contributions are small in $1/(k_{\mathrm{F}}\ell)$, and Eq. (2.3) determines the self-energy Σ in the *self-consistent Born approximation* (SCBA).

Inserting the above result into the Dyson equation yields

$$\langle G^{\pm} \rangle(\mathbf{p};\epsilon) \;=\; \frac{1}{\epsilon + \xi_{\mathbf{p}} \pm \frac{i}{2\tau}}. \tag{2.4}$$

In real space representation, this leads to a decay of the average Green function on the scale of the mean free path,

$$\langle G \rangle(\mathbf{r},\mathbf{r}') = G_0(\mathbf{r},\mathbf{r}')\, e^{-\frac{|\mathbf{r}-\mathbf{r}'|}{2\ell}}. \tag{2.5}$$

2.2.2. Two-particle correlation functions

Having found the average Green function, the next step is to calculate correlation functions.

As we have seen, the Green function, being a spatially and energetically rapidly fluctuating object, readily vanishes on some microscopic scale[5] $l_{\min}$ upon averaging over any control parameter and is, therefore, not directly accessible. Thus, in describing fluctuation phenomena, one commonly employs correlation functions of the type $F(\mathbf{r}_1,\mathbf{r}_2;\mathbf{r}_3,\mathbf{r}_4;\omega) \equiv \langle G^-(\mathbf{r}_1,\mathbf{r}_2;\epsilon) G^+(\mathbf{r}_3,\mathbf{r}_4;\epsilon+\omega)\rangle$ as the 'most microscopic' building blocks. Due to quantum wave interference, the correlation function F becomes long-ranged whenever two of its coordinates are close to each other pairwise (on scales of $l_{\min}$). There are three possibilities of pairing the coordinates and, thus, three corresponding correlation functions. Specifically,

[5] In general, $l_{\min}$ is set by the mean free path. In strong magnetic fields, however, the classical cyclotron radius $R_c = v_{\mathrm{F}}/\omega_c$ (ω_c cyclotron frequency) may become smaller than the mean free path implying that $l_{\min} = R_c$ (see e.g. [58]).

- for $\mathbf{r} \equiv \mathbf{r}_1 \approx \mathbf{r}_2$ and $\mathbf{r}' \equiv \mathbf{r}_3 \approx \mathbf{r}_4$, $F^{[d]}(\mathbf{r}, \mathbf{r}') \equiv F(\mathbf{r}, \mathbf{r}; \mathbf{r}', \mathbf{r}')$ describes the fluctuations of the (local) density of states and, thus, the thermodynamic fluctuations and parametric correlations.
- $F^{[D]}(\mathbf{r}, \mathbf{r}') \equiv F(\mathbf{r}, \mathbf{r}'; \mathbf{r}', \mathbf{r})$ describes the total probability of propagation from $\mathbf{r}$ to $\mathbf{r}'$. This is the generalised 'diffuson', a quantity of key relevance in the context of mesoscopic transport.
- Finally, in a system with unbroken time-reversal ($\mathcal{T}$) symmetry, the correlator $F^{[C]}(\mathbf{r}, \mathbf{r}') \equiv F(\mathbf{r}, \mathbf{r}'; \mathbf{r}, \mathbf{r}')$, the so-called Cooperon, becomes long-ranged, too.

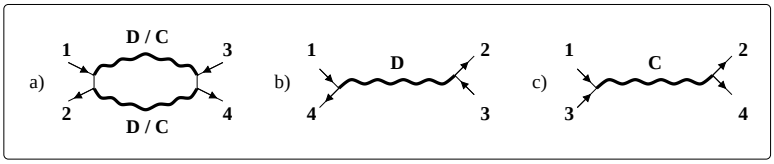

Figure 2.4.: Schematic picture of the three correlation functions: a) density-density, b) diffuson, and c) Cooperon. The wavy lines represent the sum of ladder (D) and maximally crossed (C) diagrams, respectively.

In momentum representation, the correlation functions defined above read

$$F(\mathbf{p}_1, \mathbf{p}_1', \mathbf{p}_2, \mathbf{p}_2'; \omega) = \langle G^-(\mathbf{p}_1, \mathbf{p}_1'; \epsilon) G^+(\mathbf{p}_2, \mathbf{p}_2'; \epsilon + \omega) \rangle. \tag{2.6}$$

Again – as for the averaged Green function – the diagrammatic perturbation series involves summing up diagrams with paired impurity lines. The dominant contributions are series of *ladder diagrams* and *maximally crossed diagrams*, see Fig. 2.5. With the notation $\langle AB \rangle_c = \langle AB \rangle - \langle A \rangle \langle B \rangle$, i.e. subtracting the disconnected part of the correlator, the contribution of connected diagrams can be written as

$$\begin{aligned} & \langle G^-(\mathbf{p}_1, \mathbf{p}_1'; \epsilon) G^+(\mathbf{p}_2, \mathbf{p}_2'; \epsilon + \omega) \rangle_c \\ = \; & \langle G^- \rangle(\mathbf{p}_1, \epsilon) \, \langle G^- \rangle(\mathbf{p}_1', \epsilon) \, \langle G^+ \rangle(\mathbf{p}_2, \epsilon + \omega) \, \langle G^+ \rangle(\mathbf{p}_2', \epsilon + \omega) \rangle \times \\ & \times \, \Gamma(\mathbf{p}_1, \mathbf{p}_2, \mathbf{p}_1', \mathbf{p}_2'; \omega) \, \delta(\mathbf{p}_1 - \mathbf{p}_2 - \mathbf{p}_1' + \mathbf{p}_2'), \end{aligned} \tag{2.7}$$

thus defining the reducible[6] vertex function $\Gamma(\mathbf{p}_1, \mathbf{p}_2, \mathbf{p}_1', \mathbf{p}_2'; \omega)$.

The diffuson (Ladder diagrams)

Consider first the sum of ladder diagrams depicted in the upper part of Fig. 2.5. Due to momentum conservation at each vertex, the momentum difference $\mathbf{q} \equiv \mathbf{p}_1 - \mathbf{p}_2 (= \mathbf{p}_1' - \mathbf{p}_2')$ is constant, and Γ depends on this difference only. Then $\Gamma(\mathbf{q}, \omega)$ is given by a Bethe-Salpeter equation, the two-particle analogue of the Dyson equation:

$$\Gamma(\mathbf{q}, \omega) = \gamma_{\mathrm{V}} + \gamma_{\mathrm{V}} \Big[\underbrace{\int d\mathbf{p}'' \, \langle G^- \rangle(\mathbf{p}'' + \mathbf{q}, \epsilon + \omega) \langle G^+ \rangle(\mathbf{p}'', \epsilon + \omega)}_{\equiv \, \Pi(\mathbf{q}, \omega)} \Big] \Gamma(\mathbf{q}, \omega).$$

[6] In the case of two-particle functions, a diagram is called reducible if it can be split into two separate diagrams by cutting *two* $\langle G \rangle$-lines.

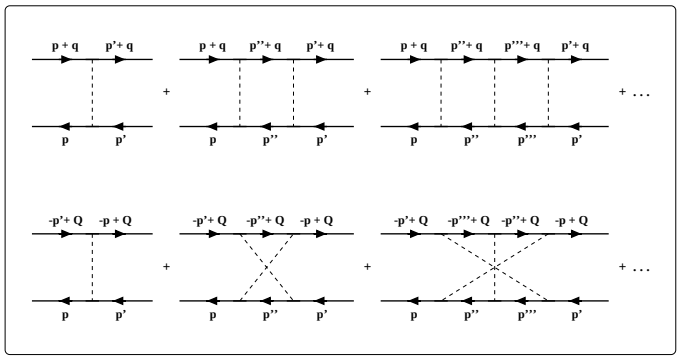

Figure 2.5.: Ladder and maximally crossed diagrams.

Anticipating the result that Γ diverges for $\mathbf{q}, \omega \to 0$, we can approximate the irreducible vertex function Π for small $|\mathbf{q}|, \omega$:

$$\Pi(\mathbf{q}, \omega) \simeq 2\pi\nu\tau(1 + i\omega\tau - D\mathbf{q}^2\tau), \tag{2.8}$$

where $D = v_\mathrm{F}^2\tau/d$ is the diffusion constant (d dimensionality of the system).

Recalling that $\gamma_\mathrm{V} = (2\pi\nu\tau)^{-1}$, the sum of ladder diagrams finally yields

$$\Gamma(\mathbf{q}, \omega) = \frac{\gamma_\mathrm{V}}{1 - \gamma_\mathrm{V}\,\Pi(\mathbf{q}, \omega)} = \frac{1}{2\pi\nu\tau^2}\frac{1}{D\mathbf{q}^2 - i\omega} \equiv \mathcal{D}(\mathbf{q}, \omega). \tag{2.9}$$

This is a diffusion pole or so-called *diffuson*. It can easily be seen that the diffuson is not affected by a weak magnetic field: Minimal coupling implies that the magnetic field shifts all momenta by the corresponding vector potential, $\mathbf{p} \to \mathbf{p} - \mathbf{A}$; however, $(\mathbf{p}_1 - \mathbf{A}) - (\mathbf{p}_2 - \mathbf{A}) = \mathbf{p}_1 - \mathbf{p}_2 = \mathbf{q}$.

The Cooperon (Maximally crossed diagrams)

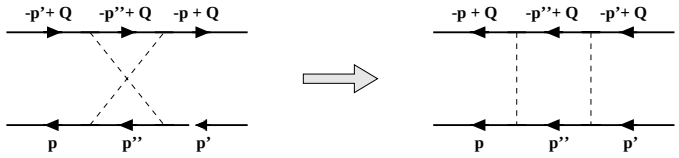

Figure 2.6.: The connection between maximally crossed and ladder diagrams.

A maximally crossed diagram [59] (for a detailed discussion see e.g. [60]) can be converted to a ladder by reversing one G-line, cf. Fig. 2.6. Since now all the arrows point in the same direction, momentum conservation at the vertices requires the momentum sum $\mathbf{Q} = \mathbf{p}_1 + \mathbf{p}_2'$ to be constant. Apart from that, the structure of all equations is the same as for the ladder diagrams. Thus,

$$\Gamma(\mathbf{Q}, \omega) = \frac{1}{2\pi\nu\tau^2}\frac{1}{D\mathbf{Q}^2 - i\omega} \equiv \mathcal{C}(\mathbf{Q}, \omega). \tag{2.10}$$

This is called a *Cooperon* – in analogy to superconductivity, as it corresponds to a correlator in the particle-particle channel (as opposed to the particle-hole channel for the diffuson). Now the presence of a magnetic field requires replacing $\mathbf{Q} \to \mathbf{Q} - 2\mathbf{A}$ which leads to a decaying of the Cooperon.

The connected part of averages of the form $\langle G^+G^+\rangle$ or $\langle G^-G^-\rangle$ vanishes, i.e. no long-ranged correlations exist. The density-density correlator, $F^{[d]}$, can be expressed in terms of diffusons and Cooperons (see also Fig. 2.4) and, therefore, will not be discussed here separately. Note that $F^{[d]}$ is closely related to the two-level correlation function employed in spectral statistics, see Sec. 3.4.

2.3. Functional field integration: The non-linear σ-model

Diagrammatics as a perturbative theory fails at small energies of the order of the mean level spacing, where it produces unphysical infra-red divergences. In this regime, a *non-perturbative* approach is needed. This approach is provided by the coherent state path integral (see also App. A.2).

The (retarded) Green function can be represented as a field integral,

$$G^+(\mathbf{r},\mathbf{r}';\epsilon) \;=\; \langle\mathbf{r}|(\epsilon+i0-\hat{\mathcal{H}})^{-1}|\mathbf{r}'\rangle \;=\; -\frac{i}{\mathcal{Z}}\int Ds\,Ds^*\; s^*(\mathbf{r})s(\mathbf{r}')\; e^{i\int d\mathbf{r}\, s^*(\epsilon^+-\hat{\mathcal{H}})s},$$

where

$$\mathcal{Z}=\int Ds\,Ds^*\, e^{i\int d\mathbf{r}\, s^*(\epsilon^+-\hat{\mathcal{H}})s},$$

and $\hat{\mathcal{H}}=\hat{\mathbf{p}}^2/(2m)+V(\mathbf{r})$. Here V represents the impurity potential which we assume to be drawn from a Gaussian white noise distribution, cf. (2.1).

Unfortunately, in this form it is not possible to carry out the disorder averaging: the random potential appears in the numerator as well as in the denominator. The presence of the partition function as a normalisation factor, $\mathcal{Z}^{-1}$, causes this problem. It is important, however, because neglecting the V-dependence of $\mathcal{Z}$ would generate unphysical 'vacuum loops'.

There are three different methods to circumvent this problem: the replica trick [61], supersymmetry [62, 63] and the Keldysh formalism [64–66]. The former two will be used in the present work and, thus, are discussed here. The most elegant formalism is supersymmetry introduced by Efetov [62, 63]; a brief review follows in Sec. 2.3.1. Its use is, however, restricted to non-interacting systems. For interacting systems, the replica trick (or the Keldysh formalism) may be used instead which is presented in Sec. 2.3.2.

2.3.1. Supersymmetry

When one is considering only *single-particle* properties of a system, there are two equivalent formulations of the path integral, namely by using bosonic or fermionic fields. Supersymmetry now exploits the following property of commuting (s) versus anti-commuting or Grassmann (χ) variables:

$$\int ds^*\,ds\, e^{-s^*Ms}=\det{}^{-1}M,\qquad \int d\bar{\chi}\,d\chi\, e^{-\bar{\chi}M\chi}=\det M.$$

Thus, combining both into a 'supervector', $\psi^T=(s,\chi)$, yields

$$\int d\psi^\dagger\, d\psi\, e^{-\psi^\dagger M\otimes\mathbb{1}_{\mathrm{BF}}\,\psi}=1, \tag{2.11}$$

where the subscript 'BF' stands for 'boson-fermion'.

Applying this to the partition sum, it is automatically normalised to unity, $\mathcal{Z} = 1$. The unphysical vacuum loops cancel, and the impurity averaging is straightforward. As a guiding example, here we construct the NLσM for a normal system. The extension to the superconducting case will be discussed in chapter 6.

The evaluation of a two-particle correlation function requires the introduction of two sets of fields, covering the advanced and retarded sector. With $\psi^T = (s_1, \chi_1, s_2, \chi_2)$ the correlator can be written as

$$\langle G^+(\epsilon+\frac{\omega}{2})G^-(\epsilon-\frac{\omega}{2})\rangle = -\left\langle \int D[\psi,\bar{\psi}]\, s_1^* s_1 s_2^* s_2\, e^{-i\int d\mathbf{r}\,\bar{\psi}(\epsilon-\frac{\omega^+}{2}\sigma_3^{\mathrm{AR}}-\hat{\mathcal{H}})\psi} \right\rangle,$$

where $\omega^+ = \omega + i0$ and σ_3^{AR} is a Pauli matrix in advanced/retarded space. Furthermore, $\bar{\psi} = \psi^\dagger L$ with $L = \sigma_3^{\mathrm{AR}} \otimes E_{\mathrm{BB}} + \mathbb{1}^{\mathrm{AR}} \otimes E_{\mathrm{FF}}$, where E_{BB} and E_{FF} are projectors onto the boson-boson and fermion-fermion block, respectively. This metric factor is required due to convergence criteria for the bosonic sector [67].

By introducing a source term,

$$\mathcal{Z}[J] = \int D[\psi,\bar{\psi}]\, e^{-i\int d\mathbf{r}\,\bar{\psi}(\epsilon-\frac{\omega^+}{2}\sigma_3^{\mathrm{AR}}-\hat{\mathcal{H}})\psi} e^{\int d\mathbf{r}\,(J^\dagger\psi+\bar{\psi}J)}, \tag{2.12}$$

different correlators of Green functions can be obtained from the generating functional $\mathcal{Z}$ by taking derivatives with respect to the source field J. In the following, we will suppress the sources and consider only $\mathcal{Z}[0]$.

Now the impurity averaging of the partition function leads to a quartic term in the fields ψ,

$$\langle e^{i\int d\mathbf{r}\,\bar{\psi}V\psi}\rangle = \exp[-\frac{1}{4\pi\nu\tau}\int d\mathbf{r}\,(\bar{\psi}\psi)^2]. \tag{2.13}$$

By Fourier transformation to momentum representation, one can identify the slow modes (cf. Fig. 2.7),

$$\begin{aligned}\int d\mathbf{r}\,(\bar{\psi}\psi)^2 &= \sum_{\sum \mathbf{p}_i=0} (\bar{\psi}_{\mathbf{p}_1}\psi_{\mathbf{p}_2})(\bar{\psi}_{\mathbf{p}_3}\psi_{\mathbf{p}_4}) \qquad (2.14)\\ \approx \sum_{\mathbf{p},\mathbf{p}';\mathbf{q}} &\Big((\bar{\psi}_{\mathbf{p}}\psi_{-\mathbf{p}+\mathbf{q}})(\bar{\psi}_{-\mathbf{p}'}\psi_{\mathbf{p}'-\mathbf{q}}) + (\bar{\psi}_{\mathbf{p}}\psi_{-\mathbf{p}'})(\bar{\psi}_{\mathbf{p}'-\mathbf{q}}\psi_{-\mathbf{p}+\mathbf{q}}) + (\bar{\psi}_{\mathbf{p}}\psi_{\mathbf{p}'-\mathbf{q}})(\bar{\psi}_{-\mathbf{p}+\mathbf{q}}\psi_{-\mathbf{p}'})\Big),\end{aligned}$$

where $|\mathbf{q}| \ll \ell^{-1}$.

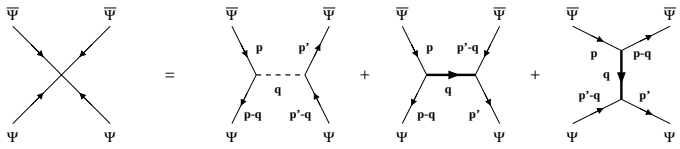

Figure 2.7.: Decoupling of the quartic interaction.

The first term corresponds to slow fluctuations of the energy which can be absorbed by a local redefinition of the chemical potential. Thus, we concentrate on the remaining terms: The second term generates the diffuson contribution while the third term yields the Cooperon contribution.

Enlarging the field space[7] by defining $\Psi^T = (\psi^T, \psi^\dagger)/\sqrt{2}$, the last two terms can be rewritten into a single contribution,

$$\exp\Big[-\frac{1}{2\pi\nu\tau}\sum_{\mathbf{q}} \zeta(\mathbf{q})\zeta(-\mathbf{q}) \Big], \tag{2.15}$$

where $\zeta(\mathbf{q}) = \sum_{\mathbf{p}} \Psi(\mathbf{p}-\mathbf{q})\bar{\Psi}(-\mathbf{p})$. The components of the newly defined vector Ψ fulfill the symmetry relation $\Psi^\dagger = (C\Psi)^T$, where $C = \sigma_1^{\mathrm{TR}} \otimes E_{\mathrm{BB}} + i\sigma_2^{\mathrm{TR}} \otimes E_{\mathrm{FF}}$. This symmetry corresponds to time-reversal ($\psi \to \psi^*$, $\mathcal{H} \to \mathcal{H}^T$).

In the absence of the symmetry-breaking energy difference, $\omega = 0$, the action is invariant under rotations $\Psi \to U\Psi$, where $ULU^\dagger = L$ and $U^T = CU^\dagger C^T$. Thus, $U \in \mathrm{Osp}(4|4)$.

As a next step the quartic interaction is decoupled by a Hubbard-Stratonovich transformation, introducing the new (supermatrix-) fields Q:

$$\exp\left[-\frac{1}{4\pi\nu\tau}\int d\mathbf{r}\,(\bar{\Psi}\Psi)^2\right] \;=\; \int DQ\, \exp\left[\frac{\pi\nu}{8\tau}\int d\mathbf{r}\ \mathrm{Str}\, Q^2 - \frac{1}{2\tau}\int d\mathbf{r}\,\bar{\Psi}Q\Psi\right], \tag{2.16}$$

where $\mathrm{Str}\, M = \mathrm{tr}\, M_{\mathrm{BB}} - \mathrm{tr}\, M_{\mathrm{FF}}$. The symmetries of Q reflect the symmetries of the dyadic product $\Psi \otimes \bar{\Psi}$, namely

$$Q = CLQ^T(CL)^T. \tag{2.17}$$

Now the resulting exponent is only quadratic in the original Ψ-fields. Therefore, the Gaussian integral can be readily evaluated, yielding the action

$$S[Q] = -\frac{\pi\nu}{8\tau}\int d\mathbf{r}\ \mathrm{Str}\, Q^2 + \frac{1}{2}\int d\mathbf{r}\ \mathrm{Str}\, \ln \mathcal{G}^{-1}, \tag{2.18}$$

where $\langle \mathcal{Z} \rangle = \int DQ\, \exp(-S[Q])$ and

$$\mathcal{G}^{-1} = \frac{1}{2m}\hat{\mathbf{p}}^2 - \epsilon_{\mathrm{F}} + \frac{\omega^+}{2}\sigma_3^{\mathrm{AR}} + \frac{i}{2\tau}Q.$$

To extract an effective low-energy, long-wavelength field theory from this action, a saddle point analysis has to be performed. Variation of (2.18) with respect to Q yields

$$Q_{\mathrm{SP}}(\mathbf{r}) = \frac{i}{\pi\nu}\mathcal{G}(\mathbf{r},\mathbf{r}). \tag{2.19}$$

Neglecting the small energy ω (as well as the source terms), the Ansatz Q_{SP} constant and diagonal leads to

$$Q_{\mathrm{SP}} = -\frac{i}{\pi}\int d\xi\, \frac{1}{\xi - \frac{i}{2\tau}Q_{\mathrm{SP}}} = \mathrm{sgn}(Q_{\mathrm{SP}}). \tag{2.20}$$

Thus, the saddle point Q_{SP} has the meaning of a self-energy. Analytic properties of the Green function single out the solution $Q_{\mathrm{SP}} = \sigma_3^{\mathrm{AR}}$.

In fact, the action is invariant under transformations $Q \to TQT^{-1}$, where T constant: instead of one saddle point one obtains – at $\omega = 0$ and in the absence of symmetry breaking sources – a degenerate saddle point manifold $Q^2 = \mathbb{1}$. Fluctuations around the saddle point can be subdivided into longitudinal modes, $[\delta Q_l, Q_{\mathrm{SP}}] = 0$, and transverse modes, $\{\delta Q_t, Q_{\mathrm{SP}}\} = 0$. The longitudinal modes δQ_l leave the saddle point manifold $Q^2 = \mathbb{1}$. Therefore, they are massive and

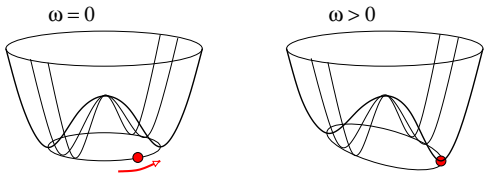

Figure 2.8.: Saddle-point manifold. At $\omega = 0$ the saddle point spans an entire manifold while for finite ω the degeneracy is lifted.

do not contribute to the low-energy physics of the system. In the following, we concentrate on the transverse modes δQ_t. The parameter which stabilises this distinction is $k_F \ell \sim \epsilon_F \tau$, i.e. the following considerations are valid in the *quasi-classical* limit.

We proceed by expanding the action around the saddle point in the slowly varying fields $Q(x) = T(x) Q_{SP} T^{-1}(x)$. Separating the fast and slow degrees of freedom with $\hat{\mathbf{p}} \to \mathbf{p} + \hat{\mathbf{q}}$, this expansion yields

$$S \simeq \frac{1}{2} \int d\mathbf{r} \int d\mathbf{p}\ \mathrm{Str} \left[\frac{\omega^+}{2} \mathcal{G}_0 T^{-1} \sigma_3^{\mathrm{AR}} T - \frac{1}{2m^2} \left(\mathcal{G}_0\, T^{-1}\, \mathbf{p}\hat{\mathbf{q}}\, T \right)^2 \right]. \tag{2.21}$$

The integral over fast momenta, $\mathbf{p}$, can be performed using the following representation for the Green function,

$$\mathcal{G}_0(\mathbf{p}) = \frac{1}{2} \sum_{s=\pm} \frac{1 + s\sigma_3^{\mathrm{AR}}}{-\xi_p + s\frac{i}{2\tau}} \equiv \frac{1}{2} \sum_{s=\pm} (1 + s\sigma_3^{\mathrm{AR}}) G_0^s(\mathbf{p}).$$

Then, $\int d\mathbf{p}\ \mathcal{G}_0(\mathbf{p}) = -i\pi\nu\sigma_3^{\mathrm{AR}}$, and

$$\begin{aligned} &\int d\mathbf{p}\ \mathrm{Str}\left[\mathcal{G}_0(\mathbf{p})\, T^{-1}\, \mathbf{p}\hat{\mathbf{q}}\, T\, \mathcal{G}_0(\mathbf{p})\, T^{-1}\, \mathbf{p}\hat{\mathbf{q}}\, T\right] = \\ = \underbrace{\frac{\nu p_F^2}{4d} \int d\xi\ G_0^+ G_0^-}_{= m^2 \pi \nu D/2}\ &\mathrm{Str}\left[(1+s\sigma_3^{\mathrm{AR}}) T^{-1}\, \hat{\mathbf{q}}\, T (1-s\sigma_3^{\mathrm{AR}}) T^{-1}\, \hat{\mathbf{q}}\, T\right]. \end{aligned}$$

Finally, summing over s and using the cyclic invariance under the trace, the effective action takes the form of a non-linear σ model,

$$S[Q] = -\frac{\pi\nu}{8} \int d\mathbf{r}\ \mathrm{Str}\left[D(\partial Q)^2 + 2i\omega^+ \sigma_3^{\mathrm{AR}} Q\right]. \tag{2.22}$$

(Note that the effect of a weak magnetic field is to generalise the derivatives to $\tilde{\partial} = \partial - i\mathbf{A}[\sigma_3^{\mathrm{TR}}, .]$; this will be discussed in more detail in chapter 5.)

In the perturbative regime, an expansion of the effective action around the saddle point in the generators W, where $Q = e^{-W/2} \sigma_3^{\mathrm{AR}} e^{W/2}$ and $\{W, \sigma_3^{\mathrm{AR}}\} = 0$, reproduces the diagrammatic results. By contrast, in the *non*-perturbative regime, the action is dominated by zero-modes which require an integration over the whole saddle point manifold $\mathrm{Osp}(4|4)/(\mathrm{Osp}(2|2) \otimes \mathrm{Osp}(2|2))$.

[7] Generally, each discrete symmetry leads to a doubling of the low-lying modes and, thus, should be incorporated by doubling the field space [68].

2.3.2. Replica trick

As two-particle interactions are not the same for bosons and fermions, they prohibit the use of the supersymmetry method. An alternative approach is the replica trick. Again – as for supersymmetry – this is only a convenient way to write the path integral (in order to admit for impurity averaging) which has no physical interpretation.

The replica trick enables one to directly construct a path integral for $\ln \mathcal{Z}$ (instead of $\mathcal{Z}$), making use of the identity

$$\ln \mathcal{Z} = \lim_{N\to 0} \frac{1}{N}(\mathcal{Z}^N - 1). \tag{2.23}$$

The generating functional can be written as

$$\mathcal{Z}^N = \int D[\Psi] e^{-S[\Psi]} = \int \prod_{a=1}^{N} D\psi^a D\bar{\psi}^a \, e^{-\sum_{a=1}^{N} S[\psi^a]}. \tag{2.24}$$

Again Green functions and their correlators are obtained by taking functional derivatives with respect to some source terms. Here the action for a single replica reads

$$S[\psi^a] = \int d\mathbf{r}\, \bar{\psi}^a (i\epsilon_n - \hat{\mathcal{H}})\psi^a + S_I[\psi^a], \tag{2.25}$$

where $\epsilon_n = \pi(2n+1)/\beta$ (with β inverse temperature) are fermionic Matsubara frequencies. $\hat{\mathcal{H}}$ denotes the non-interacting Hamiltonian while interactions are contained in S_I. Note that in addition to the replica index a, the fields carry a Matsubara index – corresponding to the advanced/retarded sector above. Again the field space has to be doubled if additional discrete symmetries are present.

With the above definitions, the on-site Green function – necessary to calculate the density of states $\nu(\epsilon) = -\pi^{-1} \operatorname{tr} \Im\left[G(\mathbf{r},\mathbf{r}; i\epsilon_n \to \epsilon^+)\right]$ – e.g. obtains as

$$G(\mathbf{r},\mathbf{r};\epsilon_n) = i \lim_{N\to 0} \frac{1}{N} \frac{\partial}{\partial \epsilon_n} \left\langle \mathcal{Z}^N \right\rangle_V . \tag{2.26}$$

The derivation of an effective low-energy, long-wavelength action follows exactly the same lines as for the supersymmetric version of the path integral. The resulting NLσM for the non-interacting case reads

$$S[Q] = \frac{\pi\nu}{8} \int d\mathbf{r} \ \operatorname{tr} \left[D(\partial Q)^2 - 4\epsilon_n Q \right]. \tag{2.27}$$

Now – as the ψ-fields – the Q-matrices carry Matsubara (n,m) as well as replica (a,b) indices, Q^{ab}_{nm}. Furthermore, they are Hermitian and obey the symmetry relation $Q = \sigma_1^{\mathrm{TR}} Q^T \sigma_1^{\mathrm{TR}}$.

The term replica '*trick*' is used because the method does not stand on very firm mathematical grounds. In fact, the limiting procedure $N \to 0$ is only strictly justified for analytic functions of N – which is generally not the case: As long as perturbative results are concerned the method is safe. By contrast, in the non-perturbative regime naively taking the limit $N \to 0$ may lead to unphysical results [69]. However, a number of recent publications [70, 71] has shown that – in some cases! – allowing for replica symmetry breaking one is able to recover the correct non-perturbative results. E.g. in Ref. [70], the large energy asymptotics of the two-level correlation

function have been reproduced for the Gaussian orthogonal, unitary, and symplectic ensembles (cf. Secs. 2.4 and 3.4 below) within the replica formalism.

In the derivation of the NLσM, the dimensionality of the systems has not been specified. Of special interest is the zero-dimensional case or the so-called *ergodic* regime, where the system is given long enough time to explore the entire phase space ($t > E_{\mathrm{Th}}^{-1}$). Here universality plays an important role. In fact, the spectral and transport properties in this regime can be described by a 'random matrix' Hamiltonian which knows only about the fundamental symmetries of the system. It has been shown that the random matrix formulation is equivalent to the $0d$-version of the supersymmetric NLσM. A short introduction to random matrix theory (RMT) is given in the following section.

2.4. Random matrix theory

Random matrix theory (RMT) was developed in the 50s and 60s, starting with the pioneering work by Wigner [72] on the statistics of energy levels in heavy nuclei. Since then RMT has been applied successfully to an increasing number of different physical problems. A first application of RMT to disordered systems dates back to Gor'kov and Eliashberg [73] who used it to describe level spectra in small metallic grains. The underlying assumption of RMT is that – in the ergodic regime – the relevant physical properties of a complex system are determined by fundamental symmetries. Thus, one may attempt to describe these properties by considering ensembles of random Hamiltonians which are subject only to some common symmetry condition. A classification of many-body systems into symmetry classes was introduced by Dyson [74, 75]. He found three universality classes reflecting the fundamental symmetries of the Hamiltonian. The discovery of a connection between RMT and classical chaos further enhanced its range of applicability: even if it possesses only few degrees of freedoms, a system whose behaviour is chaotic in the classical limit follows the predictions of RMT (Bohigas-Giannoni-Schmit conjecture [76]).

Wigner-Dyson ensembles

Conventionally, three different symmetry classes are distinguished which are characterised by the symmetry index β. I.e. one considers an ensemble of $N \times N$ Hermitian matrices $\mathcal{H}$ with a Gaussian probability distribution,

$$P(\mathcal{H})\, d\mu[\mathcal{H}] \sim e^{-\beta \frac{N}{\lambda^2} \operatorname{tr} \mathcal{H}^2} d\mu[\mathcal{H}]. \tag{2.28}$$

The presence of symmetries in the system imposes additional constraints on $\mathcal{H}$, and the index β counts the number of degrees of freedom for each matrix element. Physically, $\beta = 2$ applies to systems with broken time-reversal symmetry e.g. due to a magnetic field. If $\mathcal{T}$-invariance is present, $\beta = 1$ describes systems with and $\beta = 4$ systems without spin-rotation symmetry, e.g. due to spin-orbit scattering. These properties are summarised in the following table:

symmetry class		β	time-reversal	spin-rotation
orthogonal	GOE	1	✓	✓
unitary	GUE	2	–	(irrelevant)
symplectic	GSE	4	✓	–

The denotation 'orthogonal', 'unitary' or 'symplectic' characterises the group which diagonalises the corresponding random Hamiltonians. Furthermore, the abbreviation 'G(O,U,S)E' stands for Gaussian (Orthogonal, Unitary, Symplectic) Ensemble.

Time-reversal invariant systems can be described by real symmetric matrices $\mathcal{H}_{nm} = \mathcal{H}_{mn} = \mathcal{H}^*_{nm}$. These are diagonalised by an orthogonal matrix $O \in \mathrm{O}(N)$, i.e. $\mathcal{H} = O^\dagger \,\mathrm{diag}(\lambda_1, \ldots, \lambda_N)\, O$.

If $\mathcal{T}$-invariance is broken, the appropriate matrix Hamiltonian is Hermitian, $\mathcal{H}_{nm} = (\mathcal{H}^\dagger)_{nm} = \mathcal{H}^*_{mn}$, which can be transformed to diagonal form by a unitary matrix $U \in \mathrm{U}(N)$.

Finally, in the absence of spin-rotation symmetry, the matrix elements are real quaternions $\hat{\mathcal{H}}_{nm} = \mathcal{H}^{(0)}_{nm}\mathbb{1}_2 + i\sum_i \mathcal{H}^{(i)}_{nm}\sigma_i$ (where σ_i are Pauli matrices). The diagonalisation yields $\hat{\mathcal{H}}_{nm} = S^\dagger \,\mathrm{diag}(\lambda_1\mathbb{1}_2, \ldots, \lambda_N\mathbb{1}_2)\, S$ with a symplectic matrix S.

To find the distribution of eigenvalues, one has to link the volume element $d\mu[\mathcal{H}]$ to the corresponding volume elements in terms of eigenvalues and eigenvectors. The Jacobian depends only on the eigenvalues and the symmetry index [77]:

$$J(\{\lambda_n\}) = \prod_{i<j} |\lambda_i - \lambda_j|^\beta. \tag{2.29}$$

The outline of the derivation of a σ-model for the case $\beta = 2$ (GUE) is shown in appendix B.1. For a general review on RMT see e.g. [78–80].

Novel symmetry classes

Only very recently, it has been realised that this classification scheme is not complete [47]. In fact, there are ten symmetry classes in total, corresponding to the ten compact symmetric spaces – identified and labelled by Cartan. The classification scheme is shown in Table 2.1.

Denotation		Compact symmetric space
A	GUE (Dyson)	$\mathrm{U}(N)$
AI	GOE (Dyson)	$\mathrm{U}(N)/\mathrm{O}(N)$
AII	GSE (Dyson)	$\mathrm{U}(2N)/\mathrm{Sp}(N)$
AIII	chiral GUE	$\mathrm{U}(N+M)/\mathrm{U}(N)\times\mathrm{U}(M)$
BDI	chiral GOE	$\mathrm{SO}(N+M)/\mathrm{SO}(N)\times\mathrm{SO}(M)$
CII	chiral GSE	$\mathrm{Sp}(N+M)/\mathrm{Sp}(N)\times\mathrm{Sp}(M)$
BD		$\mathrm{SO}(N)$
C		$\mathrm{Sp}(N)$
DIII		$\mathrm{SO}(2N)/\mathrm{U}(N)$
CI		$\mathrm{Sp}(N)/\mathrm{U}(N)$

Table 2.1.: The ten symmetry classes.

Common to the novel symmetry classes is the invariance of the energy spectrum under the inversion $E \to -E$. For large energies, this additional symmetry is irrelevant, but for small energies novel features – clearly distinct from the properties of the conventional Wigner-Dyson (WD) classes – arise. Obviously the band centre, $E = 0$, plays a special role while in the WD classes the energy spectrum is uniform on average.

Instead of one index, here two symmetry indices α, β are needed. The Jacobian is now of the form

$$J(\{\lambda_n\}) = \prod_{i<j} |\lambda_i^2 - \lambda_j^2|^\beta \prod_k |\lambda_k|^\alpha. \tag{2.30}$$

Notice that all eigenvalues come in pairs $\pm\lambda_i$. The spectral properties in the vicinity of $E = 0$ are determined by the exponent α.

The chiral symmetry classes (AIII, BDI, CII) find their application in quantum chromodynamics [81] while the remaining four symmetry classes become relevant in connection with superconductivity [82]. These classes (BD, C, DIII, CI) – whose low-energy properties have been discussed in Ref. [82] – possess the following symmetries:

	time-reversal	spin-rotation
BD	–	–
C	–	✓
DIII	✓	–
CI	✓	✓

Examples of systems belonging to class C and CI will appear in chapter 7.

This concludes the introduction on theoretical methods. Concepts relevant for the different parts of this work will be presented in the first chapter of each part.

Part I.

Mesoscopic correlations in two-dimensional electron systems

3. Low-dimensional electron systems

3.1. Experimental realisation of 2DEGs

Even though the 'real world' is three-dimensional, quantum mechanics admits for the existence of (quasi) two-dimensional systems. If the width d of a (three-dimensional) system is of the order of the wavelength of the particles, momentum quantisation in that direction becomes important. Now at low temperatures, the particle energies are limited by the Fermi energy. Thus, for $d < \lambda_F$, only the lowest mode is allowed and, therefore, the particle motion is confined to a two-dimensional plane.

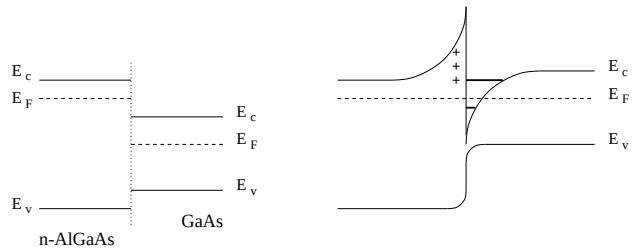

Figure 3.1.: Band diagram of a 2DEG in an GaAs/AlGaAs heterostructure [25] (E_v: energy of the valence band, E_c: energy of the conduction band).

Technically, these two-dimensional systems or 2DEGs can be realised in Si-MOSFETs and GaAs/AlGaAs heterostructures [83]. The properties of heterojunctions between dissimilar semiconductors are governed by the lineup of the valence and conduction bands at the interface, as depicted schematically in Fig. 3.1. Selective doping of the wide gap material AlGaAs (usually with Si), leads to a diffusion of free carriers from the n-AlGaAs into the GaAs, leaving positively charged donors behind. This charge separation causes an electrostatic potential which traps the electrons within a short distance from the interface. Due to this confinement, momentum quantisation occurs in the perpendicular direction whereas free motion along the interface is possible. The mobility is limited only by scattering from the remote donors.

Typical values of relevant parameters for GaAs- and Si-2DEGs are listed in table 3.1.

3.2. Weak localisation and negative magnetoresistance

In Sec. 2.2.2 correlation functions have been introduced. How do these long-ranged correlators affect physical observables?

	GaAs	Si	(units)
Effective mass m	0.067	0.19	m_e
Density of states ν	0.28	1.59	$10^{11}\,\mathrm{cm}^{-2}/\mathrm{meV}$
Electronic density n_s	4.0	$1-10$	$10^{11}\,\mathrm{cm}^{-2}$
Fermi wavevector k_F	1.58	$0.56-1.77$	$10^{6}\,\mathrm{cm}^{-1}$
Mean free path ℓ	10^2-10^4	$37-118$	$10^{-4}\,\mathrm{cm}$

Table 3.1.: Electronic properties of 2DEGs in GaAs/AlGaAs heterostructures and Si inversion layers (taken from [84]). Here m_e is the electron mass.

The conductance of a system is related to the transition probability from points $\mathbf{r}_i$ to $\mathbf{r}_f$. Quantum-mechanically, this probability is obtained by summing the transition *amplitudes* A_j of all possible paths from $\mathbf{r}_i$ to $\mathbf{r}_f$ and, then, taking the mean square,

$$P(\mathbf{r}_i \to \mathbf{r}_f) = \left| \sum_j A_j \right|^2 . \tag{3.1}$$

Due to the random scattering on impurities, in general, different paths acquire different phases and, therefore, cannot interfere constructively. Thus, upon averaging, the result assumes the classical value

$$P(\mathbf{r}_i \to \mathbf{r}_f) = \sum_j |A_j|^2 . \tag{3.2}$$

A first quantum correction obtains by considering time-reversed paths. If a path linking $\mathbf{r}_\mathrm{i}$ and $\mathbf{r}_\mathrm{f}$ contains a loop (as depicted in Fig. 3.2), this loop can be traversed in different directions. Now, the paths j and j' going clockwise and anti-clockwise, respectively, are scattered by the same impurities. If the system possesses time-reversal symmetry, $A_j = A_{j'}$, i.e. the amplitudes for going both ways are the same. Thus, when calculating the transition probability, their phases just cancel. As such contributions exist only for closed loops, the probability to stay at a given point $\mathbf{r}$ is larger than expected classically. This enhanced return probability reduces the conductance of a $\mathcal{T}$-invariant system as compared to its classical value. Quantitatively, the resulting *weak localisation* corrections are determined by the Cooperon correlator $F^{[C]}$.

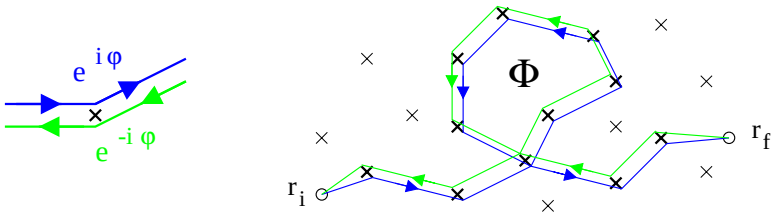

Figure 3.2.: Interfering electron paths in a random medium.

Now, a magnetic field breaks time-reversal symmetry and, thus, gradually destroys the interference effects. Therefore, when applying a magnetic field, the conductance increases – or, equivalently, the resistance decreases. This effect is called *negative magnetoresistance*.

Now, what is the relevant field scale for the suppression of weak localisation corrections? Quantum interference becomes ineffective as soon as the phase difference between the interfering paths is of order 2π. In a magnetic field, an electron acquires an additional phase $\int \mathbf{A}(\mathbf{s})\, d\mathbf{s}$ while its time-reversed counterpart picks the opposite phase $-\int \mathbf{A}(\mathbf{s})\, d\mathbf{s}$. When travelling through a closed loop, the phase difference equals

$$2 \oint \mathbf{A}(\mathbf{s})\, d\mathbf{s} = 2 \int \nabla \times \mathbf{A}(\mathbf{s})\, d\mathbf{F} = 2 \int \mathbf{H}\, d\mathbf{F} = 2HF_\perp = 2\Phi. \tag{3.3}$$

Thus, the characteristic field scale is determined such that the typical area $F_\perp$ encloses one flux quantum, ϕ_0. For a perpendicular magnetic field, this obtains $H_\perp l_{H_\perp}^2 \simeq \phi_0$, i.e. a magnetic length $l_{H_\perp} \sim H_\perp^{-1/2}$ (see also Fig. 3.3). For a parallel magnetic field, the situation is more complicated as we will discuss in detail in chapter 5. Geometrical arguments suggest that thickness of the 2DEG, d, comes into play as a second length scale, and the relevant area is given as $F_\perp \sim l_{H_\parallel} d$. This leads to $l_{H_\parallel} \sim (H_\parallel d)^{-1}$. The magnetic length scales come with the corresponding time scales $\tau_H^{-1} = D/l_H^2$. Thus, this simple estimate admits for determining the field dependence of the 'magnetic decoherence times': $\tau_{H_\perp} \sim H_\perp^{-1}$ [33], whereas for parallel magnetic fields one expects $\tau_{H_\parallel} \sim H_\parallel^{-2}$ [34].

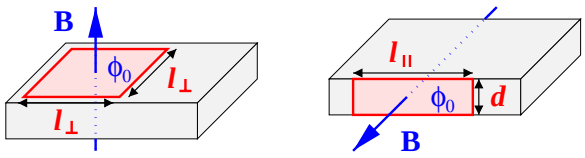

Figure 3.3.: Relevant areas for perpendicular and parallel magnetic fields.

3.3. Quantum dots

Starting from a two-dimensional electron gas, a quantum dot (QD) can be realised by depleting certain regions with a gate voltage. For this purpose, metallic gates are created on top of the GaAs/AlGaAs structure. A typical geometry is shown in Fig. 3.4. The electron motion is, thus, confined in all directions. Furthermore, via gate voltages it is not only possible to define the area of the dot, but also to vary its chemical potential as well as its coupling to the leads.

As opposed to an extended system which has a continuous spectrum, the energy levels of a QD are discrete. This discreteness of the excitation spectrum is not dissimilar to the electronic structure in atoms, and QDs are sometimes referred to as 'artificial atoms'. In fact, in so-called vertical QDs which contain only a small number of electrons even a shell structure has been observed [85, 86]. The advantage of QDs as compared to natural atoms is that they are easily manageable experimentally, and a number of (external) control parameters admits for investigating various effects which are not realisable otherwise.

A quantum dot can be either diffusive or ballistic, depending on whether the mean free path is smaller or larger than the size of the dot. In the latter case, the dynamics will be integrable or chaotic – as determined by the boundaries. In the ergodic regime, diffusive and chaotic QDs can be described by random matrix theory. This is the content of the Bohigas-Giannoni-Schmit conjecture [76] mentioned earlier: The spectral properties of quantum systems which are chaotic in their classical limit are *universal*.

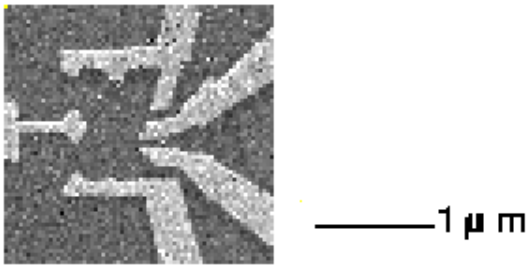

Figure 3.4.: Quantum dot confined by gates (picture taken from Ref. [6]). Here the lighter shaded areas are the metallic gates on top of the sample.

3.4. Spectral statistics

Quantum interference phenomena do not only affect the transport behaviour, but also spectral properties. As mentioned above, the energy spectrum of a finite system is discrete and, therefore, can be characterised by a mean level spacing δ and fluctuations. In many cases, the mean level spacing varies only slowly with energy and can be assumed to be constant. More interesting are the fluctuations. The strength of fluctuations is determined by the correlations between energy levels. The latter are characterised by the two-point correlator of DoS fluctuations

$$R_2(\omega) \;=\; \frac{1}{\delta^2}\left\langle \delta\nu(\epsilon+\frac{\omega}{2})\,\delta\nu(\epsilon-\frac{\omega}{2})\right\rangle \;=\; \frac{1}{\delta^2}\left\langle \nu(\epsilon+\frac{\omega}{2})\,\nu(\epsilon-\frac{\omega}{2})\right\rangle - 1, \tag{3.4}$$

where $\nu(\epsilon) = \operatorname{tr}\delta(\epsilon-\mathcal{H})$ and $\delta\nu = \nu - \langle\nu\rangle$.

If the levels are uncorrelated (Poisson statistics), R_2 vanishes. However, in a disordered or chaotic system, quantum effects induce correlations between the levels. Expressing the DoS in terms of Green functions, one can identify the relevant contributions due to interfering paths – as for the transition amplitude in Sec. 3.2. The relevant contributions are depicted schematically in Fig. 3.5. Using diagrammatic perturbation theory, one obtains [87]

$$R_2(\omega) = \frac{1}{\pi^2\beta}\Re\sum_{\mathbf{q}}\frac{\delta^2}{(D\mathbf{q}^2-i\omega)^2}, \tag{3.5}$$

where β is the symmetry index introduced in the previous chapter. As a reminder: $\beta = 1$ (orthogonal) corresponds to $\mathcal{T}$-invariant systems while $\beta = 2$ (unitary) describes systems with broken $\mathcal{T}$-symmetry.

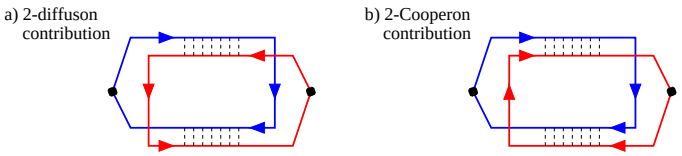

Figure 3.5.: Diagrams contributing to R_2. If $\mathcal{T}$-invariance is broken, the Cooperon term (right) vanishes.

At energies $\omega \ll E_{\mathrm{Th}}$, i.e. in the ergodic regime, the dominant contribution to R_2 is given by

the spatial zero-mode $\mathbf{q} = 0$,

$$R_2(\omega) \simeq -\frac{1}{\beta}\left(\frac{\delta}{\pi\omega}\right)^2.$$

As expected – this result does not depend on any details of the system like e.g. geometry and is, therefore, universal. Furthermore, this expression signals that perturbation expansion fails at small energies $\omega < \delta$. The divergence of the above result cannot be cured by taking into account higher order contributions and a non-perturbative approach is needed. As pointed out in the previous chapter, in the non-perturbative regime random matrix theory provides a valuable method for calculating system properties. One obtains (see, e.g., Ref. [79])

$$\begin{aligned} R_2^o(s) &= -\frac{\sin^2 s}{s^2} - \pi\frac{d}{ds}\left(\frac{\sin s}{s}\right)\int_s^\infty ds'\,\frac{\sin s'}{s'}, \\ R_2^u(s) &= -\frac{\sin^2 s}{s^2}, \end{aligned} \tag{3.6}$$

where $s = \pi\omega/\delta$. Furthermore, 'o' ('u') stands for orthogonal (unitary). For $s \to 0$, this admits for the following approximations $R_2^o(s) - 1 \simeq \pi s/6$ while $R_2^u(s) - 1 \simeq s^2/3$, i.e. $R_2(s \to 0) - 1 \sim s^\beta$.

In the ergodic regime, the two-level correlation function is related to the correlator $F^{[d]}$ introduced in Sec. 2.2.2 through

$$\Re F^{[d]}(s) = \pi\delta(s) - R_2^u(s). \tag{3.7}$$

Note that for small s the function R_2 approximates the nearest neighbour distribution which encodes the (energetically) short-ranged correlations. Long-ranged correlations are described by the level number variance

$$\Sigma_2(L) \;=\; \langle \delta\hat{N}^2(L)\rangle \;=\; L - 2\int_0^L dr\,(L-r)\,R_2(\pi r) \tag{3.8}$$

which measures the fluctuations of the number of levels $\hat{N}(L)$ in a given energy window $E = L\delta$. By construction, $\langle\hat{N}(L)\rangle = L$. Using the above expressions for R_2, one obtains $\langle\delta\hat{N}^2\rangle \sim \beta^{-1}\ln\langle\hat{N}\rangle$. This expresses the rigidity of the spectrum – in contrast to Poisson statistics, where $\langle\delta\hat{N}^2\rangle \sim \langle\hat{N}\rangle$.

3.5. Zero-bias anomaly and Coulomb blockade

So far we have neglected interactions. In fact, many of the characteristic phenomena in mesoscopics are well described within a non-interacting theory. When does Coulomb interaction play a role – and how does it manifest itself?

The most direct manifestation of interaction effects is the so-called Coulomb blockade. Consider the tunnelling conductance through an (almost) *closed* system, i.e., to be more specific, a quantum dot (QD) coupled only via point contacts. As a function of gate voltage – which tunes the chemical potential – a series of resonance peaks is observed, see Fig. 3.6. Typically, the spacing of these peaks is controlled by the charging energy $E_c = e^2/(2C)$, where C denotes the capacitance of the dot. This can be understood within the 'orthodox' or constant interaction model: The electrostatic energy of n electrons on the dot is given as

$$U(n) = n^2 E_c - nV_\mathrm{g},$$

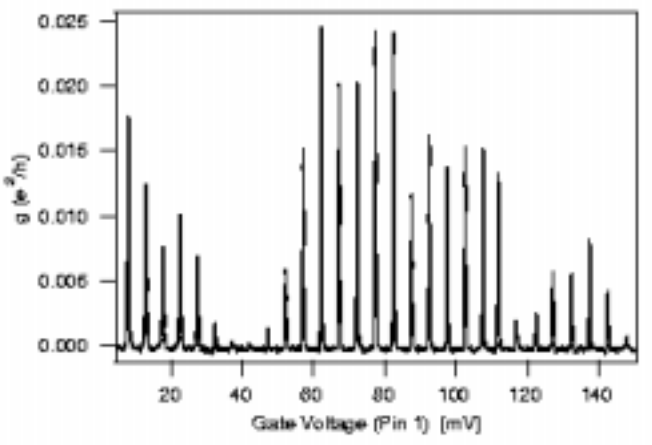

Figure 3.6.: Tunnelling conductance through a quantum dot: Experimental results by Marcus et al. measured with the QD depicted in Fig. 3.4 (picture taken from Ref. [6]).

where V_g represents the external gate voltage.

Now, tunnelling of an extra electron onto the dot is only possible if two states with a different number of electrons, n and $n+1$, are degenerate. The energy balance reads

$$E(n+1) - E(n) = \big(\epsilon_{n+1} + U(n+1)\big) - \big(\epsilon_n + U(n)\big), \tag{3.9}$$

where ϵ_n is the single-particle energy corresponding to the n-th level.

In a typical system, the charging energy exceeds the mean level spacing, $\delta = \langle\, \epsilon_{n+1} - \epsilon_n \,\rangle_n$, by far. Thus, the degeneracy condition $E(n+1) - E(n) = 0$ is given approximately as

$$V_\mathrm{g} = (2n+1)E_c,$$

which leads to equally spaced conductance peaks with a voltage difference $\delta V_\mathrm{g} = 2E_c$, see e.g. [31].

Taking into account the finite level spacing, deviations from the regular pattern of peaks occur. Due to the double occupancy of each level (spin $\uparrow\downarrow$), naively one would expect a bi-modal peak distribution with a δ-peak at $2E_c$ and a Wigner-Dyson curve centred around $\delta + 2E_c$. This is, however, not observed experimentally. In fact, the peak spacing distribution is still the subject of current investigation: the orthodox model alone is not sufficient to explain the experimental findings. Instead, one has to take into account residual interactions as well as scrambling of the wavefunctions when changing the gate voltage [88].

Although much weaker, an effect analogous to the Coulomb blockade occurs in *open* dirty systems, too. Taking into account the long-range Coulomb repulsion, when an electron tunnels onto the system, the other electrons have to rearrange in order to accommodate the additional charge. If all electrons are localised, this leads to a vanishing of the density of states (DoS) at the Fermi level, the so-called Coulomb gap [89, 90]. This can be understood within a simplified picture as follows: Consider an energy interval of small width $|\epsilon|$ centred around the Fermi energy. Creating a one-particle excitation from the ground state by transferring an electron from state j below the Fermi energy, $\epsilon_j < \epsilon_\mathrm{F}$, to state i above the Fermi energy, $\epsilon_i > \epsilon_\mathrm{F}$, *increases* the energy by $\Delta_{ij} = \epsilon_i - \epsilon_j - E_{ij} > 0$, where $E_{ij} = e^2/r_{ij}$ is the Coulomb interaction energy of the

created electron-hole pair. Thus, the distance between the states has to obey $r_{ij} > 1/(\epsilon_i - \epsilon_j)$, and the mean 'volume per state' is $\mathcal{V}_0 \sim \bar{r}^{\,d} > |\epsilon|^{-d}$. Now, this admits for estimating the density of states at small energies,

$$\nu(\epsilon) \simeq \frac{1}{|\epsilon|\mathcal{V}_0} < \text{const.} \times |\epsilon|^{d-1}, \tag{3.10}$$

which implies that the DoS vanishes at the Fermi level.

In the delocalised regime, the DoS develops a singularity at the Fermi level. Due to the diffusive dynamics, the rearrangement of electrons is slow. Until the charge redistribution is achieved the system is in a classically forbidden state which causes the suppression of the tunnelling DoS at zero bias. This effect has been discussed first by Altshuler and Aronov [91, 92].

INFO: The change in the density of states, $\nu(\epsilon)$, can be related to the interaction self-energy $\Sigma_{\rm ee}(\mathbf{p}, i\epsilon_n)$ as [93]

$$\frac{\delta\nu(\epsilon)}{\nu} = -\frac{2}{\pi}\int d\xi_p\, \Im\left[\mathcal{G}_0^2(\mathbf{p}, i\epsilon_n)\Sigma_{\rm ee}(\mathbf{p}, i\epsilon_n)\right]_{i\epsilon_n\to\epsilon},$$

where $\mathcal{G}_0$ is the (Matsubara) Green function in the absence of interaction.

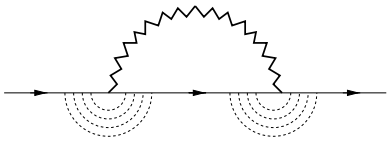

Figure 3.7.: Exchange contribution to $\Sigma_{\rm ee}$. Here the zigzag-line represents the effective Coulomb propagator, cf. 3.8.

Using the method introduced in Sec. 2.2, the dominant contribution to $\Sigma_{\rm ee}$ comes from the diagram shown in Fig. 3.7,

$$\Sigma_{\rm ee}(\mathbf{p}, i\epsilon_n) = \frac{1}{\beta}\sum_{\omega_m}\int d\mathbf{q}\; U_{\rm eff}(\mathbf{q}, i\omega_m)\,\frac{\mathcal{G}_0^2(\mathbf{p}, i\epsilon_n - i\omega_m)}{(Dq^2 + |\omega_m|)^2\tau^2}\,\theta(\epsilon_n(\omega_m - \epsilon_n)),$$

where $U_{\rm eff}$ is the effective interaction potential in the random phase approximation (RPA); cf. Fig. 3.8.

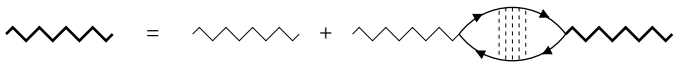

Figure 3.8.: Random phase approximation.

One obtains

$$\frac{\delta\nu_2(\epsilon)}{\nu} - \sim g^{-1}\ln\left(\frac{|\epsilon|}{D\kappa^2\tau}\right)\ln\left(|\epsilon|\tau\right), \qquad \frac{\delta\nu_3(\epsilon)}{\nu} \sim g^{-1}\sqrt{\frac{|\epsilon|}{E_{\rm Th}}}, \tag{3.11}$$

where $\kappa = 2\pi e^2\nu$ is the inverse screening length.

Thus, the DoS exhibits a logarithmic singularity in $2d$ and a square-root singularity in $3d$. Note that the suppression of the DoS by Coulomb interaction is small in the inverse dimensionless conductance $1/g$.

An extension of these results to the non-perturbative regime has been derived by Finkel'stein [94] within a replicated field theory and confirmed later by Kamenev and Andreev [66] using the Keldysh non-linear σ-model. In $2d$, the corresponding expression reads

$$\nu_2(\epsilon) = \nu \exp\Big[-\frac{1}{8\pi^2 g} \ln\left(\frac{|\epsilon|}{D\kappa^2\tau}\right) \ln\left(|\epsilon|\tau\right) \Big] \tag{3.12}$$

which reduces to the Altshuler-Aronov expression for $g \gg 1$.

4. Tunnelling spectroscopy

As correlation functions ($F^{[d;D;C]}$) are the key elements in *theoretical* investigations into mesoscopic systems, probing them *experimentally* is of great interest. Why do we need tunnelling spectroscopy with an *extended* probe as in double quantum well structures?

In a standard device-contact-electron system architecture, the continuous experimental spectroscopy of transport and spectral correlation functions proves to be difficult: First, the *fixed* attachment of local current/voltage electrodes prevents one from continuously monitoring the scale (r) dependence of transport correlation functions. This problem does not exist in measurements based on local tunnelling tips [95]. In those, however, the electronic state of the tunnelling device as well as its coupling to the electron system have to be precisely known to draw quantitatively reliable conclusions on the nature of the bulk electronic correlations of the latter. In particular, the distance between the device and the electron system has to be kept constant with atomic precision. These conditions can hardly be met under realistic conditions. Second, both local contacts and tunnelling tips tend to disturb the electron system under investigation. In interacting systems, they lead to various manifestations of the orthogonality catastrophe [96]: A localised perturbation in a Fermi system entails a modified ground state that is orthogonal to the ground state of the unperturbed system. As a consequence, much of the measured current/voltage characteristics describes the process of local accommodation of charge carriers at the interface, rather than the electronic correlations of the bulk system. Third, a division between system and contacts of a mesoscopic conductor is, to a large extent, arbitrary. Quantum interference phenomena in mesoscopic systems tend to be highly non-local in space, and often it is not clear, where the physical processes responsible for the outcome of an experiment took place, in the 'device', the 'contacts', or all over the place.

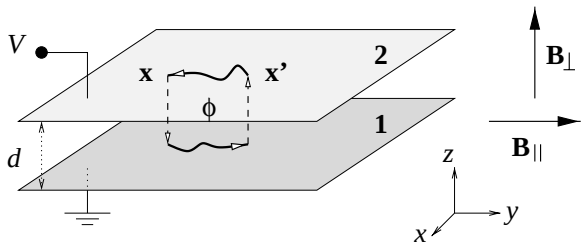

Figure 4.1.: Schematic setup with dominant process contributing to the tunnelling current indicated.

These difficulties can be overcome by using an extended system in a double well setup as a spectrometer. In fact, we will see below that detailed information on the correlation functions can be extracted from the tunnelling current fluctuations. Moreover, (i) the tunnelling takes place uniformly at all points of the layers which means that an averaging over spatially fluctuating structures (e.g. details of the microscopic wavefunction amplitudes) is intrinsic to the data contained in the current. (ii) Several parameters can be tuned to gain information: The

bias voltage resolves energetic correlations, a parallel magnetic field resolves spatial correlations, and a perpendicular magnetic field may serve as a control parameter for parametric correlations (i.e. correlations between Green functions evaluated at different values of external control parameters). (iii) The geometry of the layers can be designed freely, so that it is possible to study different regimes of particle dynamics (e.g. ergodic, ballistic, diffusive, etc.).

The setup is shown schematically in Fig. 4.1: Two electron systems confined in parallel wells separated by an isolating barrier of uniform thickness $d \sim 10 - 20$ nm form a double-layer system of two 2DEGs. A tunnelling current I from one layer to the other is driven by applying a voltage difference V between them. The tunnelling region is typically a few 100×100 μm^2 in extent. In the absence of any disorder scattering and/or tunnelling amplitude inhomogeneities, the tunnelling from one layer to the other can only occur if energy and momentum are conserved. This leads to the resonant behaviour of the tunnelling current that is characteristic of two-dimensional systems. More generally, for constrained geometries (e.g. quantum wire/two-dimensional electron system) the field dependence of these resonances can be analysed to obtain information on the dispersion of the fundamental excitations in the two systems [24].

However, in 'real' systems, inhomogeneities in the tunnelling barrier thickness, static disorder, and other non-momentum conserving imperfections will lead to modifications of the idealised resonant current profile. Of these intruding mechanisms, the first appears to be the most serious: the current will respond with exponential sensitivity to any fluctuations of the layer separation; for strong enough spatial variations one may run into a scenario, where tunnelling occurs only at a sparse set of 'hot spots', with no traces of a resonant profile left [97]. (Some characteristics of this type of current flow will be discussed below.) However, recent technological advances have made it possible to manufacture double well systems with near atomic monolayer precision. In such devices, fluctuations in the tunnelling matrix elements are reduced down to values of $\mathcal{O}(10\%)$ [98] and can be absorbed into a renormalisation of the effective in-plane disorder. In the present work, the focus will be on transport in these near-planar devices.

Even if the tunnelling is homogeneous, static disorder will broaden the resonant behaviour and introduce fluctuations. The broadening of the average current is related to the dynamics on short time scales [21]. In contrast, the fluctuations contain information about physical processes on much larger time scales [25, 26] of the order of, e.g., the diffusion time through the system. It is the purpose of this work to investigate the nature of these fluctuations and their relation to the aforementioned electronic correlation functions.

4.1. Theory of tunnelling currents

4.1.1. The current formula

Consider a double-layer system consisting of two parallel two-dimensional electron gases, labelled 1 and 2, respectively (see Fig. 4.1). We aim to analyse the tunnelling current I under conditions, where the tunnelling is weak (in a sense to be specified momentarily). After matching the electron densities in both layers by adjusting their chemical potential μ, the current becomes a function of bias voltage V, temperature T, and, optionally, a magnetic field $\mathbf{B}$.

Quantum-mechanically, the system can be represented in terms of a tunnelling Hamiltonian [99],

$$\mathcal{H} = \mathcal{H}_1 + \mathcal{H}_2 + \mathcal{H}_\mathcal{T}, \tag{4.1}$$

where $\mathcal{H}_1$ and $\mathcal{H}_2$ describe layer 1 and 2, respectively, while $\mathcal{H}_\mathcal{T}$ describes the transfer of electrons between the layers. Choosing a gauge where the bias voltage has been transferred to the tunnelling matrix elements, $\mathcal{H}_\mathcal{T}$ can be written as

$$\mathcal{H}_\mathcal{T} = \int d\mathbf{x}\, d\mathbf{x}' \left(\mathcal{T}_{\mathbf{x}\mathbf{x}'} e^{-iVt} {\psi^\dagger}_1(\mathbf{x}) \psi_2(\mathbf{x}') + \text{h.c.} \right), \tag{4.2}$$

where $\mathcal{T}_{\mathbf{x}\mathbf{x}'}$ is the tunnelling amplitude from $\mathbf{x}$ in layer 1 to $\mathbf{x}'$ in layer 2, and $\psi_j^\dagger$, ψ_j are electron creation and annihilation fields for layer $j = 1, 2$. The tunnelling current is defined as the rate of change of the number of particles N_j in one layer, say layer 2, multiplied by their charge, i.e.

$$I(t) = -e\dot{N}_2. \tag{4.3}$$

We are interested in the tunnelling current for the *weak tunnelling regime*. Here, 'weak' means that the typical energy scale associated with the tunnelling, $\Gamma_\mathcal{T} \propto |\mathcal{T}|^2$, is much smaller than the other relevant energy scales. In this regime, single-tunnelling events dominate whereas the amplitude for multiple-tunnelling processes is negligibly small. In principle, the effect of higher order tunnelling processes can systematically be taken into account. Within an approximation whereby higher order tunnelling is treated as an incoherent process this leads to the level smearing mentioned in the text (see also section 4.3 below). Due to the assumption, $V > \Gamma_\mathcal{T}$, a more complicated, coherent description is not necessary. Furthermore, since the tunnelling matrix elements $\mathcal{T}_{\mathbf{x}\mathbf{x}'}$ decrease exponentially (on atomic scales) as a function of $|\mathbf{x} - \mathbf{x}'|$ one can model $\mathcal{T}_{\mathbf{x}\mathbf{x}'}$ as a spatially local object, $\mathcal{T}_{\mathbf{x}\mathbf{x}'} = \mathcal{T}_\mathbf{x} \delta(\mathbf{x} - \mathbf{x}')$.

Although $\mathcal{H}_1, \mathcal{H}_2$ may contain intra-layer electron-electron (e-e) interactions, the Hamiltonian description of our system, Eq. (4.1), does, so far, not include any inter-layer interactions. Roughly speaking, e-e interaction effects can be divided into three groups: momentum transfer between the layers ('Coulomb drag'), charging effects associated with the tunnelling process, and self-energy corrections (due to inelastic scattering and dephasing). As for the Coulomb drag, the relevant time scale $\tau_{1\leftrightarrow 2}$ is much larger than the momentum relaxation τ within each layer (see Ref. [29]). However, charging effects will inevitably influence the tunnelling current at low bias; a quantitative discussion of these corrections is postponed until Sec. 4.1.2. Finally, we assume that our devices are highly phase coherent in the sense that the characteristic 'non-interacting' energy scales of the problem exceed the inverse dephasing and/or inelastic collision times by far (i.e. the system is in a 'mesoscopic regime').

All these assumptions understood, the tunnelling current reads [21, 100]

$$I(V, \mathbf{B}) = 2 \int d\mathbf{x}\, d\mathbf{x}' \int (d\epsilon^{[V]}) \mathcal{T}_\mathbf{x} \mathcal{T}^*_{\mathbf{x}'}\, e^{i\mathbf{q}_\text{B}(\mathbf{x}-\mathbf{x}')} A_1(\mathbf{x}, \mathbf{x}'; \epsilon, B_\perp) A_2(\mathbf{x}', \mathbf{x}; \epsilon - V, B_\perp), \tag{4.4}$$

with the abbreviation $\int (d\epsilon^{[V]}) = \int_{-\infty}^{\infty} \frac{d\epsilon}{2\pi} [n_\text{F}(\epsilon - V) - n_\text{F}(\epsilon)]$. Here $n_\text{F}(\epsilon) = (1 + e^{(\epsilon - \epsilon_\text{F})/T})^{-1}$ is the Fermi distribution function at temperature T and Fermi energy ϵ_F. The characteristic momentum scale set by the parallel field is

$$\mathbf{q}_\text{B} = d\mathbf{B}_\parallel \times \mathbf{e}_z,$$

where $\mathbf{e}_z$ is a unit vector perpendicular to the plane.

In Eq. (4.4) the quantities of main interest are the spectral functions A_j of layer j. The spectral functions depend on the bias voltage V applied to layer 2, and on the perpendicular magnetic field $B_\perp$. In fact, it will be our main objective to infer information on these objects *through* these parameter dependences. In this context, it is crucial to note that $\mathbf{B}_\parallel$ does not change

the dynamics within the individual layers, but merely weighs the tunnelling current with an Aharonov-Bohm type phase.[1] The sensitivity of the current to this flux will help to gain information about the long-range propagation within the layers. A caricature of the basic idea is depicted in Fig. 4.1. This figure illustrates the basic physical processes underlying the current flow as described by Eq. (4.4): An electron tunnels at point $\mathbf{x}$ from layer 2 to 1, leaving a hole behind. It propagates within that layer to point $\mathbf{x}'$, where it tunnels back to layer 2 and recombines with the hole. The in-plane magnetic field enters the formula via the flux through this electron-hole loop. Therefore, the in-plane magnetic field dependence of the tunnelling current contains information about the typical area enclosed in the loop which in turn is determined by the typical range of propagation within the layers. The condition of weak tunnelling is fulfilled, provided the typical time after which an electron tunnels is larger than the characteristic time scale that is to be resolved in the experiment.

To further simplify the analysis, note that under the conditions stated above the spectral functions themselves do not exhibit temperature dependence. (Temperature would enter through significant interaction corrections.) Under these conditions, a simple integral relation between currents at zero and finite temperatures holds:

$$I(T, \epsilon_{\mathrm{F}}) = -\int d\epsilon \left(\frac{\partial n_{\mathrm{F}}}{\partial \epsilon}\right) I(T = 0, \epsilon_{\mathrm{F}} = \epsilon). \tag{4.5}$$

In the following, unless stated otherwise, all results will be given for $T = 0$ only. The generalisation to finite temperature – essentially a smearing of the $T = 0$ results – obtains from Eq. (4.5).

Here we are primarily interested in the tunnelling current flowing between disordered systems. The microscopic properties of these systems will be described by some disorder distribution function about which three (idealising) assumptions an be made:

1.) The disorder potentials of the two layers are essentially uncorrelated.

2.) The e-e interaction and higher order tunnelling processes are not able to introduce significant inter-layer correlations in the motion of the charge carriers. Technically, this means that impurity averages can be taken for each layer independently.

3.) Disorder does not significantly affect the spatial homogeneity of the tunnelling, i.e. the tunnelling matrix elements do not depend on position, $\mathcal{T}_{\mathbf{x}} \equiv \mathcal{T}$.

All three conditions can be met experimentally: 1.) Correlations in the disorder potentials would become important if the impurities were placed between the 2DEGs – which, in a usual setup, is not the case. In principle, long-ranged fluctuations of the Coulomb potential due to remote impurity sites may be felt by both layers simultaneously. In practice, however, these potentials are strongly screened by the layers themselves which implies that no significant inter-layer correlation remains. (Notice that correlation effects become 'significant' once the amplitude of the correlated part of the scattering potential parametrically exceeds that of the uncorrelated potential.) 2.) Sizeable inter-layer Coulomb correlations may arise in very clean systems subject to strong perpendicular magnetic fields. In such systems, the e-e interaction can stabilise a fractional quantum Hall phase [101] and inter-layer e-e interactions lead to additional correlation phenomena (spontaneous coherence and quantum Hall ferromagnets [102]). In contrast, for

[1] As mentioned earlier, this is strictly true for the $2d$ system, corrections due to the finite width of the well are the subject of the following chapter.

strong enough disorder, the e-e interaction is less significant and, thus, the effective random potentials in each layer can be treated as statistically independent of each other. This assumption can be tested experimentally, as will be discussed below. Finally, 3.) the spatial homogeneity of the tunnelling is very sensitive to the thickness of the barrier. However, it is now possible to grow heterostructures with near atomic monolayer precision and, thus, achieve a tunnelling probability that is almost spatially constant [103, 104]: In high precision devices, the space dependent relative fluctuations in the tunnelling probability can be reduced to about ten percent and lower [98]. Furthermore, the validity of this assumption can be tested experimentally. In the extreme case, where tunnelling occurs only through tunnelling centres or 'pinholes' [97], the resonant behaviour of the tunnelling current disappears. If the spacing between pinholes exceeds the mean free path, the average current is just proportional to the product of the local densities of states, $\langle I\rangle \sim \nu_1\nu_2$, and, furthermore, becomes independent of magnetic field. In principle, a full (angle-resolved) analysis of the field-dependence of the current would allow one to extract information about the distribution of tunnelling centres [105]. However, further discussion of this type of 'tunnelling centre spectroscopy' is beyond the scope of this work.[2] Keeping in mind that the working assumption of near-homogeneous tunnelling can be put to experimental test, let us hereafter concentrate on the case $\mathcal{T}_{\mathbf{x}} \equiv \mathcal{T}$.

4.1.2. Average current

Under the assumptions formulated above the average current is given by

$$\langle I(V,\mathbf{B})\rangle = \frac{L^2}{\pi}\,|\mathcal{T}|^2 \int_0^V d\epsilon \int d\mathbf{x}\, e^{i\mathbf{q}_{\text{B}}\mathbf{x}} \langle A_1(\mathbf{x};\epsilon,B_\perp)\rangle\langle A_2(-\mathbf{x};\epsilon-V,B_\perp)\rangle. \tag{4.6}$$

The current, Eq. (4.6), is characterised by the averaged one-particle Green function $\langle {G^{\pm}}_j(\mathbf{x},\mathbf{x}';\epsilon)\rangle$. This quantity is short-ranged on a scale $l_{\min}$. For small perpendicular magnetic fields $B_\perp$, $l_{\min}$ is set by the mean free path[3] $\ell = v_{\text{F}}\tau$. (In cases, where the scattering times in the layers are different, one needs to generalise to τ_j, $j = 1, 2$.)

The average current has been studied theoretically [21] and experimentally [103, 104]. For vanishing magnetic fields, the theoretical result reads

$$\frac{\langle I(V,\mathbf{B}=0)\rangle}{V} = G_0 \frac{\Gamma^2}{(V+\delta\epsilon_{\text{F}})^2+\Gamma^2}, \tag{4.7}$$

where $\Gamma = \Gamma_1+\Gamma_2$. Here $\Gamma_j = 1/(2\tau_j)$ is the line-width of the Lorentzian shaped average spectral function in layer j, ν the single-particle level density of states per unit area, and

$$G_0 = \frac{2\nu|\mathcal{T}|^2}{\Gamma}L^2 \tag{4.8}$$

the characteristic low-bias average conductance of the system. Finally, $\delta\epsilon_{\text{F}}$ denotes a possible difference between Fermi energies of the two layers. For the average current, the condition of weak tunnelling is

$$\Gamma_{\mathcal{T}} < \Gamma, \tag{4.9}$$

[2] Note that, although significant inhomogeneities would largely obstruct the detection of transport correlations, they only have a minor effect on the analysis of *spectral* correlations.

[3] In contrast to many other transport characteristics of electronic systems, the average tunnelling current is related to the mean free path ℓ and *not* the transport mean free path ℓ_{tr}. In systems with small angle scattering events, the latter can exceed ℓ by an order of magnitude.

where $\Gamma_{\mathcal{T}} \equiv |\mathcal{T}|^2/\Gamma$ is the inverse of the (golden rule) rate at which a particle propagating in one layer tunnels to the other (cf. appendix B.2). Henceforth we will focus on the regime of small bias voltage $V \ll \Gamma$ and not take the possibility of an externally induced Fermi energy mismatch into account. Under these conditions, $\langle I(V, \mathbf{B} = 0)\rangle/V \approx G_0$. In the presence of a moderately weak in-plane magnetic field ($|\mathbf{q}_{\mathrm{B}}|^{-1} \gg \lambda_{\mathrm{F}}$), this generalises to

$$\frac{\langle I(V,\mathbf{B})\rangle}{V} = G_0 f(|\mathbf{q}_{\mathrm{B}}|\ell), \tag{4.10}$$

where the scaling function f exhibits the asymptotic behaviour $f(x \ll 1) = 1 + \mathcal{O}(x^2)$ and $f(x \gg 1) \sim x^{-1}$ [21, 25]. In the following, let us concentrate on the weak field regime, $|\mathbf{q}_{\mathrm{B}}|\ell \ll 1 \Rightarrow f \approx 1$.

Before moving on to the main issue, mesoscopic fluctuations of $I(V, \mathbf{B})$, here a few more remarks on the average current – in order to argue that, from the known behaviour of $\langle I\rangle$, conclusions on the validity of some of the assumptions made above can be drawn. In [103, 104] the influence of a perpendicular magnetic field on the average current between high mobility samples was investigated. It was found that strong fields lead to a suppression of the differential tunnelling conductance, $G_{\mathcal{T}} \equiv \partial I/\partial V$, at zero bias. This phenomenon is called the 'tunnelling-gap'. The splitting of the conductance peak at $V = 0$, characterised by some field dependent gap-energy, $\Delta(B)$, is due to the Coulomb interaction within and between the layers. As shown theoretically in [106] and confirmed experimentally in [103, 104], the total current flowing at the split-peaks (positioned at $V = \pm\Delta$) equals the peak current at $V = 0$ in the absence of interactions. This observation implies that interactions in these experiments largely manifest themselves in the form of self-energy corrections to the single-particle poles. In contrast, if strong inter-layer correlation effects were present, the peak current would increase. Indeed, for strong inter-layer correlations, the momenta of the particle and the hole constituting the 'current-loop' would be partially correlated. This should lead to a gradual resurrection of the resonant behaviour characteristic for the clean case and, therefore, to an un-split zero-bias conductance peak.

4.1.3. Fluctuations

We next turn our attention to the fluctuations of the tunnelling current. As a starting point serves the formula

$$I(V,\mathbf{B}) \;=\; \frac{1}{\pi}\,|\mathcal{T}|^2 \int d\mathbf{x}\, d\mathbf{x}' \int_{\epsilon_{\mathrm{F}}}^{\epsilon_{\mathrm{F}}+V} d\epsilon\, e^{i\mathbf{q}_{\mathrm{B}}(\mathbf{x}-\mathbf{x}')} A_1(\mathbf{x},\mathbf{x}';\epsilon,B_\perp)\, A_2(\mathbf{x}',\mathbf{x};\epsilon-V,B_\perp) \tag{4.11}$$

for the zero-temperature current at uniform tunnelling probability. As we are interested in correlations on large time scales, Eq. (4.9) for the range of applicability of the weak tunnelling approximation has to be replaced by the more restrictive condition

$$\Gamma_{\mathcal{T}} < \max\left(\tau_\phi^{-1}, V, v_{\mathrm{F}}|\mathbf{q}_{\mathrm{B}}|\right), \tag{4.12}$$

where τ_ϕ is the phase coherence time and $v_{\mathrm{F}}|\mathbf{q}_{\mathrm{B}}|$ the characteristic energy scale set by the parallel magnetic field. This inequality states that the probability for an electron to tunnel, while moving coherently within one layer, is low.

To describe fluctuations of the current and related quantities, it is convenient to consider correlation functions of the type

$$C_X(z,z') \equiv \frac{\langle X(z)X(z')\rangle_c}{\langle X\rangle^2}, \tag{4.13}$$

where X is an observable, $\langle AB\rangle_c \equiv \langle AB\rangle - \langle A\rangle\langle B\rangle$, and $z^{(\prime)}$ represents the set of parameters $\{V^{(\prime)}, \mathbf{B}^{(\prime)}, \epsilon_{\rm F}^{(\prime)}\}$. The suppression of the parameter dependence in the normalisation denominator indicates that, on the z-scales relevant for the structure of fluctuations, the parameter dependence of the averaged observables is negligibly weak.[4]

In most of the following, we will concentrate on the correlation function C_G of the differential conductance $G_{\mathcal{T}}$. This quantity is a) experimentally more relevant than the current correlation function C_I and b) tends to exhibit more pronounced structure. Indeed, it is straightforward to show that the current and the conductance correlation function, respectively, are related through

$$C_I(V) = \frac{2}{V^2}\int_0^V d\omega\,(V-\omega)\,C_G(\omega), \tag{4.14}$$

i.e. C_I is obtained from C_G through an integral average.

Averaging (the square of) Eq. (4.11) over disorder, one verifies that

$$\begin{aligned} C_G(\omega,\mathbf{B},\mathbf{B}') &= \frac{1}{G_0^2}\langle G_{\mathcal{T}}(V;\mathbf{B})G_{\mathcal{T}}(V';\mathbf{B}')\rangle = \\ &= \frac{4|\mathcal{T}|^4}{\pi^2 G_0^2}\int\prod_{n=1}^{4} d\mathbf{x}_n\, e^{i\mathbf{q}_{\rm B}(\mathbf{x}_1-\mathbf{x}_2)+i\mathbf{q}_{\rm B'}(\mathbf{x}_3-\mathbf{x}_4)}\times \\ &\quad\times \Re F_1(\mathbf{x}_1,\mathbf{x}_2,\mathbf{x}_3,\mathbf{x}_4;\alpha)\,\Re F_2(\mathbf{x}_2,\mathbf{x}_1,\mathbf{x}_4,\mathbf{x}_3;\alpha), \end{aligned} \tag{4.15}$$

where $G_0 = \langle G_{\mathcal{T}}\rangle$ as discussed in the previous section and $\alpha = \{\omega, B_\perp, B'_\perp\}$ with $\omega = V - V'$. The objects

$$F_{1/2}(\mathbf{x}_1,\mathbf{x}_2,\mathbf{x}_3,\mathbf{x}_4;\alpha) = \langle G^-_{1/2}(\mathbf{x}_1,\mathbf{x}_2;\epsilon,B_\perp)G^+_{1/2}(\mathbf{x}_3,\mathbf{x}_4;\epsilon+\omega,B'_\perp)\rangle$$

are the basic two-particle correlation functions discussed in the introduction. The fact that Eq. (4.15) contains the product of two of these correlators is a direct consequence of our assumption of negligible inter-layer disorder correlations. Notice that while the correlation functions F of non-interacting systems categorically depend only on the energy difference between the two Green functions, the dependence on the perpendicular fields can be more complicated.

The four-fold integration over the coordinates $\mathbf{x}_i$ implies that all three contributions discussed above, density-density $F^{[d]}$, diffuson $F^{[D]}$, and Cooperon $F^{[C]}$, contribute to Eq. (4.15) (see Fig. 2.4). At this stage, the role of the weak in-plane magnetic field becomes clear. As discussed above, the correlators $F^{[d;D;C]}$ are long-ranged (as compared to the microscopic spatial extent of the average Green functions contributing to $\langle I\rangle$). This means that Eq. (4.15) is field sensitive – through the magnetic wavevector – on *small* magnetic field scales. The characteristic field strength is determined through $|\mathbf{q}_{\rm B}| = dB_\parallel \sim L_\omega^{-1}$, where L_ω is the typical distance a particle propagates during time ω^{-1}. E.g. for a medium characterised by diffusive motion with diffusion constant D, $L_\omega \sim (D/\omega)^{1/2}$. Using that for the three fundamental correlators the coordinates are pairwise equal (with an accuracy of $\mathcal{O}(l_{\rm min})$) and neglecting factors $\sim |\mathbf{q}_{\rm B}|l_{\rm min} \ll 1$, Eq. (4.15)

[4] To avoid confusion, let us reiterate that here angular brackets stand for averaging over an external set of parameters, *not* for a quantum-mechanical average. E.g. in the discussion below, $X(z) \equiv G_{\mathcal{T}}(V,\mathbf{B})$ may stand for the conductance measured at a certain field/voltage configuration. The subsequent $\langle\dots\rangle$-average will then be over configurational fluctuations.

assumes the form

$$C_G(\omega,\mathbf{B},\mathbf{B}') = \left(\frac{8\pi\ell^2|\mathcal{T}|^2}{gG_0}\right)^2 \int d\mathbf{x}\, d\mathbf{x}' \Big(\Re F_1^{[d]}(\mathbf{x},\mathbf{x}';\alpha)\,\Re F_2^{[d]}(\mathbf{x}',\mathbf{x};\alpha) + \times\Big(e^{i(\mathbf{q}_B-\mathbf{q}_{B'})(\mathbf{x}-\mathbf{x}')}\,\Re F_1^{[D]}(\mathbf{x},\mathbf{x}';\alpha)\,\Re F_2^{[D]}(\mathbf{x}',\mathbf{x};\alpha) + + e^{i(\mathbf{q}_B+\mathbf{q}_{B'})(\mathbf{x}-\mathbf{x}')}\,\Re F_1^{[C]}(\mathbf{x},\mathbf{x}';\alpha)\,\Re F_2^{[C]}(\mathbf{x}',\mathbf{x};\alpha)\Big), \tag{4.16}$$

where $g = 2\pi D\nu$ is the dimensionless conductance.

Eq. (4.16) states that the diffuson contribution $F^{[D]}$ couples to the difference, $\mathbf{B}_\parallel^- \equiv \mathbf{B}_\parallel - \mathbf{B}'_\parallel$, of the two in-plane field vectors, the Cooperon contribution $F^{[C]}$ to the sum, $\mathbf{B}_\parallel^+ \equiv \mathbf{B}_\parallel + \mathbf{B}'_\parallel$, whereas the density-density contribution $F^{[d]}$ is $\mathbf{B}_\parallel$-insensitive. (Later on we will see how information on $F^{[d]}$ can be extracted from the dependence on the bias voltage and/or the perpendicular field $B_\perp$.) Note that Eq. (4.16) holds true for extended systems, where the unconstrained integration over x, x' implies momentum conservation, as well as for restricted systems, where the in-plane momentum is not conserved in tunnelling.

Finally, if both systems are extended, Fourier transforming Eq. (4.16) in the magnetic field yields

$$\Re F_1^{[D]}(\Delta\mathbf{x};\alpha)\,\Re F_2^{[D]}(-\Delta\mathbf{x};\alpha) = \left(\frac{\nu^2 dL}{8\pi}\right)^2 \int d^2B_\parallel^+ e^{-id(\Delta\mathbf{x}\times\mathbf{B}_\parallel^+)_z} C_G(\omega,\mathbf{B}^+,\mathbf{B}^-), \tag{4.17}$$

$$\Re F_1^{[C]}(\Delta\mathbf{x};\alpha)\,\Re F_2^{[C]}(-\Delta\mathbf{x};\alpha) = \left(\frac{\nu^2 dL}{8\pi}\right)^2 \int d^2B_\parallel^- e^{-id(\Delta\mathbf{x}\times\mathbf{B}_\parallel^-)_z} C_G(\omega,\mathbf{B}^+,\mathbf{B}^-), \tag{4.18}$$

where $\Delta\mathbf{x}$ is the difference between the two spatial arguments of the correlation functions F, and $\mathbf{q}_B\mathbf{x} = d(\mathbf{x}\times\mathbf{B}_\parallel)_z$ as well as the result (4.7) for G_0 have been used.

Eqs. (4.17,4.18) contain a central message: Detailed spectral and spatial information on the correlation functions F can be obtained from the dependence of the tunnelling current on a parallel magnetic field. (In contrast to contact measurements,) the current approach to exploring correlation functions enables one to continuously measure spatial scale dependences and does not incorporate strong local perturbations. If one of the layers is a finite quantum dot, Eq. (4.16) still gives the general relation between the current fluctuations and the spectral correlation functions. In the next two sections, we will discuss applications of this general concept to some concrete problems.

4.2. Anomalous diffusion

In this section, Eqs. (4.17,4.18) will be applied to (anomalous) diffusion in spatially extended structures. We first note that for the limiting cases of purely ballistic and diffusive dynamics, the correlation functions $F^{[D;C]}$ can be calculated explicitly. For ballistic systems, a straightforward integration over the momenta of the single-particle Green functions obtains

$$\Re\left[F^{[D;C]}(r;\omega)\right] \sim \frac{\nu}{v_F r}\cos\frac{\omega r}{v_F}. \tag{4.19}$$

For diffusive systems, leading order diagrammatic perturbation theory (one diffuson/Cooperon approximation) leads to

$$\Re\left[F^{[D;C]}(r;\omega)\right] \sim \frac{\nu^2}{g}\mathrm{ker}\left(\frac{r}{L_\omega}\right) + \dots, \tag{4.20}$$

where $\ker(x)$ is the Thomson function [107]. For small x, this function can be approximated as $\ker(x) \approx -\mathrm{C} - \ln(x/2)$ ($\mathrm{C} \approx 0.58$ Euler's constant). The ellipses stand for weak localisation type contributions of higher order in the number of diffusons and Cooperons. These corrections scale with negative powers of the dimensionless conductance g. By definition, a system will be denoted as 'diffusive' if $g \gg 1$ and weak localisation does not play a significant role.

To get some idea about the strength of the tunnelling current fluctuations let us briefly discuss the $\mathbf{B} = 0$ current correlation function $C_I(V)$ for two different setups: a) two disordered layers and b) only one disordered layer and one 'clean' layer. Here 'clean' means that ℓ exceeds the system size L. Substituting Eqs. (4.19) and (4.20) into (4.15) and integrating over frequencies one finds in case a)

$$C_I(V) = g^{-2} \frac{E_{\mathrm{Th}}}{V} \left(c^{[d]} + 2c^{[D]} \ln(V/E_{\mathrm{Th}}) \right), \tag{4.21}$$

where $E_{\mathrm{Th}} = g\delta$ is the Thouless energy. Eq. (4.21) has been derived under the assumption $V > E_{\mathrm{Th}}$. Physically, this means that on time scales $t \sim V^{-1}$, the charge carriers do not have enough time to diffusively explore the entire system area. For smaller voltages, a crossover to an ergodic regime, discussed in the next section, takes place. The two numerical coefficients $c^{[d]} = 9/(8\pi)$ and $c^{[D]} = 1/(4\pi)$ determine the strength of the density-density and diffuson contribution, respectively. The factor of two multiplying $c^{[D]}$ expresses the fact that in the field free case, the diffuson and Cooperon contribution are equal and add. For case b), the expression looks similar, however instead of the logarithm a factor $\sqrt{V/\Gamma}$ appears. This means that in the regime of interest, $V \ll \Gamma$, the current fluctuations between a clean and a disordered layer are largely due to fluctuations in the density of states. This result can easily be understood qualitatively: In a clean system, the charge carriers move much faster than in a disordered system. As a result, the particles propagating in the disordered system do not have enough time to diffusively travel over large distances. This in turn implies that the diffuson and Cooperon contribution to the correlator are reduced by a phase space reduction factor. By contrast, the density-density contribution, involving only Green functions taken at coinciding points (within the clean system), remains unaffected. Actually, the density-density contribution to the current correlation is proportional to the variance of the number of levels in an energy window V. This is very similar to the conductance fluctuations in conventional transport, which are related to the level number variance in an energy window of the size of E_{Th}. For completeness, we mention that for case b) $c^{[d]} = 4/\pi$ and $c^{[D]} = 16/(3\pi)$. Note that the conductance is self averaging ($\sim L^{-2}$) in the thermodynamic limit. Furthermore, the fluctuations are suppressed by a factor g^{-2}. This is a phase space reduction factor expressing the fact that to obtain averaging-insensitive contributions, two of the four spatial arguments of the correlation function F must be close to each other on scales ℓ, cf. Eq. (4.16). Finally, notice that already weak *perpendicular* magnetic fields of $\mathcal{O}(1/\Delta x^2)$, where Δx^2 is the characteristic area of extent of $F^{[C]}$, suffice to suppress the Cooperon contribution. This means that the dependence of the current fluctuations on a perpendicular field can be used to determine the maximum range of the correlation functions at frequencies $\omega \sim V$. For $V < \tau_\phi^{-1}$, this scale is set by the dephasing length, L_ϕ. In analogy to the classical experiments by Bergmann [60], the field dependence of the current for these low voltages can be used to estimate L_ϕ.

What can be said about systems with more complex types of dynamics, i.e. systems where localisation and/or interaction corrections play some role? In principle, both weak localisation and interaction corrections can be taken into account perturbatively, where the inverse of the dimensionless conductance, g^{-1}, represents the expansion parameter [108]. As g is lowered, these non-diffusive corrections become stronger and eventually, for $g = \mathcal{O}(1)$, the perturbative

description breaks down. However, relying on concepts of scaling theory, it is still possible to make some general statements about the behaviour of the strongly disordered electron gas: For $g \sim 1$, localisation phenomena begin to qualitatively affect the dynamics. According to the one-parameter scaling theory [109], the weakly interacting electron gas eventually flows into a localised regime provided that (a) spin-orbit scattering is negligible and (b) no strong perpendicular magnetic fields are present. In contrast, systems with significant spin-orbit scattering, are expected to exhibit a true metal-insulator transition at some critical value $g_c \sim \mathcal{O}(1)$ [110]; $2d$ electrons (interacting as well as non-interacting) subject to strong magnetic fields undergo a metal-insulator transition responsible for the quantum Hall effect [111]. Finally, in a number of experiments on $2d$ electrons with strong interaction parameter $r_s > 1$, transport behaviour has been observed that resembles a metal-insulator transition [112], too.

In all these phenomena (except, perhaps, the not sufficiently well understood transport phenomena discussed in Ref. [112]) the concept of 'anomalous diffusion' plays a key role [113]. Prior to the onset of strong localisation, the electron dynamics undergoes a crossover from ordinary diffusive ($g \gg 1$) to anomalously diffusive ($g \sim 1$). Quite generally, the correlation function of anomalously diffusive electrons has the scaling form

$$F^{[D]}(r,\omega) \sim \left(\frac{r}{L_\omega}\right)^{-\eta} e^{-2r/\xi}, \tag{4.22}$$

where ξ is the localisation length and η a characteristic exponent related to the multifractal nature of states that are neither regularly extended nor fully localised [7]. The length L_ω is related to the energy ω by the so-called *dynamical exponent* z,

$$L_\omega \sim \omega^{-1/z}. \tag{4.23}$$

Whereas for non-interacting systems $z = 2$ as in ordinary diffusive systems, the value of z for interacting systems is controversial [114]. In systems with a true localisation-delocalisation transition, the localisation length diverges with a characteristic exponent ν upon approaching the transition point. In Eq. (4.22), it has been assumed that ξ is smaller than L_ω. In the opposite case, L_ω would be the scale of exponential decay of the correlation function.

According to Eq. (4.22), the 'non-diffusivity' of the electron dynamics can be characterised in terms of the three exponents z, ν, and η. To obtain these quantities one needs to know both the spatial and the energetic profile of the correlation function. In fact, the aforementioned difficulty to continuously monitor the spatial structure of electronic correlations has prevented previous experiments from determining the exponent η. In contrast, the basic relations (4.17,4.18) do, at least in principle, contain all the information needed to extract all exponents of anomalous diffusion. In the following, we shall try to assess whether this approach might work *in practice*.

One aspect counteracting the application of the current approach to the analysis of anomalous diffusion is that to date semiconductor devices tend to be 'too clean': In state-of-the-art high-mobility samples, the mean free path is of the same order as the low-temperature phase coherence length, roughly about 10 μm. In such devices, the phase coherent electron transport is ballistic and not even conventionally diffusive. We, thus, need to consider low-mobility devices, where the disorder concentration is increased either by doping or by lowering the separation between the 2DEG and the donor impurities. We expect that by artificially increasing the disorder, an order of magnitude separation between ℓ and L_ϕ might be attainable [115]. Second, to observe significant deviations from standard diffusion, one needs to be in a regime of a low global conductance g. In low-mobility systems showing integer quantum Hall transitions (when placed in strong perpendicular magnetic fields), the typical Coulomb energy is low as compared to the

disorder energy scale. In such systems, the conductance g is of order unity in the transition regimes, and anomalous diffusion could be observed by our method.

4.3. Spectral correlations

Tunnelling spectroscopy of double-layer systems does not only provide information on extended 2DEGs [25, 26], where the field dependence of the tunnelling current admits for investigating the spatial structure of correlation functions. A somewhat modified setup can be used to study spectral properties or parametric correlations in quantum dots through the tunnelling current statistics. Now, the system under investigation is a layered structure of a chaotic QD, defined by gates, and a clean (extended) 2DEG. By studying the autocorrelation of the tunnelling current between the two layers as a function of applied voltage V and *perpendicular* magnetic field difference $\Delta B_\perp$, one obtains information on spectral properties and parametric correlations of the QD. Again the parallel field acts as a tool to distinguish different contributions to the current/conductance fluctuations.

Note that a similar situation has already been studied experimentally by Sivan et al. [27], where a single level served as a spectrometer for a thick QD. A short discussion of their results and the differences to the proposed setup follows below.

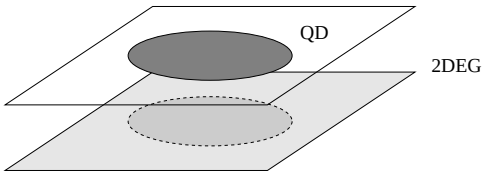

Figure 4.2.: Setup for investigating spectral and parametric correlations: QD – 2DEG.

In the finite size setup under consideration, Coulomb charging effects are likely to play some role and, therefore, have to be considered. However, in contrast to other QD systems, here these obscuring effects are comparatively small as will be discussed below. Furthermore, it will be argued that the impact of interactions on the current fluctuations sensitively depends on the parameter regime. For didactic reasons, we will begin by discussing the idealised non-interacting situation in subsection 4.3.2. Coulomb corrections will then be considered in subsection 4.3.3.

4.3.1. Modelling of the quantum dot

We are interested in the behaviour of a chaotic quantum dot on time scales, where the electron dynamics is ergodic – a 'zero-dimensional' system in the standard terminology of mesoscopic physics. For a diffusive system, the time to establish ergodic dynamics is set by the inverse Thouless energy, E_{Th}^{-1}. For nearly clean quantum dots, the ergodicity time depends on the boundary scattering potential.

As mentioned earlier, an appropriate method for modelling such systems is random matrix theory. For simplicity, let us assume that the magnetic field is sufficiently strong to break time-reversal invariance, while, on the other hand, it is still too weak to significantly affect the ballistic dynamics of the charge carriers, i.e. $R_c \gg \min(L, \ell)$. Then, the system can be described within RMT by a random $N \times N$ matrix Hamiltonian $\mathcal{H}_{\mathrm{GUE}}$ drawn from the Gaussian Unitary

Ensemble (GUE), cf. Sec. 2.4. In addition, a possible magnetic field difference is modelled by the following Ansatz:

$$\mathcal{H}_{\mu\nu} = \mathcal{H}^{\mathrm{GUE}}_{\mu\nu} + i\Phi_{\mu\nu}, \tag{4.24}$$

where Φ is an anti-symmetric ($\Phi = -\Phi^T$), constant matrix.[5]

The matrix indices $\mu, \nu = 1, \ldots, N$ can, roughly, be interpreted as discretised spatial coordinates. Thus, the (spatial) correlation functions $F(\mathbf{r}_1, \mathbf{r}_2, \mathbf{r}_3, \mathbf{r}_4)$ have to be replaced by their discretised version,

$$F_{\mu\nu\mu'\nu'} \quad \equiv \quad \langle G^-_{\mu\nu} G^+_{\mu'\nu'} \rangle_{\mathrm{GUE}}.$$

The derivation of these correlation functions can be found in the literature [28]. The main steps are summarised in appendix B.1 while here we only state the results.

As time-reversal symmetry is broken by the magnetic field, the Cooperon contribution vanishes. Therefore, the correlations are composed as a sum of two contributions,

$$F_{\mu\nu\mu'\nu'} \sim F^{[d]} \delta_{\mu\nu}\delta_{\mu'\nu'} + F^{[D]} \delta_{\mu\nu'}\delta_{\nu\mu'}. \tag{4.25}$$

$F^{[d]}$ and $F^{[D]}$ are dimensionless functions of the variables s and b, measuring the 'mismatch' of the two Green functions. To be specific, $s = \pi\omega/\delta$. The other parameter, $b \sim (N\delta)^{-2}\,\mathrm{tr}\,(\Phi^2)$, describes the field difference. As shown in Ref. [28], this parameter can unambiguously be related to the magnetic field threading the dot. Comparison of the RMT σ-model and its microscopic counterpart leads to the identification,

$$2b = \pi^2 C_\phi\, \phi^2,$$

where $C_\phi = \delta^{-2}\langle(\frac{\partial\epsilon_n}{\partial\phi})^2\rangle$ describes the sensitivity of levels to the applied field, and $\phi = \Delta B_\perp L^2$ is the magnetic flux threading the dot. For a disordered system, C_ϕ is proportional to the conductance g.

The two functions $F^{[d;D]}$ are given by the following integral expressions,

$$F^{[d]}(s;b) \;=\; \frac{1}{2b}\int_0^\infty \frac{d\lambda}{\lambda}\, e^{is^+\lambda}\left[e^{-b\lambda|\lambda-2|} - e^{-b\lambda(\lambda+2)}\right], \tag{4.26}$$

$$F^{[D]}(s;b) \;=\; \frac{1}{2b^2}\int_0^\infty \frac{d\lambda}{\lambda^3}\, e^{is^+\lambda}\left[(b\lambda|\lambda-2|+1)\, e^{-b\lambda|\lambda-2|} - (b\lambda(\lambda+2)+1)\, e^{-b\lambda(\lambda+2)}\right], \tag{4.27}$$

where $s^+ = s + i0$.

Note that the $F^{[d]}$ and $F^{[D]}$ are related by the equality [117]

$$\frac{\partial}{\partial b} F^{[d]}(s;b) = \frac{\partial^2}{\partial s^2} F^{[D]}(s;b). \tag{4.28}$$

In the limit of large magnetic fields, $b \gg 1$, one recovers the perturbative result,

$$F^{[d]}(s; b\gg 1) = \frac{1}{(2b - is^+)^2}, \qquad F^{[D]}(s; b\gg 1) = \frac{2}{2b - is^+}.$$

[5] Alternatively, one could model this part by another random Hamiltonian; this does not change the result qualitatively [116].

At small magnetic fields, however, the correlation functions $F^{[d;D]}$ are non-perturbative. One obtains

$$\begin{aligned} F^{[d]}(s;b) &= 2i\,\frac{\sin s^+}{s^{+\,2}}\,e^{is^+} + \frac{4ib}{s^{+\,3}} + \mathcal{O}(b^2), \\ F^{[D]}(s;b) &= \frac{2i}{s^+} + \frac{4b}{s^{+\,2}}(1 + i\frac{\sin s^{+\,2}}{s^{+\,2}}\,e^{is^+}) + \mathcal{O}(b^2). \end{aligned}$$

As pointed out in Sec. 3.4, the density-density correlator $F^{[d]}(s, b = 0)$ is related to the two-level correlation function $R_2^u(s) = -(\sin s/s)^2$ through $\Re F^{[d]} = \pi\delta(s) - R_2^u(s)$ (the index 'u' standing for unitary). Similarly, the real part of the zero-field diffuson correlation function is given by $\Re F^{[D]}(s, b = 0) = \pi\delta(s)$ (where the δ-type dependence on s follows from the condition of particle number conservation). It is straightforward to generalise the $\Delta B_\perp = 0$ result to the orthogonal case by replacing $R_2^u(s)$ in $F^{[d]}$ by the corresponding function $R_2^o(s)$ and multiplying the diffuson contribution by a factor of 2 ($F^{[C]} = F^{[D]}$ at $B_\perp = 0$).

Note that the $s = 0$ singularity displayed by the two correlation functions is of no relevance for our theory. For small s, the finite level width is essential, i.e. $s^+ \to s + i\gamma$, where $\gamma = \pi\Gamma_{\mathcal{T}}/\delta$. The level broadening $\Gamma_{\mathcal{T}}$ due to the tunnel coupling to the 2DEG is calculated in appendix B.2. In principle, the σ-model description can consistently be extended to include the effect of *coherent* multiple tunnelling. The resulting theory, however, would be significantly more complicated than the present formalism and we will not discuss it any further (thereby paying the price that the very-low-voltage regime remains out of reach).

Having found the proper correlation functions for the QD, one may proceed by evaluating the tunnelling current/conductance with the help of these expressions.

4.3.2. Non-interacting system

Let us start by briefly discussing the average current. To be specific, one assumes – a condition easily met experimentally – that the electron dynamics on scales L is ballistic. As mentioned earlier the average current is governed by processes on rather short time scales. On these time scales the dynamics of the QD is not ergodic, yet. I.e. the system cannot be considered as zero-dimensional and the RMT description does not apply. Instead, using Eq. (4.6), the 'clean' spectral functions $A_i^{(0)}$ have to be integrated over the finite area of the dot. This amounts to replacing in Eq. (4.8) the scale Γ by its equivalent for a clean but finite system namely $\Gamma^{(\mathrm{b})} \sim v_{\mathrm{F}}/L$, where the superscript '(b)' stands for ballistic. Thus, at small voltages $V \ll \Gamma^{(\mathrm{b})}$,

$$\langle I \rangle = \frac{2|\mathcal{T}|^2}{\Gamma^{(\mathrm{b})}\delta} V. \tag{4.29}$$

Turning to the fluctuations, within the RMT description, space type matrix elements will be represented as $L^2 A(\mathbf{x}, \mathbf{x}') \to N A_{\mu\nu}$ and the integration over the coordinates of the upper system becomes a matrix trace, $L^{-2}\int d^2x \to N^{-1}\sum_\mu$. On the other hand, the dynamics in the 2DEG spectrometer underneath is integrable-ballistic implying that, as before, it has to be described in terms of the microscopic Hamiltonian of the two-dimensional electron gas. This type of hybrid modelling, involving RMT in combination with a microscopic Hamiltonian, does not pose any conceptual problems. In the basic formula (4.15), quantities assigned to the upper system will be described through their RMT representations whereas the correlation functions of the lower system are given by the ballistic expression (4.19). Notice that none of the functions $F^{[d;D]}$ actually depends on the coordinate arguments – due to the ergodic zero-dimensional nature of

the dot – which is why no conflicts arise from the simultaneous appearance of RMT and truly space dependent correlation functions.

INFO: Keeping this in mind, the tunnelling conductance correlator, Eq. (4.15), can be rewritten in a discrete version (in the absence of a parallel magnetic field, $\mathbf{q}_{\text{B}} = \mathbf{q}_{\text{B}'} = 0$)

$$C_G(V;\Delta B_\perp) \sim \sum_{\mu\nu,\mu'\nu'} \langle A_1^{\mu\nu}(\epsilon;B_\perp) A_1^{\mu'\nu'}(\epsilon';B'_\perp)\rangle_c \, A_2^{\nu\mu}(\epsilon+V;B_\perp) A_2^{\nu'\mu'}(\epsilon'+V;B'_\perp),$$

where $\Delta B_\perp = B'_\perp - B_\perp$. Making use of the properties of RMT correlation functions found in section 4.3.1, one obtains

$$\begin{aligned}
\sum_{\mu\nu,\mu'\nu'} \langle A_1^{\mu\nu} A_1^{\mu'\nu'}\rangle_c \, A_2^{\nu\mu} A_2^{\nu'\mu'} &= 2\sum_{\mu\nu} \left[\Re\langle G_1^{+\,\mu\mu} G_1^{-\,\nu\nu}\rangle_c \, A_2^{\mu\mu} A_2^{\nu\nu} + \Re\langle G_1^{+\,\mu\nu} G_1^{-\,\nu\mu}\rangle_c \, A_2^{\nu\mu} A_2^{\mu\nu}\right] \qquad (4.30)\\
&= 2\left(\frac{\pi}{N\delta}\right)^2 \Big(\Re[F^{[d]}] \big(\underbrace{\sum_{\mu} A_2^{\mu\mu}}_{=2\pi L^2\nu}\big)^2 + \Re[F^{[D]}] \underbrace{\sum_{\mu\nu} A_2^{\nu\mu} A_2^{\mu\nu}}_{\approx 2\pi L^2\nu/\Gamma^{(\text{b})}}\Big)\\
&= 8\pi^4 (\frac{L^2\nu}{\delta})^2 N^{-2} \Big(\Re[F^{[d]}] + \frac{\delta}{2\pi\Gamma^{(\text{b})}}\Re[F^{[D]}]\Big).
\end{aligned}$$

Thus, in the ergodic regime, the conductance autocorrelations are given by

$$C_G(V,\Delta B) = 2\left(\frac{\Gamma^{(\text{b})}}{\epsilon_{\text{F}}}\right)^2 \left(\Re[F^{[d]}] + \frac{\delta}{2\pi\Gamma^{(\text{b})}}\Re[F^{[D]}]\right). \qquad (4.31)$$

The global suppression factor $(\Gamma^{(\text{b})}/\epsilon_{\text{F}})^2 \sim (k_{\text{F}}L)^{-2}$ stems from the fact that an averaging over the area of the QD is intrinsic to the setup. The further suppression factor $\delta/\Gamma^{(\text{b})} \sim (k_{\text{F}}L)^{-1}$ multiplying the diffuson contribution results from the integration over the Green functions of the lower 2DEG. Unlike the density-density contribution, $F^{[D]}$ is weighted by Green functions taken at different coordinates. Integration over these arguments leads to the k_{F}-dependent suppression.

According to Eq. (4.31), the fluctuations of the tunnelling conductance are linearly related to the sum of two ergodic correlation functions $F^{[d]}$ and – multiplied by a small constant – $F^{[D]}$. These are precisely the objects which have been discussed above in Sec. 4.3.1. Thus, analysing the parameter dependence of the tunnelling conductance fluctuations, one can extract detailed information on these correlation functions.

For completeness, the results for the current-current correlator C_I are given in appendix B.3.

We finally ask, how the two contributions $F^{[d]}$ and $F^{[D]}$ to the conductance correlation function can be distinguished. In general, the factor $(k_{\text{F}}L)^{-1} \ll 1$ leads to a massive suppression of the diffuson contribution as compared to the density-density contribution. Since corrections of $\mathcal{O}((k_{\text{F}}L)^{-1})$ have been neglected in applying random matrix theory, anyway, an additional parameter is necessary to resolve the diffuson contribution. As discussed previously within the context of two extended systems, this is exactly what an *in-plane* magnetic field does: Coupling only to the D-contribution, an in-plane field difference $\mathbf{B}_\parallel^- = \mathbf{B}_\parallel - \mathbf{B}'_\parallel$ can be used to selectively identify the $F^{[D]}$-correlation function. In fact, for finite $\mathbf{B}_\parallel^-$, the tunneling matrix elements pick up a phase factor that modifies the subsequent integration over the Green functions of the 2DEG.

INFO: The additional phase factors in Eq. (4.30) read $e^{-i(\mathbf{q}_{\rm B}(\mathbf{x}-\mathbf{x}')+\mathbf{q}_{\rm B'}(\mathbf{y}-\mathbf{y}'))}$, where $\mathbf{q}_{\rm B} = ed\mathbf{B}_\parallel \times \mathbf{e}_z$. This does not affect the density-density correlations, where $\mathbf{x} \simeq \mathbf{x}'$ and $\mathbf{y} \simeq \mathbf{y}'$. However, the 'prefactor' to the diffuson contribution becomes field dependent. Since $\mathbf{x} \simeq \mathbf{y}'$ and $\mathbf{x}' \simeq \mathbf{y}$ only the field difference $\mathbf{B}_\parallel^-$ enters. I.e. in Eq. (4.30) $\sum_{\mu\nu} A_2^{\nu\mu} A_2^{\mu\nu} = \int d\mathbf{x}\, d\mathbf{y}\, A_2(\mathbf{y},\mathbf{x}) A_2(\mathbf{x},\mathbf{y})$ has to be replaced by

$$\begin{aligned} M(\mathbf{B}_\parallel^-) &\equiv \int d\mathbf{x}\, d\mathbf{y}\, e^{-i\Delta\mathbf{q}_{\rm B}(\mathbf{x}-\mathbf{y})} A_2(\mathbf{y},\mathbf{x}) A_2(\mathbf{x},\mathbf{y}) \\ &= 4\pi^2 L^2\nu^2 \int d\mathbf{r}\, e^{-i\Delta\mathbf{q}_{\rm B}\mathbf{r}} \mathrm{J}_0^2(k_{\rm F} r) \;=\; 8\pi^3 L^2\nu^2 \int r\, dr\, \mathrm{J}_0(\Delta q_{\rm B} r) \mathrm{J}_0^2(k_{\rm F} r). \end{aligned} \tag{4.32}$$

At small magnetic fields, $B_\parallel^- \ll (dL)^{-1}$, one obtains

$$M(\mathbf{B}_\parallel^-) \;\simeq\; 8\pi^3 L^2\nu^2 \int r\, dr \left(1 - \frac{1}{4}(\Delta q_{\rm B} r)^2\right) \mathrm{J}_0^2(k_{\rm F} r) \;\simeq\; \frac{2\pi L^2\nu}{\Gamma^{(\rm b)}} \left(1 - \frac{c_g}{12}(eB_\parallel^-\, dL)^2\right).$$

This leads to

$$\begin{aligned} & C_G(V, \Delta B_\perp; \Delta\mathbf{q}_{\rm B}) - C_G(V, \Delta B_\perp; 0) \sim \\ \sim\; & -\frac{c_g}{(k_{\rm F}L)^3} (|\Delta\mathbf{q}_{\rm B}|L)^2\, F^{[D]}(s,b) + \mathcal{O}\left((|\Delta\mathbf{q}_{\rm B}|L)^4\right), \end{aligned} \tag{4.33}$$

where c_g is a constant of order unity.

The relevant field scale is one flux quantum through the area spanned by the linear size of the QD, L, and the distance between the layers, d, i.e. $B_\parallel^{\rm c} \sim 1/(dL)$. This field scale is typically much larger than the characteristic scale of the perpendicular magnetic field $B_\perp^{\rm c} \sim 1/(\sqrt{g}L^2)$.

Before leaving this section, here some brief comments on the connection between the present analysis and previous experimental work by Sivan et al. [27]. As mentioned in the introduction, Ref. [27] investigated a setup dot/dot, where the second dot was very small, with extreme level quantisation. (That is, in [27], the role of our 2DEG is assumed by a single quantised level of an ultra-small device.) Arguing semi-quantitatively, Sivan et al. related the statistics of the tunnelling conductance to density-density type parametric correlation functions. Indeed, the experimental data turned out to be in good accord with the RMT prediction, Eq. (4.26), discussed above. There are two differences to the presently discussed setup: first, the fact that in our system a 2DEG is used as a spectrometer implies that the second, diffuson type correlation function plays a more important role than in [27]. (In fact, this type of correlation function should contribute to the data of [27], too. Due to the fact, that the current flows into a single level, however, this contribution is minute and can safely be neglected.) Second, one expects that the spatial averaging involved in our formalism leads to a far reaching elimination of all non-spectral structures (as opposed to single-level spectroscopy, where non-universal wavefunction characteristics may affect the result). The prize one has to pay is the suppression factor $(k_{\rm F}L)^{-2}$ which is not present in the dot/dot setup.

Summarising, we have found that the statistics of the dot/2DEG-conductance (in a regime of broken time-reversal invariance) can be described in terms of two basic correlations functions $F^{[d]}$ and $F^{[D]}$. As compared to the previously discussed case of two extended systems, the information contained in $F^{[d;D]}$ is now purely spectral. (All spatial structures have equilibrated due to the ergodicity of the system.) Indeed, these two functions are fully universal in the sense that they depend only on the two basic parameters s and b measuring bias voltage and

perpendicular magnetic field strength, respectively. There is one *non*-universal element affecting the conductance fluctuations, viz. a geometry dependent factor suppressing the contribution of $F^{[D]}$. Still the contributions of the d- and D-correlation function can be disentangled, namely by measuring the dependence of the conductance on a *parallel* magnetic field. How are these results which have been obtained within a non-interacting theory affected once Coulomb interactions are switched on?

4.3.3. Interaction effects

In principle, an interacting systems cannot be treated within the supersymmetric formalism. However, the aim of this section is to show that the interaction effects decouple from the statistics due to disorder (or the chaotic dynamics) in the QD. Thus, with some modifications, the results previously obtained remain valid. The analysis presented here follows closely Ref. [118]. Details of the calculation can be found in appendix B.4.

As far as quantum dots are concerned, the most important manifestation of interaction phenomena is the Coulomb blockade: due to the repulsive interaction, it costs an extra energy E_c to add an electron to the dot. For an isolated dot, this charging energy is determined by the self capacitance C through $E_c = e^2/(2C)$. In typical systems the charging energy exceeds the level spacing by large because $\delta \sim L^{-d}$ and $E_c \sim L^{-1}$. However, for a dot in close vicinity to an extended conducting system, a 2DEG say, an excess charge on the dot will be compensated for by the accumulation of positive background charge in the large system. Under such circumstances it is the geometric capacitance *between* the systems that determines the charging energy. This is the situation given presently.

For a planar dot/2DEG setup, the geometric capacitance estimates to $C = \epsilon\epsilon_0 L^2/d$, where $\epsilon_0 \approx 8.9 \cdot 10^{-12} F/\mathrm{m}$ and ϵ is the dielectric constant of the filling medium. For GaAs, $\epsilon \approx 10$. The charging energy E_c determined by this capacitance has to be compared with the other characteristic energy scales of the problem. The smallest scale one might hope to resolve is the single-particle level spacing δ of the dot. (It is this energy scale on which non-perturbative structures in the parametric correlation functions are observed.) Notice that both, $\delta = (\nu L^2)^{-1}$ and E_c, scale inversely with the dot area. Thus, it must be the spacing between dot and 2DEG that determines the crossover criterion. Specifically, with $\nu \approx 3 \cdot 10^{10}$ meV^{-1}cm^{-2}, one finds that $E_c \approx \delta$ for $d \approx 4$ nm. Realistically, d is somewhat larger than that, i.e. of the order of up to a few tens of nm. We thus conclude that interaction effects are of relevance once one gets interested in low-energy structures of the order of the level spacing.

In previous sections, fluctuations of tunnelling transport coefficients have been described through disorder correlation functions[6] $\mathcal{F}_0(\epsilon_1 - \epsilon_2) \equiv \langle A_0(\epsilon_1) A_0(\epsilon_2)\rangle$, where $A_0(\epsilon)$ are the energy dependent spectral functions, and the subscript '0' means 'non-interacting'. As mentioned above, interactions will mainly manifest themselves through global charging mechanisms. This sector of the Coulomb interaction does not couple to the coordinate dependence of the correlation functions. To simplify the notation, therefore spatial coordinates are temporarily suppressed in the notation.

Our main goal will be to show that interaction and disorder are largely separable in the analysis of correlation functions. Yet, unlike in the non-interacting case, it will no longer be sufficient to compute the zero-temperature correlation functions and to account for finite temperature effects

[6] In fact, we have largely focused on the correlator of Green functions $F_0 \sim \langle G_0^- G_0^+ \rangle$. Presently, however, it will be more convenient to concentrate on the spectral functions themselves. The two quantities F_0 and $\mathcal{F}_0$ are related through $\mathcal{F}_0 = \langle A_0 A_0\rangle_c = 2\Re\langle G_0^- G_0^+\rangle_c = 2\Re F_0$.

in the end (through an integration over the Fermi distribution functions). Instead, one has to work in a finite temperature formalism from the outset.

To model the interaction let us employ the 'orthodox model', that is we add a charging term,

$$\mathcal{H}_c = E_c(\hat{N}_{QD} - \bar{N})^2, \tag{4.34}$$

to the Hamiltonian of the dot. Here $\bar{N}$ is the preferred occupation number that can be set by the gate voltage.

To incorporate this term into the model, it is convenient to use a functional integral formulation. Within this approach, it is straightforward to see that the theory essentially splits into two sectors: one that describes non-interacting Green functions (albeit subject to some imaginary time dependent voltage σ), and an interaction and temperature dependent weight function that controls the fluctuations of σ. This approach of describing charging was introduced by Kamenev and Gefen [118]. In the following, we shall briefly review its main elements and apply it to our present problem.

Within a fermionic field integral approach, the imaginary-time action describing the quantum dot is given by

$$S = \int d\tau\, \bar{\psi}(\partial_\tau + \mathcal{H}_0 - \mu)\psi + E_c \int d\tau (\bar{\psi}\psi - \bar{N})^2,$$

where ψ is a time and position dependent Grassmann field and the rest of the notation is self-explanatory. (Unless stated otherwise, the notation $\bar{\psi}\psi \equiv \int d\mathbf{r}\, \bar{\psi}(\mathbf{r})\psi(\mathbf{r})$ contains a spatial integration.) Decoupling the interaction by a Hubbard-Stratonovich transformation, one obtains the effective action

$$\begin{aligned} S[\psi,\sigma] &= S[\sigma] + S_{\rm d}[\psi,\sigma], \\ & S[\sigma] = \int d\tau\, (\frac{1}{4E_c}\sigma^2 - i\bar{N}\sigma), \\ & S_{\rm d}[\psi,\sigma] = \int d\tau\, \bar{\psi}(\tau)\, (\partial_\tau + \mathcal{H}_0 - \mu + i\sigma)\, \psi(\tau), \end{aligned}$$

where $\sigma(\tau)$ is a scalar bosonic field. Next, all but the static component $\sigma_0 \equiv \beta \int d\tau\, \sigma$ are removed from the fermionic action $S_{\rm d}$ through the gauge transformation $\psi(\tau) \to \exp[-\int^\tau d\tau'(\sigma(\tau') - \sigma_0)]\psi(\tau)$. (That the static component cannot be removed has to do with the fact that gauging out σ_0 would, in general, lead to a violation of the time-antiperiodic boundary condition $\psi(\tau) = -\psi(\tau+\beta)$.) This makes the action of the system oblivious to the time-dependent components of the Coulomb field. However, the (imaginary-time) Green functions $\mathcal{G}(\tau)$, we actually wish to compute, being non-gauge invariant objects, pick up a gauge factor $\mathcal{G}(\tau,\sigma) \to \mathcal{G}(\tau,\sigma_0)B(\tau)$ to be specified momentarily. For temperatures larger than the level spacing, the integration over the static component σ_0 can be done in a saddle point approximation. As a result, $\mathcal{G}(\tau,\sigma_0) \to \mathcal{G}_0(\tau,\bar{\mu}) \equiv \mathcal{G}_0(\tau)$, where $\bar{\mu}$ has the significance of an effective (real) chemical potential determined through the optimal occupation number $\bar{N}$.

We are thus led to consider the combination $\mathcal{G}(\tau) = \mathcal{G}_0(\tau)B(\tau)$. Roughly speaking, the physics of interactions resides in the factor $B(\tau)$. Disorder, the external fields, etc. are contained in $\mathcal{G}_0 = \mathcal{G}_0(\mathbf{x},\mathbf{x}';\tau)$. This is the 'splitting' of the zero-mode interaction theory into two components mentioned above.

Transformation of $\mathcal{G}$ back to frequency space obtains [118]

$$\mathcal{G}(i\epsilon_n) = -\frac{1}{2}\int \frac{d\omega'}{2\pi}\frac{d\epsilon'}{2\pi} B(\omega')A_0(\epsilon')\frac{\coth\frac{\omega'}{2T} + \tanh\frac{\epsilon'}{2T}}{i\epsilon_n - \omega' - \epsilon'}, \tag{4.35}$$

where A_0 is the spectral function associated with the (real-time) Green function $\mathcal{G}_0$ and

$$B(\omega) = 2\sqrt{\frac{\pi}{TE_c}}\exp[-\frac{1}{4TE_c}(E_c^2+\omega^2)]\sinh\frac{\omega}{2T}.$$

This representation holds for any particular realisation of the disorder and the external fields.

We next turn to the discussion of the correlator of two spectral functions $\mathcal{F}(\omega;\epsilon) \equiv \langle A(\epsilon+\frac{\omega}{2})A(\epsilon-\frac{\omega}{2})\rangle$. Making use of Eq. (4.35) and noting that the disorder average couples only to the functions A_0, one obtains

$$\mathcal{F}(\omega;\epsilon) \;=\; \frac{\pi}{TE_c}\,e^{-\frac{E_c}{2T}}\int\frac{d\eta}{2\pi}\,\mathcal{F}_0(\omega-\eta)\,e^{-\frac{\eta^2}{8TE_c}}\int\frac{dW}{2\pi}e^{-\frac{W^2}{2TE_c}}\,\frac{\cosh\frac{\epsilon}{T}+\cosh\frac{\omega}{2T}}{\cosh\frac{\epsilon-W}{T}+\cosh\frac{\omega-\eta}{2T}}. \quad (4.36)$$

Notice that, unlike $\mathcal{F}$, the non-interacting $\mathcal{F}_0$ depends only on the energy difference ω.

Eq. (4.36) represents the most general form of our result for the correlation function in the presence of a charging interaction. To understand the structure of this expression, and to identify physically distinct regimes, realise that $\mathcal{F}$ depends on four characteristic energy scales: the temperature T, the charging energy E_c, the bias voltage V, and an intrinsic scale ϵ_0 over which the non-interacting correlator $\mathcal{F}_0$ varies. Notice that the dependence on V is implicit, through the limits imposed on the variables ϵ and ω.

To exemplify the dependence of the correlator on these scales, let us assume that $\mathcal{F}_0(\omega)$ is proportional to a delta function smeared over the intrinsic level broadening $\Gamma_{\mathcal{T}}$, i.e. $\mathcal{F}_0(\omega) \sim \delta_{\Gamma_{\mathcal{T}}}(\omega)$ (as is the case, e.g., for the diffuson-contribution to the ergodic correlation functions discussed above). In this limit,

$$\mathcal{F}^{(\delta)}(\omega;\epsilon) \;\sim\; \frac{1}{2\sqrt{TE_c}}e^{-\frac{\omega^2}{8TE_c}}f(\epsilon). \quad (4.37)$$

This expression displays a feature common to *all* correlation functions $\mathcal{F}$ affected by charging: Formerly sharp energy dependences are broadened to Gaussians of width $\sigma = 2\sqrt{TE_c}$. In other words, energetically sharp features of $\mathcal{F}_0$ are washed out and a lower limit to what can be resolved in an experiment is set.

To make further progress, one has to distinguish between two different regimes: a) weak interaction or high temperature, $E_c \ll T$, and b) strong interaction or low temperature, $E_c \gg T$. We begin by discussing the first case, a).

For $E_c \ll T$, interaction corrections are small and an expansion to first order in the parameter E_c/T obtains

$$\mathcal{F}(\omega;\epsilon) \;=\; \bar{\mathcal{F}}_0(\omega)\big(1+\mathcal{O}(E_c/T)\big),$$

where $\bar{\mathcal{F}}_0$ stands for an energy average of the non-interacting correlator $\mathcal{F}_0$ over a scale $2\sqrt{TE_c}$ (as in Eq. (4.37)). This means that weak interactions leave the result essentially unaltered, albeit lowering its spectral resolution.

We next turn to the discussion of case b), $E_c \gg T$. Given that the principal setup of the theory favours low temperatures, this regime is more relevant than a). On the other hand, it also has to be kept in mind that the applicability of the theory [118] is limited to temperatures $T > \delta$. Thus, the structures discussed below apply to a temperature regime $\delta < T \ll E_c$.

In the extreme limit[7] $T \to 0$, the interactions produce a hard Coulomb gap, i.e. $\mathcal{F} = \mathcal{F}_0\,\theta(\epsilon - |\omega|/2 - E_c)$. At finite temperatures the gap becomes softer but its essential features remain robust: For small bias V, the correlation function is strongly suppressed while at large bias there are only small changes. The relevant limits are b1) $V \ll T\sqrt{E_c/T}$ and b2) $T \ll E_c \ll V$.

In the first case, when the applied voltage is small, Eq. (4.36) simplifies to

$$\mathcal{F}(\omega;\epsilon) \quad = \quad c\,\bar{\mathcal{F}}_0(0) e^{-\frac{E_c}{2T}} (\cosh\frac{\epsilon}{T} + \cosh\frac{\omega}{2T}),$$

i.e. the correlator is exponentially suppressed. Here c is a factor depending algebraically on T/E_c.

In the opposite case, when the applied voltage is large, one obtains

$$\mathcal{F}(\omega;\epsilon) \quad \simeq \quad \bar{\mathcal{F}}_0(\omega) - e^{-\frac{\epsilon-2E_c}{T}} \left(\bar{\mathcal{F}}_0(\omega-)\, e^{-\frac{\omega}{2T}} + \bar{\mathcal{F}}_0(\omega+)\, e^{\frac{\omega}{2T}}\right),$$

where the dominant contribution $\bar{\mathcal{F}}_0(\omega)$ is the non-interacting $\mathcal{F}_0$ smeared out over energies $2\sqrt{TE_c}$ as before and $\omega\pm = \omega \pm 2E_c$.

Summarising, large charging energies, $E_c > T$, change the non-interacting theory in two different ways. First, to avoid the Coulomb blockade, large bias voltages $V > E_c$ have to be applied. Second, even for those voltages, a lower limit $2\sqrt{TE_c}$ on the maximal energetic resolution of the theory is imposed. For the reasons outlined above, one is lead to believe that, at least for sufficiently weak magnetic fields and impure samples, the effect of other interaction mechanisms is relatively minor. At any rate, since the functional dependence of the Coulomb blockade corrections follows from Eq. (4.36), the applicability of the theory can be put to test.

4.4. Discussion

The main idea presented in this chapter is to monitor the current flowing between two parallel 2DEGs as a function of three qualitatively different control parameters – a parallel magnetic field, a perpendicular field, and a bias voltage – in order to extract information on the three basic two-particle correlation functions of mesoscopic physics, the generalised diffuson $F^{[D]}$, the Cooperon $F^{[C]}$, and the density-density correlator $F^{[d]}$.

As compared to standard transport measurement architectures, the most important advantage of the approach is that electronic correlations are detected without disturbing the 'bulk' system through *local* contacts. Instead the entire planar electron system acts as an 'extended contact' whose spatial structure is, non-disturbingly, scanned by means of the two magnetic fields; *spectral* electronic structures are resolved by measuring the bias voltage dependence of the current. Importantly, the relevant information carried by the tunnelling current is solely contained in its fluctuations. E.g., we have shown that the Fourier transform of the conductance-conductance correlation function with respect to the parallel field directly obtains the two spatially resolved transport functions $F^{[D;C]}$. In contrast, previous analyses of magneto-tunnelling currents, both experimentally and theoretically, focused on the average current profile that is unrelated to any 'mesoscopic' type of information.

To exemplify the usefulness of the approach, two different applications have been considered: tunnelling between two extended 2DEGs and tunnelling from a quantum dot geometry into a

[7] Strictly speaking, the limit $T \to 0$ is not compatible with the condition $T \gg \delta$, but it yields qualitatively correct results.

2DEG. As for the former, we have shown how, at least in principle, the exponents characterising localisation/delocalisation transitions can be extracted from the current data. In contrast, for a quantum dot with ergodic dynamics, the focus is on spectral rather than on spatial structures. We have explicitly worked out the connection between the tunnelling current statistics and various parametric correlation functions (a connection previously used on a semi-quantitative basis to interpret the data of the experiment [27]) and discussed how these correlations can be monitored by changing external fields and bias voltage.

As with any other tunnelling setup, Coulomb interactions are likely to change the outcome of the non-interacting theory. We have provided evidence in favour of the Coulomb blockade being the most relevant interaction mechanism. The presence of the Coulomb blockade will result in two principal effects: first, it forces one to use bias voltages in excess of the blockade threshold. Second, the spectral structure of the correlation functions is washed out. This reduces the information content that can be extracted from the tunnelling current statistics. The extent to which these obstructive mechanisms affect the theory is set by the Coulomb charging energy. In the present system, the latter is largely determined by the inverse of the inter-layer capacitance which, owing to the extended geometry of the systems, is small. Thus, charging phenomena will be less pronounced than in small islands. All in all, we believe that for realistic values of the relevant system parameters, a significant parameter range over which electronic correlations can be resolved through the current approach remains.

5. Weak localisation properties of 2DEGs in parallel magnetic fields

In the previous chapter the parallel magnetic field served as a tool to resolve in-plane correlations that do not depend on this field. By contrast, in this chapter, the influence of a parallel field on the dynamics of a (quasi) two-dimensional system is studied.

To a first approximation, a magnetic field couples to the dynamics of the charge carriers in a 2DEG (2DHG) in two different ways: a) due to the spin degree of freedom, it induces a Zeeman splitting, and b) it couples to the orbital motion. Here the second aspect is analysed for the case of a *parallel* (or *in-plane*) magnetic field. In particular, the effect of the magnetic field on weak localisation (WL) properties is investigated.

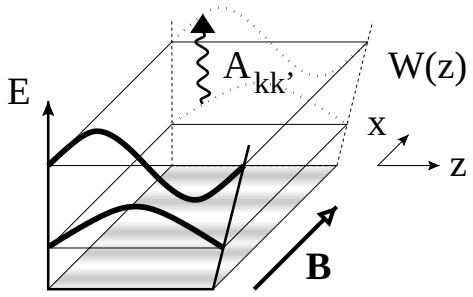

Figure 5.1.: Schematic picture of the quantum well. Two exemplary subband wavefunctions are shown. The spatial profile of the impurity potential is sketched on the bottom of the well.

This effect will sensitively depend on the microscopic structure of the wavefunctions in the direction perpendicular to the plane (the z-direction). It is the spatial extent of these wavefunctions that distinguishes the 2DEG from an ideal plane: A truly two-dimensional system would not feel the orbital coupling of a parallel field at all, as was assumed e.g. in the previous chapter. A particularly interesting situation arises when the confining potential in z-direction, $W(z)$, is symmetric in the sense $W(z) = W(-z)$. Assuming that the disorder potential, induced by remote donors, does not vary significantly on the microscopic scales of variation of W, the *entire* Hamiltonian commutes with z-inversion ($\mathcal{P}_z$). As shown by Berry and Robnik [119], discrete symmetries of this type may compensate for the time-reversal symmetry breaking induced by an external field. Thus, in spite of the presence of an external field the system may still exhibit signatures of time-reversal invariant behaviour, e.g. non-vanishing WL corrections to the conductance.

Before describing the analysis in more detail, let us briefly sketch the resulting physics. An

in-plane magnetic field H manifests itself through the phase coherence time, $\tau_\phi(H)$ [34, 35]:

$$\Delta\sigma = \frac{e^2}{\pi h}\ln(\tau/\tau_\phi(H)); \quad 1/\tau_\phi(H) = 1/\tau_\phi + 1/\tau_H, \tag{5.1}$$

where $\Delta\sigma$ is the WL correction to the conductivity, and $\tau_H \propto H^{-2}$. At $H = 0$, the WL correction shows a logarithmic temperature dependence due to $\tau_\phi \propto T^{-p}$. Consider now the system displayed in Fig. 5.1. The finite motion in z-direction implies a splitting of the electronic spectrum into different subbands of 'size quantisation', i.e. the finite width d of the quantum well imposes momentum quantisation in multiples of $p = 2\pi/d$. If $H = 0$ and the disorder is z-independent, these subbands are decoupled and contribute separately to the conductivity, σ. Universality of the WL implies that in this case the correction $\Delta\sigma$, Eq. (5.1), is proportional to the number M of the occupied subbands: $\Delta\sigma = M(e^2/\pi h)\ln(\tau/\tau_\phi)$.

The magnetic field plays *two* complementary roles: it breaks time-reversal ($\mathcal{T}$) symmetry and (together with a possible z-dependence of the random potential) couples different subbands. In fact, the second role determines the first one: $\mathcal{T}$-invariance is preserved as long as the subbands remain decoupled, since the vector potential of the parallel field can be gauged out in each particular subband. Therefore, the coupling governs the magnetoconductance. For strong inter-subband coupling, we return to the disordered film situation, and the WL correction is determined by Eq. (5.1). When the coupling is weak, the WL correction is determined by M different decoherence times τ_H^k:

$$\Delta\sigma = \frac{e^2}{\pi h}\sum_{k=0}^{M-1}\ln(\tau/\tau_\phi^k(H)); \quad 1/\tau_\phi^k(H) = 1/\tau_\phi + 1/\tau_H^k. \tag{5.2}$$

It turns out that $1/\tau_H^{k\neq 0} > 0$, i.e. all WL corrections, except maybe one ($k=0$), are temperature-independent at $H \neq 0$ and low enough T. Whether the remaining $1/\tau_H^0$ vanishes or not crucially depends on the $\mathcal{P}_z$-symmetry of the confining potential. If the system is fully $\mathcal{P}_z$-symmetric, $W(z) = W(-z)$, the original Hamiltonian is invariant under the combination of $H \to -H$ and $\mathcal{P}_z$-inversions. This symmetry implies orthogonal rather than unitary level statistics [119]. As a result, the decoherence rate $1/\tau_H^0$ remains zero, and a WL correction $\Delta\sigma \sim \ln(\tau/\tau_\phi)$ exists at arbitrary fields. (As $\tau_\phi \propto T^{-p}$, the logarithmic $\sigma(T)$-dependence persists.) All other decoherence times $\tau_H^{k\neq 0}$ are proportional to H^{-2}. Accordingly, the WL correction reads

$$\Delta\sigma_{\rm s}(H,T) = \frac{e^2}{\pi h}\,[p\ln T + 2(M-1)\ln H]. \tag{5.3}$$

By contrast, any violation of $\mathcal{P}_z$-symmetry (by either confining or disorder potentials) suppresses *all* WL corrections, i.e.

$$\Delta\sigma_{\rm as}(H,T) = 2M\frac{e^2}{\pi h}\ln H \tag{5.4}$$

for $M \neq 1$. Therefore, the WL effects sensitively probe the symmetry properties of the confining (and disorder) potential. All in all, it is the interplay of the three factors – inter-band coupling, $\mathcal{T}$-invariance, and $\mathcal{P}_z$-invariance – that determines the conductivity $\sigma(T,H)$.

A special situation arises when just one subband is occupied, $M = 1$. In the absence of high-lying unoccupied bands, the parallel field has no effect whatsoever – a one-band system, being structureless in z-direction, cannot accommodate magnetic flux. Formally, the vector potential of the field can be removed by a gauge transformation [cf. the analysis below]. Thus, $\mathcal{T}$-breaking

at $M = 1$ requires virtual excursions into unoccupied subbands [36]. This fact substantially reduces the magnetoconductance. If the random potential is z-independent, a residual effect exists, albeit of high order in the magnetic field, $\tau_{H,M=1} \propto H^{-6}$. This dependence can be understood as follows: The matrix elements controlling the inter-band hopping are proportional to H. This amounts to a hopping probability $\sim H^2$. Since the square of the field strength is $\mathcal{T}$-invariant, the virtual propagation *within* the empty bands must contribute another H, and we arrive at $\sim H^3$ for the $\mathcal{T}$-breaking contribution to the self-energy. Finally, to obtain a quantum-mechanical intensity, the propagation amplitudes have to be squared which brings us to H^6. It is again essential that the parallel field performs both $\mathcal{T}$-breaking *and* subband coupling. Accordingly one should expect a crossover $(\tau_H \propto H^{-2}) \leftrightarrow (\tau_H \propto H^{-6})$ in the WL profile upon sweeping the Fermi energy through the bottom of the second subband. If one allows for z-dependent scattering although, even for $M = 1$ the usual H^2-dependence is recovered.

After the qualitative discussion above, the next step is the construction of a quantitative description for this system. To explore such type of phenomena one needs to construct an approach which on the one hand is sensitive to microscopic details in z-direction whilst on the other hand should be capable of efficiently describing large scale in-plane properties. This task can efficiently be addressed within a field integral formalism.[1]

5.1. Field theory for the quasi two-dimensional system

The starting point of the derivation is a supersymmetric field integral (as introduced in Sec. 2.3.1) with action

$$S[\psi] \;=\; -i\int dV\,\bar{\psi}\Big(\omega^{+}\sigma_3^{\mathrm{AR}}+E_{\mathrm{F}}+\frac{1}{2m}(\partial_x^2+(\partial_y-iHz)^2+\partial_z^2)-W(z)-V(x,y)\Big)\psi, \quad (5.5)$$

where ω is the energy difference between a retarded and an advanced Green function ($\omega^{+} = \omega + i0$) that will be used to probe transport in the system, σ_3^{AR} is a Pauli matrix in advanced/retarded space, W is the confining potential of the 2DEG, and V a disorder potential. To simplify the analysis,

- the fields ψ are treated as spinless. The spin degrees of freedom can straightforwardly be reintroduced at any stage. More seriously,

- it is assumed that the disorder potential does not depend on the z-coordinate. Given the typical architecture of 2DEGs, this is certainly a justified zeroth order assumption. In, e.g., high mobility 2DEGs (or 2DHGs) in GaAs/AlGaAs heterostructures, the mobility is limited by a long-range random potential, created by charged impurities located far from the plane. Later on, this condition will be relaxed by generalising V according to $V(x,y) \to V(x,y) + U(x,y,z)$, where U is weak and can be treated perturbatively in a sense to be specified below.

[1] Of course, the present, perturbative problem is equally well accessible by diagrammatic methods. However, to get the interplay between inter-band correlations and disorder scattering reliably under control, the formalism of field integration has the advantage that the fully microscopic aspects of the problem are processed in the early stages of the derivation [62, 63].

5.1.1. Subband structure

The confinement in z-direction is responsible for the size quantisation which entails a subband structure of the system. To make progress with the action, Eq. (5.5), an orthonormalised set of wavefunctions $\{\phi_k\}$, diagonalising the z-dependent part of the problem, is introduced:

$$\left(-\frac{1}{2m}\partial_z^2 + W(z) - \epsilon_k\right)\phi_k = 0. \tag{5.6}$$

Expanding the original fields ψ in the complete set of functions ϕ_k, that is $\psi(x,y,z) = \sum_k \psi_k(x,y)\phi_k(z)$, the action takes the form

$$S[\psi] \;=\; -i\int dS\,\bar\psi_k\Big(\big[\omega^+\sigma_3^{\rm AR} + E_{\rm F} - \epsilon_k + \frac{\partial_x^2}{2m} - V(x,y)\big]\delta_{kk'} + \frac{1}{2m}\left((\partial_y - i\hat A)^2\right)_{kk'}\Big)\psi_{k'},$$

where the integration extends over the x-y–plane, summation over k, k' is implied, and

$$A_{kk'} \equiv H\int dz\,\phi_k(z) z \phi_{k'}(z) \tag{5.7}$$

is the vector potential.[2] I.e. the magnetic field couples to the dipole matrix elements $d_{kk'} = \int dz\,\phi_k(z) z \phi_{k'}(z)$ that contain detailed information about the microscopic symmetry properties of the system as will be discussed below in section 5.2.

As a next step, one has to average over disorder, decouple the resulting quartic term in the ψ-fields by a Hubbard-Stratonovich transformation (thus introducing the supermatrix fields Q), and then integrate out the ψ-fields.

INFO: To account for phenomena related to time-reversal symmetry, one introduces the standard doubled field space [63],

$$\bar\Psi = \frac{1}{\sqrt{2}}(\bar\psi, \psi^T\sigma_3^{\rm BF}), \qquad \Psi \equiv \frac{1}{\sqrt{2}}\begin{pmatrix}\psi\\ \bar\psi^T\end{pmatrix}, \tag{5.8}$$

to obtain

$$S[\Psi] \;=\; -i\int dS\,\bar\Psi_k\Big(\big[\omega^+\sigma_3^{\rm AR} + E_{\rm F} - \epsilon_k + \frac{\partial_x^2}{2m} - V(x,y)\big]\delta_{kk'} + \frac{1}{2m}\left((\partial_y - i\hat A\sigma_3^{\rm TR})^2\right)_{kk'}\Big)\Psi_{k'}, \tag{5.9}$$

where $\sigma_3^{\rm BF}$ is a Pauli matrix in boson/fermion space, and the matrix $\sigma_3^{\rm TR}$ acts in the newly introduced time-reversal space.

Then the average of the functional over the in-plane disorder V can be performed. Assuming a standard white noise potential, the averaged action assumes the form

$$\begin{aligned} S_V[\Psi] \;&=\; \frac{1}{4\pi\nu\tau}\int dS\,(\bar\Psi_k\Psi_k)(\bar\Psi_{k'}\Psi_{k'}) \;\to \\ \to S_V[\Psi,Q] \;&=\; -\frac{\pi\nu}{8\tau}\int dS\ {\rm Str}\,(Q_{kk'}Q_{k'k}) + \frac{1}{2\tau}\int dS\,\bar\Psi_k Q_{kk'}\Psi_{k'}. \end{aligned}$$

Then, $S[\Psi,Q] = S_0[\Psi] + S_V[\Psi,Q]$, where $S_0 = S|_{V=0}$ is the clean action, and a Hubbard-Stratonovich field Q, decoupling the disorder generated interaction, has been introduced. Performing the Gaussian integration over the fermion fields yields the Q-field action.

[2] Notice that the completeness of the set $\{\phi_k\}$, $\sum_k \phi_k(z)\phi_k(z') = \delta(z-z')$, implies $\hat A^2 = \hat A^{\rm dia}$, where $A^{\rm dia}_{kk'} \equiv H^2\int dz\,\phi_k(z) z^2 \phi_{k'}(z)$. Thus, the diamagnetic contribution $\sim H^2 z^2$ to the Hamiltonian is indeed reproduced correctly by the above expansion.

In terms of the slow supermatrix fields $Q_{kk'}$, the action reads

$$\begin{aligned} S[Q] &= -\frac{\pi\nu}{8\tau}\int dS\ \mathrm{Str}\, Q^2 + \\ &+ \frac{1}{2}\int dS\ \mathrm{Str}\ \ln\left(\omega^+\sigma_3^{\mathrm{AR}} + E_{\mathrm{F}} - \hat{\epsilon} + \frac{1}{2m}(\partial_x^2 + (\partial_y - i\hat{A}\sigma_3^{\mathrm{TR}})^2) + \frac{i}{2\tau}Q\right), \end{aligned} \tag{5.10}$$

where a compact k-index free notation has been introduced. Here $\hat{\epsilon} \equiv \mathrm{diag}(\epsilon_0, \epsilon_1, \dots)$ contains the subband energies. The next step in the construction of the effective theory is the saddle point analysis. Functional differentiation of the action with respect to Q obtains the equation

$$\Lambda_k = \frac{i}{\pi\nu}\int d^2p \frac{1}{i\delta\sigma_3^{\mathrm{AR}} + E_{\mathrm{F}} - \epsilon_k - \frac{p^2}{2m} + \frac{i}{2\tau}\Lambda_k} \tag{5.11}$$

for the diagonal elements Λ_k of the saddle point matrix $Q_{kk'}$. At this stage one has to specify the relative position of the Fermi energy E_{F} and the subband energies ϵ_k. Below, we will explore the case where M bands with energy $\epsilon_k < E_{\mathrm{F}}$ $(k = 0, \dots, M-1)$ exist. This leads to

$$\Lambda_k = \begin{cases} \sigma_3^{\mathrm{AR}} & k < M, \\ 0 & k \geq M, \end{cases} \tag{5.12}$$

where it has been assumed that the highest occupied subband ϵ_{M-1} lies well below (farther than τ^{-1}) the Fermi level. Based on this solution, the low-lying fields of the theory can be represented as $Q = T\Lambda T^{-1}$, where $\Lambda = \{\Lambda_k \delta_{kk'}\}$.

The next step is the derivation of an effective low-energy action for the matrix field Q which is described in appendix C.1. The final expression for the general slow action reads

$$\begin{aligned} S[Q] &= -\frac{\pi\nu}{8}\int dS\ \tilde{\sum_k}\ \mathrm{Str}\left(4i\omega\sigma_3^{\mathrm{AR}}Q_k + D_k(\tilde{\partial}_k Q_k)^2\right) + \\ &+ \frac{\pi\nu}{4}\int dS\ \tilde{\sum_{k,k'}}\ \mathrm{Str}\left(\mathcal{X}_{kk'}\sigma_3^{\mathrm{TR}}Q_k\sigma_3^{\mathrm{TR}}Q_{k'}\right), \end{aligned} \tag{5.13}$$

where $\tilde{\partial}_k = \partial - i\mathbf{e}_y A_{kk}[\sigma_3^{\mathrm{TR}}, .]$. The sum $\tilde{\sum}_k$ involves only the occupied subbands $k = 0, \dots,$ M-1. Furthermore,

$$\mathcal{X}_{kk'} = \frac{1}{2}(D_k + D_{k'})\frac{1}{(E_{kk'}\tau)^2 + 1}A_{kk'}A_{k'k}(1 - \delta_{kk'}). \tag{5.14}$$

Here D_k is the diffusion constant of subband k, and $E_{kk'} = \epsilon_k - \epsilon_{k'}$.

The first line of (5.13) gives the conventional result of a $2d$ system while the second line describes the coupling of the subbands induced by the magnetic field.

5.1.2. Perturbative analysis

To prepare the lowest order perturbative analysis of the problem, i.e. the one Cooperon approximation to the conductivity, we a) adopt a fermion-replica approach (whereupon all supertraces

'str' become a '− tr' over replica indices) and b) expand the fields Q to lowest non-trivial order in some generators. Explicitly,

$$Q = \sigma_3^{\mathrm{AR}}(1 + 2W + 2W^2 + \dots), \qquad \text{where } W = \begin{pmatrix} & B \\ -B^\dagger & \end{pmatrix}.$$

The time-reversal structure of the theory enforces

$$W^T = -\sigma_2^{\mathrm{TR}} W \sigma_2^{\mathrm{TR}} \qquad \text{or} \qquad B^* = \sigma_2^{\mathrm{TR}} B \sigma_2^{\mathrm{TR}}.$$

It is convenient to decompose the generators B into 'diffuson' and 'Cooperon' blocks, $B = B^d + B^c$, where the components with superscript 'd' ('c') commute (anti-commute) with σ_3^{TR}. Inserting these expressions into the action and expanding to second order in the generators obtains

$$\begin{aligned} S[B, B^\dagger] \;=\; & -\pi\nu \int dS \left(2i\omega \,\mathrm{tr}\, \left(BB^\dagger \right) - \right. \\ & -\tilde{\sum_{k,k'}} C_{kk'} \,\mathrm{tr}\, \left([\delta_{kk'}\partial B_k - i\mathbf{A}_{kk'}(\sigma_3^{\mathrm{TR}} B_{k'} - B_k \sigma_3^{\mathrm{TR}})] \cdot \right. \\ & \left. \left. \cdot [\delta_{k'k}\partial B^\dagger_{k'} - i\mathbf{A}_{k'k}(\sigma_3^{\mathrm{TR}} B^\dagger_k - B^\dagger_{k'} \sigma_3^{\mathrm{TR}})] \right) \right). \end{aligned} \tag{5.15}$$

It is clear from the structure of the second order action, that it does not couple between the 'd' and the 'c' sector, i.e. $S = S^d + S^c$. Next the two actions $S^{d,c}$ will be explored separately. We start with a discussion of the Cooperon action, being responsible for WL corrections. For completeness, a short discussion of the diffuson action follows in section 5.2.3.

5.2. The Berry-Robnik phenomenon

The time-reversal structure of the theory implies that the Cooperon sector of the generators has the explicit form

$$B^c = \begin{pmatrix} & b \\ -b^* & \end{pmatrix},$$

where b is a matrix in replica space. Substituting this representation into Eq. (5.15), the action takes the form

$$S^c[b, b^\dagger] \;=\; -2\pi\nu L^2 \tilde{\sum_{\mathbf{q};k,k'}} \,\mathrm{tr}\, \left\{ b_{k,\mathbf{q}} \Big(2i\omega\delta_{kk'} - \Big[D_k(\mathbf{q} - 2\mathbf{A}_{kk})^2 + 2\tilde{\sum_{k''}} \mathcal{X}_{kk''} \Big] \delta_{kk'} - 2\mathcal{X}_{kk'} \Big) b^\dagger_{k',\mathbf{q}} \right\},$$

where we switched to the momentum representation in the $2d$-plane, $\mathbf{q}^T = (q_x, q_y)$, and L^2 is the $2d$-extension of the system.

The kernel appearing between b and $b^\dagger$ is the 'inverse of the Cooperon'. More explicitly, the Cooperon $\mathcal{C}$, which in our formulation is a matrix in the discrete space of k-indices and diagonal in $\mathbf{q}$-space, is obtained by inverting the matrix

$$(\mathcal{C}^{-1}_{\mathbf{q}})_{kk'} \;=\; \left(-\frac{2i\omega}{D_k} + (\mathbf{q} - 2\mathbf{A}_{kk})^2 + \frac{2}{D_k} \sum_{k''} \mathcal{X}_{kk''} \right) \delta_{kk'} + \frac{2}{\sqrt{D_k D_{k'}}} \mathcal{X}_{kk'}. \tag{5.16}$$

The magnetoconductance is determined by the specific form of this matrix. Before investigating its dependence on the system properties, let us derive an expression for the WL corrections to the conductivity in terms of $\mathcal{C}$.

We apply the above results for the Cooperon to a one-loop calculation of the in-plane conductivity. The latter is defined as

$$\sigma(\mathbf{r},\mathbf{r}') = \frac{1}{2\pi}\langle j_x(\mathbf{r})G^+(\mathbf{r},\mathbf{r}')j_x(\mathbf{r}')G^-(\mathbf{r}',\mathbf{r})\rangle, \tag{5.17}$$

where $\mathbf{r} \equiv (x,y)^T$ is an in-plane vector. Furthermore, j_x is a current operator. Note that, using the "right" units, the prefactor in Eq. (5.17) reads e^2/h.

Correlation functions of this type can efficiently be generated by means of a vector potential type source [120]. As shown in appendix C.2, one finally obtains $\sigma = \sigma^0 + \Delta\sigma$ with

$$\sigma^0 = \sum_{k=0}^{M-1} \sigma_k^0, \tag{5.18}$$

where $\sigma_k^0 = \nu D_k$ is the Drude conductivity of subband k, and

$$\Delta\sigma = -\frac{2}{\pi}\sum_{k=0}^{M-1}\sum_{\mathbf{q}} (\mathcal{C}_{\mathbf{q},\omega=0})_{kk}. \tag{5.19}$$

In general, the field dependent terms will render $\mathcal{C}$ massive, i.e. the weak localisation corrections will suffer from a field induced suppression. However, there is the situation mentioned above, where z-inversion, $\mathcal{P}_z : z \mapsto -z$, is an (approximate) symmetry of the Hamiltonian, $[\mathcal{H},\mathcal{P}_z] \approx 0$. We begin our analysis of the consequences of the presence of such a symmetry by considering an idealised system for which $[\mathcal{H},\mathcal{P}_z] = 0$ is exact.

5.2.1. Exact inversion symmetry

For systems with an exact $\mathcal{P}_z$ symmetry, the z-eigenstates obey

$$\mathcal{P}_z\phi_k = (-)^k\phi_k, \tag{5.20}$$

where we have assumed that (a) the ground state ϕ_0 is symmetric under reflection and (b) the z-parity of the states alternates. Both features can be proven true under rather general conditions by using theorems on $1d$ Schrödinger operators. The definition of the vector potential matrix $\hat{A}$ then implies

$$A_{kk'} = \begin{cases} A_{kk'} & \text{k+k' odd,} \\ 0 & \text{k+k' even,} \end{cases}$$

and, thus, the same holds true for $\mathcal{X}_{kk'}$.

This structure bears consequences on the Cooperon mass. To analyse this point, consider the spatial Cooperon zero-mode,

$$(\mathcal{C}^{-1}_{\mathbf{0},\omega=0})_{kk'} = 2\left(\frac{1}{D_k}\sum_{k''}\mathcal{X}_{kk''}\delta_{kk'} + \frac{\mathcal{X}_{kk'}}{\sqrt{D_k D_{k'}}}\right). \tag{5.21}$$

This matrix has determinant zero implying that *there is a Cooperon mode which is not affected by the field*. In fact, it is straightforward to verify that the M-dimensional vector

$$\mathbf{X} \equiv \mathcal{N}^{-1/2} \sum_k (-)^k \sqrt{D_k}\, \mathbf{e}_k \tag{5.22}$$

is annihilated by $\mathcal{C}^{-1}_{\mathbf{0},\omega=0}$. For convenience we have normalised $\mathbf{X}$ to unity, i.e. $\mathcal{N} = \sum_k D_k$. Owing to the fact that the zero-mode matrix is symmetric, one can, in principle, construct a complete set of orthonormal eigenvectors, $\{\mathbf{X}_0 \equiv \mathbf{X}, \mathbf{X}_1, \ldots \mathbf{X}_{M-1}\}$, with eigenvalues $\{0, \lambda_1, \ldots, \lambda_{M-1}\}$.

We next observe that, due to $A_{kk} = 0$, the full Cooperon kernel is separable (i.e. it is the sum of a spatial and an 'internal' operator). This implies that the complete real space representation of the Cooperon can readily be written down as

$$\mathcal{C}_{\omega=0}(\mathbf{x}, \mathbf{x}') = \tilde{\sum_{\mathbf{q};k}} e^{i\mathbf{q}(\mathbf{x}-\mathbf{x}')}\, \frac{\mathbf{X}_k \mathbf{X}_k^T}{q^2 + \lambda_k}. \tag{5.23}$$

Inserting this result into Eq. (5.19) yields

$$\Delta\sigma(H) = -\frac{2}{\pi} \tilde{\sum_{k;\mathbf{q}}} \frac{1}{q^2 + \lambda_k}, \tag{5.24}$$

(based on the fact that the eigenvectors $\mathbf{X}_k$ are normalised to unity, $\mathbf{X}^T\mathbf{X} = 1$). This is our final result for the conductivity. Notice that, due to $\lambda_0 = 0$, the weak localisation corrections do survive the magnetic field; carrying out the $\mathbf{q}$-summation leads to the usual logarithmic correction to the Drude conductance. Thus, even at high magnetic fields, a logarithmic temperature dependence – see Eq. (5.3) – of the conductance should be observable. All other eigenvalues are proportional H^2 and, thus, display the usual field dependence.

To simplify our further analysis, we assume that all non-zero eigenvalues of the (symmetric) zero-mode Cooperon matrix are negligible in the sense that the eigenvalue gap leads to exponentially decaying, and therefore irrelevant correlations.

5.2.2. Perturbed inversion symmetry

We next explore what happens if the system is not exactly inversion symmetric. An asymmetry can be caused either by the confining potential or by a z-dependence of the random impurity potential.

Asymmetric confining potential

In this case, Eq. (5.21) generalises to

$$A_{kk'} = \begin{cases} A_{kk'} + \delta A_{kk'} & \text{k+k' odd,} \\ \delta A_{kk'} & \text{k+k' even,} \end{cases}$$

where $\delta A_{kk'}$ is assumed to be much weaker than the symmetry allowed elements $A_{kk'}$, $k + k'$ odd. Similarly, there are non-vanishing but small matrix elements $\delta\mathcal{X}_{kk'}$ for both $k + k'$ even and odd.

We compute the effect of the presence of these matrix elements within lowest order perturbation theory. That is, to lowest order the zero-mode eigenvalue $\lambda_0(\mathbf{q})$ of the unperturbed Cooperon mode at momentum $\mathbf{q}$ will shift by the amount

$$\delta\lambda_0^{(\mathrm{as})}(\mathbf{q}) = \mathbf{X}^T \delta\mathcal{C}_{\mathbf{q}}^{-1}\mathbf{X}, \tag{5.25}$$

where $\delta\mathcal{C}_{\mathbf{q}}^{-1}$ is the perturbation contribution to the Cooperon operator. Explicitly,

$$\left(\delta\mathcal{C}_{\mathbf{q}}^{-1}\right)_{kk'} = \Big[-4q_y\delta A_{kk} + 4\delta A_{kk}^2 + 2\sum_{k''}\delta\mathcal{X}_{kk''}\Big]\delta_{kk'} + 2\delta\mathcal{X}_{kk'}. \tag{5.26}$$

Combining these equations and making use of the definition of the zero-mode eigenvectors (5.22) yields

$$\begin{aligned}\delta\lambda_0^{(\mathrm{as})}(\mathbf{q}) &= \frac{1}{\mathcal{N}}\sum_k D_k(q-2\delta\mathbf{A}_{kk})^2 + \frac{2}{\mathcal{N}}\sum_{k,k'}(1+(-)^{k+k'})\delta\mathcal{X}_{kk'} = \\ &= (q-\frac{2}{\mathcal{N}}\sum_k D_k\delta\mathbf{A}_{kk})^2 + \frac{2}{\mathcal{N}^2}\sum_{k,k'}D_kD_{k'}(\delta A_{kk}-\delta A_{k'k'})^2 + \frac{4}{\mathcal{N}}\sum_{k+k'\,\mathrm{even}}\delta\mathcal{X}_{kk'}.\end{aligned}$$

Accordingly, in the Cooperon denominator of the massless mode (cf. Eq. (5.23)) we have to substitute

$$q^2 \to q^2 + \frac{2}{\mathcal{N}^2}\sum_{k,k'}D_kD_{k'}(\delta A_{kk}-\delta A_{k'k'})^2 + \frac{4}{\mathcal{N}}\sum_{k+k'\,\mathrm{even}}\delta\mathcal{X}_{kk'}.$$

Thus, the Cooperon acquires a mass term $\sim H^2$.

z-dependent impurities

A potential with a generic z-dependence will not be inversion symmetric, implying that, somehow, the Cooperon must pick up a mass. Deriving this mass for a Gaussian distributed potential $U(\mathbf{r},z)$,

$$\langle U(\mathbf{r},z)\rangle = 0, \qquad \langle U(\mathbf{r},z)U(\mathbf{r}',z')\rangle = \gamma^2\delta(\mathbf{r}-\mathbf{r}')\delta(z-z'),$$

will be the main goal of this section. For small U, it is sufficient to consider the lowest non-vanishing order in U.

INFO: Assuming that U is much weaker than the z-independent part of the potential, V, one can proceed by simply substituting $E_{\mathrm{F}} \to E_{\mathrm{F}} + U$ under the logarithm in Eq. (5.10). Expanding to second order in U obtains

$$S[Q] = S_0[Q] + \frac{1}{4}\,\mathrm{tr}\,(\mathcal{G}U\mathcal{G}U), \tag{5.27}$$

where the trace extends over both, internal degrees of freedom and real space, and $\mathcal{G}$ is the full Q-dependent Green function of the problem. Averaging over disorder then yields

$$S[Q] = S_0[Q] + \frac{\gamma^2}{4}\int dS\,dz\,\mathrm{tr}\left[\mathcal{G}(\mathbf{r},z;\mathbf{r},z)\mathcal{G}(\mathbf{r},z;\mathbf{r},z)\right],$$

Since this contribution is small already, one is allowed to neglect in $\mathcal{G}$ all contributions that are small as compared to the Fermi scales (A, ω, etc.). Thus, the saddle point equation gives

$$\mathcal{G}(\mathbf{r},z;\mathbf{r},z) = -i\pi\nu\langle z|Q(\mathbf{r})|z\rangle + \dots, \tag{5.28}$$

where the ellipses denote real contributions that are Q-independent. Notice that, at this level, Q still is a (bilocal) operator in z-space. Representing the z-content of the matrix element in terms of the eigenfunctions ϕ_k and keeping in mind that Q is k-diagonal, we find

$$\mathcal{G}(\mathbf{r}, z; \mathbf{r}, z) = -i\pi\nu \tilde{\sum_k} \phi_k^2(z) Q_k(\mathbf{r}) \tag{5.29}$$

which has to be substituted back into the action.

We arrive at

$$S[Q] = S_0[Q] - \left(\frac{\pi\gamma\nu}{2}\right)^2 \int dS \tilde{\sum_{kk'}} \Gamma_{kk'} \operatorname{tr}\left(Q_k(\mathbf{r}) Q_{k'}(\mathbf{r})\right), \tag{5.30}$$

where the coefficient

$$\Gamma_{kk'k''k'''} = \int dz\, \phi_k(z)\phi_{k'}(z)\phi_{k''}(z)\phi_{k'''}(z),$$

and $\Gamma_{kk'} \equiv \Gamma_{kkk'k'}$ is positive. This expression tells that the z-dependent scattering tends to lock the fields Q_k. For γ large, only field configurations $\{Q_k \equiv Q\}$ with no k-dependence survive. The physical mechanism is the following: Scattering in z-direction leads to a coupling between the different k-bands. Thus, the formerly independent diffusons and Cooperons are coupled, too.

Do the former results, in particular the massless Cooperon channel survive this coupling? The answer is no. The k-space eigenvector $\mathbf{X}_0$ associated with the eigenvalue $\lambda_0 = 0$ in the Cooperon channel is staggered in k, cf. Eq. (5.22), i.e. it stands orthogonal on the field configurations that are compatible with the locking.

If the coupling due to the impurity scattering is smaller than the field induced subband coupling, the shift of the lowest eigenvalue is again obtained by first order perturbation theory. Then,

$$\delta\lambda_0^{(\mathrm{imp})} = \frac{1}{\mathcal{N}} \pi\nu\gamma^2 \sum_{k+k' \text{ odd}} \Gamma_{kk'}. \tag{5.31}$$

Or, $\delta\lambda_0^{(\mathrm{imp})} \sim 1/(\mathcal{N}\tau')$, where τ' has the meaning of a scattering time perpendicular to the plane, i.e. between the subbands.

This result which does not depend on the magnetic field holds true only for sufficiently large fields. For smaller fields, the disorder induced mass term fixes the preferred eigenvector. To compute the mass of the completely locked Cooperon, consider

$$\lambda_l \equiv \mathbf{X}_l^T \mathcal{C}^{-1}_{\mathbf{0},\omega=0} \mathbf{X}_l,$$

where the Cooperon operator is given by Eq. (5.21), and the 'locked' vector $\mathbf{X}_l$ reads

$$\mathbf{X}_l \equiv \mathcal{N}^{-1/2} \sum_k \sqrt{D_k}\, \mathbf{e}_k. \tag{5.32}$$

Explicitly computing the matrix element leads to

$$\lambda_l = \frac{2}{\mathcal{N}^2} \sum_{k,k'} D_k D_{k'} (A_{kk} - A_{k'k'})^2 + \frac{4}{\mathcal{N}} \sum_{k,k'} \mathcal{X}_{kk'}. \tag{5.33}$$

At low fields, the mass of the Cooperon increases quadratically with H according to Eq. (5.33), but then, due to Eq. (5.31), it levels off at large fields. The characteristic field H_c can be estimated by comparing Eqs. (5.31) and (5.33) which yields $H_c \sim E/v_{\rm F}\sqrt{\tau/\tau'}/d$, where E stands for the typical energy separation between subbands and d sets the scale for the width of the quantum well.

As the expressions obtained above are rather lengthy, it is helpful to consider some specific examples. We concentrate on the experimentally most relevant case $M = 2$ and, for simplicity, choose[3] $D_0 = D_1 \equiv D$. Diagonalisation of the 2×2 Cooperon matrix,

$$\mathcal{C}^{-1} = \begin{pmatrix} (\mathbf{q}-\mathbf{A})^2 + \frac{2}{D}(\mathcal{X}_{01} + \frac{1}{2\tau_\phi}) & \frac{2}{D}\mathcal{X}_{01} \\ \frac{2}{D}\mathcal{X}_{01} & (\mathbf{q}+\mathbf{A})^2 + \frac{2}{D}(\mathcal{X}_{01} + \frac{1}{2\tau_\phi}) \end{pmatrix},$$

yields

$$\lambda = q^2 + A^2 + \frac{2}{D}(\mathcal{X}_{01} + \frac{1}{2\tau_\phi}) \pm 2\sqrt{(\mathbf{Aq})^2 + \frac{1}{D^2}\mathcal{X}_{01}^2}, \tag{5.34}$$

where $\mathbf{A} = \mathbf{A}_{00} - \mathbf{A}_{11}$, and $\mathcal{X}_{01} = DA_{01}^2/(1 + (E_{10}\tau)^2)$ obtains from (5.14). The corresponding magnetic decoherence times read $1/\tau_\phi(H) = D\lambda$.

Note that at small magnetic fields, $2\mathcal{X}_{01} \ll 1/\tau_\phi$, the symmetry mechanism is ineffective. Irrespective of A, the magnetoconductance yields

$$\sigma(H) - \sigma(0) \simeq 2\frac{e^2}{\pi h}\mathcal{X}_{01}\tau_\phi, \tag{5.35}$$

which shows the usual low-field quadratic dependence on H. However, the coefficient is diminished by the factor $1/(1 + (E_{10}\tau)^2)$.

At large magnetic fields, $2\mathcal{X}_{01} \gg 1/\tau_\phi$, if the confining potential is fully symmetric ($\mathbf{A} = 0$), the result reduces to

$$1/\tau_\phi(H) = \frac{1}{\tau_\phi} + 2\mathcal{X}_{01}(1 \pm 1).$$

While $1/\tau_\phi^1(H) \simeq 4\mathcal{X}_{01}$ leads to a logarithmic field dependence (see Eq. (5.2)), due to the field-insensitive $1/\tau_\phi^0(H) = 1/\tau_\phi$, the conductance maintains its temperature dependence through τ_ϕ even at large fields.

A slight asymmetry of the confining potential entails a finite $\mathbf{A}$, which leads to

$$1/\tau_\phi(H) \simeq DA^2 + \frac{1}{\tau_\phi} + 2\mathcal{X}_{01}(1 \pm 1).$$

Thus, the temperature dependence remains as long as $DA^2 < 1/\tau_\phi$.

The simplest model is a symmetric quantum well with a box potential of width d. In this case, one obtains[4] $A_{01} = -16Hd/(9\pi^2)$ as the only non-vanishing matrix element. Adding a small perturbation $\delta W(z) = wz$ to the confining potential, in addition, yields the diagonal term $A = 4wA_{01}^2/(HE_{10})$.

As discussed above, the physically most interesting systems are close to symmetric. The experimentally most generic case, however, is a triangular quantum well which is far from symmetric

[3] Admitting for different diffusion constants $D_0 \neq D_1$ does not change the results qualitatively.
[4] The corresponding eigenfunctions and matrix elements $A_{kk'}$ are calculated in appendix C.4.

– at least as far as the low-lying subbands are concerned ($A_{kk} > A_{kk+1}$, cf. App. C.4). In the strongly asymmetric case, one obtains

$$1/\tau_\phi^k(H) = 2\mathcal{X}_{01} \qquad (k = 0, 1),$$

where specifically for the triangular well ($W(z) = \infty$ for $z < 0$ and $W(z) = wz$ for $z > 0$) the relevant matrix element reads $A_{01} \approx -0.67(2mw)^{-1/3}H$.

Fortunately, the shape of the confining potential can be tuned via gate voltages. Thus, close to symmetric scenarios, admitting for the experimental observation of symmetry effects, should be feasible.

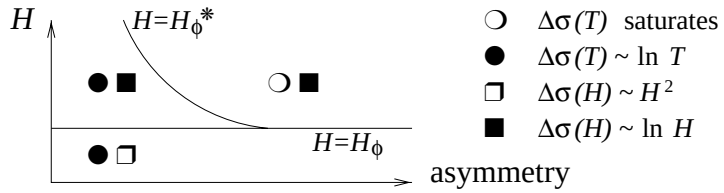

Figure 5.2.: Different regimes of H- and T-dependence of the weak localisation corrections.

The regimes with different field and temperature dependences of the conductance are schematically shown in Fig. 5.2. The fields H_ϕ and H_ϕ^* are defined through $2\mathcal{X}_{01}\tau_\phi = 1$ and $DA^2\tau_\phi = 1$, respectively. I.e.

$$H_\phi \equiv \frac{1}{\sqrt{D\tau_\phi}\, d_{01}\sqrt{\frac{2}{1+(\Delta_{10}\tau)^2}}}, \qquad H_\phi^* \equiv \frac{1}{\sqrt{D\tau_\phi}\,(d_{00}-d_{11})},$$

where $d_{kk'}$ are the dipole matrix elements defined above.

5.2.3. The diffuson action

For completeness, let us discuss the behaviour of the diffuson. Substituting the explicit, time-reversal resolved structure of the diffuson generators,

$$B^d = \begin{pmatrix} b & \\ & -b^* \end{pmatrix},$$

into the quadratic action obtains

$$S^d[b, b^\dagger] \;=\; -2\pi\nu L^2 \tilde{\sum_{\mathbf{q};k,k'}} \operatorname{tr}\Big\{ b_{k,\mathbf{q}}\Big(2i\omega\delta_{kk'} - \Big[D_k q^2 + 2\tilde{\sum_{k''}}\mathcal{X}_{kk''}\Big]\delta_{kk'} + 2\mathcal{X}_{kk'}\Big) b^\dagger_{k',\mathbf{q}}\Big\}.$$

The diffuson kernel $\mathcal{D}$, thus, reads

$$(\mathcal{D}_\mathbf{q}^{-1})_{kk'} = \left(-\frac{2i\omega}{D_k} + q^2 + \frac{2}{D_k}\sum_{k''}\mathcal{X}_{kk''}\right)\delta_{kk'} - \frac{2}{\sqrt{D_k D_{k'}}}\,\mathcal{X}_{kk'}. \tag{5.36}$$

Note that the – possibly non-vanishing! – diagonal elements A_{kk} do not appear in this expression. In the absence of subband coupling, $\mathcal{X}_{kk'} = 0$, Eq. (5.36) reduces to the conventional form of the diffuson, $(\mathcal{D}_\mathbf{q}^{-1})_{kk'} = (-2i\omega/D_k + q^2)\delta_{kk'}$.

Even when the subbands are coupled, the diffuson matrix possesses always – irrespective of the symmetry of the confining potential and the z-dependence of the scattering potential – an eigenvalue $\lambda_0 = 0$ corresponding to the locked eigenvector $\mathbf{X}_l$ (see Eq. (5.32)). The diffuson is insensitive to $\mathcal{T}$-invariance and, therefore, to the Berry-Robnik symmetry phenomenon as well. One observes, however, that the other $M-1$ diffuson modes become massive in the presence of the magnetic field. This is not related to $\mathcal{T}$-breaking, but only to the coupling between the subbands. As pointed out earlier, this coupling induces some splitting mechanism, leaving only one mode massless.

5.3. One subband: Virtual processes

If only one subband is occupied, $M = 1$, according to the previous analysis, the in-plane magnetic field shows no effect. In the symmetric case, $A_{00} = 0$. In the asymmetric case, $q^2 - 4q_y A_{00} + 4A_{00}^2 = (\mathbf{q} - 2\mathbf{A}_{00})^2$, and, therefore, the vector potential can be removed by a gauge transformation. This is easily understood due to the fact that paths within the plane cannot accommodate magnetic flux, as mentioned earlier.

So far the contribution of unoccupied subbands has been disregarded because diffusons and Cooperons can only be constructed within occupied subbands. There are, however, virtual processes. Can virtual processes alone break time-reversal symmetry? For the z-inversion symmetric problem, due to the Berry-Robnik phenomenon [119], one mode always remains massless. Thus, if only the lowest subband is occupied there is no magnetoresistance at all. What happens if z-inversion symmetry is broken? In order to answer this question let us study a toy model first.

The simplest model containing all the relevant features of the system is a random matrix model for the occupied subband, coupled to two degenerate unoccupied, i.e. energetically high-lying, levels, see Fig. 5.3. The analysis, shown in appendix C.3, yields that a) if the coupling between the levels is solely due the magnetic field, the action contains a term $\sim H^6 \,\mathrm{Str}\,(\sigma_3^{\mathrm{TR}} Q)^2$, whereas b) if one allows for an additional coupling (which is not $\mathcal{T}$-breaking), one obtains the lower order contribution $\sim H^2 \,\mathrm{Str}\,(\sigma_3^{\mathrm{TR}} Q)^2$ instead.

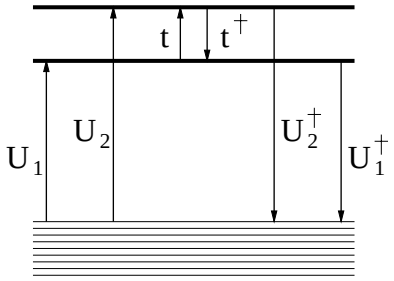

Figure 5.3.: Toy model: A RMT system (modelling the occupied subband) is coupled to two energetically high-lying levels.

Having shown by means of a simple toy model that virtual processes may break $\mathcal{T}$-symmetry, let us return to the magnetic field case. The starting point is the action $S[Q]$ in Eq. (5.10). The Q-matrices now live only in the occupied subband because there are no slow modes within the unoccupied subbands; see also page 130.

Usually it is sufficient to take into account only the paramagnetic term. Here we are going to obtain higher order corrections in the magnetic field, and, therefore, the diamagnetic term might become relevant. It is possible, however, to include the diamagnetic term in a redefinition of the perpendicular wavefunctions ϕ_k, i.e.

$$\left(-\frac{1}{2m}\partial_z^2+\frac{1}{2m}A^2+W(z)-\epsilon_k^{(\mathrm{d})}\right)\phi_k^{(\mathrm{d})}=0. \tag{5.37}$$

Then, instead of $A_{kk'}$ the action contains $A^{(\mathrm{d})}_{kk'}=H\int dz\,\phi_k^{(\mathrm{d})}z\phi_{k'}^{(\mathrm{d})}$. However, as this does not change the structure of the action, the lowest order contribution is still obtained by neglecting the diamagnetic term. Thus, we drop the superscript '(d)' in the following.

Furthermore, it is convenient to choose a gauge where the vector potential in the occupied subband vanishes, i.e. $\tilde{A}_{kk'}=A_{kk'}-A_{00}\delta_{kk'}$. Note that the off-diagonal elements of $\hat{A}$ are completely fixed by the original choice of the formalism which requires $\mathbf{A}(x,y,z)$ to have no z-component. Therefore, the gauge freedom is restricted to functions $f=f(x,y)$. However, having no z-dependence, this only affects the diagonal elements A_{kk}, shifting all of them by a fixed amount, because $\int dz\,\phi_k(z)f(x,y)\phi_{k'}(z)=f(x,y)\delta_{kk'}$.

As for the toy model, a block form is useful to separate the occupied from the unoccupied subbands. Thus, the action (5.10) takes the form

$$S=\frac{1}{2}\int d\mathbf{r}\ \mathrm{Str}\ \ln\begin{pmatrix}\mathcal{G}_{oo}^{-1} & \hat{\mathcal{G}}_{ou}^{-1}\\ \hat{\mathcal{G}}_{uo}^{-1} & \hat{\mathcal{G}}_{uu}^{-1}\end{pmatrix}=\frac{1}{2}\int d\mathbf{r}\ \mathrm{Str}\ \left(\ln\hat{\mathcal{G}}_{uu}^{-1}+\ln(\mathcal{G}_{oo}^{-1}-\hat{\mathcal{G}}_{ou}^{-1}\hat{\mathcal{G}}_{uu}\hat{\mathcal{G}}_{uo}^{-1})\right), \tag{5.38}$$

where the subscripts 'o' ('u') stand for '(un-)occupied'. Here

$$\mathcal{G}^{-1}_{kk'}=(\xi_p-\epsilon_k+\frac{i}{2\tau}Q\delta_{ok})\delta_{kk'}+\frac{p_y}{m}\tilde{A}_{kk'}\sigma_3^{\mathrm{TR}}.$$

Expanding Q around the saddle point $Q=\sigma_3^{\mathrm{AR}}$ in the slowly varying fields T, the term describing virtual processes, $\delta G_V=-T^{-1}\hat{\mathcal{G}}_{ou}^{-1}\hat{\mathcal{G}}_{uu}\hat{\mathcal{G}}_{uo}^{-1}T$, reads

$$\delta G_V\ =\ -\frac{1}{m^2}T^{-1}p_y\hat{A}_{ou}\sigma_3^{\mathrm{TR}}\hat{\mathcal{G}}_{uu}p_y\hat{A}_{uo}\sigma_3^{\mathrm{TR}}T\ =\ -\frac{1}{m^2}\sum_{u,u'}p_y^2A_{ou}A_{u'o}T^{-1}\mathcal{G}_{uu'}T. \tag{5.39}$$

In the (field-dependent) Green functions of the unoccupied subbands, $\hat{\mathcal{G}}_{uu}$, one can replace ξ_p by its value at the poles of $\mathcal{G}_{oo}$, i.e. $\xi_p=\epsilon_o$. Then, $\hat{\mathcal{G}}_{uu}$ can be expanded in $\delta\hat{G}_{uu}=\frac{p_y}{m}\hat{A}_{uu}\sigma_3^{\mathrm{TR}}$ around the large energy difference $E_{uo}=\epsilon_u-\epsilon_o$:

$$\hat{\mathcal{G}}_{uu}\ =\ -\hat{E}_{uo}^{-1}\sum_n\left(\delta\hat{G}_{uu}\hat{E}_{uo}^{-1}\right)^n\simeq-\hat{E}_{uo}^{-1}-\hat{E}_{uo}^{-1}\delta\hat{G}_{uu}\hat{E}_{uo}^{-1}-\dots\ .$$

Reinserting this expression into Eq. (5.39) yields

$$\delta G_V=g_V^{\mathrm{even}}+g_V^{\mathrm{odd}}T^{-1}\sigma_3^{\mathrm{TR}}T,$$

where g_V^{even} (g_V^{odd}) contains only even (odd) terms in the magnetic field.

As one can see from the action, Eq. (5.38), this means that the even terms contribute to the diamagnetic term for the lowest subband whereas the odd terms contribute to the paramagnetic term. Thus, the effect of the virtual processes is to reintroduce an effective vector potential in the occupied subband, $\mathcal{A}(\mathbf{p})=m/p_y\,g_V^{\mathrm{odd}}(\mathbf{p})$, and to replace

$$\xi_p\ \ \rightarrow\ \ \mathcal{E}(\mathbf{p})=\xi_p-g_V^{\mathrm{even}}(\mathbf{p}).$$

As the 'diamagnetic' term $g_V^{\rm even}$ only shifts the energy of the band, we will neglect this effect and concentrate on the paramagnetic contribution. The action can now be written in its standard form though with a modified, momentum dependent vector potential:

$$S = \frac{1}{2}\int d\mathbf{r}\,\mathrm{Str}\,\ln\left(\mathcal{G}_0^{-1}+\frac{1}{m}\mathbf{p}T^{-1}(\partial - i\mathcal{A}(\mathbf{p})\mathbf{e}_y\sigma_3^{\rm TR})T\right).$$

A straightforward gradient expansion of this expression yields

$$S_{\omega=0} = -\frac{\pi\nu D}{4}\int d\mathbf{r}\int\frac{d\phi}{2\pi}\sin^2(\phi)\,\mathrm{Str}\,\left((\partial - i\mathcal{A}(\phi)\mathbf{e}_y[\sigma_3^{\rm TR},\,.\,])Q\right)^2.$$

In order to obtain the lowest order contribution in the magnetic field, the following terms contributing to $\mathcal{A}(\phi)$ are needed:

$$\begin{aligned} g_V^{(3)} &= \frac{p_y^2 A_{ou}A_{uu'}A_{u'o}}{m^2 E_{uo}E_{u'o}} \equiv \sin^2\phi\,\mathcal{A}_3, \\ g_V^{(5)} &= \frac{p_y^4 A_{ou}A_{uu_1}A_{u_1u_2}A_{u_2u'}A_{u'o}}{m^4 E_{uo}E_{u'o}E_{u_1o}E_{u_2o}} \equiv \sin^4\phi\,\mathcal{A}_5, \end{aligned}$$

where a summation over the internal indices $u, u', \ldots$ is implied, and $p_y \simeq p_{\rm F}\sin\phi$.

Thus, keeping terms up to $6^{\rm th}$ order in the magnetic field, we finally get

$$\begin{aligned} S &= -\frac{\pi\nu D}{8}\int d\mathbf{r}\left(\mathrm{Str}\,(\partial Q)^2 - 2i\underbrace{\left(\frac{3}{4}\mathcal{A}_3+\frac{5}{8}\mathcal{A}_5\right)}_{\mathcal{A}_{oo}}\mathrm{Str}\,([\sigma_3^{\rm TR},Q]\partial_y Q) - \frac{5}{8}\mathcal{A}_3^2\,\mathrm{Str}\,[\sigma_3^{\rm TR},Q]^2\right) = \\ &= -\frac{\pi\nu D}{8}\int d\mathbf{r}\;\mathrm{Str}\left[\left((\partial - i\mathcal{A}_{oo}\mathbf{e}_y[\sigma_3^{\rm TR},\,.\,])Q\right)^2 - \frac{1}{16}\mathcal{A}_3^2[\sigma_3^{\rm TR},Q]^2\right], \end{aligned}$$

where $\mathcal{A}_3 = v_{\rm F}^2\sum_{u,u'}A_{ou}A_{uu'}A_{u'o}/(E_{uo}E_{u'o})$. The relevant diagram for the present one-band problem is contrasted with the multi-subband case in Fig. 5.4.

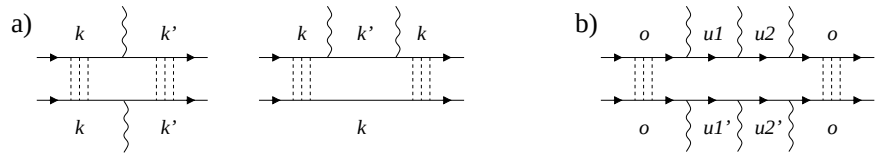

Figure 5.4.: Basic diagrams for a) $M > 1$, and b) $M = 1$. The wavy lines show interactions with the magnetic field while the dashed lines represent impurity scattering.

$\mathcal{A}_{oo}$ is a pure gauge and can be removed from the action. The mass of the Cooperon is determined by the second term, i.e.

$$\tau_H^{-1} = \frac{1}{16}D\mathcal{A}_3^2. \tag{5.40}$$

This result changes drastically when the strict condition of z-independence of the impurity potential is relaxed. Then, virtual transitions into unoccupied subbands are possible even in the absence of a magnetic field.

INFO: As for the multi-subband case, if $U(x,y,z) \to U_{kk'}(x,y)$ is sufficiently weak, it can be taken into account perturbatively, i.e. by expanding 'Str ln' up to quadratic order in U. The diagonal components U_{kk} can be neglected while the off-diagonal ones lead to an additional coupling between the subbands.

Starting from Eq. (5.27), one obtains

$$\begin{aligned} S_U &= -\frac{1}{4}\sum_{k',k'',k''',k} \int d\mathbf{r}\, d\mathbf{r}' \Big\langle \mathrm{Str}\, \left[\mathcal{G}_{kk'}(\mathbf{r},\mathbf{r}')U_{k'k''}(\mathbf{r}')\mathcal{G}_{k''k'''}(\mathbf{r}',\mathbf{r})U_{k'''k}(\mathbf{r})\right] \Big\rangle = \\ &= -\frac{\gamma^2}{4}\sum_{k',k'',k''',k} \Gamma_{k'k''k'''k} \int d\mathbf{r}\ \mathrm{Str}\, \left[\mathcal{G}_{kk'}(\mathbf{r},\mathbf{r})\mathcal{G}_{k''k'''}(\mathbf{r},\mathbf{r})\right]. \end{aligned} \tag{5.41}$$

To evaluate this expression to lowest non-vanishing order in the magnetic field, one needs the following approximations for the Green functions:

$$\begin{aligned} \mathcal{G}_{oo}(\mathbf{r},\mathbf{r}) &\simeq -i\pi\nu Q(\mathbf{r}), \\ \mathcal{G}_{uu'}(\mathbf{r},\mathbf{r}) &\simeq -i\pi\nu v_{\mathrm{F}}^2 \frac{A_{uo}A_{ou'}}{E_{uo}E_{u'o}} \sigma_3^{\mathrm{TR}} Q(\mathbf{r}) \sigma_3^{\mathrm{TR}}. \end{aligned}$$

Inserting this into (5.41) yields a second oreder term in H.

The final expression for the symmetry breaking term reads [36]

$$S_U = \frac{1}{2}(\pi\nu v_{\mathrm{F}}\gamma)^2 \sum_{u,u'} \tilde{\Gamma}_{uu'} \frac{A_{uo}A_{ou'}}{E_{uo}E_{u'o}}\, \mathrm{Str}\, \left(\sigma_3^{\mathrm{TR}} Q\right)^2, \tag{5.42}$$

where $\tilde{\Gamma}_{uu'} \equiv \Gamma_{oouu'} = \int dz\, \phi_o^2 \phi_u \phi_{u'}$. Here $1/\tau'_{uu'} \equiv 2\pi\nu\gamma^2\tilde{\Gamma}_{uu'}$ can be roughly interpreted as an inter-band scattering rate. Thus, one obtains

$$1/\tau_H^{(\mathrm{imp})} = v_{\mathrm{F}}^2 \sum_{u,u'} \frac{A_{uo}A_{ou'}}{\tau'_{uu'}\, E_{uo}E_{u'o}}. \tag{5.43}$$

Comparing Eqs. (5.40) and (5.43), a crossover $H^2 \to H^6$ is to be expected at the characteristic field $H_c \sim \sqrt{E/D}\,(\tau/\tau')^{1/4}/d$.

5.4. Discussion

We have shown that the magnetoresistance of two-dimensional electron gases in an in-plane field responds sensitively to both the geometric structure of the confining potential and the nature of the impurity scattering. Those phenomena are intimately related to the Berry-Robnik symmetry mechanism [119]. The presence of an additional discrete symmetry compensates for the breaking of $\mathcal{T}$-invariance and, thus, in the fully symmetric case, a WL signal remains even at strong magnetic fields. Furthermore, $M = 1$ represents a special case. The response in the magnetoconductance profile should be visible in experiment. A summary of the results is shown in Table 5.1.

	$M = 1$
$\mathcal{P}_z$-symmetry	$1/\tau_H = 0$
no $\mathcal{P}_z$-symmetry due to - $W(z) \neq W(-z)$	$1/\tau_H \sim D\,(v_\mathrm{F}/E)^4\,(Hd)^6$
- $V = V(x,y,z)$	$1/\tau_H \sim 1/\tau'\,(v_\mathrm{F}/E)^2\,(Hd)^2$
	$M > 1$
$\mathcal{P}_z$-symmetry	$1/\tau_H^0 = 0$, $1/\tau_H^{k\neq 0} \sim D/(E\tau)^2\,(Hd)^2$
no $\mathcal{P}_z$-symmetry due to - $W(z) \neq W(-z)$	$1/\tau_H^k \sim D/(E\tau)^2\,(Hd)^2$
- $V = V(x,y,z)$	$1/\tau_H^0 \sim \min\{D/(E\tau)^2\,(Hd)^2\,,\ 1/\tau'\}$, $1/\tau_H^{k\neq 0} \sim D/(E\tau)^2\,(Hd)^2$

Table 5.1.: Field-dependent decoherence times, $\tau_H^{(k)}$. Here d sets the scale for the width of the quantum well, E is the typical energy separation between subbands, and τ' the transverse or inter-band mean scattering time.

This concludes the discussion of two-dimensional electron gases and, thus, the first part of this work. The second part of the present work is motivated by a question related to the preceding chapter: How does a parallel magnetic field affect the properties of a two-dimensional *superconducting* system? The answer belongs to the larger context of gapless superconductivity.

Part II.

Gapless phenomena in superconductors

6. Superconductivity

While in a normal, non-interacting system the density of states is an essentially "boring" quantity, being flat on the scales of interest, this changes drastically for a superconductor. A conventional s-wave superconductor possesses a hard gap in its energy spectrum; i.e. there is a minimal excitation energy below which there are no quasi-particle states. In the second part of this work we are studying how this characteristic feature of the superconductor behaves under different perturbations. To establish a basis for further investigation, we start with a short introduction to the main characteristics of superconductivity and its theoretic description in Secs. 6.1 and 6.2. In Sec. 6.3, the Abrikosov-Gor'kov (AG) theory of gap suppression is discussed. To prepare the discussion of 'sub-gap' tail states, in Sec. 6.4 the so-called Lifshitz tails are introduced. Before leaving this chapter and presenting our results in Chaps. 7 and 8, a brief review of the NLσM description of a superconductor is given in Sec. 6.5.

6.1. Some basics about BCS

Here only a very terse introduction to the phenomenology and the basic principles can be given; for review, see e.g. Refs. [121–123].

The electrical resistance of a superconducting material drops to zero below a certain critical temperature T_c. This most prominent feature of superconductivity is accompanied by various other characteristic effects:

- Due to the Meissner effect [46], superconductors are perfectly diamagnetic. The magnetic field is expelled from the interior of the superconductor – except for a thin surface layer whose thickness is given by the London penetration depth δ_L. One distinguishes type I and II superconductors according to the ratio of the penetration depth and the coherence length ξ [124]:

$$\kappa \sim \delta_L/\xi \qquad \begin{cases} < 1/\sqrt{2} & \text{type I,} \\ > 1/\sqrt{2} & \text{type II.} \end{cases}$$

  Pure metals are usually type I superconductors. However, disorder reduces the coherence length and may turn them into type II materials.

- Strong magnetic fields as well as strong electric currents destroy superconductivity. The critical current is determined such that it induces the critical magnetic field at the surface of the superconductor [125].

- At low temperatures, the electronic heat capacity follows an exponential law [126, 127]

$$C_{\text{el}} \sim \exp[-\frac{\Delta}{T}],$$

where Δ is the order parameter. This is a direct consequence of the energy gap in the quasi-particle spectrum. By contrast, in normal metals (and gapless superconductors!) the electronic heat capacity depends linearly on temperature.

An important step towards the understanding of superconductivity was the observation by Cooper [128] that the ground state of an electron gas becomes unstable as soon as an (arbitrarily weak) attraction between electrons exists. Then, for the electrons, it is preferable to form so-called Cooper pairs which – in the simplest case (s-wave) – consist of two electrons with opposite momenta and spins. But what could lead to an attractive interaction between equally charged particles? A hint to a possible mechanism came from the 'isotope effect' [129, 130] which made obvious that the lattice – and not the electronic system alone – is involved in the appearance of superconductivity: indeed the electron-*phonon* interaction may cause an attraction between electrons [131, 132]. In their seminal work [41] Bardeen, Cooper and Schrieffer (BCS) constructed a theory, approximating this attractive interaction by an effective potential

$$V_{\mathrm{BCS}}(\mathbf{r},\mathbf{r}';\epsilon) = \begin{cases} -g\,\delta(\mathbf{r}-\mathbf{r}') & |\epsilon| < \omega_{\mathrm{D}}, \\ 0 & |\epsilon| > \omega_{\mathrm{D}}, \end{cases} \tag{6.1}$$

where g is the BCS coupling constant, ω_{D} the Debye frequency, and the energy ϵ is measured from the Fermi energy. The corresponding BCS-Hamiltonian reads

$$\mathcal{H}_{\mathrm{BCS}} = \sum_{\sigma=\uparrow,\downarrow} \psi_\sigma^\dagger \mathcal{H}_0 \psi_\sigma - \frac{g}{2} \sum_{\sigma=\uparrow,\downarrow} \int d\mathbf{r}\, \psi_\sigma^\dagger(\mathbf{r}) \psi_{-\sigma}^\dagger(\mathbf{r}) \psi_{-\sigma}(\mathbf{r}) \psi_\sigma(\mathbf{r}),$$

where $\mathcal{H}_0$ is the Hamiltonian of the non-interacting system. Then the quartic interaction can be decoupled by introducing a pairing field or order parameter, $\Delta = g\,\langle \psi_\uparrow \psi_\downarrow \rangle$, i.e.

$$\mathcal{H}_\Delta = \sum_{\sigma=\uparrow,\downarrow} \psi_\sigma^\dagger \mathcal{H}_0 \psi_\sigma + \int d\mathbf{r}\, \left(\Delta(\mathbf{r}) \psi_\uparrow^\dagger(\mathbf{r}) \psi_\downarrow^\dagger(\mathbf{r}) + \mathrm{h.c.} \right) - \frac{1}{2g} \int d\mathbf{r}\, |\Delta|^2(\mathbf{r}). \tag{6.2}$$

The presence of a non-vanishing order parameter has important consequences. Introducing a particle-hole (PH) space, one can define the Bogoliubov-de Gennes (or Gor'kov) Hamiltonian

$$\mathcal{H}_{\mathrm{BdG}} = \begin{pmatrix} \mathcal{H}_0 & \Delta \\ \Delta^\dagger & -\mathcal{H}_0^T \end{pmatrix}_{\mathrm{PH}}. \tag{6.3}$$

If the order parameter is spatially constant[1] and the system possesses $\mathcal{T}$-invariance (i.e. $\mathcal{H}_0 = \mathcal{H}_0^T$), it is straightforward to diagonalise the above BdG-Hamiltonian. One finds the eigenvalues $\epsilon_{\mathrm{BCS}}(\mathbf{p}) = \pm(\epsilon_{\mathbf{p}}^2 + \Delta^2)^{1/2}$, where $\epsilon_{\mathbf{p}}$ are the single-particle energies of the normal system. This admits for deriving the corresponding single-particle DoS which takes the form

$$\nu_{\mathrm{BCS}}(\epsilon) = \nu_0 \frac{|\epsilon|}{\sqrt{\epsilon^2 - \Delta^2}}\, \theta(|\epsilon| - \Delta), \tag{6.4}$$

where ν_0 is the DoS in the normal state. A plot of the BCS density of states is shown in Fig. 1.3.

The spectrum has a gap of size $E_{\mathrm{gap}} = \Delta$. I.e. in a conventional bulk superconductor the order parameter Δ and the energy gap E_{gap} are the same.[2] As we will see below, this does not have to be the case in restricted or perturbed systems.

[1] Note that in this case Δ can be chosen to be real.

[2] Note that the full size of the gap is 2Δ, i.e. from $-\Delta$ to Δ. Here we concentrate on energies $\epsilon > 0$. Thus, more precisely, E_{gap} should be denoted the position of the gap edge.

The order parameter has to be determined self-consistently from the condition

$$1 = g \sum_{|\epsilon_{\mathbf{p}}|<\omega_{\mathrm{D}}} \frac{n_{\mathrm{F}}(|\epsilon_{\mathrm{BCS}}(\mathbf{p})|) - \frac{1}{2}}{|\epsilon_{\mathrm{BCS}}(\mathbf{p})|},$$

where n_{F} is the Fermi distribution function. At zero temperature, one obtains

$$\Delta(T{=}0) = 2\,\omega_{\mathrm{D}}\, e^{-2/(\nu_0 g)}.$$

Note that the order parameter is associated with a length scale which can be roughly understood as the size of a Cooper pair. For a clean superconductor the coherence length is defined as $\xi_0 = v_{\mathrm{F}}/|\Delta|$. In the 'dirty' limit, $\ell \ll \xi_0$, this has to be replaced by $\xi = \sqrt{D/(2|\Delta|)}$ (see Section 2.1).

The Gor'kov Green functions corresponding to the Hamiltonian (6.3) have a matrix structure, too:

$$\hat{G} = \begin{pmatrix} G & F \\ F^\dagger & G^\dagger \end{pmatrix}, \tag{6.5}$$

where F is the so-called anomalous Green function – which would vanish in a normal system. (The advanced/retarded index $(+/-)$ has been dropped for notational simplicity.) The Green function $\hat{G}$ obeys the Gor'kov equation

$$(\epsilon - \mathcal{H}_{\mathrm{BdG}})\, \sigma_3^{\mathrm{PH}} \hat{G}(\mathbf{r}, \mathbf{r}') = \delta(\mathbf{r} - \mathbf{r}'). \tag{6.6}$$

In general the solution to this equation is complicated. Therefore, in the following section, we consider simplifications that apply in the *quasi-classical* limit [133, 134].

6.2. The Usadel equation

As in the normal case, the single-particle Green function oscillates rapidly on the scale of the Fermi wavelength – superimposed on a slowly varying background. If the length scales one is interested in exceed λ_{F}, one can use the quasi-classical approximation which averages over the fast fluctuations and retains only the slow modes.

The Eilenberger Green function is defined as the Wigner transform of the Gor'kov Green function integrated over the kinetic energy, $\xi_p = v_{\mathrm{F}}(|\mathbf{p}| - p_{\mathrm{F}})$, i.e.

$$\hat{g}(\mathbf{n}, \mathbf{r}) \equiv \frac{i}{\pi} \int d\xi_p \int d(\mathbf{r}_1 - \mathbf{r}_2)\, \hat{G}(\mathbf{r}_1, \mathbf{r}_2) e^{-i\mathbf{p}(\mathbf{r}_1 - \mathbf{r}_2)}. \tag{6.7}$$

Then, after impurity averaging, the Gor'kov equation (6.6) can be reduced to the simpler Eilenberger equation [133]

$$v_{\mathrm{F}}\mathbf{n} \cdot \partial \hat{g}(\mathbf{n}, \mathbf{r}) = \left[i(\epsilon - \hat{\Delta}(\mathbf{r}))\sigma_3^{\mathrm{PH}} - \frac{1}{2\tau} \langle \hat{g}(\mathbf{n}', \mathbf{r}) \rangle_{\mathbf{n}'}, \hat{g}(\mathbf{n}, \mathbf{r}) \right], \tag{6.8}$$

where $\mathbf{r} = (\mathbf{r}_1 + \mathbf{r}_2)/2$ is the 'centre of mass' coordinate, $\mathbf{n} = \mathbf{p}/|\mathbf{p}|$, and $\langle \ldots \rangle_{\mathbf{n}}$ denotes an angular average. Furthermore, $\hat{\Delta} = \Re[\Delta]\, \sigma_1^{\mathrm{PH}} - \Im[\Delta]\, \sigma_2^{\mathrm{PH}}$. Note that $\hat{g}$ obeys the normalisation condition $\hat{g}^2 = \mathbb{1}$ [135, 136].

Further simplification is possible in the dirty limit, i.e. when the mean free path is shorter than the superconducting coherence length, $\ell \ll \xi$ (or $\Delta \ll \tau^{-1}$). In this limit the angular dependence of the Green function is weak and an expansion in spherical harmonics keeping only the first two terms is a good approximation:

$$\hat{g}(\mathbf{n}, \mathbf{r}) \simeq \hat{g}_0(\mathbf{r}) + \mathbf{n} \cdot \hat{\mathbf{g}}_1(\mathbf{r}), \tag{6.9}$$

where $\hat{g}_0 \gg \mathbf{n} \cdot \hat{\mathbf{g}}_1$. By means of Eq. (6.8), supplemented with the normalisation condition, the first harmonic $\hat{\mathbf{g}}_1$ can be expressed through $\hat{g}_0$ as $\hat{\mathbf{g}}_1(\mathbf{r}) = -\ell\, \hat{g}_0(\mathbf{r}) \partial \hat{g}_0(\mathbf{r})$. After averaging over $\mathbf{n}$, this leads to the *Usadel equation* [137], expressed in terms of the zeroth harmonic $\hat{g}_0$ only,

$$D\partial(\hat{g}_0 \partial \hat{g}_0) + [i\epsilon\sigma_3^{\mathrm{PH}} - \Delta(\mathbf{r})\sigma_2^{\mathrm{PH}}, \hat{g}_0] = 0, \tag{6.10}$$

where $\hat{g}_0^2 = \mathbb{1}$. In order to solve this equation, appropriate boundary conditions have to be specified.

As we will see below, a generalised Usadel equation appears as the saddle point equation of the NLσM. Let us, however, first discuss the mechanism of gap suppression as described by the AG theory.

6.3. The Abrikosov-Gork'ov theory of gapless superconductivity

As discussed in the Sec. 6.1, the density of states of a bulk s-wave superconductor exhibits a quasi-particle energy gap and a singularity at the gap edge (see Fig. 1.3). This form of the DoS was obtained by diagonalising the BdG-Hamiltonian. In fact, these considerations are not limited to the clean case. Even in the presence of disorder the BdG-Hamiltonian can be diagonalised, yielding $\epsilon'_{\mathrm{BCS}}(\mathbf{p}) = \pm(\epsilon'^2_{\mathbf{p}} + \Delta^2)^{1/2}$, where $\epsilon'_{\mathbf{p}}$ are the single-particle energies of the normal *disordered* system – which do not change much as compared to the clean system. Therefore, the gap structure remains. This is the content of the Anderson theorem [8]: The gap is robust with respect to addition of non-magnetic impurities. In fact, this statement can be formulated in a more general way: The DoS is unaffected as long as the two conditions given in Sec. 6.1 are valid – namely a) the system is $\mathcal{T}$-invariant and b) the order parameter is constant.

By contrast, the integrity of the gap is destroyed by the pair-breaking effect of time-reversal symmetry breaking perturbations. The phenomenology of gap suppression is described by the Abrikosov-Gor'kov theory [42]. Before superconductivity is completely destroyed, the system enters a gapless phase.

Now what is gapless superconductivity? The order parameter Δ corresponds to the wavefunction of the condensate of Cooper pairs while the gap energy E_{gap} describes the binding energy of Cooper pairs. In an unperturbed bulk superconductor – as can be seen from Eq. (6.4) – the two do not have to be distinguished. However, here this becomes important. The order parameter determines the characteristic features of superconductivity, namely the vanishing of the electrical resistance and the Meissner effect. On the other hand, the energy gap is responsible for e.g. the low-temperature heat capacity, thermal conductivity and absorption of electromagnetic radiation, see Ref. [48]. Thus, these secondary characteristics may be very different in a gapless superconductor whereas the defining properties remain.

A theoretical description of the suppression of the energy gap and the order parameter by paramagnetic impurities is provided by the AG theory. Magnetic impurities can be incorporated into the Hamiltonian through the term $\mathcal{H}_s = J\mathbf{S} \cdot \sigma^{\mathrm{SP}}$, where σ^{SP} is a vector of Pauli matrices

in spin space. For simplicity, we consider – as for the normal disorder – a Gaussian white noise distribution, $J^2\langle S_\alpha(\mathbf{r})S_\beta(\mathbf{r}')\rangle = (6\pi\nu\tau_s)^{-1}\delta(\mathbf{r}-\mathbf{r}')\delta_{\alpha\beta}$. Calculating the renormalisation of the (Matsubara) energy, $\epsilon_n \to \tilde{\epsilon}_n$, and the order parameter, $\Delta \to \tilde{\Delta}$, in Born approximation yields the coupled equations [42]

$$\epsilon_n = \tilde{\epsilon}_n\Big(1 - \frac{1}{2\tau_s}\frac{1}{\sqrt{\tilde{\epsilon}_n^2+\tilde{\Delta}^2}}\Big), \qquad \Delta = \tilde{\Delta}\Big(1 + \frac{1}{2\tau_s}\frac{1}{\sqrt{\tilde{\epsilon}_n^2+\tilde{\Delta}^2}}\Big).$$

With $u_n \equiv \tilde{\epsilon}_n/\tilde{\Delta}$, these equations can be combined into

$$\frac{\epsilon_n}{\Delta} = u_n\left(1 - \zeta\frac{1}{\sqrt{1+u_n^2}}\right), \tag{6.11}$$

where $\zeta = 1/(\tau_s\Delta)$. Or, switching to real frequencies,

$$\frac{\epsilon}{\Delta} = u\left(1 - \zeta\frac{1}{\sqrt{1-u^2}}\right).$$

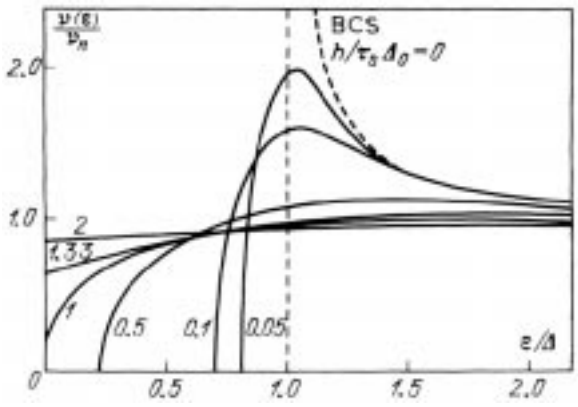

Figure 6.1.: Density of states for various values of the Abrikosov-Gor'kov parameter ζ (picture taken from Ref. [48]).

Unfortunately, there is no simple closed solution to this equation. However, much of its behaviour is known. At $\zeta = 1$, the system undergoes a crossover from a gapped phase with

$$E_{\text{gap}} = \Delta(1-\zeta^{2/3})^{3/2} \tag{6.12}$$

to a gapless phase. Close to the gap edge, the density of states, $\nu(\epsilon) = \nu_0\zeta^{-1}\Im[u]$, has the following form:

$$\frac{\nu(\epsilon)}{\nu_0} = \sqrt{\frac{2}{3}}\,\zeta^{-2/3}(1-\zeta^{2/3})^{-1/4}\sqrt{\frac{\epsilon - E_{\text{gap}}}{\Delta}}\;\theta(\epsilon - E_{\text{gap}}). \tag{6.13}$$

I.e. the AG theory predicts a hard gap with a square-root singularity. Furthermore, the gap suppression is governed by a single dimensionless parameter characterising the strength of the perturbation. As we will see below, various physical mechanisms lead to the same phenomenology of gap suppression – differing only by the respective expression for the parameter ζ. The DoS for different values of ζ is shown in Fig. 6.1.

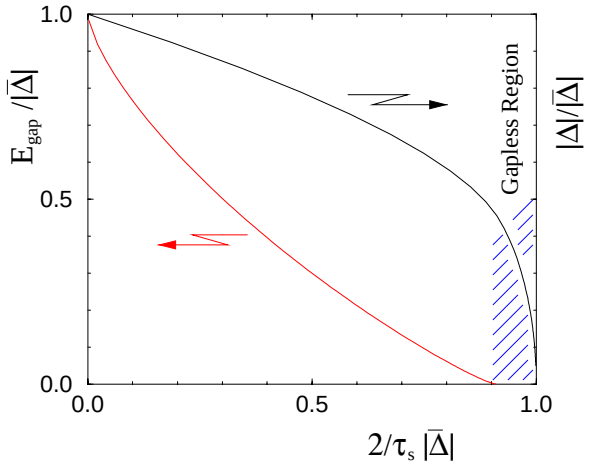

Figure 6.2.: Suppression of the energy gap $E_{\rm gap}$ and the order parameter Δ with increasing ζ (picture taken from Ref. [45]).

At $T = 0$, using Eq. (6.11), the self-consistency equation can be written in the form

$$1 \;=\; \frac{g}{\delta}\int_0^{\omega_{\rm D}} \frac{d\epsilon}{\Delta}\frac{1}{\sqrt{1+u^2}} = \frac{g}{\delta}\int_{u_0}^{\omega_{\rm D}/\Delta} du\left(1-\zeta(1+u^2)^{-3/2}\right)\frac{1}{\sqrt{1+u^2}},$$

where the lower limit is defined as $u_0 = \sqrt{\max\{0,\zeta^2-1\}}$. Carrying out the integration yields

$$\ln\frac{\Delta}{\Delta_0} = \begin{cases} -\dfrac{\pi}{4}\zeta & \zeta \le 1, \\ \operatorname{arcosh}\zeta - \dfrac{1}{2}\left(\zeta\arcsin\dfrac{1}{\zeta} - \sqrt{1-\dfrac{1}{\zeta^2}}\right) & \zeta > 1. \end{cases}$$

The onset of the gapless phase occurs at $\zeta = 1$, where $\Delta = 1/\tau_s = \Delta_0 e^{-\pi/4}$. On the other hand, superconductivity is ultimately destroyed at $1/\tau_s = \Delta_0/2$. Thus, the gapless region arises at 91% of the critical concentration of magnetic impurities. The dependence of Δ and $E_{\rm gap}$ on the pair breaking AG parameter is contrasted in Fig. 6.2.

6.4. Lifshitz tails in semiconductors

Before coming to the field theoretic description of a superconductor, let us make a detour and consider band-tail states in semiconductors. Below we will see that the hard energy gap predicted by the Abrikosov-Gor'kov mean-field theory is destroyed by fluctuations. Instead 'sub-gap' states appear, and, thus, the density of states acquires tails within the gap region [44, 138]. The appearance of these tail states bears resemblance to the case of Lifshitz tails in semiconductors [50–52]. To understand this analogy and even more important to see why it is to some extent only superficial, Lifshitz band-tails are briefly discussed here.

Using the supersymmetric field integral introduced in Sec. 2.3.1, the single-particle Green function can be obtained from the generating functional

$$\mathcal{Z} = \int D[\Psi,\bar{\Psi}]\; e^{\,i\int d\mathbf{r}\,\bar{\Psi}\left(\epsilon^+ - \frac{\hat{\mathbf{p}}^2}{2m} - V(\mathbf{r})\right)\Psi}.$$

Here again the random potential V is drawn from a Gaussian white noise distribution.

By minimising the action with respect to the fields Ψ and the potential V, one can search for 'optimal fluctuations'. This amounts to seeking inhomogeneous solutions of the non-linear Schrödinger equation

$$\Big(\epsilon - \frac{1}{2m}\hat{\mathbf{p}}^2 - V(\mathbf{r})\Big)\Psi = 0, \tag{6.14}$$

where the optimal potential is given by the self-consistency relation

$$V(\mathbf{r}) = -\frac{1}{2\pi\nu\tau}\left|\Psi(\mathbf{r})\right|^2. \tag{6.15}$$

Thus, the tail states are generated by rare configurations of the impurity potential which possess unusually low and uniform regions. In these deep minima, bound states with very low energy can exist.

For the density of states in the tails of the band, one obtains to exponential accuracy

$$\nu(\epsilon) \sim \exp\left[-\text{const.} \times |\epsilon|^{2-d/2}\right].$$

The exponent $\alpha_0 = 2$ is characteristic for Lifshitz tails in a Gaussian potential. Assuming a different distribution of the random potential yields a different exponent [139], i.e. the result depends sensitively on the distribution.

In the supersymmetric description of the problem [53], the inhomogeneous Ψ-field configurations correspond to inhomogeneous 'instanton' solutions of the saddle point equation which are non-symmetric in the boson-fermion space. This "supersymmetry breaking" is crucial[3] because it entails a finite action and, therefore, the anticipated exponentially small contribution to the DoS.

6.5. NLσM for the superconducting system

A diagrammatic description of a superconductor proves more difficult than of a normal system due to the interplay of various mechanisms of quantum interference. Furthermore, we are going to investigate non-perturbative effects. Thus, to construct a field theory is the only viable approach. The field theory approach to weakly disordered systems [61, 140, 141] has been discussed in Sec. 2.3.1. Its extension to the consideration of disordered superconducting systems follows straightforwardly [142–145].

As pointed out earlier, symmetries play an important role in determining the properties of a given system. The BdG-Hamiltonian possesses the following symmetry[4] which is reflected in the Green function:

$$\mathcal{H}_{\text{BdG}} = -\sigma_2^{\text{PH}}\mathcal{H}_{\text{BdG}}^T\sigma_2^{\text{PH}} \quad \Rightarrow \quad \hat{G}^{\pm}(\epsilon) = -\sigma_2^{\text{PH}}\left[\hat{G}^{\mp}(-\epsilon)\right]^T\sigma_2^{\text{PH}}. \tag{6.16}$$

The symmetry relation imposed on the Green function has important consequences: As retarded and advanced Green function can be transformed into one another, the introduction of an

[3] The expression "supersymmetry breaking" is a slight misuse of terminology: The non-supersymmetric saddle point is not unique but belongs to a degenerate saddle point manifold that ensures the global supersymmetry.

[4] A Hamiltonian with this symmetry belongs to symmetry class C. If, furthermore, the system is $\mathcal{T}$-invariant, $\mathcal{H}_{\text{BdG}} = \mathcal{H}_{\text{BdG}}^T$, the Hamiltonian belongs to the higher symmetry class CI. See also Sec. 7.3.

advanced-retarded space is unnecessary. This implies, too, that the Green function is now a much more complex object – comparable to G^+G^- in the normal case.

Furthermore, the band centre $\epsilon = 0$ turns out to be special. The low-energy physics is governed by soft so-called C-modes. A finite energy breaks the particle-hole symmetry and renders these modes massive. Thus, as far as the density of states is concerned, the existence of an energy gap makes the soft modes ineffective – above the gap edge the minimal mass of these C-fluctuations is set by $\epsilon > \Delta$. Therefore, in a conventional superconductor, novel effects arising from different symmetry classes do not play a significant role [145]. This changes drastically when considering e.g. d-wave superconductors [146], proximity SN structures [145] – or gapless superconductors which we study here.

In developing an effective field theory of the superconducting system, two subsequent saddle point approximations are necessary. As in the normal system the first saddle point approximation is stabilised by the large parameter $\epsilon_F\tau$ (quasi-classical limit). Due to a separation of energy scales in the dirty limit, $|\Delta| \ll 1/\tau$, at this stage the order parameter can be neglected. Then the second saddle point approximation incorporates the rotation from the conventional saddle point to the new solution for the superconductor.

Instead of a time-reversal (TR) space, here it is convenient to introduce a charge conjugation (CC) space. The particle-hole symmetry (6.16) of the BdG-Hamiltonian implies

$$\begin{aligned}
\bar\psi(\epsilon - \mathcal{H}_{\rm BdG})\psi &= \frac{1}{2}\left(\,\bar\psi(\epsilon - \mathcal{H}_{\rm BdG})\psi + \psi^T(\epsilon - \mathcal{H}_{\rm BdG}^T)\bar\psi^T\,\right) = \\
&= \frac{1}{2}\left(\,\bar\psi(\epsilon - \mathcal{H}_{\rm BdG})\psi + \psi^T(\epsilon + \sigma_2^{\rm PH}\mathcal{H}_{\rm BdG}\sigma_2^{\rm PH})\bar\psi^T\,\right) = \\
&= \frac{1}{2}\begin{pmatrix}\bar\psi & i\psi^T\sigma_2^{\rm PH}\end{pmatrix}\begin{pmatrix}\epsilon - \mathcal{H}_{\rm BdG} & \\ & -\epsilon - \mathcal{H}_{\rm BdG}\end{pmatrix}\begin{pmatrix}\psi \\ i\sigma_2^{\rm PH}\bar\psi^T\end{pmatrix} \equiv \\
&\equiv \bar\Psi(\epsilon\sigma_3^{\rm CC} - \mathcal{H}_{\rm BdG})\Psi,
\end{aligned}$$

where $\psi^T = (\psi_\uparrow^T, \bar\psi_\downarrow)$ and the last line defines vector fields $\Psi, \bar\Psi$. Furthermore, $\sigma_3^{\rm CC}$ is a Pauli matrix in the newly introduced charge conjugation space.

Our starting point is the representation of the generating functional as a supersymmetric path integral,

$$\mathcal{Z} = \int D[\Psi, \bar\Psi]\; e^{-i\int d\mathbf{r}\,\bar\Psi(\epsilon\sigma_3^{\rm CC} - \mathcal{H}_{\rm BdG})\Psi}. \tag{6.17}$$

Following the same steps as in the normal case of disorder averaging, applying a Hubbard-Stratonovich transformation and integrating out the Ψ-fields, one obtains the Q-field action

$$S[Q] = -\frac{\pi\nu_0}{8\tau}\int d\mathbf{r}\ {\rm Str}\, Q^2 + \frac{1}{2}\int d\mathbf{r}\ {\rm Str}\,\ln\hat{\mathcal{G}}^{-1},$$

where $\hat{\mathcal{G}}^{-1} = (\mathcal{H}_{\rm BdG}(V=0) - \epsilon\sigma_3^{\rm CC})\,\sigma_3^{\rm PH} + i/(2\tau)\,Q$, and the 8×8 Q-supermatrices obey the symmetry constraint $Q = \sigma_1^{\rm PH}\otimes\gamma\, Q^T(\sigma_1^{\rm PH}\otimes\gamma)^T$ with $\gamma = \sigma_1^{\rm CC}\otimes E_{\rm BB} - i\sigma_2^{\rm CC}\otimes E_{\rm FF}$.

A first saddle point approximation, setting $\epsilon = \Delta = 0$, yields $Q_{\rm SP} = \sigma_3^{\rm PH}\otimes\sigma_3^{\rm CC}$. Performing a gradient expansion around this saddle point and expanding the action up to linear order in ϵ and Δ leads to the effective action

$$S[Q] = -\frac{\pi\nu}{8}\int d\mathbf{r}\ {\rm Str}\,\left[D(\partial Q)^2 - 4(i\epsilon\sigma_3^{\rm PH}\otimes\sigma_3^{\rm CC} - \Delta\sigma_2^{\rm PH})Q\right]. \tag{6.18}$$

Now, subjecting this action to a further saddle point analysis obtains a modified saddle point equation,

$$D\partial(Q\partial Q) - [i\epsilon\sigma_3^{\mathrm{PH}} \otimes \sigma_3^{\mathrm{CC}} - \Delta\sigma_2^{\mathrm{PH}}, Q] = 0 \tag{6.19}$$

which is a generalisation of the Usadel equation (6.10).

As a simple example, let us discuss the solution of Eq. (6.19) for a bulk superconductor. The Ansatz

$$Q = \cosh\hat{\theta}\sigma_3^{\mathrm{PH}} \otimes \sigma_3^{\mathrm{CC}} + i\sinh\hat{\theta}\sigma_2^{\mathrm{PH}}, \qquad \text{where } \hat{\theta} = \begin{pmatrix} \theta_{\mathrm{B}} & \\ & i\theta_{\mathrm{F}} \end{pmatrix}$$

homogeneous, yields $\theta_{\mathrm{B}} = i\theta_{\mathrm{F}} = \operatorname{arcoth}(\epsilon/\Delta)$ [145], i.e. the order parameter rotates the saddle point away from $\sigma_3^{\mathrm{PH}} \otimes \sigma_3^{\mathrm{CC}}$. At the band centre, $\epsilon = 0$, one obtains the 'orthogonal' solution, $Q = \sigma_2^{\mathrm{PH}}$, while for large energies the result approaches the normal saddle point.

Self-consistency may be taken into account using the replica formalism. This becomes crucial for inhomogeneous superconductors as we will see in chapter 8. To do so, one starts from the replicated action

$$S[\psi^a] = \int d\mathbf{r} \sum_{n\sigma} \bar{\psi}^a_{n\sigma}(i\epsilon_n - \mathcal{H}_0)\psi^a_{n\sigma} + S_I[\psi^a], \tag{6.20}$$

where ψ^a represent Grassmann fields, $\epsilon_n = (2n+1)\pi/\beta$ fermionic Matsubara frequencies, and

$$S_I[\psi^a] = g\int_0^\beta d\tau \int d\mathbf{r}\ \bar{\psi}^a_\uparrow \bar{\psi}^a_\downarrow \psi^a_\downarrow \psi^a_\uparrow. \tag{6.21}$$

As usual, to account for the symmetry properties of the system, one enlarges the field space by incorporating a particle-hole as well as a charge conjugation sector. This introduces the four-component fields $\Psi^{aT} = (\psi^a_\uparrow, \bar{\psi}^a_\downarrow, \psi^a_\downarrow, -\bar{\psi}^a_\uparrow)/\sqrt{2}$. Decoupling the quartic BCS interaction with the introduction of the order parameter $\Delta(\mathbf{r})$ (chosen to be real), the total action assumes the canonical form

$$S[\Psi^a] = \int d\mathbf{r} \sum_n \bar{\Psi}^a_n(i\epsilon_n\sigma_3^{\mathrm{CC}} - \mathcal{H}_{\mathrm{BdG}})\Psi^a_n + \frac{1}{g}\int_0^\beta d\tau \int d\mathbf{r}\, \Delta^2(\mathbf{r},\tau), \tag{6.22}$$

where $\mathcal{H}_{\mathrm{BdG}}$ represents the BdG-Hamiltonian (6.3) defined above.

Following the standard route, one obtains the non-linear σ-model action [63, 142–145]

$$\begin{aligned} S[Q,\Delta] \;=\; & \frac{1}{g}\int d\mathbf{r} \int_0^\beta d\tau\, \Delta^2(\mathbf{r},\tau) + \\ & + \frac{\pi\nu_0}{8}\int d\mathbf{r}\ \mathrm{tr}\left[D(\partial Q)^2 - 4(\hat{\epsilon}\sigma_3^{\mathrm{PH}} \otimes \sigma_3^{\mathrm{CC}} + \Delta\sigma_2^{\mathrm{PH}})Q\right], \end{aligned} \tag{6.23}$$

where $[\hat{\epsilon}]_{nm} = \epsilon_n\delta_{nm}$. Furthermore, $Q^2 = \mathbb{1}$, and the Hermitian matrices Q obey the the symmetry relation $Q = \sigma_1^{\mathrm{PH}} \otimes \sigma_1^{\mathrm{CC}} Q^T \sigma_1^{\mathrm{PH}} \otimes \sigma_1^{\mathrm{CC}}$. Note that the fields carry replica (a,b) as well as Matsubara (n,m) indices, i.e. $Q = Q^{ab}_{nm}$.

Finally, the self-consistency equation – which obtains from varying the action (6.23) with respect to Δ – reads

$$\Delta = \frac{\pi\nu_0 g}{4\beta}\,\mathrm{tr}\,[\sigma_2^{\mathrm{PH}}Q] = \frac{\pi\nu_0 g}{\beta}\sum_n \sin\theta_n. \tag{6.24}$$

7. Thin superconducting films in strong in-plane magnetic fields

As discussed in Sec. 6.3, time-reversal symmetry breaking perturbations may drastically change the energy spectrum of a conventional dirty superconductor and lead to the occurrence of gapless superconductivity. The most common mechanism for breaking $\mathcal{T}$-invariance is to apply an external magnetic field H. However, in a bulk superconductor the Meissner effect [46] screens out the field, except for a thin surface layer. Thus, a – not too strong – magnetic field does not significantly affect the properties of a bulk superconductor. The situation is completely different for a thin film of thickness d smaller than the London penetration depth. Then the field penetration is almost complete and the magnetic field distinctly modifies the electronic properties of the system.

In the following, we consider – as in chapter 5 – the influence of a *parallel* magnetic field. In Sec. 7.1, we study how the results for magnetic impurities translate to thin films in parallel fields. Subsequently, in Secs. 7.2 and 7.3, we search for manifestations of the Berry-Robnik symmetry effect – obtained above for normal systems – in the superconducting case. To do so, a diffusive film with δ-correlated disorder is contrasted to a film with columnar defects and a symmetric confining potential.

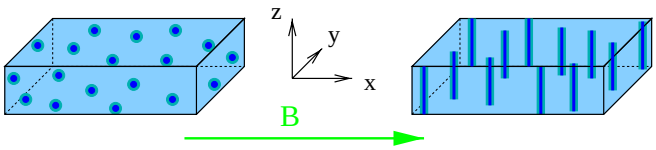

Figure 7.1.: Schematic picture of a thin film with δ-correlated disorder (left) and columnar defects (right).

Before looking at the analysis in more detail, let us briefly summarise our findings. On the mean-field level, the parallel field effect on both, thin films with δ-correlated disorder as well as thin films with columnar defects, is well described by the Abrikosov-Gor'kov theory. The parameter governing the suppression of the energy gap is given by $\zeta \sim D(Hd)^2/\Delta \sim \Phi_{d\xi}^2$, where $\Phi_{d\xi}$ is the flux through an area perpendicular to the field spanned by the width of the film and the superconducting coherence length. Within the gapped phase, as in the case of magnetic impurities [44, 45], the hard square-root edge of the mean-field solution is untenable due to the absence of an Anderson theorem. Exponentially small tails of the density of states in the sub-gap region can be associated with inhomogeneous instanton or bounce solutions of the mean-field equations as will be discussed in Sec. 7.1.2. In the vicinity of the gap edge E_{gap}, the energy scaling of these tails is universal [45], depending only on the distance from E_{gap}, the

dimensionless parameter ζ and the dimensionality. In $2d$, on obtains

$$\nu(\epsilon < E_{\rm gap}) \sim \exp\left[-a_2(\zeta)\nu_0 D\,\frac{E_{\rm gap}-\epsilon}{\Delta}\right], \tag{7.1}$$

where a_2 is a known dimensionless function of the control parameter. Note that this result is non-perturbative in the inverse dimensionless conductance $1/(\nu_0 D)$.

Within the gapless phase, as will be shown in Sec. 7.3, novel features related to the different symmetry classes arise. The presence or absence of the fundamental symmetries, namely time-reversal and spin-rotation, manifests itself in the low-energy behaviour of the density of states. As in the normal case, we will find signatures of the Berry-Robnik phenomenon [119].

7.1. Diffusive film

The magnetic field induces a Zeeman splitting and it couples to the orbital motion of the electrons. Both effects suppress superconductivity. Whereas in a bulk system the orbital effect usually dominates, in very thin films the opposite situation arises. The crossover can be estimated in the following way [147]: The critical magnetic field associated with the orbital effect is roughly determined by the condition that the flux threading an area spanned by the coherence length is of the order of one flux quantum, $H_{c2}\xi^2 \simeq \phi_0$. Now, if $d \ll \xi$, this has to be replaced by $H_{c2}^{\parallel}\xi d \simeq \phi_0$, i.e. the orbital critical field increases. The Zeeman critical field H_Z is independent of the width of the system. H_Z is obtained from the condition that the energy splitting between up($\uparrow$)- and down($\downarrow$)-spins is roughly of the size of the order parameter, $g_L\mu_B H_Z \simeq \Delta$, where g_L is the Landé g-factor and $\mu_B = e/(2m)$ the Bohr magneton. Comparing the two equations, $H_{c2} \simeq \phi_0/(\xi d)$ and $H_Z \simeq \Delta/(g_L\mu_B)$, leads to the conclusion that the orbital effect is dominant in suppressing superconductivity, i.e. $H_{c2}^{\parallel} < H_Z$, as long as $d > \frac{1}{2} g_L\,\lambda_{\rm F}\xi/\ell$. Here we restrict attention to this case. To be more specific, we consider a system, where the length scales are arranged in the following hierarchy:

$$\lambda_{\rm F} \ll d, \ell \ll \xi. \tag{7.2}$$

The inequality $\lambda_{\rm F} \ll \ell$ defines the quasi-classical limit while $\ell \ll \xi$ is the condition for the dirty limit. Finally, $\lambda_{\rm F} \ll d$ implies that the subband splitting due to size quantisation is small and many subbands are occupied. Thus, as far as the fast momenta are concerned, the system is effectively three-dimensional.

The most generic case to study is a thin film with just a 'normal' δ-correlated white noise disorder potential. We are interested in the limit, where – in addition to the conditions (7.2) specified above – $\ell \ll d$ which implies diffusive motion in all three directions.

The starting point for our analysis is the conventional NLσM for a three-dimensional system subject to a magnetic field, derived in Sec. 6.5,

$$S[Q] = -\frac{\pi\nu_0}{8}\int d^3r\ {\rm Str}\left[D(\tilde{\partial}Q)^2 - 4(i\epsilon\sigma_3^{\rm PH}\otimes\sigma_3^{\rm CC} - \Delta\sigma_2^{\rm PH})Q\right], \tag{7.3}$$

where $\tilde{\partial} = \partial - i\mathbf{A}[\sigma_3^{\rm PH},\ .\ ]$ and $\mathbf{A} = -Hz\mathbf{e}_y$.

The typical scale of variation of the Q-fields is set by the coherence length. Thus, as $d \ll \xi$, the matrices Q are constant along the z-direction. Then, the z-integration can be performed

explicitly:

$$\frac{1}{d}\int_{-d/2}^{d/2} dz\,\mathbf{A}=0, \qquad \frac{1}{d}\int_{-d/2}^{d/2} dz\,A^2=\frac{1}{12}(Hd)^2.$$

Accordingly,

$$S=-\frac{\pi\nu_0 d}{8}\int d^2r\ \mathrm{Str}\left[D(\partial Q)^2-\frac{\alpha}{2}[\sigma_3^{\mathrm{PH}},Q]^2-4(i\epsilon\sigma_3^{\mathrm{PH}}\otimes\sigma_3^{\mathrm{CC}}-\Delta\sigma_2^{\mathrm{PH}})Q\right], \tag{7.4}$$

where $\alpha=\frac{1}{6}D(Hd)^2$.

Note that the gauge choice is important here. The physical gauge to choose is the London gauge: $\nabla\cdot\mathbf{A}=0$ and $A_z(\pm d/2)=0$. Both conditions are fulfilled by $\mathbf{A}=-Hz\mathbf{e}_y$. In a superconductor the vector potential is associated with a supercurrent $\mathbf{j}_s=n_s\mathbf{A}/m$, where n_s is the density of Cooper pairs. The first condition tells us that no net current is generated while the second condition does not allow a supercurrent to flow through the superconductor-vacuum boundary.

Thus, when integrating out z, we have fixed the gauge, i.e. the resulting action is not gauge invariant. Therefore, the magnetic field does not appear within a covariant derivative, but as an additional diamagnetic term $\sim\alpha[\sigma_3^{\mathrm{PH}},Q]^2$. This distinguishes the "thick" film, $d\gg\lambda_{\mathrm{F}}$, from the single-channel case, where the magnetic field can be gauged out and, thus, has no influence – as emphasised in chapter 5.

7.1.1. Mean-field analysis

The mean-field density of states is obtained by subjecting the action (7.4) to a saddle point analysis. Varying this action with respect to Q yields the saddle point equation

$$D\partial(Q\partial Q)-\frac{\alpha}{2}[\sigma_3^{\mathrm{PH}}Q\sigma_3^{\mathrm{PH}},Q]-[i\epsilon\sigma_3^{\mathrm{PH}}\otimes\sigma_3^{\mathrm{CC}}-\Delta\sigma_2^{\mathrm{PH}},Q]=0. \tag{7.5}$$

This is the Usadel equation – see Eq. (6.19) – supplemented by an additional term due to the parallel magnetic field. With the Ansatz of Sec. 6.5, namely $Q=\cosh\hat{\theta}\,\sigma_3^{\mathrm{PH}}\otimes\sigma_3^{\mathrm{CC}}+i\sinh\hat{\theta}\,\sigma_2^{\mathrm{PH}}$, one obtains

$$D\partial^2\hat{\theta}-2i(\epsilon\sinh\hat{\theta}-\Delta\cosh\hat{\theta})-\alpha\sinh(2\hat{\theta})=0. \tag{7.6}$$

Assuming that θ is homogeneous and defining

$$\tilde{\epsilon}=\epsilon-\frac{i}{2}\alpha\cosh\hat{\theta}, \qquad \tilde{\Delta}=\Delta+\frac{i}{2}\alpha\sinh\hat{\theta},$$

the equation for $\tilde{\epsilon},\tilde{\Delta}$ takes the form of the BCS solution, $\tilde{\epsilon}/\tilde{\Delta}=\coth\theta$. Then, in terms of the 'bare' ϵ,Δ, the saddle point equation (7.6) can be brought to the conventional AG form,

$$\frac{\epsilon}{\Delta}=u\left(1-\zeta\frac{1}{\sqrt{1-u^2}}\right), \tag{7.7}$$

where $u\equiv\coth\theta$. Here the parameter governing the suppression of the energy gap is given as $\zeta=\alpha/\Delta$ [148], and $E_{\mathrm{gap}}=\Delta(1-\zeta^{2/3})^{3/2}$.

Finally, the density of states obtains as

$$\nu(\epsilon) \;=\; \frac{\nu_0}{8}\int\frac{d\mathbf{r}}{V}\,\Re\,\langle\,\mathrm{Str}\,[\sigma_3^{\mathrm{BF}}\otimes\sigma_3^{\mathrm{PH}}\otimes\sigma_3^{\mathrm{CC}}\,Q(\mathbf{r})]\rangle_Q \;=\; \nu_0\,\Re[\cosh\theta]. \tag{7.8}$$

Inserting the solution determined by Eq. (7.7), this yields the characteristic AG density of states with a square-root edge in the gapped phase.

The form of the parameter ζ has a simple intuitive explanation: Rewriting ζ in terms of the coherence length yields $\zeta = (Hd\xi)^2/3$. Now $\Phi_{d\xi} = Hd\xi$ is the flux (in units of the flux quantum ϕ_0) through an area perpendicular to the field spanned by the thickness of the film and the coherence length. Then, the gapless phase occurs when $\Phi_{d\xi} = \mathcal{O}(1)$. Coming back to our estimate of critical fields at the beginning of this chapter, it is just a numerical factor that makes the onset of gapless superconductivity happen before the complete destruction of superconductivity, see also Sec. 6.3.

7.1.2. Inhomogeneous saddle points and sub-gap states

As we have seen, the mean-field AG result predicts a square-root singularity at the gap edge. In the magnetic field case, it has been shown recently [44, 45] that this hard edge is, in fact, untenable, but destroyed by fluctuations. – In the absence of an Anderson theorem there is nothing to protect the hard gap. Instead, within the gap region the DoS develops exponentially small tails that correspond to 'droplets' of localised states.

The procedure by which these tails are obtained from the NLσM has been described in detail in Ref. [45]: The saddle point equation (7.6) has – in addition to the homogeneous AG solution, θ_{AG} – an inhomogeneous instanton or bounce solution, $\theta(\mathbf{r})$. In two dimensions, this solution cannot be found explicitly. Thus, for didactic reasons, let us start with the one-dimensional problem, where an analytical solution is available, and then generalise the results to the $2d$ case relevant here.

In order to investigate inhomogeneous solutions, we first have to understand the homogeneous solution in more detail. As the mean-field DoS vanishes below the gap edge (i.e. $\nu_{\mathrm{MF}}(\epsilon < E_{\mathrm{gap}}) = \nu_0\,\Re[\cosh\theta_{\mathrm{AG}}] = 0$), one knows that the mean-field solution of the Abrikosov-Gor'kov equation satisfies the condition $\theta_{\mathrm{AG}}(\epsilon < E_{\mathrm{gap}}) = \phi_{\mathrm{AG}}(\epsilon) + i\pi/2$, where $\phi_{\mathrm{AG}}(\epsilon)$ is real.

Now, instead of analysing the saddle point equation, it is more convenient to study its first integral

$$\xi^2(\partial\hat{\theta})^2 + V(\hat{\theta}) = \text{const.}\,, \tag{7.9}$$

where the potential is given by

$$V(\hat{\theta}) = 2i(\sinh\hat{\theta} - \frac{\epsilon}{\Delta}\cosh\hat{\theta}) - \frac{\zeta}{2}\cosh(2\hat{\theta}). \tag{7.10}$$

Inspection of the potential (7.10) shows that along the line $\theta = \phi + i\pi/2$ the potential $V_R(\phi) = V(\phi + i\pi/2)$ is *real* with a functional dependence on ϕ shown in Fig. 7.2 for different energies. The homogeneous saddle point sits at the maximum of this potential. At $\epsilon = 0$, it belongs to the fermionic contour ($\theta_{\mathrm{AG}} = i\pi/2$) and the potential is symmetric around $\phi = 0$. The bosonic contour can be deformed smoothly to include the saddle point. By increasing the energy, the saddle point moves away from the imaginary axis on the line $\theta_{\mathrm{AG}} = i\pi/2 + \phi_{\mathrm{AG}}$ – where the DoS vanishes – until the energy reaches E_{gap} and the imaginary part of θ_{AG} starts to deviate from

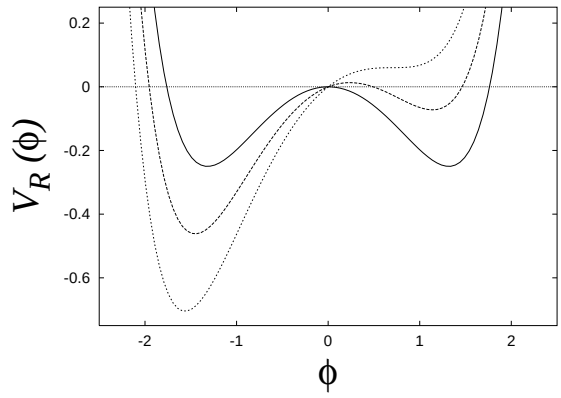

Figure 7.2.: Real potential V_R as a function of ϕ along the line $\theta = i\pi/2 + \phi$ for $\epsilon = 0, E_{\rm gap}/2, E_{\rm gap}$. At $\epsilon = E_{\rm gap}$ the maximum and the minimum merge.

$\pi/2$ implying a finite DoS. Now both contours have to be deformed smoothly (for a discussion see, e.g., Ref. [145]). Following the behaviour of the potential, one notices that, upon increasing ϵ, one minimum deepens while the other becomes more and more shallow until merging with the maximum at $\epsilon = E_{\rm gap}$.

In addition to the homogeneous Abrikosov-Gor'kov solution, the potential above admits for a bounce solution $\phi_{\rm AG} \to \phi_{\rm max}(> \phi_{\rm AG}) \to \phi_{\rm AG}$, where $V_R(\phi_{\rm max}) = V_R(\phi_{\rm AG})$. In principle, as can be seen from Fig. 7.2, this is not the only inhomogeneous solution. However, a bounce solution towards negative values of ϕ always involves a larger action and its contribution is, therefore, negligible. For $\Im[\theta] \neq \pi/2$ the imaginary part of the potential is finite, in general, and solutions which leave $\Im[\theta] = \pi/2$ can be excluded; see Ref. [45].

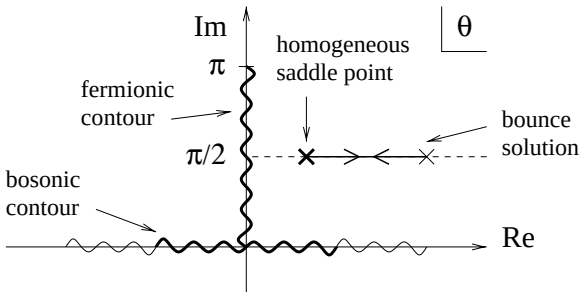

Figure 7.3.: Bosonic and fermionic integration contours. Furthermore, the homogeneous saddle point and the bounce solution are shown.

In Fig. 7.3 the integration contours are shown. Each saddle point separately is accessible from the bosonic as well as the fermionic contour by smooth deformations. However, only the bosonic contour can be deformed smoothly as to pass through *both* saddle points. Thus, on the level of the saddle point supersymmetry is broken. In fact, this had to be expected because, in order to obtain an exponentially small contribution to the density of states, a finite action is required. However, taken on its own this would violate the normalisation condition $\mathcal{Z} = 1$. Therefore, one expects a zero-mode in boson-fermion space restoring the symmetry.

The action for the instanton assumes the form

$$S_{\text{inst.}} = 4\pi\nu_0\Delta\xi \int_{\phi_{\text{AG}}}^{\phi_{\max}} d\phi\, \sqrt{V_R(\phi_{\text{AG}}) - V_R(\phi)}. \tag{7.11}$$

Coming now to the form of the instanton solution, an analytic solution of the non-linear saddle point equation is not readily available. However, close to the gap edge, one can expand $V_R(\phi)$ around the homogeneous AG solution at E_{gap} up to cubic order. Namely,

$$V_R(\phi) - V_R(\phi_{\text{AG}}) \simeq -\sqrt{6}\left(\frac{E_{\text{gap}}}{\Delta}\right)^{1/6} \gamma^{1/2}(\epsilon)\,\delta\phi^2 + \left(\frac{\zeta E_{\text{gap}}}{\Delta}\right)^{1/3} \delta\phi^3,$$

where $\gamma(\epsilon) = (E_{\text{gap}} - \epsilon)/\Delta$ and $\delta\phi = \phi - \phi_{\text{AG}}$. This admits for evaluating the action analytically with

$$\delta\phi(x) = \sqrt{6}\left(\frac{\Delta}{\zeta^2 E_{\text{gap}}}\right)^{1/6} \gamma^{1/2}(\epsilon)\, \cosh^{-2}\left(\frac{x}{2r_{\text{drop}}(\epsilon)}\right). \tag{7.12}$$

The size of the instanton, which diverges upon approaching the gap edge, is given by [44]

$$r_{\text{drop}}(\epsilon) = 6^{1/4}\,\xi \left(\frac{\Delta}{E_{\text{gap}}}\right)^{1/12} \gamma^{-1/4}(\epsilon). \tag{7.13}$$

In higher dimensions one can assume that the bounce solution possesses radial symmetry. Nevertheless, the problem becomes more complicated because the saddle point equation contains a gradient term. For the case $d = 2$, we are interested in, one obtains

$$\partial_{\tilde{r}}{}^2\phi + \frac{1}{\tilde{r}}\,\partial_{\tilde{r}}\phi + \frac{1}{2}\partial_\phi V_R(\phi) = 0,$$

where $\tilde{r} = |\mathbf{r}|/\xi$.

However, one can still determine the parameter dependence of the action by dimensional analysis using the Ansatz $\phi - \phi_{\text{AG}} = \alpha f(|\mathbf{r}|/\beta)$. Altogether, this obtains

$$S_{\text{inst.}} = c_2\,\zeta^{-2/3}(1-\zeta^{2/3})^{-1/2}\nu_0 D\,\gamma(\epsilon),$$

where c_2 is a numerical constant.

This completes our analysis of the profile and statistical weight of the bounce solution. However, since it does not depart from the line $\Im[\theta] = \pi/2$, taken alone, it provides no contribution to the DoS! To understand why sub-gap states are associated with the bounce it is necessary to explore the role of fluctuations in the vicinity of the instanton. As emphasised in Ref. [44], such a program turns out to be crucial in the present system.

As pointed out above, the supersymmetry cannot be broken globally. Thus, the non-supersymmetric saddle-point has to be embedded in a degenerate saddle point manifold, where integration over this manifold restores the symmetry. Furthermore, the inhomogeneous solution breaks translational invariance. Again this should be associated with a zero-mode. However, as the solution is a *bounce*, i.e. it has a node, the zero-mode is *not* the lowest energy mode. In addition, there exists a negative energy mode.

Using an explicit parameterisation of the fluctuations, this has indeed be verified in Ref. [44, 45]. Instead of repeating the analysis here, we simply note that:

- There is a zero-mode restoring supersymmetry and, thus, ensuring the correct normalisation $\mathcal{Z} = 1$.
- There is a zero-mode restoring translational invariance. As this zero-mode is associated with a bounce solution, furthermore, a negative-energy mode exists. The negative-energy mode requires a rotation of the integration contour which entails an additional factor of i (see e.g. Ref. [149]). Therefore, the instanton solution yields a finite contribution to the DoS.

A more thorough discussion of fluctuations can also be found in Sec. 8.2.2 in the context of inhomogeneous superconductivity.

Let us summarise. Taking into account the inhomogeneous instanton solution of the saddle point equation, and (crucially!) fluctuations around it, yields the following result for the 'sub-gap' DoS to exponential accuracy,

$$\nu(\epsilon) \sim \exp\left[-c_2 \nu_0 D\, \zeta^{-2/3}(1-\zeta^{2/3})^{-1/2}\, \frac{E_{\rm gap}-\epsilon}{\Delta}\right]. \tag{7.14}$$

Furthermore, one finds that the sub-gap states are confined to droplets of size $r_{\rm drop}(\epsilon)$ which diverges upon approaching the gap edge.

In the magnetic impurity model, it is tempting to ascribe the low-energy quasi-particle states to regions with an unusually high concentration of magnetic impurities. I.e. fluctuations of the random magnetic impurity potential may create regions, where the effective scattering rate $1/\tau_s'$ exceeds the mean scattering rate $1/\tau_s$ over a range set by the coherence length. The probability of creating such shallow potential minima is exponentially small. Within these regions – or 'droplets' – quasi-particle states with energies down to $E_{\rm gap}(\tau_s') < E_{\rm gap}(\tau_s)$ exist. Obviously, these states are bound to the region, where the scattering rate is large, and, therefore, localised.

However, this interpretation does not carry through to the present case because here the magnetic field is constant everywhere. In this regard the parallel field problem is more instructive: it makes obvious that optimal fluctuations of the pair-breaking perturbation cannot be responsible for the tails of the DoS. Instead quantum coherence effects associated with the 'normal' disorder generate these tail states. As pointed out in Refs. [44, 45], even in the magnetic impurity problem, details of the distribution of the magnetic impurity potential are not important. This contrasts the situation of Lifshitz band-tail states [50] in semiconductors: there the energy scaling depends sensitively on the nature of the disorder distribution. Therefore, a Lifshitz-type argument is not applicable in the derivation of sub-gap states. These states are quasi-classical in nature and arise due to an interplay of the normal (non-magnetic) disorder with the pair-breaking perturbation (i.e. the parallel magnetic field or the magnetic impurity potential). A further discussion about the universality of the above results can be found in chapter 8.

7.2. Columnar defects

Having seen in the normal case that the properties of a thin film in a parallel magnetic field depend sensitively on the nature of the impurity potential, we are going to ask the same question for the superconductor: Does the absence of z-dependent scattering lead to an observable symmetry effect?

One might expect that – as there is a mechanism which could possibly compensate for $\mathcal{T}$-breaking – the Anderson theorem still holds and gapless superconductivity does not occur. We

are going to show that this is not the case. On the mean-field level, one obtains the same results as for the diffusive case, although with a modified parameter ζ. In fact, self-consistency forbids a solution which could cancel the field effect. The reason is that here we are dealing with an interacting problem: when the formation of Cooper pairs is concerned, it is not possible to replace time-reversal by any other symmetry. However, as we will see in Sec. 7.3, the Berry-Robnik phenomenon is not completely ineffective in the superconducting case. Taking into account fluctuations in the gapless phase, one can show that while the diffusive film – as expected in the presence of a magnetic field – belongs to class C, the film with columnar defects is in the higher symmetry class CI. This leads to a different low-energy behaviour of the two systems: in the former case $\nu(\epsilon) \sim \epsilon^2$, while in the latter case $\nu(\epsilon) \sim \epsilon$.

To be specific, let us consider a model of a thin film superconductor subject to a random (impurity) potential which varies only along the in-plane directions as in chapter 5. In the absence of a magnetic field or superconducting order parameter, the quasi-particle Hamiltonian can be subdivided into different subbands labelled by an index k. The spectral properties of each subband is described by a two-dimensional NLσM action of conventional type. The derivation of an effective low-energy action follows closely the normal case in section 5.1. The Gor'kov Hamiltonian of the system now reads

$$\mathcal{H} = \Big(-\frac{\tilde{\partial}^2}{2m} + W(z) - V(x,y) \Big) \sigma_3^{\mathrm{PH}} + \Delta(z) \sigma_2^{\mathrm{PH}}, \tag{7.15}$$

where $\tilde{\partial} = \partial + iHz\mathbf{e}_y \sigma_3^{\mathrm{PH}}$, W is the confining potential, and V represents white noise disorder, i.e. $\langle V(\mathbf{r}) V(\mathbf{r}') \rangle = (2\pi\nu_0\tau)^{-1} \delta^{(2)}(\mathbf{r} - \mathbf{r}')$, where $\mathbf{r}^{(\prime)}$ are in-plane two-component vectors.

Diagonalising the z-dependent part of the problem, and representing $\mathcal{H}$ in the basis of the eigenfunctions $\{\phi_k\}$, i.e. $\mathcal{H}_{kk'} = \int dz\, \phi_k \mathcal{H} \phi_{k'}$, the vector potential $\mathbf{A} = -Hz\mathbf{e}_y$ as well as the order parameter become matrices in k-space:

$$\begin{aligned} \mathbf{A}_{kk'} &= -H\mathbf{e}_y \int dz\, \phi_k(z) z \phi_{k'}(z), \\ \Delta_{kk'} &= \int dz\, \phi_k(z) \Delta(z) \phi_{k'}(z). \end{aligned}$$

Let us emphasise again that, if the system possesses inversion symmetry $z \to -z$, the matrix element $A_{kk'}$ differs from zero only if $k + k'$ odd; in particular, $A_{kk} = 0$. For simplicity, here we only consider the fully symmetric case.[1]

Under the further assumption, that the subband spacing $|\epsilon_k - \epsilon_{k'}|$ is larger than the scattering rate, one finds that only the diagonal components of the order parameter are non-vanishing. Starting from the conventional superconducting $2d$ NLσM action for the k subbands and turning on an in-plane magnetic field, the total effective action assumes the form

$$\begin{aligned} S &= -\frac{\pi\nu_0}{8} \int d^2r \sum_k \mathrm{Str}\, \left[D_k (\partial Q_k)^2 - 4 \left(i\epsilon \sigma_3^{\mathrm{PH}} \otimes \sigma_3^{\mathrm{CC}} - \Delta_{kk} \sigma_2^{\mathrm{PH}} \right) Q_k \right] + \\ &\quad + \frac{\pi\nu_0}{4} \int d^2r \sum_{kk'} \mathcal{X}_{kk'}\, \mathrm{Str}\, \left[\sigma_3^{\mathrm{PH}} Q_k \sigma_3^{\mathrm{PH}} Q_{k'} \right], \end{aligned}$$

where $\mathcal{X}_{kk'} = D_{kk'} A_{kk'} A_{k'k} / (1 + (E_{kk'}\tau)^2)$. Furthermore, $D_{kk'} = (D_k + D_{k'})/2$ and $E_{kk'} = \epsilon_k - \epsilon_{k'}$. Crucially, from this result we see that there exists no linear coupling of Q to the vector potential – a paramagnetic term does not appear.

[1] As in chapter 5, it can be shown that an asymmetry of the confining potential or the presence of z-dependent scattering destroy any unusual phenomena associated with the Berry-Robnik symmetry effect [119].

To proceed, we subject the action to a mean-field analysis. Varying the action with respect to fluctuations of Q_k, one obtains the modified (set of coupled) Usadel equations

$$D_k\partial\left(Q_k\partial Q_k\right) - \left[i\epsilon\sigma_3^{\mathrm{PH}}\otimes\sigma_3^{\mathrm{CC}} - \Delta_{kk}\sigma_2^{\mathrm{PH}}, Q_k\right] - \sum_{k'}\mathcal{X}_{kk'}\left[\sigma_3^{\mathrm{PH}}Q_k\sigma_3^{\mathrm{PH}}, Q_{k'}\right] \;=\; 0\,.$$

Applying the Ansatz $Q_k = \cosh\hat{\theta}_k\sigma_3^{\mathrm{PH}}\otimes\sigma_3^{\mathrm{CC}} + i\sinh\hat{\theta}_k\sigma_2^{\mathrm{PH}}$ with θ_k homogeneous in the in-plane coordinates, the mean-field equation assumes the form

$$i(\epsilon\sinh\theta_k - \Delta_{kk}\cosh\theta_k) + \sum_{k'}\mathcal{X}_{kk'}\sinh\left(\theta_k+\theta_{k'}\right) = 0\,. \tag{7.16}$$

In principle, this equation has to be solved in parallel with the self-consistent equation for the order parameter

$$\Delta_{kk'} = 4\pi g\nu_0\sum_n \sin\theta_{k,n}\,\delta_{kk'} \tag{7.17}$$

where g is the effective BCS coupling constant.

Analysing the saddle point equation (7.16), it can be easily seen that the field dependent term $\sum_{k'}\mathcal{X}_{kk'}\sin(\theta_k+\theta_{k'})$ vanishes, if we choose the solution $\theta_k = (-1)^k\theta$ (due to $\mathcal{X}_{kk'} = 0$ for $k+k'$ even). Thus, there seems to be one mode that is not affected by the magnetic field. However, this would imply that the order parameter, too, must have an alternating sign, i.e. $\Delta_{kk} = (-1)^k\Delta$. Recalling the definition $\Delta_{kk} = \int dz\,\Delta(z)\phi_k^2$, this is not feasible. Thus, the above solution is ruled out[2] and, therefore, on the mean-field level, the symmetry mechanism is ineffective.

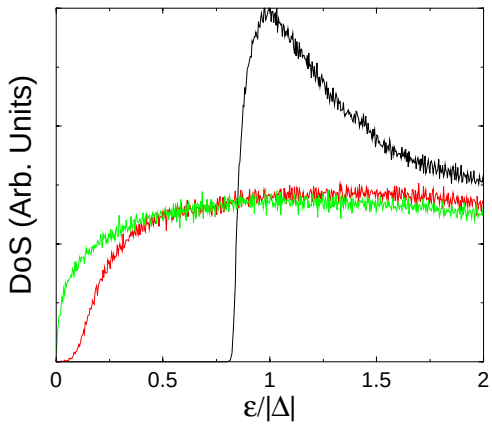

Figure 7.4.: Numerical results: DoS. Upon increasing the magnetic field, the energy gap closes and the BCS singularity disappears.

A more natural choice seems to be a spatially homogeneous order parameter. Unfortunately, for a general model, the solution of Eqs. (7.16,7.17) does not seem to be readily accessible. However, to gain some insight into the nature of the general solution, we will specialise further consideration to the particular case in which only the lowest two subbands are coupled.

With $\mathcal{X}_{12} = \mathcal{X}_{21} \equiv \mathcal{X}$ the equations for θ_1 and θ_2 coincide. Therefore, setting $\theta \equiv \theta_1 = \theta_2$ which implies $\Delta_{11} = \Delta_{22} \equiv \Delta$, the mean-field equation takes the form reminiscent of the AG equation,

$$i(\epsilon\sinh\theta - \Delta\cosh\theta) + \mathcal{X}\sinh(2\theta) = 0\,.$$

[2]One might expect that taking into account the phase of the order parameter would change the situation, but we checked that this is not the case.

As with the diffusive film, the application of a strong in-plane field suppresses the order parameter and allows for the existence of a gapless phase. According to the AG theory, the superconductor enters the gapless phase when $\zeta \equiv 2\mathcal{X}/\Delta \simeq 1$.

If $E_{12}\tau \ll 1$, the parameter ζ is of the same form as in the diffusive case, i.e. $\zeta \sim D(Hd)^2/\Delta$. In the opposite limit, ζ is greatly reduced because the wide subband spacing restricts the motion in z-direction. Now, $\zeta \sim D(Hd)^2/((E_{12}\tau)^2\Delta)$, and, thus, higher magnetic fields have to be applied in order to reach the gapless phase. As in the diffusive case, the hard edge in the gapped phase is compromised due to fluctuations – see the discussion above – and exponentially small tails in the sub-gap region arise.

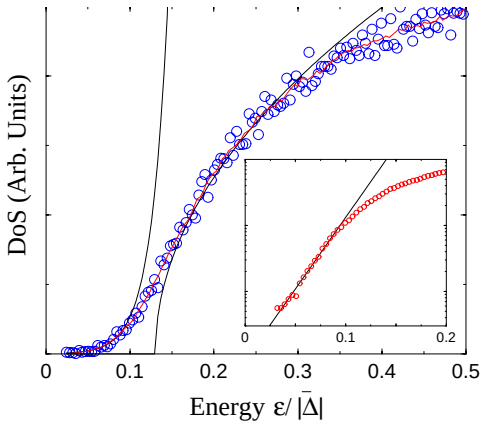

Figure 7.5.: Numerical results: Sub-gap DoS. The solid lines show the square-root edge and the exponentially small tails. In the inset, the same data are plotted on a linear-log scale.

The effect of gap suppression is born out in a simple numerical simulation. Fig. 7.4 shows the quasi-particle DoS for a two subband tight-binding model with 20×20 sites when subject to an in-plane magnetic field. The energy is measured in units of the (unperturbed) order parameter. The three curves correspond to different values of the magnetic field. Details of the result at intermediate fields are magnified in Fig. 7.5. The mean-field square-root edge as well as the exponentially small tails are indicated. Furthermore, the inset shows the linear energy dependence of the sub-gap action, cf. Eq. (7.14), on a linear-log scale: $\ln \nu(\epsilon < E_{\rm gap}) \sim E_{\rm gap} - \epsilon$.

More generally, for many subbands, one would expect the same qualitative picture to hold – although Δ_{kk} might slowly depend on k.

7.3. Phase coherence properties of the gapless phase: Massless fluctuations and the soft mode action

While on the mean-field level all perturbations, i.e. magnetic impurities as well as parallel fields in films with different disorder potentials, follow the same AG phenomenology, it is interesting to note that, in contrast to the magnetic impurity model [42, 44] which belongs to symmetry class D due to broken spin-rotation symmetry, here the soft fluctuations around the mean-field should be described by a class C or CI effective action [82]. Therefore, one expects localisation of the quasi-particle states in the gapless phase. In fact, the fluctuations are sensitive to the nature of the impurity scattering.

To assess the low-energy properties of the system, we have to identify the soft modes of the action. For frequencies $\epsilon \to 0$, the saddle point is not unique, but spans a degenerate manifold $Q = TQ_{\rm SP}T^{-1}$ with $T = \exp[W]$ and $\{Q_{\rm SP}, W\} = 0$. The symmetries of the system impose certain conditions on the generators W.

7.3.1. Diffusive film

The choice of generators W is dictated by the presence of the order parameter and the magnetic field. This leads to the following conditions:

- W has to commute with the order parameter,
$$[\sigma_2^{\rm PH}, W] = 0.$$
- As time-reversal symmetry is broken by the magnetic field, W has to fulfill the further restriction
$$[\sigma_3^{\rm PH}, W] = 0.$$

Thus, $W = \mathbb{1}^{\rm PH} \otimes W_s$. This corresponds to symmetry class C which describes superconducting systems with spin-rotation symmetry, but broken $\mathcal{T}$-invariance. The integration manifold of class C is Osp(2|2)/Gl(1|1).

The soft mode action reads [150]

$$S_{Q_s} = -\frac{\pi\nu d}{4}\int d\mathbf{r}\ \mathrm{Str}\left[D\cosh^2\theta(\partial Q_s)^2 - 4i\epsilon\cosh\theta\sigma_3^{\rm CC}Q_s\right], \tag{7.18}$$

where $Q_s = T_s\sigma_3^{\rm CC}T_s^{-1}$ and $T_s = \exp[W_s]$.

In the perturbative regime, $\epsilon \gg E_c = D|\cosh\theta|/L^2$, one obtains

$$\begin{aligned}\nu(\epsilon) &= \nu_0(\epsilon) + \Re\left[\frac{1}{\pi}\int\frac{d^2q}{(2\pi)^2}\frac{1}{D\cosh\theta q^2 - 2i\epsilon}\right] \\ &= \nu_0(\epsilon) + \Re\left[\frac{1}{8\pi^2 D\cosh\theta}\ln\left(1+\left(\frac{D\cosh\theta}{2\epsilon\ell^2}\right)^2\right)\right].\end{aligned} \tag{7.19}$$

On energy scales $\epsilon < E_c$, the zero spatial mode dominates the action which leads to the following result [82],

$$\nu(\epsilon) = \nu(E_c)\left(1 - \frac{\sin(2\pi\epsilon/\delta)}{2\pi\epsilon/\delta}\right), \tag{7.20}$$

where $\delta = 1/(\nu(E_c)L^2)$. I.e. for $\epsilon \to 0$, the DoS vanishes quadratically,

$$\frac{\nu(\epsilon)}{\nu(E_c)} \simeq \frac{2}{3}\pi^2\left(\frac{\epsilon}{\delta}\right)^2.$$

This is to be contrasted with the low-energy behaviour of the DoS in the case of columnar defects, where the system possesses $\mathcal{P}_z$-symmetry.

7.3.2. Columnar defects

Here instead of a single W, there is a set of generators W_k.

- As before, W_k has to commute with the order parameter,

$$[\sigma_2^{\mathrm{PH}}, W_k] = 0.$$

- However, even though time-reversal symmetry is broken by the magnetic field, the generators do not have to obey $[\sigma_3^{\mathrm{PH}}, W_k] = 0$. Due to $\mathcal{P}_z$-symmetry which causes all elements $\mathcal{X}_{kk'}$ with $k + k'$ even to vanish, it is sufficient to require

$$W_{k'} = \sigma_3^{\mathrm{PH}} W_k \sigma_3^{\mathrm{PH}} \qquad \text{for } k + k' \text{ odd.}$$

  I.e. one generator, take e.g. W_0, can be chosen 'freely'. Then, the others are determined through

$$W_k = (\sigma_3^{\mathrm{PH}})^k W_0 (\sigma_3^{\mathrm{PH}})^k$$

  (or: $W_k = W_0$ if $k \in 2\mathrm{N}$, and $W_k = \sigma_3^{\mathrm{PH}} W_0 \sigma_3^{\mathrm{PH}}$ if $k \in 2\mathrm{N} + 1$).

Thus, the second condition here only imposes certain relations between different W_k, but does not restrict the structure of W_k in particle-hole space. This corresponds to the higher symmetry class CI. Now the integration manifold is Osp(2|2). Again we find a manifestation of the Berry-Robnik symmetry phenomenon: the low-energy physics in the gapless phase are determined by the symmetry class associated with systems possessing time-reversal invariance.

Now the soft mode action reads

$$S_{Q_s} = -\frac{\pi\nu}{8} \int d\mathbf{r}\ \mathrm{Str}\ \left[D_k \cosh^2\theta_k (\partial Q_s)^2 - 4i\epsilon \cosh\theta_k \sigma_3^{\mathrm{PH}} \otimes \sigma_3^{\mathrm{CC}} Q_s \right], \tag{7.21}$$

where $Q_s = T_s \sigma_3^{\mathrm{PH}} \otimes \sigma_3^{\mathrm{CC}} T_s^{-1}$. Here $T_s = \exp[W_0]$, and W_0 fulfils the conditions specified above. Results for class CI are available in the literature, too [82]. For small energies, one obtains

$$\frac{\nu(\epsilon)}{\nu(E_c)} \quad = \quad \frac{\pi}{2} \int_0^{\pi\epsilon/\delta} \frac{dz}{z} J_0(z) J_1(z) = \frac{\pi^2}{4} \epsilon/\delta + \mathcal{O}(\epsilon^3), \tag{7.22}$$

and the DoS vanishes linearly for $\epsilon \to 0$.

This behaviour can be verified numerically. In Fig. 7.6, the density of states at low energies is compared for the two cases. On the log-log scale one can read out the exponent α governing the energy dependence, $|\epsilon|^\alpha$. At low energies, the two lines with slope $\alpha_{\mathrm{C}} = 2$ and $\alpha_{\mathrm{CI}} = 1$ – characteristic for the symmetry classes C and CI – fit the data for the diffusive film and the film with columnar defects, respectively.

7.4. Discussion

We have cast the problem of a thin superconducting film in a parallel magnetic field in a field theoretic description. In the mean-field approximation, known results from AG theory [42] are reproduced. The same phenomenology applies to diffusive films as well as films with columnar

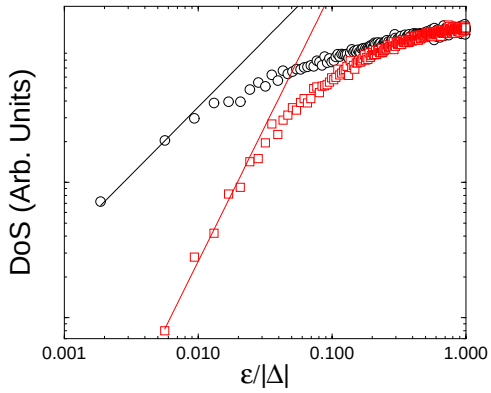

Figure 7.6.: Numerical results: Log-log plot of the low-energy DoS in the gapless phase for a diffusive film (open squares) and a film with columnar defects (open circles).

defects. In the diffusive case, we have shown that – within the gapped phase – taking into account inhomogeneous instanton solutions of the saddle point equation, the hard gap is destroyed. In analogy to the magnetic impurity problem [44, 45], exponentially small tails within the gap region arise. The same is to be expected for the columnar defects. For the two subband case, this is obvious because with $\theta_1 = \theta_2$, the saddle point equation as well as the action have exactly the same form as for the diffusive film. For $M > 2$ the coupling between different θ_k complicates the analysis, however, the general behaviour should not be affected qualitatively.

Within the gapless phase, the Berry-Robnik symmetry phenomenon leads to different low-energy properties. As confirmed by numerics, for the diffusive film, the DoS vanishes quadratically for $\epsilon \to 0$ (class C) while in the presence of only columnar defects the DoS at small energies is linear in ϵ (class CI). The latter behaviour is usually observed in systems which possess time-reversal invariance. Although the $\mathcal{P}_z$-symmetry cannot prevent the gradual destruction of superconductivity by the magnetic field, some compensation for the $\mathcal{T}$-breaking is still effective.

An evident extension of the above scheme for future work is to study the influence of an in-plane magnetic field on a NS bilayer, i.e. the interplay between gapless superconductivity and the proximity effect. In addition to the effect of the field on the individual system, here it affects the coupling, too.

8. Gap fluctuations in inhomogeneous superconductors

A more direct way of influencing the quasi-particle properties of a superconductor are inhomogeneities in the coupling constant. We consider below the influence of a spatially varying coupling constant $g(\mathbf{r})$ on the quasi-particle properties of a conventional disordered s-wave superconductor. As mentioned in the introduction, such a program is not new: the same problem was investigated in an earlier work by Larkin and Ovchinnikov [49]. However, although our aims, and indeed many of our conclusions, are broadly similar to those of Ref. [49], the present investigation is motivated by two considerations: Firstly, the development of a quasi-classical approach within the framework of the NLσM to explore the nature of the quasi-particle states in the 'sub-gap' region serves as a useful prototype for future studies of related 'droplet phase' instabilities in other interacting theories (such as that presented by the superconductor/insulator transition in the disordered interacting system [144, 151]). Secondly, in developing and applying the σ-model approach, we will find that the Lifshitz-type arguments [50] invoked in Ref. [49] to determine the profile of the DoS in the sub-gap region are flawed. Indeed, the theory developed below will expose a general scheme which establishes the universality of 'gap fluctuations' in the d-dimensional system in accord with the zero-dimensional results of Ref. [152].

With this introduction, let us formulate the model superconducting system which will be considered. Our starting point is the Gor'kov or Bogoliubov-de Gennes (BdG) Hamiltonian, $\mathcal{H} = \mathcal{H}_0\sigma_3^{\rm PH} + \Delta\sigma_1^{\rm PH}$. The order parameter, chosen to be real, has to be determined self-consistently from the condition $g^{-1}(\mathbf{r})\Delta(\mathbf{r}) = \langle\psi_\uparrow(\mathbf{r})\psi_\downarrow(\mathbf{r})\rangle/\nu_0$. Following the notation of Ref. [49], we will assume that the (inverse) coupling constant $g^{-1}(\mathbf{r})$ exhibits small fluctuations around an average value $1/\bar{g}$. As with the random impurity potential, these fluctuations of the coupling constant $\delta(g^{-1})(\mathbf{r}) \equiv g_1(\mathbf{r})$ are drawn from a Gaussian distribution with zero mean, and correlation

$$\langle g_1(\mathbf{r})g_1(\mathbf{r}')\rangle_g = \phi(|\mathbf{r}-\mathbf{r}'|). \tag{8.1}$$

Here the condition $g_1(\mathbf{r})\bar{g} \ll 1$ will be imposed so that the coupling constant remains positive everywhere. Furthermore, one assumes that the correlations are characterised by some correlation length r_c which determines the range of ϕ.

Qualitatively, the response of the ground state to inhomogeneities in the coupling constant depends sensitively on the range of the correlations. If the correlation length is much larger than the superconducting coherence length $\xi = (D/2|\Delta|)^{1/2}$, the order parameter can smoothly adjust to the local value of $g^{-1}(\mathbf{r})$. In this case $\Delta(\mathbf{r}) \sim g(\mathbf{r})$, and the local DoS, $\nu(\mathbf{r})$, is fixed by the local value of the order parameter [49]. In the opposite limit, one expects the faster fluctuations of the coupling constant to be rectified by the proximity effect coupling of neighbouring superconducting regions. It is in this limit that the system becomes sensitive to quasi-classical phase coherence processes. Therefore, to focus our discussion, in the following, we limit consideration to the quasi-classical and dirty limits, where the energy scales are arranged in the hierarchy $\epsilon_{\rm F} \gg 1/\tau \gg \Delta$.

Before turning to the formalism, let us summarise the main conclusions of this investigation. Following Ref. [49], one finds that inhomogeneities of the coupling constant are reflected in inhomogeneities of the superconducting order parameter. Setting $\Delta(\mathbf{r}) = \bar{\Delta} + \Delta_1(\mathbf{r})$, where $\bar{\Delta}$ represents the homogeneous component of the order parameter and $\Delta_1(\mathbf{r})$ its spatial fluctuation, one finds that

$$\langle \Delta_1(\mathbf{q})\Delta_1(-\mathbf{q})\rangle_g = \bar{\Delta}^2 \, \langle g_1(\mathbf{q})g_1(-\mathbf{q})\rangle_g \, f^2(|\mathbf{q}|). \tag{8.2}$$

Here $f(|\mathbf{q}|)$ represents a dimensionless function of $|\mathbf{q}|\xi$ which is determined self-consistently (see below).

By accommodating these spatial fluctuations, if the correlation length of the coupling constant is short, $r_c \ll \xi$, one finds [49] that the equation of motion for the average quasi-particle Green function obeys a local non-linear equation which has the canonical form of that encountered by the Abrikosov-Gor'kov theory [42]. Specifically, in the mean-field approximation, the BCS singularity is rounded off and the DoS exhibits a reduced quasi-particle energy gap $E_{\rm gap} = \bar{\Delta}(1-\eta^{2/3})^{3/2}$ [49], where

$$\eta \sim \phi(0) \left(\frac{r_c}{\xi \ln(\xi/r_c)^2} \right)^2 \tag{8.3}$$

is a dimensionless parameter characterising the strength of the correlations of the superconducting order parameter. Note that, in the present case, $\eta \ll 1$ due to the conditions $g_1(\mathbf{r})\bar{g} \ll 1$ (which ensures $|\Delta_1(\mathbf{r})| \ll \bar{\Delta}$) and $r_c \ll \xi$. Thus, the system remains in the gapped phase – as one would expect, if the coupling constant is positive everywhere.

However, as with $\mathcal{T}$-breaking perturbations – the conclusions of the mean-field analysis are modified significantly by optimal fluctuations of the random impurity potential. Such fluctuations, which appear as spatially inhomogeneous instanton field configurations of the mean-field equation, show the gap structure to be fragile: one finds that, within the gapped phase of the mean-field theory, spatially localised states at energies below the gap are generated by mesoscopic fluctuations. Close to the mean-field gap edge $E_{\rm gap}$, these states are confined to droplets of dimension [49]

$$r_{\rm drop}(\epsilon) \sim \xi \left(\frac{E_{\rm gap} - \epsilon}{\bar{\Delta}} \right)^{-1/4}, \tag{8.4}$$

diverging as one approaches $E_{\rm gap}$. With $r_{\rm drop} \gg \ell \gg \lambda_{\rm F}$, each of these regions is characterised by an entire band of localised states. To exponential accuracy the corresponding sub-gap DoS varies as

$$\nu(\epsilon) \sim \exp\left[-a_{\rm d}(\eta)\nu_0 D L^{d-2} \left(\frac{\xi}{L} \right)^{d-2} \left(\frac{E_{\rm gap}-\epsilon}{\bar{\Delta}} \right)^{\frac{6-d}{4}} \right], \tag{8.5}$$

which is non-perturbative in the inverse dimensionless conductance of the normal system $1/(\nu_0 D L^{d-2})$. This result, which differs from that obtained in Ref. [49], mirrors the scaling obtained in the study of sub-gap states in superconductors with magnetic impurities [44] and thin films in parallel fields. Later we will argue that the energy scaling of the DoS is not accidental but is a universal feature of the sub-gap states in the superconducting system (cf. Ref. [45]).

Now for $r_{\rm drop} \gg L$, the system enters a zero-dimensional regime. Here the expression for the DoS (8.5) applies with $d = 0$. Reassuringly, in this case one recovers the universal result predicted for gap fluctuations near a square root edge [152]. The origin of this universality in the present scheme was discussed in Ref. [45].

8.1. Field theory of the inhomogeneous superconductor

As self-consistency is essential in the present context, we are working with a replica field theory. Using this formulation, the response of the superconducting system to inhomogeneities in the BCS coupling constant will be investigated.

The starting point of the analysis is the non-linear σ model action (6.23), where now g is a function of $\mathbf{r}$ (and a factor ν_0 has been absorbed into g):

$$\begin{aligned} S[Q,\Delta] &= \nu_0 \int d\mathbf{r} \int_0^\beta d\tau\, g^{-1}(\mathbf{r})\,\Delta^2(\mathbf{r},\tau) + \\ &\quad + \frac{\pi\nu_0}{8} \int d\mathbf{r}\ \mathrm{tr}\ \left[D(\partial Q)^2 - 4(\hat{\epsilon}\sigma_3^{\mathrm{PH}} \otimes \sigma_3^{\mathrm{CC}} + \Delta\sigma_2^{\mathrm{PH}})Q\right]. \end{aligned} \tag{8.6}$$

The impurity averaged DoS can be obtained from the identity

$$\langle \nu(\epsilon) \rangle = \frac{\nu_0}{4} \int \frac{d\mathbf{r}}{V} \lim_{N\to 0} \frac{1}{N} \Re \left\langle \mathrm{tr}\left[\Lambda \otimes \sigma_3^{\mathrm{PH}} \otimes \sigma_3^{\mathrm{CC}} Q P_{\epsilon\epsilon}\right] \right\rangle_{Q,\Delta}, \tag{8.7}$$

where $\langle \cdots \rangle_{Q,\Delta} = \int DQ \int D\Delta \cdots e^{-S[Q,\Delta]}$ and $P_{\epsilon\epsilon}$ projects onto the diagonal element $\epsilon\epsilon$. Furthermore, $\Lambda_{nm} = \mathrm{sgn}(\epsilon_n)\delta_{nm}$.

8.1.1. Self-consistent fluctuations of the order parameter

To assess the influence of the inhomogeneous coupling constant on the quasi-particle properties it is necessary to subject the action to a saddle-point analysis. Varying the action (8.6) with respect to Q and Δ, one obtains the coupled saddle-point equations

$$\begin{aligned} &D\partial(Q\partial Q) + [\epsilon_n \sigma_3^{\mathrm{PH}} \otimes \sigma_3^{\mathrm{CC}} + \Delta\sigma_2^{\mathrm{PH}}, Q] = 0, \\ &g^{-1}(\mathbf{r})\Delta(\mathbf{r}) = \frac{\pi}{4\beta}\,\mathrm{tr}\ [\sigma_2^{\mathrm{PH}} Q(\mathbf{r})]. \end{aligned} \tag{8.8}$$

For a homogeneous coupling constant, these equations admit a homogeneous solution for the order parameter and Q. However, for a general inhomogeneous configuration for $g^{-1}(\mathbf{r})$, an exact solution is unavailable and an approximate scheme must be sought.

Following Ref. [49], our strategy will be to use the mean-field solution of the homogeneous problem as a platform to develop a perturbative expansion of the self-consistent order parameter. Specifically, by finding the deviation $\delta\Delta(\mathbf{r}) \equiv \Delta_1(\mathbf{r})$ of the order parameter from its mean value $\bar{\Delta}$ to leading order in $g_1(\mathbf{r})$, integrating out fast fluctuations of Q, and averaging over random configurations of $g_1(\mathbf{r})$, one will obtain an effective action for the quasi-particle degrees of freedom of the superconducting system. With this effective theory, we will again use a saddle-point analysis to explore the rearrangement of the ground state due to the inhomogeneous coupling constant. At the mean-field level, the solution reveals a homogeneous renormalisation of the superconducting gap from its bare value. On this background, one will find that the hard gap predicted by the mean-field theory is further softened by gap fluctuations which are accommodated in the effective field theory by inhomogeneous instanton configurations of the fields Q.

Applied to the saddle-point equations (8.8) above, the Ansatz

$$Q_{nm} = (\cos\hat{\theta}_n \sigma_3^{\mathrm{PH}} \otimes \sigma_3^{\mathrm{CC}} + \sin\hat{\theta}_n \sigma_2^{\mathrm{PH}})\delta_{nm} \tag{8.9}$$

where $\hat{\theta}_n = \mathrm{diag}(\theta_n^1, \ldots, \theta_n^N)$ is replica diagonal, leads to the coupled saddle-point equations

$$\begin{aligned} D\partial^2\hat{\theta}_n(\mathbf{r}) - 2\left(\epsilon_n \sin\hat{\theta}_n(\mathbf{r}) - \Delta(\mathbf{r})\cos\hat{\theta}_n(\mathbf{r})\right) &= 0, \\ g^{-1}(\mathbf{r})\Delta(\mathbf{r}) = \frac{\pi}{\beta}\sum_n \sin\hat{\theta}_n(\mathbf{r}). & \end{aligned} \tag{8.10}$$

In the following, the Matsubara indices will be dropped and only be reinstated when necessary. These equations can be identified as self-consistent Usadel equations [137, 153] for the average quasi-classical Green function in the presence of an inhomogeneous coupling constant. Specifically, the former represents the reorganisation of the ground state due to spatial inhomogeneities in the order parameter, while the second equation enforces the self-consistency condition imposed on the order parameter.

For a homogeneous coupling constant $\bar{g}$, the mean-field equations are solved by a homogeneous replica symmetric Ansatz with

$$\hat{\theta}_0 = \arccos\frac{\hat{\epsilon}}{\hat{E}}, \tag{8.11}$$

where $\hat{E}^2 = \hat{\epsilon}^2 + \bar{\Delta}^2$ and $\bar{\Delta} = (\pi\bar{g}/\beta)\sum_n \sin\theta_{0n}$. In this case, as expected, one simply recovers the BCS solution [145]. This result, being independent of disorder, is simply a manifestation of the Anderson theorem [8] on the level of the effective action – in the non-interacting system, a weak non-magnetic impurity potential has no influence on the average DoS.

To accommodate spatial fluctuations of the coupling constant and, with them, fluctuations of the order parameter one should, in principle, solve the non-linear set of equations self-consistently. Evidently, such a program is infeasible. Instead, following Ref. [49], taking the relative fluctuations of the coupling constant to be small, we look for a perturbative expansion of the mean-field equations. To develop the perturbative expansion of the mean-field equations, set $\hat{\theta} = \hat{\theta}_0 + \hat{\theta}_1(\mathbf{r})$ and, accordingly, $\Delta = \bar{\Delta} + \Delta_1(\mathbf{r})$, where both $\hat{\theta}_1$ and Δ_1 are of order g_1. Expanding to first order in g_1, one obtains the coupled linear equations for θ_1 and Δ_1,

$$D\partial^2\hat{\theta}_1 - 2\underbrace{\left(\hat{\epsilon}\cos\hat{\theta}_0 + \bar{\Delta}\sin\hat{\theta}_0\right)}_{\hat{E}}\hat{\theta}_1 + 2\Delta_1\cos\hat{\theta}_0 = 0, \tag{8.12}$$

$$\Delta_1(\mathbf{r}) = \frac{\pi}{\beta}\bar{g}\sum_n \hat{\theta}_{1n}(\mathbf{r})\cos\hat{\theta}_{0n} - g_1(\mathbf{r})\bar{g}\bar{\Delta}. \tag{8.13}$$

Transforming Eq. (8.12) to the Fourier representation, one obtains the solution

$$\hat{\theta}_1(\mathbf{q}) = 2\frac{\Delta_1(\mathbf{q})\cos\hat{\theta}_0}{D\mathbf{q}^2 + 2\hat{E}}$$

which, when inserted into Eq. (8.13), yields

$$\Delta_1(\mathbf{q}) = -\frac{\bar{\Delta}}{\frac{\pi}{\bar{\Delta}\beta}\sum_n\left(\sin\theta_{0n} - \frac{2\bar{\Delta}\cos^2\theta_{0n}}{D\mathbf{q}^2+2E_n}\right)}g_1(\mathbf{q}).$$

Finally, performing the Matsubara summation, one finds

$$\Delta_1(\mathbf{q}) \equiv -\bar{\Delta}g_1(\mathbf{q})f(|\mathbf{q}|), \tag{8.14}$$

where, normalising the wavevector $\tilde{\mathbf{q}} = \xi\mathbf{q}$ by the coherence length,

$$f(q) = \frac{2\tilde{q}^2}{\pi - (\tilde{q}^4-1)^{1/2}\ln\left[\frac{\tilde{q}^2-(\tilde{q}^4-1)^{1/2}}{\tilde{q}^2+(\tilde{q}^4-1)^{1/2}}\right]} = \begin{cases} 1 - \frac{\pi\tilde{q}^2}{4} + \ldots & \tilde{q} \ll 1, \\ \frac{1}{\ln\tilde{q}^2} & \tilde{q} \gg 1. \end{cases} \tag{8.15}$$

From this result, one obtain the response of the order parameter to spatial variations of the BCS coupling constant. The low Fourier components ($q \ll 1/\xi$) of the order parameter smoothly follow spatial fluctuations of $g^{-1}(\mathbf{r})$. Perhaps more surprising is the response of the order parameter to fast fluctuations. As one would expect, these fluctuations are suppressed by the proximity effect, however, as noted by Ref. [49], the attenuation scales only as $1/\ln\tilde{q}^2$.

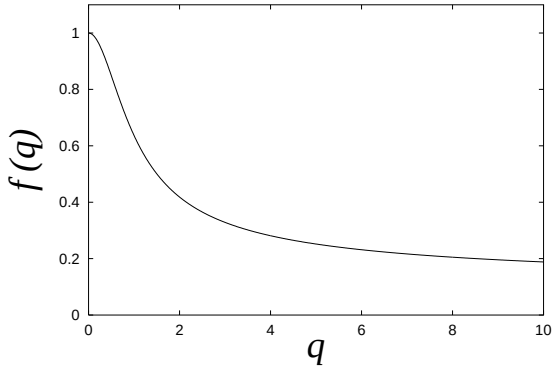

Figure 8.1.: The function $f(q)$, governing the dependence of the order parameter on variations of the coupling constant.

Now, these fast fluctuations of the order parameter can have a dramatic effect on the mean-field DoS and its fluctuation in the vicinity of the mean-field gap edge. To assimilate the effect of these fluctuations it is necessary to revisit the NLσM action taking into account the inhomogeneous order parameter.

8.1.2. Mean-field solution

Substituting the mean-field solution for the order parameter, $\bar{\Delta}$, together with its spatial fluctuation $\Delta_1(\mathbf{r})$ into the NLσM action, one obtains

$$S[Q] \;=\; \frac{\pi\nu_0}{8}\int d\mathbf{r}\ \mathrm{tr}\left[D(\partial Q)^2 - 4\big(\hat{\Sigma} + \Delta_1(\mathbf{r})\sigma_2^{\mathrm{PH}}\big)Q\right], \tag{8.16}$$

where $\hat{\Sigma} = \hat{\epsilon}\sigma_3^{\mathrm{PH}} \otimes \sigma_3^{\mathrm{CC}} + \bar{\Delta}\sigma_2^{\mathrm{PH}}$.

Now, since $\int d\mathbf{r}\,\Delta_1(\mathbf{r}) = 0$, contributions to the generating function arising from field configurations of Q which are constant or slowly varying in space are largely insensitive to the fluctuations. Therefore, to assess the influence of the spatial inhomogeneity of the order parameter, we proceed by integrating out fast fluctuations of Q [154], where 'fast' means varying on length scales shorter than the coherence length.

INFO: To do so, the fast and slow degrees are separated by expanding Q around the slowly varying $\bar{Q}$, i.e.

$$Q = T\bar{Q}T^{-1}\,, \quad \bar{Q} = e^{-W_</2}\sigma_3^{\rm PH}\otimes\sigma_3^{\rm CC}\otimes\Lambda\, e^{W_</2}, \tag{8.17}$$

where $T = \exp[-W_>/2]$ with $\{\bar{Q}, W_>\} = 0$. Integrating over $W_>$, one obtains $S_{\rm eff} = S_0 + S_{\rm AG}$, where

$$S_0 = \frac{\pi\nu_0}{8}\int d\mathbf{r}\ {\rm tr}\,\Big[D(\partial\bar{Q})^2 - 4\hat{\Sigma}\bar{Q}\Big] \tag{8.18}$$

and

$$S_{\rm AG} \;=\; \frac{\pi\nu_0}{8}\sum_{\mathbf{q},\mathbf{q}',\mathbf{q}'',\mathbf{q}'''}{\rm tr}\,\Big[\Delta_1(\mathbf{q})\Delta_1(-\mathbf{q}''')\,\hat{\Pi}_{\mathbf{q}',-\mathbf{q}''}[\bar{Q}(\mathbf{q}+\mathbf{q}'),\sigma_2^{\rm PH}][\bar{Q}(-\mathbf{q}''-\mathbf{q}'''),\sigma_2^{\rm PH}]\Big]. \tag{8.19}$$

Here Δ_1 is determined by Eq. (8.14). Furthermore, $\hat{\Pi}_{\mathbf{q},-\mathbf{q}'}$ represents the diffusion propagator, i.e.

$$\hat{\Pi}^{-1}_{\mathbf{q},-\mathbf{q}'} = Dq^2\delta_{\mathbf{q},\mathbf{q}'} + \{\hat{\Sigma}, \bar{Q}(\mathbf{q}-\mathbf{q}')\}.$$

Retaining only the diagonal part $\hat{\Pi}_{\mathbf{q},-\mathbf{q}}$ and averaging over fluctuations g_1, which to a good approximation amounts to replacing $g_1(\mathbf{q})g_1(-\mathbf{q}')$ by its average value $\langle g_1(\mathbf{q})g_1(-\mathbf{q}')\rangle_g = \phi(|\mathbf{q}|)\,\delta_{\mathbf{q},\mathbf{q}'}$, one obtains

$$S_{\rm AG} = \frac{\pi\nu_0\bar{\Delta}}{16}\int d\mathbf{r}\int d\mathbf{r}'\ {\rm tr}\,\Big[\hat{\eta}(\mathbf{r}-\mathbf{r}',\hat{\epsilon})[\bar{Q}(\mathbf{r}),\sigma_2^{\rm PH}][\bar{Q}(\mathbf{r}'),\sigma_2^{\rm PH}]\Big]$$

with

$$\hat{\eta}(\mathbf{r},\hat{\epsilon}) = \frac{2}{\bar{\Delta}}\,\langle\Delta_1^2\rangle(\mathbf{r})\,\hat{\Pi}(\mathbf{r}). \tag{8.20}$$

Upon approaching the gap edge, $\hat{\Pi}$ becomes long-ranged, the relevant scale being $\ell_E = \sqrt{D/E} \gg \xi$. Thus, the spatial dependence of η is governed by $\langle\Delta_1^2\rangle$, whose range is determined by Eq. (8.14) and the correlator $\langle g_1(\mathbf{r})g_1(\mathbf{r}')\rangle_g = \phi(|\mathbf{r}-\mathbf{r}'|)$. If ϕ is short-ranged (on the scale of the coherence length), one can use the approximation

$$S_{\rm AG} = \frac{\pi\nu_0\bar{\Delta}}{16}\int d\mathbf{r}\ {\rm tr}\,\Big[\hat{\eta}(0,\hat{\epsilon})[\bar{Q}(\mathbf{r}),\sigma_2^{\rm PH}]^2\Big]. \tag{8.21}$$

Close to the gap, where the energy dependence of $\hat{\eta}$ is negligible ($E \approx 0$), this action recovers the mean-field equation obtained in Ref. [49] – as will be shown below – with $\eta = \hat{\eta}(0, E{=}0)$.

The effective action in the vicinity of the gap edge then reads

$$S_{\rm eff} = \frac{\pi\nu_0}{8}\int d\mathbf{r}\ {\rm tr}\,\left[D(\partial\bar{Q})^2 - 4\hat{\Sigma}\bar{Q} + \frac{1}{2}\bar{\Delta}\eta[\bar{Q},\sigma_2^{\rm PH}]^2\right], \tag{8.22}$$

where

$$\eta \simeq \frac{1}{\xi^2}\int\frac{d\mathbf{q}}{q^2}\,f^2(|\mathbf{q}|)\phi(|\mathbf{q}|).$$

To summarise, quenched inhomogeneities in the coupling constant induce spatial fluctuations of the order parameter which are accommodated by a rearrangement of the quasi-particles in the superconducting condensate. In the disordered system, this rearrangement is governed by the same Usadel equations that describe the proximity effect in hybrid SN systems [137]. Taking into account the inhomogeneities in the order parameter, one obtains an effective action for the disordered superconductor in which the bulk action for the non-disordered system is supplemented by an additional term (8.21) which, as we will see presently, leads to a suppression of the superconducting quasi-particle gap.

To explore the influence of the fluctuations on the quasi-particle gap structure, once again varying the effective action with respect to $\bar{Q}$, one obtains the saddle-point equation

$$D\partial(\bar{Q}\partial\bar{Q}) - \left[\hat{\Sigma}, \bar{Q}\right] + \frac{1}{2}\bar{\Delta}\eta\left[\sigma_2^{\rm PH}\,\bar{Q}\,\sigma_2^{\rm PH}, \bar{Q}\right] = 0. \tag{8.23}$$

Adopting the parameterisation (8.9), this saddle-point equation can be rewritten as

$$D\partial^2\hat{\theta} - 2\hat{\epsilon}\sin\hat{\theta} + 2\bar{\Delta}\cos\hat{\theta} - 2\bar{\Delta}\eta\sin\hat{\theta}\cos\hat{\theta} = 0. \tag{8.24}$$

The saddle-point equation (8.24) has a form which coincides with the Abrikosov-Gor'kov (AG) equation obtained in the theory of gapless superconductivity [42]. There, the parameter η has to be interpreted as the spin scattering rate $\eta = 1/\tau_s\bar{\Delta}$ induced by magnetic impurities in the superconducting system. The analysis of the AG equation shows that, for $\eta > 1$ the system enters a gapless phase while for $\eta < 1$ the quasi-particle energy gap is suppressed but not destroyed. Here the parameter values are restricted to $\eta \ll 1$ as pointed out earlier.

Thus, as a first step, we look for homogeneous solutions of Eq. (8.24), i.e. $\hat{\theta}(\mathbf{r}) \equiv \hat{\theta}_{\rm AG}$:

$$\hat{\epsilon}\sin\hat{\theta}_{\rm AG} - \bar{\Delta}\cos\hat{\theta}_{\rm AG} + \bar{\Delta}\eta\sin\hat{\theta}_{\rm AG}\cos\hat{\theta}_{\rm AG} \;\; = \;\; 0. \tag{8.25}$$

Combined with the gap equation, the solution is obtained self-consistently from the equation

$$\frac{\hat{\epsilon}}{\bar{\Delta}} = \cot\hat{\theta}_{\rm AG}\Big(1 - \eta\frac{1}{\sqrt{1+\cot^2\hat{\theta}_{\rm AG}}}\Big) \tag{8.26}$$

which coincides with Eq. (18) of Ref. [49].

The mean-field density of states, $\nu(\epsilon) = \nu_0\,\Re\left[\cos\theta_{\rm AG}(i\epsilon_n \to \epsilon)\right]$, reveals a reduced energy gap $E_{\rm gap} = \bar{\Delta}(1-\eta^{2/3})^{3/2}$. Furthermore, in the vicinity of the gap, the density of states is given by Eq. (6.13). More concisely, setting

$$\Delta_{\rm g} = (\frac{2}{3}\,\bar{\Delta}\delta^2)^{1/3}\eta^{4/9}(1-\eta^{2/3})^{1/6}, \tag{8.27}$$

where $\delta = 1/(\nu_0 L^d)$ is the average level spacing of the normal system, this result can be brought to a more compact form and written as [152]

$$\nu(\epsilon > E_{\rm gap}) = \frac{1}{\pi L^d}\sqrt{\frac{\epsilon - E_{\rm gap}}{\Delta_{\rm g}^3}}. \tag{8.28}$$

As expected, quenched disorder in the coupling constant is reflected in an overall suppression of the quasi-particle energy gap. Importantly, quasi-classical processes imply that the suppression of the gap does not simply follow the distribution of the order parameter. However, as recognised by Larkin and Ovchinnikov [49], the square root singularity in the DoS predicted by the mean-field theory is untenable: optimal fluctuations associated with the impurity potential $V(\mathbf{r})$ give rise to sub-gap states which cause the gap to fluctuate. Such states are invisible to the mean-field theory. At first sight it is tempting to seek gap fluctuations within the perturbative fluctuations around the symmetric mean-field saddle-point configuration $\theta_{\rm AG}$. However, when taken into account, it is found that the integrity of the gap is maintained by the analytical properties of the mean-field solution: perturbative fluctuations influence only the profile of the DoS about the mean-field energy gap. (For a discussion of this point in the context of the hybrid SN system, see Ref. [145]). Instead, it is necessary to revisit the saddle-point equation (8.24) and seek inhomogeneous instanton field configurations that are non-trivial in replica space.

8.2. Inhomogeneous saddle points

To develop a theory of sub-gap states in the present system one can draw intuition both from the analysis of Larkin and Ovchinnikov [49] as well as a related study of gap fluctuations in the superconductor with $\mathcal{T}$-breaking perturbations (cf. Ref. [44, 45] and Chap. 7). In Ref. [49] sub-gap states were shown to be associated with inhomogeneous solutions of the Abrikosov-Gor'kov equation (8.24). In the framework of the non-interacting field theory, these inhomogeneous solutions are identified with 'supersymmetry broken' instanton or bounce configurations of the action. In the present case, one can therefore anticipate that the relevant bounce configurations are replica non-symmetric, providing an exponential suppression of the DoS below the mean-field edge. Further, we will find that the replica symmetry of the theory is restored by a zero-mode in the replica space. The analysis is very similar to the supersymmetric version discussed in Sec. 7.1.2

8.2.1. Replica non-trivial instanton solutions

Except for a change of notation, $\theta \to -i\theta$, the saddle-point equation (8.24) has exactly the same form as Eq. (7.6). I.e. switching from Matsubara to real energies, the potential is given by

$$V(\theta) = -2i\frac{\epsilon}{\Delta}\cos\theta + 2\sin\theta + \frac{\eta}{2}\cos 2\theta, \tag{8.29}$$

and the (fermionic) integration contour now covers the interval $[0, \pi]$ as shown in Fig. 8.2.

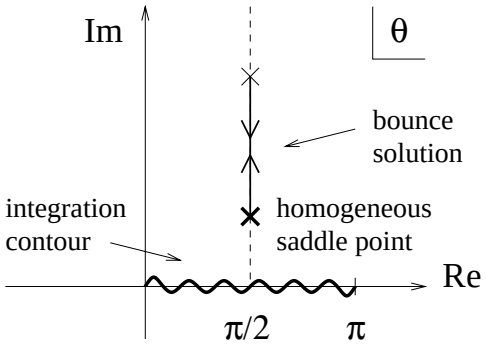

Figure 8.2.: Bounce solution.

In order to obtain a finite though exponentially small sub-gap density of states, one needs to find a solution with finite action. All replica symmetric solutions lead to a vanishing action in the limit $N \to 0$. Therefore, the solution we are looking for necessarily involves "replica symmetry breaking". Leaving aside the homogeneous mean-field configuration, the configuration which incurs the lowest action is one in which the bounce inhabits only a single replica, say, $a = 1$, i.e.

$$\hat{\theta}(x) = \frac{\pi}{2} + i\,\mathrm{diag}(\phi(x), \phi_{\mathrm{AG}}, \ldots, \phi_{\mathrm{AG}}). \tag{8.30}$$

Then, in the one-dimensional case, $\phi(x)$ is described by Eq. (7.12). The inhomogeneous solution, thus, varies on length scales much longer than the coherence length – justifying the separation into slow and fast degrees of freedom in Sec. 8.1.2.

As shown in Sec. 7.1.2, in higher dimensions, the parameter dependence of the action can be extracted by dimensional analysis which finally yields

$$S_{\text{inst.}} = a_{\text{d}}(\eta)\nu_0 D\xi^{d-2}\gamma(\epsilon)^{(6-d)/4}, \tag{8.31}$$

where $a_{\text{d}}(\eta) = c_{\text{d}}\eta^{-2/3}(1-\eta^{2/3})^{-(2+d)/8}$ and c_{d} a numerical constant; $c_1 = 2^7\pi\sqrt{6}/5$. Then, making use of Eq. (8.27), the action can be cast in the more compact form

$$S_{\text{inst.}} = \sqrt{\frac{3}{2}}\, c_{\text{d}} \left(\frac{r_{\text{drop}}(\epsilon)}{L}\right)^d \gamma_{\text{g}}^{3/2}(\epsilon), \tag{8.32}$$

where $\gamma_{\text{g}}(\epsilon) = (E_{\text{gap}} - \epsilon)/\Delta_{\text{g}}$. This allows an explicit connection with the zero-dimensional limit. Indeed, the factor $(r_{\text{drop}}/L)^d$ can be further absorbed into Δ_{g} by replacing the level spacing of the system, δ, with the level spacing of the droplet, $\delta_{\text{drop}}(\epsilon) = 1/(\nu_0 r_{\text{drop}}^d)$, in its definition (8.27): $\tilde{\Delta}_{\text{g}} = (\delta_{\text{drop}}(\epsilon)/\delta)^{2/3}\Delta_{\text{g}}$.

The action for solutions with more than one instanton is always larger and, therefore, possible small contributions to the DoS can be safely neglected.

8.2.2. Fluctuation analysis

As we have seen, the lowest energy bounce configuration involves a "breaking" of replica symmetry at the level of the mean-field solution. Taking into account fluctuations in the vicinity of the bounce solution, we will see below that there exists a zero-mode and a negative-energy mode – as discussed briefly in Sec. 7.1.2. The former restores global replica symmetry of the theory and, thus, ensures the integrity of the normalisation of the generating functional $\mathcal{Z} = 1$. Furthermore, the negative-energy mode necessitates a $\pi/2$ rotation of the contour which, imparting a factor of i, renders the contribution of the instanton to the DoS non-vanishing.

To explore the influence of the fluctuations, let us introduce the parameterisation

$$Q = Re^{-W/2}\sigma_3^{\text{PH}} \otimes \sigma_3^{\text{CC}} \otimes \Lambda e^{W/2}R^{-1}, \tag{8.33}$$

where $R(x) = \exp[i\sigma_1^{\text{PH}} \otimes \sigma_3^{\text{CC}}\theta(x)/2]$ is the rotation from the metallic saddle point to $Q_{\text{SP}}(\theta)$. The matrices W are subject to the symmetry condition in replica space $W_{ba} = W_{ab}^\dagger$. Expanding the action up to second order in the generators obtains the following term:

$$\begin{aligned} S[W] \;\simeq\; & -\frac{\pi\nu_0}{8}\int d\mathbf{r} \sum_{a,b} \text{tr}\Big[\partial W_{ab}\partial W_{ba} + \frac{1}{2}\partial\phi_a\partial\phi_b\sigma_2^{\text{PH}}W_{ab}\sigma_2^{\text{PH}}W_{ba} + \\ & + (F_a - \eta\cosh\phi_a\cosh\phi_b)W_{ab}W_{ba} - \eta\sinh\phi_a\sinh\phi_b\sigma_1^{\text{PH}}\otimes\sigma_3^{\text{CC}}W_{ab}\sigma_1^{\text{PH}}\otimes\sigma_3^{\text{CC}}W_{ba}\Big], \end{aligned}$$

where $F_a = ((\partial\phi_a)^2 + V(\phi_a) - \eta\cosh 2\phi_a)/2$. There are two types of fluctuations:

(a) replica-diagonal fluctuations and

(b) fluctuations mixing the replicas.

Within the replica-diagonal part, the most relevant contributions are due to fluctuations of the angle ϕ, i.e. $W_{ab} = \sigma_1^{\text{PH}} \otimes \sigma_3^{\text{CC}}\varphi_a(x)\delta_{ab}$. In the $N-1$ 'trivial' replicas ($\theta = \theta_{\text{AG}}$), these fluctuations

are massive and, therefore, only lead to a weakly energy dependent prefactor. More important are the fluctuations in the replica with the inhomogeneous saddle point, $a = 1$:

$$S[\varphi_1] = \frac{1}{2}\int dx \int dx'\, \varphi_1(x)\, \frac{\delta^2 S}{\delta\phi(x)\delta\phi(x')}\, \varphi_1(x'). \tag{8.34}$$

Now this class of fluctuations has been studied extensively in the standard literature [149]. The operator $\delta^2 S/\delta\phi(x)\delta\phi(x')$ has a zero-mode, $\varphi_1^{(0)} \sim \partial\phi$, due to translational invariance, i.e. the action is independent of the position of the bounce. Furthermore, as the zero-mode is associated with a *bounce* solution it has a node. This implies the existence of one negative-energy eigenmode. To account for this, one has to rotate the contour away from the imaginary axis. This deformation of the contour provides a factor of i. Therefore, the result – which was purely imaginary ($\Re[\theta] = \pi/2$) before – becomes real and, thus, gives a finite contribution to the DoS.

Turning to the fluctuations mixing the replicas, the replica non-symmetric saddle point must be accompanied by a zero-mode in replica space. Writing $W = W^- + W^+$, where $W^-(W^+)$ (anti-)commutes with $\sigma_1^{\mathrm{PH}} \otimes \sigma_3^{\mathrm{CC}}$, the part of the action coupling between the replicas '1' and '$a \neq 1$' reads

$$S_{1a}^{\pm} \simeq -\sum_{a\neq 1} \mathrm{tr}\left[\partial W_{1a}^{\pm}\partial W_{a1}^{\pm} + \frac{V[\phi(\mathbf{r})] - \tilde{V}^{\pm}}{2}\, W_{1a}^{\pm} W_{a1}^{\pm}\right], \tag{8.35}$$

where

$$\tilde{V}^{\pm} = \frac{\eta}{2}\Big(\cosh 2\phi_{\mathrm{AG}} + \cosh 2\phi(\mathbf{r}) + 4\cosh(\phi_{\mathrm{AG}} \pm \phi(\mathbf{r}))\Big). \tag{8.36}$$

Although its presence is disguised by the choice of parameterisation, the action involving this class of fluctuations exhibits a zero-mode. In principle, the zero-mode can be easily identified by choosing a different parameterisation, namely $Q = UQ_{\mathrm{SP}}U^\dagger$ where U constant. This parameterisation, however, leads to a non-trivial measure. Nevertheless, it is useful for determining the dependence of the integration over zero-modes on the number of replicas, N. Close to the gap edge, i.e. at finite energies $\epsilon > 0$, the structure of the saddle point within the PH- and CC-space is completely fixed. – The only freedom left are rotations in replica space, $U \in \mathrm{U}(N)$. Thus, dividing off the matrices which leave the saddle point invariant, the relevant matrices U belong to the coset space $\mathrm{U}(N)/(\mathrm{U}(1)\times\mathrm{U}(N-1))$. Integration over the zero-modes gives a prefactor which is proportional to the volume $\mathcal{V}$ of the coset. In the limit $N \to 0$, one finds $\mathcal{V} \sim N$ [70] (see also App. D). Or, in other words, there are N saddle points that contribute to the integral. Using the parameterisation (8.33) does not change the N dependence but only the spatial structure of the zero-mode. Therefore, without calculating the value of the prefactor, one knows that the result has the following form:

$$\begin{aligned}\nu(\epsilon) &\sim \lim_{N\to 0}\frac{1}{N}\int dx\, N\left[\sinh\phi(x) + (N-1)\sinh\phi_{\mathrm{AG}}\right]\, |\chi_0(x)|^2\, e^{-S_{\mathrm{inst.}}} \\ &= \int dx\, \left[\sinh\phi(x) - \sinh\phi_{\mathrm{AG}}\right] |\chi_0(x)|^2\, e^{-S_{\mathrm{inst.}}},\end{aligned} \tag{8.37}$$

where $|\chi_0(x)|^2$ describes the spatial profile of the zero-mode.

8.3. Discussion

This concludes our derivation of the sub-gap DoS: by itself the instanton or bounce configuration provides the leading exponential dependence of the DoS while the fluctuations render the pre-exponential factors positive definite. More precisely:

(1) The prefactor becomes real due to the negative-energy eigenmode and the consequential deformation of the contour.

(2) The sub-gap DoS is non-vanishing only in the vicinity of the bounce as can be seen from Eq. (8.37).

Altogether, taking the action for the d-dimensional system (8.32), one obtains the expression for the DoS defined by Eq. (8.5):

$$\nu(\epsilon) \sim \exp\left[-c_{\mathrm{d}}\nu_0 D\xi^{d-2}\eta^{-2/3}(1-\eta^{2/3})^{-\frac{2+d}{8}}\left(\frac{E_{\mathrm{gap}}-\epsilon}{\bar{\Delta}}\right)^{\frac{6-d}{4}}\right],$$

or, after rescaling,

$$\nu(\epsilon) \sim \exp\left[-\sqrt{\frac{3}{2}}\,c_{\mathrm{d}}\left(\frac{E_{\mathrm{gap}}-\epsilon}{\tilde{\Delta}_{\mathrm{g}}}\right)^{3/2}\right]. \tag{8.38}$$

As noted in Ref. [152], if the mean-field DoS exhibits a square-root singularity of the form (8.28), fluctuations of the edge due to optimal fluctuations of the impurity potential are predicted to assume a universal form

$$\nu(\epsilon) \sim \exp\left[-\frac{2}{3}\left(\frac{E_{\mathrm{gap}}-\epsilon}{\Delta_{\mathrm{g}}}\right)^{3/2}\right] \tag{8.39}$$

obtained by random matrix theory. Now, as we have seen, when $r_{\mathrm{drop}} > L$ (inevitable as $\epsilon \to E_{\mathrm{gap}}$), the system enters a zero-dimensional regime. In this limit, with $d = 0$ the expression for the DoS reassuringly assumes the universal form (8.39).

In the present context, the mechanism by which the universal expression develops at the level of the action has been elucidated in Ref. [45]. Specifically, in the zero-dimensional regime, the instanton configuration must be supplemented by a homogeneous replica symmetry broken solution of stationary phase which sits at the shallow minimum of the potential $V(\theta)$, c.f. Fig. 7.2. There the integration contour leaves the axis $\theta = \pi/2 + i\phi$, and the minimum represents in fact a maximum along the perpendicular direction [45]. Physically, gap fluctuations in the zero-dimensional system correspond to sample-to-sample fluctuations rather than spatial variations of the gap.

Although the saddle-point analysis as well as the size of the instanton agree with the result found in Ref. [49], the energy dependence of the action does not, i.e. while we obtain the exponent $\alpha = 3/2 - d/4$, the solution obtained in Ref. [49] is compatible with an exponent $\alpha_{\mathrm{Lif}} = 2 - d/4$. As mentioned earlier the exponent $3/2$ is a direct consequence of the square-root behaviour of the mean-field result [45]. This is most obvious in the zero-dimensional case, where the action assumes the universal form proposed in Ref. [152].

The discrepancy of the results can be traced back to the application of a Lifshitz-type argument [50] to the present scheme. Although the problem bears close similarity to the Lifshitz problem of band-tail states in semiconductors [50–52], the correspondence is superficial. In particular, Lifshitz tail states at the band-edge of a semiconductor are typically associated with wavefunctions which vary smoothly on the scale of their extent. As such, an estimate of the optimal character of the tail state distribution can be established on the level of the ψ-field action. By contrast, the sub-gap tail states associated with gap fluctuations in the superconducting

system involve a superposition of states close to the Fermi level, where spatial fluctuations vary rapidly oscillating at the scale of the Fermi wavelength — the sub-gap states are quasi-classical in origin. It therefore does not seem possible to develop a Lifshitz argument for the present system. As a further consequence, in contrast to the band-tail states, the quasi-classical nature of the sub-gap states in the superconductor makes their properties insensitive to the nature of the impurity distribution.

It is interesting to note that the analysis in this work has a number of relatives in the recent literature. As emphasised earlier, at the level of the soft mode action, the theory of gap fluctuations mirrors that obtained in the Abrikosov-Gor'kov theory of a superconductor with magnetic impurities [44, 45] and, later, that encountered in the description of sub-gap states in the hybrid SN system [155]. Furthermore, various results which are non-perturbative in the (inverse) dimensionless conductance and involve replica (or super-)"symmetry breaking" have been reported in the literature [54, 156–158]. Of these investigations, it is particularly interesting to contrast the present scheme with the prediction of 'anomalously localised states' in the weakly disordered normal conductor.

By exploiting instanton configurations of the NLσM action, Khmel'nitskii and Muzykantskii [156] proposed that the long-time current relaxation in a disordered wire was dominated by rare localised states which coexist in a background of extended states (see also, Ref. [157]). These states, which are ascribed to optimal fluctuations of the random potential, are penalised by a statistical weight which depends exponentially on the dimensionless conductance. This scaling mirrors that found in the present system. However, crucially, scaling in the superconducting system involves an energy dependence which allows the exponent to become small as one approaches the energy gap.

In hindsight, it is easy to understand why optimal fluctuations can more readily induce localised states in the superconducting system. In the normal disordered system, as pointed out by Mott, hybridisation makes the coexistence of localised states in a background of extended states difficult to sustain. However, in the superconducting system, fluctuations of the order parameter provide a natural mechanism by which quasi-particle states can localise in regions, where the order parameter is suppressed.

9. Summary

In the present work various quantum interference effects in weakly disordered systems have been studied. While in the 'normal' case those effects are mainly present in quantum corrections or fluctuations, both described by correlation functions of the form $\langle G^+G^-\rangle$, in a superconductor already the averaged quantities show rich physics. Thus, in part I of this work, when studying normal systems, the main emphasis has been put on correlation functions. By contrast, in part II, we have concentrated on the density of states of superconducting systems.

After an introduction on relevant concepts and methods, in the **first part**, correlation functions in two-dimensional electron gases (2DEGs) have been investigated.

An approach for experimentally studying the three correlation functions – density-density ($F^{[d]}$), diffuson ($F^{[D]}$) and Cooperon ($F^{[C]}$) – has been presented in chapter 4. In double-layer systems, fluctuations of the tunnelling conductance between the layers reflect the in-plane properties of the single layer. The dependence of the fluctuations on a parallel magnetic field allows one to monitor the diffuson and Cooperon correlation functions, $F^{[D;C]}$. One may hope to extract the relevant exponents for anomalous diffusion from these measurements. The same concept applies, too, if one of the layers is in the ergodic regime, i.e. when it is confined to an effectively zero-dimensional system or so-called quantum dot (QD). Then, the conductance autocorrelations encode the spectral and parametric correlations in the QD contained in $F^{[d;D]}$. A similar setup has been used earlier by Sivan et al. [27] to study the density-density correlator $F^{[d]}$.

In zeroth order approximation, a parallel magnetic field does not influence the dynamics within a single 2DEG. We next turned to the analysis of magnetic field effects in quantum wells with a finite width in chapter 5. Clearly, the effect depends sensitively on the structure of wavefunctions in the perpendicular direction. We have shown that in the absence of z-dependent scattering, the Berry-Robnik phenomenon [119] leads to unusual magnetoresistance. An inversion symmetry of the confining potential compensates for time-reversal symmetry breaking and, thus, entails a non-vanishing weak localisation correction to the conductivity. The effect is destroyed, both, by a slight asymmetry of the confining potential as well as a weak z-dependence of the impurity scattering.

A special situation arises when just one subband of size quantisation is occupied. Here only virtual processes may cause a residual magnetoresistance. The corresponding magnetic decoherence rate $1/\tau_H$ scales with the 6^{th} power of the applied field (as opposed to the usual H^2 dependence).

In the **second part** of this work, gapless phenomena in superconductors have been studied. The link between the two parts is the parallel field which is one mechanism that entails gapless superconductivity.

As shown in chapter 7, both, in thin films with δ-correlated impurities or columnar defects, the suppression of the quasi-particle gap is governed by the Abrikosov-Gor'kov mean-field equations [42]. At a critical value of the magnetic field, a transition from a gapped to a gapless phase

takes place. Even within the gapped phase, however, the hard gap is destroyed by optimal fluctuations, and the density of states develops exponentially small tails within the gap region. As found recently for the case of magnetic impurities [44], using a field theoretic approach, these 'sub-gap' states can be associated with inhomogeneous, 'supersymmetry breaking' saddle points. In this context, it is crucial to take into account fluctuations which a) restore the global symmetry and b) make the contribution of these instanton solutions to the density of states finite.

A symmetry effect as described in chapter 5 is visible only in the gapless phase, where the low-energy physics is determined by universality classes [47]. While – as one would expect – the diffusive film belongs to class C (spin-rotation, but no time-reversal symmetry), the film with columnar defects is described by class CI (spin-rotation and time-reversal symmetry). This implies, for $\epsilon \to 0$, a quadratic energy dependence of the DoS in the diffusive case whereas for the columnar defects the DoS depends linearly on the energy.

A similar scenario is found in a completely different class of systems. A much more direct way of destroying the integrity of the quasi-particle energy gap are spatial fluctuations of the BCS coupling constant. The parameter regime considered here excludes the gapless phase. However, the suppression of the gap within the gapped phase follows along the same lines.

In chapter 8, following the work of Larkin and Ovchinnikov [49], we have shown that, in a weakly disordered superconductor, short-scale fluctuations of the BCS coupling constant lead to a suppression of the quasi-particle energy gap. At the level of mean-field, the integrity of the gap edge is maintained. However, optimal fluctuations of the impurity potential induce a narrow band of states, localised at the scale of the coherence length, which extend below the mean-field gap edge. Within the framework of the statistical field theory developed here, these states appear as replica symmetry broken instanton configurations of the mean-field equations – the global symmetry of the theory being restored by a zero-mode in the replica space. To exponential accuracy, we have obtained the spectrum of gap fluctuations. The generality of these results has been emphasised. Specifically, in the d-dimensional system, once normalised by the mean-field DoS at the gap edge, we have shown that the spectrum of tail states depends only on the dimensionless parameter η and, in particular, is independent of the nature of the disorder potential. Moreover, in the zero-dimensional system, the spectrum of gap fluctuations is truly universal and coincides with that obtained by Vavilov et al. [152] in the study of gap fluctuations in the SN system.

List of symbols and abbreviations

$A(\mathbf{r}, \mathbf{r}'; \epsilon)$	spectral function
$\mathbf{A}$	vector potential
AG	Abrikosov-Gor'kov
$\mathbf{B}$ *or* $\mathbf{H}$	magnetic field
BCS	Bardeen-Cooper-Schrieffer
BdG	Bogoliubov-de Gennes
β	symmetry index of random matrix ensemble
	or inverse temperature
C	capacitance
CB	Coulomb blockade
$\mathcal{C}$	Cooperon
d	dimensionality of the system
	or distance between layers in DQW
	or width of a quantum well/thin film
$d\mathbf{p} = d^d p/(2\pi)^d$	
$d\mathbf{r} = d^d r$	
$D = v_{\mathrm{F}}^2 \tau/d$	diffusion constant
DoS	density of states
DQW	double quantum well
$\mathcal{D}$	diffuson
$\delta = 1/(\nu L^d)$	mean level spacing
δ_L	London penetration depth
Δ	order parameter
e	electron charge
$E_c = e^2/(2C)$	charging energy
E_{BB}	projector onto the boson-boson block
E_{FF}	projector onto the fermion-fermion block
E_{gap}	quasi-particle energy gap
$E_{\mathrm{Th}} = 2\pi D/L^2$	Thouless energy
ϵ_k	subband energies
$\epsilon_n = (2n+1)\pi/\beta$	fermionic Matsubara frequency
ϵ_{F} *or* E_{F}	Fermi energy
$F^{[d]}$	density-density correlation function
$F^{[C]}$	Cooperon correlation function
$F^{[D]}$	diffuson correlation function
FT	field theory

$\phi_0 = h/e^2$	flux quantum
g	dimensionless conductance $g = E_{\rm Th}/\delta$
	or BCS coupling constant
$G^{\pm}(\mathbf{r}, \mathbf{r}'; \epsilon)$	retarded/advanced Green function
$G_{\mathcal{T}}$	tunneling conductance
$\Gamma = 1/(2\tau)$	
$\Gamma_{\mathcal{T}}$	level broadening
$\mathcal{H}$	Hamiltonian
$k_{\rm F}$ *or* $p_{\rm F}$	Fermi momentum
κ	inverse screening length
$\ell = v_{\rm F}\tau$	elastic mean free path
L	linear system size
L_ϕ	phase coherence length
$\lambda_{\rm F}$	Fermi wavelength
μ	chemical potential
$\mu_B = e/(2m)$	Bohr magneton
$n_{\rm F}$	Fermi distribution function
NLσM	non-linear sigma model
ν	density of states
$\omega_n = 2n\pi/\beta$	bosonic Matsubara frequency
$\omega_{\rm D}$	Debye frequency
Ω	thermodynamic potential
$\mathcal{P}_z$	inversion symmetry $z \to -z$
R_2	two-level correlation function
RMT	random matrix theory
RSB	replica symmetry breaking
$s = \pi\omega/\delta$	
S	action (e.g. $S[Q]$)
$\mathrm{Str}\, M = \mathrm{tr}\, M_{\rm BB} - \mathrm{tr}\, M_{\rm FF}$	supertrace
SCBA	self-consistent Born approximation
σ	conductivity
$\sigma_i^{\rm AR}$	Pauli matrix in advanced/retarded space
$\sigma_i^{\rm BF}$	Pauli matrix in boson/fermion space
$\sigma_i^{\rm CC}$	Pauli matrix in charge conjugation space
$\sigma_i^{\rm PH}$	Pauli matrix in particle/hole space
$\sigma_i^{\rm TR}$	Pauli matrix in time-reversal space
Σ	self-energy
Σ_2	level number variance
T	temperature
$\mathcal{T}$	tunneling matrix element
	or time-reversal symmetry
τ	elastic mean scattering time
τ_H	magnetic (field) decoherence time
τ_s	magnetic (impurity) scattering time

τ_ϕ	decoherence time
v_F	Fermi velocity
V	bias voltage
V_g	gate voltage
$W(z)$	confining potential
WD	Wigner-Dyson
ξ	superconducting coherence length
	or localisation length
$\xi_p = \epsilon_\mathrm{F} - \mathbf{p}^2/(2m)$	
$\mathcal{Z}$	partition sum/generating functional
ζ *or* η	AG parameter
2DEG	two-dimensional electron gas

A. Some useful definitions and formulae

A.1. Green functions

Consider a system of electrons described by a Hamiltonian $\mathcal{H}$. At zero temperature the electron Green function is defined as

$$G(\mathbf{p},\mathbf{p}';t-t') = -i\,\langle\,|\mathrm{T}\,c_{\mathbf{p}}(t)c^{\dagger}_{\mathbf{p}'}(t')|\,\rangle, \tag{A.1}$$

where T is the time ordering operator,

$$\mathrm{T}c_{\mathbf{p}}(t)c^{\dagger}_{\mathbf{p}'}(t') = \begin{cases} c_{\mathbf{p}}(t)c^{\dagger}_{\mathbf{p}'}(t') & \text{for } t > t' \ , \\ -c^{\dagger}_{\mathbf{p}'}(t')c_{\mathbf{p}}(t) & \text{for } t < t'. \end{cases} \tag{A.2}$$

$|\,\rangle$ denotes the ground state with respect to $\mathcal{H}$. Furthermore, $c^{\dagger}_{\mathbf{p}}, c_{\mathbf{p}}$ is a complete set of Fermi creation and annihilation operators. Eq. (A.1) is defined in the Heisenberg representation, i.e.

$$c^{(\dagger)}_{\mathbf{p}}(t) = e^{i\mathcal{H}t}c^{(\dagger)}_{\mathbf{p}}\mathrm{e}^{-i\mathcal{H}t} \tag{A.3}$$

while $|\,\rangle$ is time independent.

At finite temperatures the so-called Matsubara formalism has to be used instead. The imaginary-time Matsubara Green function is defined as

$$\mathcal{G}(\mathbf{p},\mathbf{p}';\tau-\tau') = -\,\langle \mathrm{T}_{\tau}\,c_{\mathbf{p}}(\tau)c^{\dagger}_{\mathbf{p}'}(\tau')\rangle. \tag{A.4}$$

The τ-ordering operator T_{τ} arranges the operators by increasing τ from right to left. Here the angular bracket $\langle\dots\rangle$ denotes the thermodynamic average $\mathrm{Tr}(\mathrm{e}^{-\beta(\mathcal{H}-\mu N-\Omega)}\dots)$ with β inverse temperature, μ chemical potential, and N number of particles. The thermodynamic potential Ω is a normalisation factor, $\mathrm{e}^{-\beta\Omega} = \mathrm{Tr}(\mathrm{e}^{-\beta(\mathcal{H}-\mu N)})$. The τ-dependence of the operators is given by

$$c^{(\dagger)}_{\mathbf{p}}(\tau) = \mathrm{e}^{(\mathcal{H}-\mu N)\tau}c^{(\dagger)}_{\mathbf{p}}\mathrm{e}^{-(\mathcal{H}-\mu N)\tau}.$$

Since $\mathcal{G}$ is a function of the difference $\Delta\tau = \tau - \tau'$ only, we can also write $\mathcal{G}(\mathbf{p},\mathbf{p}';\tau) = -\,\langle \mathrm{T}_{\tau}\,c_{\mathbf{p}}(\tau)c^{\dagger}_{\mathbf{p}'}(0)\rangle$. Expanding $\mathcal{G}$ in a Fourier series, one obtains the energy Green function

$$\mathcal{G}(\mathbf{p},\mathbf{p}';i\epsilon_n) = \int_0^{\beta} \mathrm{d}\tau\,\mathrm{e}^{\mathrm{i}\epsilon_n\tau}\mathcal{G}(\mathbf{p},\mathbf{p}';\tau) \tag{A.5}$$

with the fermionic Matsubara frequencies $\epsilon_n = (2n+1)\pi/\beta$.

Finally, the retarded (+) and advanced (−) Green functions which are the quantities of physical interest are related to the Matsubara Green function by analytic continuation, i.e.

$$G^{\pm}(\mathbf{p},\mathbf{p}';\epsilon) = \mathcal{G}(\mathbf{p},\mathbf{p}';i\epsilon_n \to \epsilon \pm i0). \tag{A.6}$$

Note that $G^{-} = (G^{+})^{*}$. Thus, we can define the spectral function $A(\mathbf{p},\mathbf{p}';\epsilon)$ as

$$A(\mathbf{p},\mathbf{p}';\epsilon) = i[G^{+}(\mathbf{p},\mathbf{p}';\epsilon) - G^{-}(\mathbf{p},\mathbf{p}';\epsilon)] = -2\,\Im\left[G^{+}(\mathbf{p},\mathbf{p}';\epsilon)\right]. \tag{A.7}$$

For a more detailed review see e.g. [100].

A.2. Coherent state path integrals

The partition sum $\mathcal{Z}$ can be thought of as the sum over diagonal elements of the *imaginary*-time evolution operator U, i.e. $\int dx\, U(x,0;x,-i\beta)$. With the appropriate resolution of unity, the time evolution $U(x_\mathrm{i},t_\mathrm{i};x_\mathrm{f},t_\mathrm{f}) = \langle\phi_\mathrm{f}|e^{-iH(t_\mathrm{f}-t_\mathrm{i})}|\phi_\mathrm{i}\rangle$ can be broken up into small pieces and, finally, be written as a path integral.

The resolution of unity used here is expressed in terms of coherent states, see e.g. [159], which can be defined for bosons as well as for fermions. The fermion statistics requires the introduction of anti-commutating 'numbers', the so-called Grassmann variables.

A.2.1. Grassmann variables

Grassmann variables are numbers with the following property:

$$\eta_i\eta_j = -\eta_j\eta_i. \tag{A.8}$$

Crucially, this implies $\eta^2 = 0$. Furthermore, multiplication by complex numbers ($c_i\eta_i$, where $c_i \in \mathbb{C}$) and addition ($\eta_i + \eta_j$) is defined. Then, the set of numbers $c_0 + \sum_{n=1}^{N} c_{j_1\ldots j_n}\eta_{j_1}\ldots\eta_{j_n}$ forms the so-called Grassmann algebra.

Functions of Grassmann numbers are defined via their Taylor expansion $f(\eta) = \sum_j f^{(j)}(0)\,\eta^j/j!$ which contains only a finite number of terms. The definition of differentiation is $\partial_{\eta_j}\eta_i = \delta_{ij}$. Finally, integration over Grassmann numbers is defined in the following way:

$$\int d\eta_i = 0, \qquad \int d\eta_i\,\eta_i = 1.$$

Note that $\partial_\eta\eta = \int d\eta\,\eta$, i.e integration and differentiation are the same.

A.2.2. Coherent states

Coherent states are eigenstates of the annihilation operator. It is straightforward to show that the creation operator has no eigenstates [159].

Boson coherent states

In second quantisation, the bosonic creation and annihilation operators obey the commutation relations $[a_i, a_j^\dagger] = \delta_{ij}$; furthermore, $[a_i, a_j] = 0$ and $[a_i^\dagger, a_j^\dagger] = 0$. The states

$$|\phi\rangle = \exp\left[\sum_i \phi_i a_i^\dagger\right]|0\rangle \tag{A.9}$$

are eigenstates of all annihilation operators, a_i. Using these states, the resolution of unity reads

$$\int\prod_j \frac{d\bar{\phi}_j d\phi_j}{2\pi i}\, e^{-\bar{\phi}_j\phi_j}\,|\phi\rangle\langle\phi| = 1,$$

i.e. the set of states is over-complete.

Fermion coherent states

The fermionic *anti*-commutation relations imposed on the creation and annihilation operators read $\{c_i, c_j^\dagger\} = \delta_{ij}$ and $\{c_i, c_j\} = 0$ as well as $\{c_i^\dagger, c_j^\dagger\} = 0$. Here the eigenstates of the annihilation operator, c_i, obtain

$$|\eta\rangle = \exp\left[-\sum_i \eta_i c_i^\dagger\right]|0\rangle\,, \tag{A.10}$$

where η_i are Grassmann numbers. The corresponding resolution of unity is given as

$$\int \prod_j d\bar{\eta}_j d\eta_j\, e^{-\bar{\eta}_j \eta_j}\, |\eta\rangle\langle\eta| = 1.$$

For a derivation of the path integral see e.g. Ref. [159].

A.2.3. Gaussian integrals

Gaussian integrals play an important role in field theory. Here some important formulae are summarised.

The simplest of Gaussian integrals is

$$\int_{-\infty}^{\infty} dx\; e^{-\frac{1}{2}ax^2} = \sqrt{\frac{2\pi}{a}},$$

where $\Re[a] > 0$.

This can be generalised to the multi-dimensional case. Furthermore, linear terms in the exponent or prefactors may be included:

$$\begin{aligned}\int dv^\dagger\, dv\, e^{-v^\dagger A v + u^\dagger v + v^\dagger u'} &= \pi^N(\det{}^{-1} A)\, e^{u^\dagger A^{-1} u'},\\ \int dv^\dagger\, dv\, v_i v_j^*\, e^{-v^\dagger A v} &= \pi^N A_{ij}^{-1}(\det{}^{-1} A),\end{aligned}$$

where v, u are N-component complex vectors and A is a $N \times N$ complex matrix with positive definite Hermitian part.

Using Grassmann variables, one obtains instead

$$\begin{aligned}\int d\bar{\eta}\, d\eta\, e^{-\bar{\eta}^T A \eta + \bar{\nu}^T \eta + \bar{\eta}^T \nu} &= (\det A)\, e^{\bar{\nu}^T A^{-1} \nu},\\ \int d\bar{\eta}\, d\eta\, \eta_j \bar{\eta}_i\, e^{-\bar{\eta}^T A \eta} &= A_{ij}^{-1}(\det A),\end{aligned}$$

where $\bar{\eta}, \eta, \bar{\nu}, \nu$ are N-component vectors of Grassmann numbers and A is now an arbitrary $N \times N$ complex matrix. The properties of the Grassmann variables ensure the convergence of the integral.

B. Spectroscopy of quantum dots

In Sec. 4.3, spectral and parametric correlations in QDs and their relation to the tunnelling conductance fluctuations are discussed. Here some details of the calculations as well as results for the tunnelling *current* fluctuations are presented.

B.1. Parametric correlations in GUE

We consider an ergodic, zero-dimensional system, where time-reversal symmetry is broken by a magnetic field $B_\perp$. This belongs to the unitary symmetry class and can be described by a random Hamiltonian drawn from the Gaussian Unitary Ensemble, $\mathcal{H}^{\rm GUE}$; i.e.

$$\langle \mathcal{H}^{\rm GUE}_{\mu\nu}\rangle = 0, \qquad\qquad \langle \mathcal{H}^{\rm GUE}_{\mu\nu}\mathcal{H}^{\rm GUE}_{\nu'\mu'}\rangle = \frac{\lambda^2}{N}\,\delta_{\mu\mu'}\delta_{\nu\nu'}. \tag{B.1}$$

An additional possible magnetic field difference $\Delta B_\perp$ can be modelled by an anti-symmetric matrix Φ, i.e. the total system Hamiltonian reads $\mathcal{H} = \mathcal{H}^{\rm GUE} \pm i\Phi$. We are, thus, led to consider correlation functions of the form

$$F_{\mu\nu\mu'\nu'} \;\equiv\; \Big\langle (\epsilon^+ + \frac{\omega}{2} - \mathcal{H}^{\rm GUE} - i\Phi/2)^{-1}_{\mu\nu}\; (\epsilon^- - \frac{\omega}{2} - \mathcal{H}^{\rm GUE} + i\Phi/2)^{-1}_{\mu'\nu'}\Big\rangle.$$

Correlation functions of this type can conveniently be calculated from the functional integral [63]

$$\int D[\bar\psi,\psi]\, e^{-S[\bar\psi,\psi]}\,(\dots), \tag{B.2}$$

where

$$S = i\bar\psi\{\epsilon - \mathcal{H}^{\rm GUE} - (\frac{\omega^+}{2} - i\Phi)\sigma_3^{\rm AR}\}\psi\,.$$

Here the ellipses stand for pre-exponential terms specific to the index configuration of the correlation function under consideration [28, 63, 116]. Following a by now standard procedure [28, 63, 116] – similar to the one outlined in Sec. 2.3.1 – the average over the RMT Hamiltonian leads to the effective action of the NLσM,

$$S_{\rm eff}[Q] = \frac{s^+}{2}\,{\rm STr}(Q\sigma_3^{\rm AR}) - \frac{b}{4}\,{\rm STr}(Q\sigma_3^{\rm AR})^2, \tag{B.3}$$

where Q is a four-dimensional supermatrix subject to the constraint $Q^2 = \mathbb{1}$. The parameters, $s = \pi\omega/\delta$ and $b = 2\,{\rm tr}\,(\phi\phi^{\rm T})/\lambda^2$, appearing in this expression measure the 'mismatch' of our two Green functions. Note that $\lambda = N\delta/\pi$.

Now for the different correlation functions, one obtains the following expressions:

$$F^{[d]} = \int DQ\, e^{-S_{\rm eff}[Q]}\, {\rm Str}\,(\sigma_3^{\rm BF} Q_{11})\, {\rm Str}\,(\sigma_3^{\rm BF} Q_{22}) - 1, \tag{B.4}$$

$$F^{[D]} = \int DQ\, e^{-S_{\rm eff}[Q]}\, {\rm Str}\,(\sigma_3^{\rm BF} Q_{12} \sigma_3^{\rm BF} Q_{21}). \tag{B.5}$$

Furthermore, $F^{[C]} = 0$ as $\mathcal{T}$-invariance is broken.

In order to access non-perturbative results, integration over the whole saddle point manifold is required. Using the parameterisation of Ref. [28] yields for $F^{[d]}$ and $F^{[D]}$, respectively,

$$\begin{aligned} F^{[d]}(s;b) &= \int_1^\infty d\lambda_1 \int_{-1}^1 d\lambda_2\, e^{is^+(\lambda_1-\lambda_2)-b(\lambda_1^2-\lambda_2^2)} = \\ &= \frac{1}{2b}\int_0^\infty \frac{dv}{v}\, e^{is^+ v}\left[e^{-bv|v-2|} - e^{-bv(v+2)}\right], \end{aligned} \tag{B.6}$$

$$\begin{aligned} F^{[D]}(s;b) &= \int_1^\infty d\lambda_1 \int_{-1}^1 d\lambda_2\, \frac{\lambda_1+\lambda_2}{\lambda_1-\lambda_2}\, e^{is^+(\lambda_1-\lambda_2)-b(\lambda_1^2-\lambda_2^2)} = \\ &= \frac{1}{2b^2}\int_0^\infty \frac{dv}{v^3}\, e^{is^+ v}\left[(bv|v-2|+1)\, e^{-bv|v-2|} - (bv(v+2)+1)\, e^{-bv(v+2)}\right]. \end{aligned} \tag{B.7}$$

The integral (B.7) can be performed analytically, leading to

$$\Re\left[F^{[d]}(s;b)\right] = \frac{\pi}{2b}\,\Im\left[{\rm Erf}\frac{s^+ + 2ib}{2\sqrt{b}}\right]\Re\left[{\rm Erfc}\frac{2b - is^+}{2\sqrt{b}}\right]. \tag{B.8}$$

Asymptotics of both correlation functions for small and large b are discussed in the main text.

The parameter b characterises the magnetic field dependence of the fluctuations. How is it related to the actual field difference $\Delta B_\perp$? The magnetic field $\Delta B_\perp$ enters the formula via the magnetic flux through the QD, $\phi = \Delta B_\perp L^2$. For a diffusive system b is given by

$$2b = \frac{\pi}{\delta} D\langle(\frac{r}{L^2}\frac{\phi}{\phi_0})^2\rangle = \frac{1}{2} g \frac{\langle r^2\rangle}{L^2}\left(\frac{\phi}{\phi_0}\right)^2, \tag{B.9}$$

where $g = E_{\rm Th}/\Delta$ is the dimensionless conductance.[1] For a ballistic chaotic system it is more complicated to determine b though it is still of the same form, i.e. $b \sim (\phi/\phi_0)^2$. The prefactor now strongly depends on the geometry. If the dynamics are completely chaotic, it may be estimated by replacing $E_{\rm Th}$ in the above formula by $v_{\rm F}/L$. However, in both cases, the prefactor to $(\phi/\phi_0)^2$ is large. Thus, the correlations are sensitive to magnetic flux $\phi \ll \phi_0$.

B.2. Level broadening

Here we briefly show how the level broadening due to the coupling between the layers is computed. Adopting a matrix notation, the Green function of the combined QD/2DEG system

[1] In the case of a circular QD of radius $L/\sqrt{\pi}$ we get $\langle r^2\rangle = L^2/(2\pi)$ while in the case of a square QD $\langle r^2\rangle = L^2/6$.

reads

$$G = \begin{pmatrix} G_{11} & G_{12} \\ G_{21} & G_{22} \end{pmatrix} = \begin{pmatrix} E - \mathcal{H}_1 & \mathcal{T}^\dagger \\ \mathcal{T} & E + eV - \mathcal{H}_2 \end{pmatrix}^{-1}. \tag{B.10}$$

Thus, the modified Green function of the QD, G_{11}, is given as

$$G_{11} \;=\; \left[(E - \mathcal{H}_1) - \mathcal{T}^\dagger \underbrace{(E+eV-\mathcal{H}_2)^{-1}}_{G^0_{22}} \mathcal{T}\right]^{-1} \;=\; \left[(G^0_{11})^{-1} - \mathcal{T}^\dagger G^0_{22} \mathcal{T}\right]^{-1}.$$

Thus, the action acquires an additional term $S_\mathcal{T} = i\bar{\psi}\mathcal{T}^\dagger G^0_{22}\mathcal{T}\psi$. Including this term only in the lowest order, the effective action changes by

$$\delta S_\mathcal{T} = -i\,\mathrm{Str}\left(\mathcal{G}\mathcal{T}^\dagger G^0_{22}\mathcal{T}\right) = -i\,|\mathcal{T}|^2\;\mathrm{Str}\left(\mathcal{G}G^0_{22}\right). \tag{B.11}$$

The Green function of the 2DEG is given as[2]

$$G^0_{22}(\mathbf{r},\mathbf{r}') = -i\pi\nu J_0(k_\mathrm{F}|\mathbf{r}-\mathbf{r}'|)\sigma_3^\mathrm{AR}.$$

Furthermore, $\mathcal{G}(\mathbf{r},\mathbf{r}') = -i\pi\nu J_0(k_\mathrm{F}|\mathbf{r}-\mathbf{r}'|)Q$ [160, 161]. I.e. the additional term in the effective action reads

$$\delta S_\mathcal{T} = i\frac{\pi\,|\mathcal{T}|^2}{2\Gamma^{(\mathrm{b})}\delta}\,\mathrm{Str}\,(Q\sigma_3^\mathrm{AR}). \tag{B.12}$$

This has to be compared to $\frac{\pi\omega^+}{2\delta}\,\mathrm{Str}\,(Q\sigma_3^\mathrm{AR})$ in Eq. (B.3), i.e. the combination of the two terms gives

$$\frac{\pi}{2\delta}\left(\omega^+ + i\frac{|\mathcal{T}|^2}{\Gamma^{(\mathrm{b})}}\right)\;\mathrm{Str}\,(Q\sigma_3^\mathrm{AR}).$$

Thus, we get

$$\Gamma_\mathcal{T} = \frac{|\mathcal{T}|^2}{\Gamma^{(\mathrm{b})}}, \qquad \text{or} \qquad \gamma = \frac{\pi\,|\mathcal{T}|^2}{\Gamma^{(\mathrm{b})}\delta},$$

where $s^+ \to s + i\gamma$. I.e. in order to resolve structures on the scale of the mean level spacing, we have to require $\Gamma_\mathcal{T} \ll \delta \Leftrightarrow |\mathcal{T}|^2 \ll \Gamma^{(\mathrm{b})}\delta$.

B.3. The current-current correlator

As shown in Sec. 4.3.2, the tunnelling conductance fluctuations C_G are directly proportional to the correlation functions $F^{[d;D]}$ of the QD. The tunnelling current fluctuations C_I are obtained from C_G by a simple integral relation (4.14). Here the results are summarised.

$$C_I(V;\Delta B) \;=\; \left(\frac{2\Gamma^{(\mathrm{b})}}{\epsilon_\mathrm{F}V}\right)^2 \int_0^{eV} d\omega\,(eV-\omega)\left(\Re[F^{[d]}] + \frac{\delta}{2\pi\Gamma^{(\mathrm{b})}}\Re[F^{[D]}]\right).$$

[2] As pointed out earlier, the effect of the magnetic field on the 2DEG can be neglected.

At $\Delta B = 0$ this yields the following result,[3]

$$\begin{aligned} C_I(V;0) &= \left(\frac{2\Gamma^{(\mathrm{b})}\delta}{\epsilon_{\mathrm{F}}V}\right)^2 (\Sigma_2\left(\frac{V}{\delta}\right) + \frac{1}{2\pi\Gamma^{(\mathrm{b})}}V) = \\ &= \left(\frac{2\Gamma^{(\mathrm{b})}\delta}{\pi\epsilon_{\mathrm{F}}V}\right)^2 \begin{cases} \pi s(1+\frac{\delta}{2\pi\Gamma^{(\mathrm{b})}}) & s \ll 1, \\ \ln(s) + s\frac{\delta}{2\Gamma^{(\mathrm{b})}} & s \gg 1. \end{cases} \end{aligned} \tag{B.13}$$

The level number variance $\Sigma_2(S)$ is given as [79]

$$\begin{aligned} \Sigma_2(S) &= S - 2\int_0^S dr\,(S-r)\frac{\sin^2(\pi r)}{(\pi r)^2} = \\ &= \frac{1}{\pi^2}(\ln(2\pi S) + 2\sin^2(\pi S) + \mathrm{C} - \mathrm{ci}(2\pi S) - 2\pi S\,\mathrm{si}(2\pi S)), \end{aligned} \tag{B.14}$$

where $\mathrm{C} \approx 0.577$ (Euler constant).

The results given above are valid only for $s \gg \gamma$. In the opposite limit one obtains instead

$$C_I(V \to 0;0) \simeq \frac{4(\Gamma^{(\mathrm{b})})^2\delta}{\pi\epsilon_{\mathrm{F}}\Gamma_{\mathcal{T}}}. \tag{B.15}$$

I.e. as expected for linear response, the current fluctuations are quadratic in the applied voltage. The field dependence is given by the following formulae:

• <u>b small:</u>

$$\begin{aligned} C_I(V;\Delta B) - C_I(V;0) &= -\left(\frac{2\Gamma^{(\mathrm{b})}}{\epsilon_{\mathrm{F}}s}\right)^2 \frac{b}{\gamma}\Bigg[\underbrace{\frac{s^2}{s^2+\gamma^2}}_{\text{density-density}} + \\ &\quad + \underbrace{\frac{\delta}{2\pi\Gamma^{(\mathrm{b})}} \times \begin{cases} (\frac{s}{\gamma})^2 & s \ll \gamma, \\ (1+\frac{2}{3}\pi\gamma s) & \gamma \ll s \ll 1, \\ (1+\gamma(2\ln(2s) + 2\mathbf{C} - 1)) & s \gg 1. \end{cases}}_{\text{diffuson}} \Bigg] \end{aligned}$$

• <u>b large:</u>[4]

$$\begin{aligned} C_I(V;\Delta B) &= 2\left(\frac{\Gamma^{(\mathrm{b})}}{\epsilon_{\mathrm{F}}s}\right)^2 \Big(\underbrace{\ln(1+(\frac{s}{2b})^2)}_{\text{density-density}} + \underbrace{\frac{2\delta}{\pi\Gamma^{(\mathrm{b})}}\big(s\arctan\frac{s}{2b} - b\ln(1+(\frac{s}{2b})^2)\big)}_{\text{diffuson}} \Big) = \\ &\simeq \left(2\frac{\Gamma^{(\mathrm{b})}}{\epsilon_{\mathrm{F}}}\right)^2 \times \begin{cases} \dfrac{1}{8b^2}(1 + b\dfrac{2\delta}{\pi\Gamma^{(\mathrm{b})}}) & s \ll b, \\ \dfrac{1}{s^2}\left(\ln\dfrac{s}{2b} + \dfrac{\delta}{2\pi\Gamma^{(\mathrm{b})}}\big(\pi s - 4b(1+\ln\dfrac{s}{2b})\big)\right) & s \gg b. \end{cases} \end{aligned}$$

[3] This result can be easily generalised to the orthogonal case by replacing Σ_2^u with Σ_2^o (cf. [79], for example) and multiplying the second term by a factor 2 due to the Cooperon contribution.

[4] Note that in this case we still assume $\phi \ll \phi_0$ ($g^{-1/2} \ll \phi/\phi_0 \ll 1$), i.e. the effect of the magnetic field on the 2DEG is negligible.

B.4. Interaction effects: Calculation of the modified correlation functions

As – in our model, i.e. taking into account charging only – the interaction has no spatial structure, in the following spatial coordinates are suppressed in the notation. The imaginary-time single-particle Green function is given as

$$\mathcal{G}(\tau_1,\tau_2;\mu) = \frac{1}{\mathcal{Z}(\mu)} \int D[\bar\psi,\psi]\, e^{-S[\bar\psi,\psi]}\, \bar\psi(\tau_2)\psi(\tau_1), \tag{B.16}$$

where

$$S[\bar\psi,\psi] = \int_0^\beta d\tau \left\{ \int d\mathbf{r}\, \bar\psi[\partial_\tau + \mathcal{H}_0 - \mu]\psi + E_c\Big(\int d\mathbf{r}\, \bar\psi\psi - \bar N\Big)^2 \right\},$$

and $\mathcal{Z}(\mu) = \int D[\bar\psi,\psi]\, \exp\{-S[\bar\psi,\psi]\}$ is the partition function.

The interaction is decoupled by a Hubbard-Stratonovich transformation, introducing a Bose field $\sigma(\tau)$,

$$e^{-\int_0^\beta d\tau\, E_c\left(\int d\mathbf{r}\, \bar\psi\psi - \bar N\right)^2} = \int D\sigma\, e^{-\int_0^\beta d\tau (\frac{1}{4E_c}\sigma^2 - i\bar N\sigma + i\bar\psi\sigma\psi)}. \tag{B.17}$$

This leads to the following expression for the Green function,

$$\begin{aligned} \mathcal{G}(\tau_1,\tau_2;\mu) &= \frac{1}{\mathcal{Z}(\mu)} \int D\sigma\, e^{\int_0^\beta d\tau (\frac{1}{4E_c}\sigma^2 - i\bar N\sigma)} \times \\ &\quad \times \int D[\bar\psi,\psi]\, e^{-\int_0^\beta d\tau \int d\mathbf{r}\, \bar\psi[\partial_\tau - \mu + i\sigma + \mathcal{H}_0]\psi}\, \bar\psi(\tau_2)\psi(\tau_1). \end{aligned} \tag{B.18}$$

Choosing a (bosonic) Matsubara representation for the field σ, i.e. $\sigma(\tau) = \sum_n e^{i\omega_n\tau}\sigma_n$, where $\omega_n = 2\pi n/\beta\,(n\in\mathbb{Z})$, all but the zero component, σ_0, can be removed from the action by the gauge transformation

$$\bar\psi(\tau) \longrightarrow \bar\psi(\tau) e^{-i\int^\tau d\tau'(\sigma(\tau')-\sigma_0)}, \;\; \psi(\tau) \longrightarrow e^{i\int^\tau d\tau'(\sigma(\tau')-\sigma_0)}\psi(\tau).$$

Note that σ_0 has to be retained as (in general) it would change the periodicity, $\psi(\tau+\beta) = -\psi(\tau)$.

Then

$$\begin{aligned} \mathcal{G}(\tau_1,\tau_2;\mu) &= \frac{1}{\mathcal{Z}(\mu)} \int D\sigma\, e^{-\int_0^\beta d\tau (\frac{1}{4E_c}\sigma^2 - i\bar N\sigma)}\, e^{i\int_{\tau_1}^{\tau_2} d\tau'(\sigma(\tau')-\sigma_0)} \times \\ &\quad \times \int D[\bar\psi,\psi]\, e^{-\int_0^\beta d\tau \int d\mathbf{r}\, \bar\psi[\partial_\tau - \mu + i\sigma_0 + \mathcal{H}_0]\psi}\, \bar\psi(\tau_2)\psi(\tau_1) = \\ &= \frac{1}{\mathcal{Z}(\mu)} \int d\sigma_0\, e^{-\frac{\beta}{4E_c}\sigma_0^2 + i\beta\bar N\sigma_0} \int D[\bar\psi,\psi]\, e^{-\int_0^\beta d\tau \int d\mathbf{r}\, \bar\psi[\partial_\tau - \mu + i\sigma_0 + \mathcal{H}_0]\psi}\, \bar\psi(\tau_2)\psi(\tau_1) \times \\ &\quad \times \prod_{n\neq 0} \int d\sigma_n\, e^{-\frac{\beta}{4E_c}\sigma_n\sigma_{-n} + \frac{\sigma_n}{\omega_n}(\exp\{i\omega_n\tau_2\} - \exp\{i\omega_n\tau_1\})}. \end{aligned}$$

The integrals over the components $n \neq 0$ can be easily calculated, giving

$$e^{-2\frac{E_c}{\beta}\sum_{n\neq 0}\frac{1}{\omega_n^2}(1-\exp\{-i\omega_n\tau\})} = e^{-E_c(|\tau|-\beta^{-1}\tau^2)} \equiv \mathcal{B}(\tau), \tag{B.19}$$

where $\tau = \tau_2 - \tau_1$.

Thus, $\mathcal{G}(\tau,\sigma) \to \mathcal{B}(\tau)\mathcal{G}(\tau,\sigma_0)$. Evaluating the integral over σ_0 at the saddle point yields

$$\begin{aligned}
&\frac{1}{\mathcal{Z}(\mu)}\int d\sigma_0\, e^{-\frac{\beta}{4E_c}\sigma_0^2+i\beta\bar{N}\sigma_0}\int D[\bar{\psi},\psi]\, e^{-\int_0^\beta d\tau\int d\mathbf{r}\,\bar{\psi}[\partial_\tau-\mu+i\sigma_0+\mathcal{H}_0]\psi}\bar{\psi}(\tau_2)\psi(\tau_1) = \\
= &\frac{1}{\mathcal{Z}(\mu)}\int d\sigma_0\, e^{-\frac{\beta}{4E_c}\sigma_0^2+i\beta\bar{N}\sigma_0}\underbrace{\mathcal{Z}_0(\mu-i\sigma_0)}_{=\exp\{-\beta\Omega(\mu-\sigma_0)\}}\mathcal{G}_0(\tau_1,\tau_2;\mu-i\sigma_0) \simeq \\
\simeq &\mathcal{G}_0(\tau_1,\tau_2;\mu-i\bar{\sigma}_0),
\end{aligned}$$

where $\bar{\sigma}_0$ solves the equation $\bar{\sigma}_0/(2E_c) - i\bar{N} - i\partial_\mu\Omega|_{\mu-i\bar{\sigma}_0} = 0$ which can be rewritten as $\bar{\sigma}_0 = 2iE_c(\langle\hat{N}\rangle_{\mu-i\bar{\sigma}_0} - \bar{N})$. The condition for this approximation to be valid is $1/(2E_c) - \partial_\mu^2\Omega|_{\mu-\bar{\sigma}_0} = 1/(2E_c) + \delta^{-1} \gg \beta$.

Thus, the result is a shift of the chemical potential $\mu \to \bar{\mu} = \mu - i\bar{\sigma}_0$ (where $\bar{\sigma}_0$ real). I.e. in combination with the prefactor coming from non-zero frequencies,

$$\mathcal{G}(\tau;\mu) = \mathcal{B}(\tau)\cdot\mathcal{G}_0(\tau;\bar{\mu}). \tag{B.20}$$

Or, using (fermionic) Matsubara frequencies, $\epsilon_n = 2\pi(n+\frac{1}{2})/\beta$,

$$\begin{aligned}
\mathcal{G}(i\epsilon_n) &= \sum_m \mathcal{B}(i\omega_m)\,\mathcal{G}_0(i\epsilon_n - i\omega_m) = \\
&= -\frac{1}{2}\int\frac{d\omega'}{2\pi}\frac{d\epsilon'}{2\pi}B(\omega')A_0(\epsilon')\frac{\coth\frac{\beta\omega'}{2}+\tanh\frac{\beta\epsilon'}{2}}{i\epsilon_n-\omega'-\epsilon'},
\end{aligned} \tag{B.21}$$

where the second line is the Lehmann representation with the spectral function B (A_0) corresponding to $\mathcal{B}$ ($\mathcal{G}_0$). The spectral function of the so-called "Coulomb boson" $\mathcal{B}$ reads

$$B(\omega) = 2\sqrt{\frac{\pi\beta}{E_c}}e^{-\frac{\beta}{4E_c}(E_c^2+\omega^2)}\sinh\frac{\beta\omega}{2}. \tag{B.22}$$

After some straightforward manipulation of the above formula one obtains the following expression for the spectral function [118]:

$$\begin{aligned}
A(\epsilon) &= \frac{1}{2}\int\frac{d\omega'}{2\pi}B(\omega')A_0(\epsilon-\omega')(\tanh\frac{\beta}{2}(\omega'-\epsilon) - \coth\frac{\beta\omega'}{2}) = \\
&= \sqrt{\frac{\pi\beta}{E_c}}\,e^{-\frac{1}{4}\beta E_c}\cosh\frac{\beta\epsilon}{2}\int\frac{d\omega'}{2\pi}\frac{e^{-\frac{\beta}{4E_c}\omega'^2}}{\cosh\frac{\beta}{2}(\epsilon-\omega')}A_0(\epsilon-\omega').
\end{aligned}$$

Thus, the density of states – which is energy dependent in the presence of interaction – reads

$$\frac{\nu(\epsilon)}{\nu_0} = \sqrt{\frac{\pi\beta}{E_c}}\,e^{-\frac{1}{4}\beta E_c}\cosh\frac{\beta\epsilon}{2}\int\frac{d\omega'}{2\pi}e^{-\frac{\beta}{4E_c}\omega'^2}\cosh^{-1}\frac{\beta}{2}(\epsilon-\omega'). \tag{B.23}$$

The results for different ranges of energy, temperature and interaction strength are given in Ref. [118].

For the correlator of two spectral functions $\langle A(\epsilon+\frac{\omega}{2})A(\epsilon-\frac{\omega}{2})\rangle$, one obtains

$$\langle A(\epsilon+\frac{\omega}{2})A(\epsilon-\frac{\omega}{2})\rangle = \frac{\pi\beta}{E_c}\, e^{-\frac{1}{2}\beta E_c}\int\frac{d\eta}{2\pi}\,\mathcal{F}_0(\omega-\eta)\,e^{-\frac{\beta}{8E_c}\eta^2}\times \\ \times\int\frac{dW}{2\pi}e^{-\frac{\beta}{2E_c}W^2}\frac{\cosh\beta\epsilon+\cosh\frac{\beta\omega}{2}}{\cosh\beta(\epsilon-W)+\cosh\frac{\beta}{2}(\omega-\eta)}, \tag{B.24}$$

where we have made use of the fact that without interaction the disorder average $\langle A_0(\epsilon_1)A_0(\epsilon_2)\rangle \equiv \mathcal{F}_0(\epsilon_1,\epsilon_2)$ does depend on the energy difference $\omega=\epsilon_1-\epsilon_2$ only.

For further evaluation one has to make approximations. The two interesting limits are a) small charging or high temperature, $\beta E_c \ll 1$, and b) large charging or low temperature, $\beta E_c \gg 1$.

In the limit $\beta E_c \ll 1$, expanding $\cosh\beta(\epsilon-W)$ around $W=0$, Eq. (B.24) reduces to

$$\mathcal{F}(\epsilon,\omega) \;=\; \bar{\mathcal{F}}_0(\omega)(1+\mathcal{O}(\beta E_c)), \tag{B.25}$$

where

$$\bar{\mathcal{F}}_0(\omega)=\frac{1}{2}\sqrt{\frac{\beta}{E_c}}\int\frac{d\eta}{\sqrt{2\pi}}e^{-\frac{\beta}{8E_c}\eta^2}\mathcal{F}_0(\omega-\eta). \tag{B.26}$$

Thus, the correlation functions are only slightly modified. One an distinguish two effects: 1.) sharp features of $\mathcal{F}_0$ get smeared over the scale $2\sqrt{E_c/\beta}$, and 2.) corrections which are algebraically small in βE_c arise.

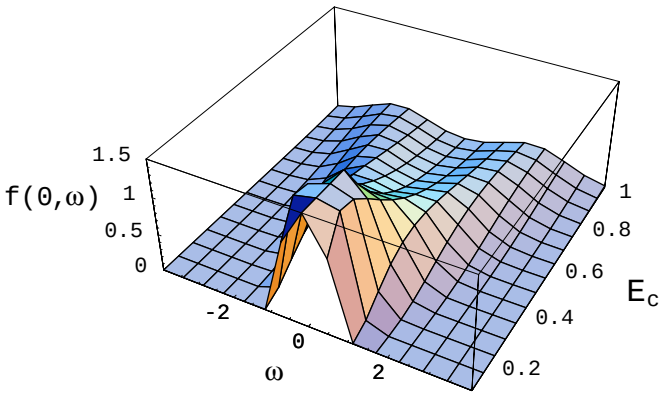

Figure B.1.: The interacting correlation function $\mathcal{F}(0,\omega)$ in the case $\mathcal{F}_0(\omega)\sim\delta(\omega)$ for varying E_c at $\beta^{-1}=0.2$.

The opposite limit, $\beta E_c \gg 1$, is experimentally more relevant, because mesoscopic effects in general favour low temperatures. Let us start by discussing the extreme case, $\beta\to\infty$ (which – although in principle out of the range of validity of the theory – yields qualitatively correct results). As the spectral function of the Coulomb boson reduces to $B(\omega)=2\pi[\delta(\omega+E_c)-\delta(\omega-E_c)]$, the result takes the simple form

$$A(\epsilon) \;=\; \frac{1}{2}\big(1+\theta(\epsilon-E_c)-\theta(E_c-\epsilon)\big)A_0(\epsilon-E_c) \;=\; A_0(\epsilon-E_c)\,\theta(\epsilon-E_c),$$

$$\langle A(\epsilon+\frac{\omega}{2})A(\epsilon-\frac{\omega}{2})\rangle \;=\; \mathcal{F}_0(\omega)\,\theta(\epsilon+\frac{\omega}{2}-E_c)\theta(\epsilon-\frac{\omega}{2}-E_c) \;=\; \mathcal{F}_0(\omega)\,\theta(\epsilon-\frac{|\omega|}{2}-E_c).$$

Integration over the 'centre of mass' energy ϵ results in

$$\int_{\frac{\omega}{2}}^{V-\frac{\omega}{2}} d\epsilon\, \theta(\epsilon-\frac{\omega}{2}-E_c) \;=\; \big(V-E_c-\omega\big)\cdot\theta(V-E_c-\omega),$$

i.e. in the original formulae for the current correlator C_I without interaction we just have to make the following replacement:

$$\int_0^V d\omega\,(V-\omega) \;\to\; \theta(V-E_c)\int_0^{V-E_c} d\omega\,(V-E_c-\omega). \tag{B.27}$$

As expected, one obtains a hard gap: at energies below E_c the correlator (as well as the average current) is completely suppressed while at higher energies ($V > E_c$) the result is unchanged except for replacing $V \to V_{\rm eff} = V - E_c$.

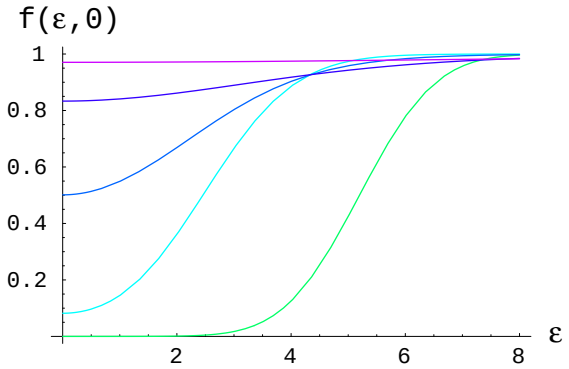

Figure B.2.: The interacting correlation function $\mathcal{F}(\epsilon,0)$ in the case $\mathcal{F}_0(\omega) \sim \delta(\omega)$ for various values of E_c and β, keeping $E_c/\beta = 1$ fixed.

This suggests that at finite temperatures, too, one has to distinguish two different cases, namely $V \ll \sqrt{E_c/\beta}$ and $\beta^{-1} \ll E_c \ll V$ (V sets the characteristic scale for ϵ,ω).

- $\underline{V \ll \sqrt{E_c/\beta}}$:

$$\begin{aligned}\mathcal{F}(\epsilon,\omega) \;&\simeq\; \frac{\beta}{2E_c}\, e^{-\frac{1}{2}\beta E_c}(\cosh\beta\epsilon+\cosh\frac{\beta\omega}{2})\int\frac{d\eta}{2\pi}\,\mathcal{F}_0(\omega-\eta)\,e^{-\frac{\beta}{8E_c}\eta^2}\,\frac{\omega-\eta}{\sinh\frac{\beta}{2}(\omega-\eta)} \simeq \\ &\simeq\; \bar{\mathcal{F}}_0(0)\,e^{-\frac{1}{2}\beta E_c}(\cosh\beta\epsilon+\cosh\frac{\beta\omega}{2})\cdot c(\beta E_c),\end{aligned} \tag{B.28}$$

  where $c(x)$ is an algebraic function.

- $\underline{\beta^{-1} \ll E_c \ll V}$:

$$\begin{aligned}\mathcal{F}(\epsilon,\omega) \;&\simeq\; \sqrt{\frac{\pi\beta}{2E_c}}\int\frac{d\eta}{2\pi}\,\mathcal{F}_0(\omega-\eta)\,e^{-\frac{\beta}{8E_c}\eta^2}\Big(1-2\cosh\frac{\beta}{2}(\omega-\eta)\,e^{-\beta(\epsilon-\frac{3}{2}E_c)}\Big) \simeq \\ &\simeq\; \bar{\mathcal{F}}_0(\omega) - e^{-\beta(\epsilon-2E_c)}(\bar{\mathcal{F}}_0(\omega+)e^{\frac{\beta\omega}{2}}+\bar{\mathcal{F}}_0(\omega-)e^{-\frac{\beta\omega}{2}}),\end{aligned} \tag{B.29}$$

  where $\omega\pm = \omega \pm 2E_c$.

Thus, in the regime $\beta E_c \gg 1$, the importance of interaction effects depends sensitively on the applied voltage. At small voltages, the correlators are exponentially suppressed, while at large voltages the interaction does not significantly change the results (except for the smearing over the scale $2\sqrt{E_c/\beta}$).

C. Weak localisation

In chapter 5 WL effects in quasi-2d systems subject to an in-plane magnetic field are studied. For transparency in the main text, some technical details are presented here.

C.1. Derivation of the slow action

Although the outcome of this construction is very much prescribed by criteria of gauge invariance, we prefer to derive the action explicitly. Making the quasi-classical replacement, $-i\partial \to \mathbf{p} - i\partial$, where $\mathbf{p}$ is a c-number momentum close to the Fermi momentum and $-i\partial$ on the r.h.s. is meant to be a derivative acting on slow fields, the action (5.10) transforms to

$$\tilde{S}[Q] = \frac{1}{2}\,\mathrm{Str}\,\ln\left(\hat{\mathcal{G}}_p^{-1} + \omega^{+}T^{-1}\sigma_3^{\mathrm{AR}}T - [T^{-1},\hat{\epsilon}]T + \frac{1}{m}\mathbf{p}\cdot\mathbf{B}\right) \tag{C.1}$$

with the following definitions:

$$\hat{\mathcal{G}}_p \equiv \left(\xi_p - \hat{\epsilon} + \frac{i}{2\tau}\sigma_3^{\mathrm{AR}}\right)^{-1}, \qquad \mathbf{B} \equiv T^{-1}\begin{pmatrix}\partial_x \\ \partial_y - i\hat{A}\sigma_3^{\mathrm{TR}}\end{pmatrix}T,$$

and $\xi_p = E_{\mathrm{F}} - p^2/(2m)$. To simplify the analysis, we next assume that the spacing between the subbands, $E_{kk'} = \epsilon_k - \epsilon'_k$ is by far in excess of the low energy scales of interest. Physically, this assumption entails that correlations between the subbands, i.e. diffusons and Cooperons connecting Green functions in different subbands, are negligible. Technically, the presence of the mass-operator $\sim [T^{-1},\hat{\epsilon}]T$ implies that the relevant matrices T must be diagonal in the subband-index space. Thus, the effective Qs can be represented as

$$Q = \{Q_k\delta_{kk'}\}, \qquad Q_k = T_k\Lambda_k T_k^{-1}. \tag{C.2}$$

A straightforward expansion of the action to first order in ω and to lowest non-vanishing order in the operators $\mathbf{B}$ yields

$$S[Q] \;=\; \int dS\,\frac{1}{4m^2}\sum_{\mathbf{p}}\mathrm{Str}\,(\mathcal{G}_p\mathbf{p}\cdot\mathbf{B}\,\mathcal{G}_p\mathbf{p}\cdot\mathbf{B}) - \frac{i\pi\nu\omega}{2}\int dS\;\mathrm{Str}\,(Q\sigma_3^{\mathrm{AR}})\,.$$

Setting temporarily $\omega = 0$, let us next focus on the further evaluation of the kinetic part of the action,

$$S_{\omega=0}[Q] = \frac{1}{4m^2}\sum_{\mathbf{p};k,k'}\int dS\;\mathrm{Str}\,\left(\mathcal{G}_p^k\,\mathbf{p}\cdot\mathbf{B}_{kk'}\,\mathcal{G}_p^{k'}\,\mathbf{p}\cdot\mathbf{B}_{k'k}\right). \tag{C.3}$$

In principle, the sum over k,k' extends over all subbands. Effectively, however, only the contribution of the occupied subbands is of relevance. For an empty subband, $E_{\mathrm{F}} - \epsilon_k < 0$, the pole

of the momentum dependent SCBA-Green function lies far off the integration contour, and the integral does not depend on whether the Green function is advanced or retarded. Technically, this pole structure implies that we do not obtain a slowly varying contribution to the action: No diffusons or Cooperons can be constructed from such types of Green functions. Therefore, the action is approximated by

$$S_{\omega=0}[Q] = \frac{1}{4m^2} \tilde{\sum_{\mathbf{p};k,k'}} \int dS \ \mathrm{Str} \left(\mathcal{G}_p^k \, \mathbf{p} \cdot \mathbf{B}_{kk'} \, \mathcal{G}_p^{k'} \, \mathbf{p} \cdot \mathbf{B}_{k'k} \right) + S^{\mathrm{no}}, \tag{C.4}$$

where $\tilde{\sum}$ extends over all occupied subbands, and S^{no} denotes the collective contribution of the empty subbands. These contributions are due to virtual processes which are negligible as long as the number of occupied subbands $M > 1$. The case $M = 1$ is special and will be treated separately in section 5.3. Using the representation

$$\mathcal{G}_p^k = \frac{1}{2} \sum_{s=\pm 1} \frac{1 + s\sigma_3^{\mathrm{AR}}}{\xi_p - \epsilon_k + s\frac{i}{2\tau}}, \tag{C.5}$$

it can be shown that

$$S_{\omega=0}[Q] \ = \ \frac{\pi\nu}{8} \tilde{\sum_{s=\pm 1;k,k'}} \frac{D_{kk'}}{-isE_{kk'}\tau + 1} \int dS \ \mathrm{Str} \left((1 + s\sigma_3^{\mathrm{AR}}) \mathbf{B}_{kk'} \cdot (1 - s\sigma_3^{\mathrm{AR}}) \mathbf{B}_{k'k} \right),$$

where $D_{kk'} = (D_k + D_{k'})/2$ (D_k diffusion coefficient of the subband k). Summing over s, the action decomposes into two parts, $S = S^I + S^{II}$, where

$$S^I[Q] \ = \ -\frac{i\pi\nu}{2} \tilde{\sum_{k,k'}} C_{kk'} E_{kk'} \tau \int dS \ \mathrm{Str} \left(\sigma_3^{\mathrm{AR}} \mathbf{B}_{kk'} \mathbf{B}_{k'k} \right), \tag{C.6}$$

$$S^{II}[Q] \ = \ -\frac{\pi\nu}{8} \tilde{\sum_{k,k'}} C_{kk'} \int dS \ \mathrm{Str} \left([\sigma_3^{\mathrm{AR}}, \mathbf{B}_{kk'}] \cdot [\sigma_3^{\mathrm{AR}}, \mathbf{B}_{k'k}] \right), \tag{C.7}$$

and

$$C_{kk'} \equiv \frac{D_{kk'}}{(E_{kk'}\tau)^2 + 1}.$$

Considering S^I first, notice that due to $E_{kk} = 0$, the operator $\mathbf{B}_{kk'}$ reduces to its off-diagonal component $-iT_k^{-1} A_{kk'} \sigma_3^{\mathrm{TR}} T_{k'} \mathbf{e}_y$ in that part of the action. However,

$$\mathrm{Str} \left(\sigma_3^{\mathrm{AR}} T_k^{-1} A_{kk'} \sigma_3^{\mathrm{TR}} T_{k'} T_{k'}^{-1} A_{k'k} \sigma_3^{\mathrm{TR}} T_k \right) = A_{kk'} A_{k'k} \, \mathrm{Str} \, (Q_k) = 0$$

because the matrices Q_k are traceless. Thus, $S^I = 0$.

Turning to the second contribution, S^{II}, and defining $\hat{\mathbf{\Xi}}^T \equiv (\partial_x, \partial_y - i\hat{A}\sigma_3^{\mathrm{TR}})$, one obtains

$$\begin{aligned} \mathrm{Str} \left([\sigma_3^{\mathrm{AR}}, \mathbf{B}_{kk'}] \cdot [\sigma_3^{\mathrm{AR}}, \mathbf{B}_{k'k}] \right) \ &= \ \mathrm{Str} \left([\sigma_3^{\mathrm{AR}}, T_k^{-1} \mathbf{\Xi}_{kk'} T_{k'}] \, [\sigma_3^{\mathrm{AR}}, T_{k'}^{-1} \mathbf{\Xi}_{k'k} T_k] \right) = \\ &= \ \mathrm{Str} \left((\mathbf{\Xi}_{kk'} Q_{k'} - Q_k \mathbf{\Xi}_{kk'}) \, (\mathbf{\Xi}_{k'k} Q_k - Q_{k'} \mathbf{\Xi}_{k'k}) \right). \end{aligned}$$

Making use of the operator identity $[\hat{\partial}, \hat{O}] = \widehat{\partial O}$, holding for coordinate-diagonal operators $\hat{O}$, yields

$$\begin{aligned} S_{\omega=0}[Q] = -\frac{\pi\nu}{8} \int dS \tilde{\sum_{k,k'}} C_{kk'} \, \mathrm{Str} \Big(\, & [\delta_{kk'} \partial Q_k - i\mathbf{A}_{kk'} (\sigma_3^{\mathrm{TR}} Q_{k'} - Q_k \sigma_3^{\mathrm{TR}})] \cdot \\ & \cdot [\delta_{k'k} \partial Q_{k'} - i\mathbf{A}_{k'k} (\sigma_3^{\mathrm{TR}} Q_k - Q_{k'} \sigma_3^{\mathrm{TR}})] \Big). \end{aligned}$$

Substituting this result back into the full action and completing the square yields the final expression for the general slow action given by Eq. (5.13).

C.2. Evaluation of the conductivity within the NLσM

Here we apply the results of Sec. 5.2 for the Cooperon to a one-loop calculation of the in-plane conductivity,

$$\sigma(\mathbf{r},\mathbf{r}') = \frac{1}{2\pi}\langle j_x(\mathbf{r})G^+(\mathbf{r},\mathbf{r}')j_x(\mathbf{r}')G^-(\mathbf{r}',\mathbf{r})\rangle. \tag{C.8}$$

Let us introduce a vector potential type source [120], $\mathbf{A}_s = (A_\pm + A_\mp)\mathbf{e}_x$, where

$$A_\pm = a_\pm E_{12}^{\rm AR}\otimes\mathcal{P}, \qquad A_\mp = a_\mp E_{21}^{\rm AR}\otimes\mathcal{P},$$

$a_\pm$ and $a_\mp$ are scalar source fields, and $\mathcal{P}\equiv E_{11}^R$ is a projector on the replica-index 1. We next minimally couple this 'vector potential' to the action, i.e. we substitute the momentum according to

$$-i\partial - \mathbf{A} \to -i\partial - \mathbf{A} - \mathbf{A}_s,$$

where $\mathbf{A}$ stands for the physical vector potential. Then the above correlation function can be generated as

$$\sigma(\mathbf{r},\mathbf{r}') = -\frac{1}{2\pi}\frac{\delta^2}{\delta a_\pm(\mathbf{r})\delta a_\mp(\mathbf{r}')}\bigg|_{a=0}\mathcal{Z}[a_\pm,a_\mp], \tag{C.9}$$

where $\mathcal{Z}[a_\pm,a_\mp]$ denotes the minimally coupled functional integral. The time-reversal doubling operation transforms the above momentum operator into

$$-i\partial - \mathbf{A} - \mathbf{A}_s \to -i\partial - \mathbf{A}\sigma_3^{\rm TR} - \mathbf{A}_s^{\rm TR},$$

where $\mathbf{A}_s^{\rm TR} = (A_\pm^{\rm TR} + A_\mp^{\rm TR})\mathbf{e}_x$, and

$$\begin{aligned} A_\pm^{\rm TR} &= a_\pm(E_{12}^{\rm AR}\otimes E_{11}^{\rm TR} - E_{21}^{\rm AR}\otimes E_{22}^{\rm TR})\otimes\mathcal{P},\\ A_\mp^{\rm TR} &= a_\mp(E_{21}^{\rm AR}\otimes E_{11}^{\rm TR} - E_{12}^{\rm AR}\otimes E_{22}^{\rm TR})\otimes\mathcal{P}. \end{aligned}$$

To keep the notation simple, we will omit the source field superscript 'TR' throughout.

The advantage of introducing a vector potential type source field is that we do not need to explicitly trace the fate of the sources under the gradient expansion. Gauge invariance alone implies that the mere effect of the presence of sources is to generalise the derivatives in the slow mode action (5.13) to

$$\delta_{kk'}\partial Q_k \to \delta_{kk'}(\partial Q_k - i[\mathbf{A_s}, Q_k]),$$

Note that the source field, not depending on the z-coordinate, is proportional to the unit matrix in k-space. We next need to expand to second order in $\mathbf{A}_s$. The contribution relevant for computing the conductance comes from the source-field diamagnetic term. Explicitly,

$$S[Q,\mathbf{A}_s] \to S[Q,0] - \frac{\pi\nu}{8}\tilde{\sum_k}\int dS\, D_k\,\mathrm{tr}\,[\mathbf{A}_s,Q_k]^2,$$

which means that the conductance obtains as

$$\sigma(\mathbf{r},\mathbf{r}') = -\frac{\nu}{16}\frac{\delta^2}{\delta a_\pm(\mathbf{r})\delta a_\mp(\mathbf{r}')}\bigg|_{a=0}\left\langle\tilde{\sum_k} D_k\int dS\ \mathrm{tr}\,[\mathbf{A}_s,Q_k]^2\right\rangle_Q. \tag{C.10}$$

(As for the signs, notice that (5.13) has been derived within supersymmetry, whilst we are now working with replicas.) Carrying out the differentiation, we arrive at $\sigma(\mathbf{r},\mathbf{r}') = \sigma\,\delta(\mathbf{r}-\mathbf{r}')$ and

$$\sigma = -\frac{\nu}{8}\tilde{\sum_k} D_k \Big\langle \mathrm{tr}\,\big([(E_{12}^{\mathrm{AR}}\otimes E_{11}^{\mathrm{TR}} - E_{21}^{\mathrm{AR}}\otimes E_{22}^{\mathrm{TR}})\otimes\mathcal{P}, Q_k(\mathbf{r})]\times \\ \times[(E_{21}^{\mathrm{AR}}\otimes E_{11}^{\mathrm{TR}} - E_{12}^{\mathrm{AR}}\otimes E_{22}^{\mathrm{TR}})\otimes\mathcal{P}, Q_k(\mathbf{r})]\big)\Big\rangle_Q.$$

Expanding Q around σ_3^{AR} in the generators B^c as before, it is straightforward to show that evaluating the expression '$\mathrm{tr}\,(\dots)$' to lowest order yields

$$-8\left\{1+\mathrm{tr}\Big((E_{11}^{\mathrm{TR}}\otimes\mathcal{P})B^\dagger(E_{22}^{\mathrm{TR}}\otimes\mathcal{P})B^\dagger+(E_{11}^{\mathrm{TR}}\otimes\mathcal{P})B(E_{22}^{\mathrm{TR}}\otimes\mathcal{P})B\Big)\right\} \;=\; -8\left\{1-2\,\mathrm{tr}\,(\mathcal{P}b\mathcal{P}b^*)\right\},$$

where we have temporarily dropped the position and k-arguments for notational transparency. Substituting this into the expression for the conductivity obtains

$$\sigma \;=\; \nu\tilde{\sum_k} D_k\left(1-2\sum_{\mathbf{q}}\left\langle \mathrm{tr}\,(\mathcal{P}b_{k,\mathbf{q}}\mathcal{P}b^*_{k,\mathbf{q}})\right\rangle\right) \;=\; \nu\tilde{\sum_k} D_k - \frac{2}{\pi}\tilde{\sum_{k;\mathbf{q}}}(\mathcal{C}_{\mathbf{q},\omega=0})_{kk} \qquad \text{(C.11)}$$

which finally leads to Eqs. (5.18,5.19).

C.3. Toy model for one occupied subband

A simple RMT model can reproduce the relevant features of the $M=1$ case: We couple a system described by a RMT Hamiltonian (modelling the occupied level) to two high-lying energy levels. After doubling the field space to account for time-reversal symmetry in the occupied subband, the action is given by the following expression:

$$S \;=\; -\frac{i}{2}\bar{c}(\omega^+\sigma_3^{\mathrm{AR}}-\mathcal{H}_{\mathrm{RMT}})c + \frac{i}{2}\sum_j\left[\bar{c}\,\hat{U}_j^\dagger\,d_j + \mathrm{h.c.}\right] + \frac{i}{2}\bar{d}\begin{pmatrix}\epsilon & \hat{t}^\dagger\\ \hat{t} & \epsilon\end{pmatrix}d, \qquad \text{(C.12)}$$

where $d^T=(d_1^T,d_2^T)$ and $\hat{x}=\begin{pmatrix}x & \\ & x^*\end{pmatrix}_{\mathrm{TR}}$ for $x=U_j,t$.

Averaging over the random Hamiltonian $\mathcal{H}_{\mathrm{RMT}}$ and then applying a Hubbard-Stratonovich transformation leads to

$$S_o = -\frac{i}{2}\bar{c}(\omega^+\sigma_3^{\mathrm{AR}}-\mathcal{H}_{\mathrm{RMT}})c \to \bar{S}_o = -\frac{N}{4}\,\mathrm{Str}\,Q^2 - \frac{i}{2}\bar{c}(\omega^+\sigma_3^{\mathrm{AR}}+i\lambda Q)c.$$

Defining $\psi^T=(c^T,d^T)$, the fermionic action is given as

$$S_F = -\frac{i}{2}\bar{\psi}\begin{pmatrix}\omega^+\sigma_3^{\mathrm{AR}}+i\lambda Q & -\hat{U}_1^\dagger & -\hat{U}_2^\dagger\\ -\hat{U}_1 & -\epsilon & -\hat{t}^\dagger\\ -\hat{U}_2 & -\hat{t} & -\epsilon\end{pmatrix}\psi \equiv -\frac{i}{2}\bar{\psi}\hat{G}^{-1}\psi.$$

Gaussian integration yields

$$S[Q] \;=\; -\frac{N}{4}\,\mathrm{Str}\,Q^2 + \frac{1}{2}\,\mathrm{Str}\,\ln\hat{G}^{-1}.$$

The saddle point manifold is described by $Q = T^{-1}\sigma_3^{\mathrm{AR}}T$. Thus,

$$S[Q] \;=\; \frac{1}{2}\,\mathrm{Str}\,\ln\begin{pmatrix}\omega^+ T\sigma_3^{\mathrm{AR}}T^{-1} + i\lambda\sigma_3^{\mathrm{AR}} & -T\hat{U}_1^\dagger & -T\hat{U}_2^\dagger \\ -\hat{U}_1 T^{-1} & -\epsilon & -\hat{t}^\dagger \\ -\hat{U}_2 T^{-1} & -\hat{t} & -\epsilon\end{pmatrix}.$$

By means of the identity $\mathrm{Str}\,\ln\begin{pmatrix}A & B\\ C & D\end{pmatrix} = \mathrm{Str}\,\ln D + \mathrm{Str}\,\ln(A - BD^{-1}C)$ and retaining only the lowest order term in ω, we get

$$S[Q] \;=\; -\frac{i\omega^+}{2\lambda}\,\mathrm{Str}\,(\sigma_3^{\mathrm{AR}}Q) + \frac{1}{2}\,\mathrm{Str}\,\ln\Big[i\lambda Q + X\Big], \tag{C.13}$$

where $X = \begin{pmatrix}\hat{U}_1^\dagger & \hat{U}_2^\dagger\end{pmatrix}\begin{pmatrix}\epsilon & \hat{t}^\dagger\\ \hat{t} & \epsilon\end{pmatrix}^{-1}\begin{pmatrix}\hat{U}_1\\ \hat{U}_2\end{pmatrix}$. With

$$\begin{pmatrix}\epsilon & \hat{t}^\dagger\\ \hat{t} & \epsilon\end{pmatrix}^{-1} = \begin{pmatrix}\epsilon(\epsilon^2 - \hat{t}^\dagger\hat{t})^{-1} & -\hat{t}^\dagger(\epsilon^2 - \hat{t}\hat{t}^\dagger)^{-1}\\ -\hat{t}(\epsilon^2 - \hat{t}^\dagger\hat{t})^{-1} & \epsilon(\epsilon^2 - \hat{t}\hat{t}^\dagger)^{-1}\end{pmatrix}\;\Big(\!\Big(\simeq \frac{1}{\epsilon^2}\begin{pmatrix}\epsilon & -t^\dagger\\ -t & \epsilon\end{pmatrix}\Big)\!\Big)$$

this term reads

$$X \;=\; \epsilon\Big(\hat{U}_1^\dagger(\epsilon^2 - \hat{t}^\dagger\hat{t})^{-1}\hat{U}_1 + \hat{U}_2^\dagger(\epsilon^2 - \hat{t}\hat{t}^\dagger)^{-1}\hat{U}_2\Big) - \Big(\hat{U}_1^\dagger\hat{t}^\dagger(\epsilon^2 - \hat{t}\hat{t}^\dagger)^{-1}\hat{U}_2 + \hat{U}_2^\dagger\hat{t}(\epsilon^2 - \hat{t}^\dagger\hat{t})^{-1}\hat{U}_1\Big).$$

The simplest model is to assume $U_1 = U_2 \equiv U$ and take all couplings to be time-reversal breaking, i.e. $U^T = -U$ as well as $t^T = -t$. This leads to

$$X = -\frac{1}{\epsilon^2 + |t|^2}|U|^2\big(2\epsilon - (t - t^*)\sigma_3^{\mathrm{TR}}\big).$$

Inserting this into the action, Eq. (C.13), and expanding the logarithm yields

$$\begin{aligned} S_{\omega=0}[Q] \;&=\; \frac{1}{2}\,\mathrm{Str}\,\ln\Big[i\lambda Q - \frac{1}{\epsilon^2 + |t|^2}|U|^2\big(2\epsilon - (t - t^*)\sigma_3^{\mathrm{TR}}\big)\Big] \\ &=\; \frac{|U|^4(t - t^*)^2}{4\lambda^2(\epsilon^2 + |t|^2)^2}\,\mathrm{Str}\,(\sigma_3^{\mathrm{TR}}Q)^2. \end{aligned} \tag{C.14}$$

Thus, the symmetry breaking first occurs in 6^{th} order of the perturbation (U^4t^2).

This simple toy model also allows one to get some information on what to expect when the impurity potential is z-dependent. If electrons are scattered in z-direction, even in the absence of a magnetic field the subbands are coupled. To model this, we now choose the couplings to have an additional term which is time-reversal invariant, i.e. $x \to x_s + x_a$ ($x = U, t$), where $x^T \to x_s - x_a$. Then, the lowest order term with σ_3^{TR} does not include any coupling between the two unoccupied levels, but is simply given as

$$X \simeq \frac{2}{\epsilon}\left(|U_s|^2 - |U_a|^2 + (U_s^*U_a - U_a^*U_s)\sigma_3^{\mathrm{TR}}\right).$$

Expanding the logarithm, now, the symmetry breaking occurs already in 2^{nd} order of the coupling U_a modelling the magnetic field, namely

$$S_{\omega=0}[Q] \;=\; \frac{(U_s^*U_a - U_a^*U_s)^2}{\lambda^2\epsilon^2}\,\mathrm{Str}\,(\sigma_3^{\mathrm{TR}}Q)^2. \tag{C.15}$$

C.4. Examples of confining potentials

As two examples we choose a) a symmetric quantum well with a box potential, and b) an asymmetric, triangular quantum well. Note that the labelling of the subbands, $k = 1, \ldots M$, is shifted as compared to the main text ($k = 0, \ldots M-1$).

Symmetric quantum well

A box with infinitely high walls is described by the potential

$$W(z) = \begin{cases} 0 & |z| < \frac{d}{2}\,, \\ \infty & \text{otherwise}\,. \end{cases}$$

The eigenfunctions for this potential are given as

$$\phi_k(z) = \sqrt{\frac{2}{d}} \sin(\frac{\pi k}{d}(z + \frac{d}{2})). \tag{C.16}$$

whereas the corresponding eigenenergies read $\epsilon_k = \frac{\pi^2 k^2}{2md^2}$. Thus,

$$A_{kk'} \;=\; \begin{cases} 0 & \text{k+k' even}\,, \\ \dfrac{8Hd}{\pi^2}\dfrac{kk'}{(k^2-k'^2)^2} = \dfrac{2Hd}{\pi^2}\dfrac{\bar{k}^2-\Delta k^2}{\bar{k}^2\Delta k^2} & \text{k+k' odd}\,, \end{cases}$$

where $\bar{k} = k + k'$, $\Delta k = k - k'$ are 'centre of mass' coordinates.

The matrix elements $\mathcal{X}_{kk'}$ appearing in the saddle point equation are then given by the following expression,

$$\mathcal{X}_{kk'} \;=\; D_{kk'} \left(\frac{2Hd}{\pi^2}\right)^2 \frac{1}{\left(\bar{k}\Delta k \frac{\pi^2\tau}{2md^2}\right)^2 + 1} \frac{(\bar{k}^2-\Delta k^2)^2}{\bar{k}^4\Delta k^4}.$$

Notice that $\mathcal{X}_{kk'}$ decays rapidly with increasing $\bar{k}, \Delta k$.

For the experimentally most relevant case of only two occupied subbands we obtain

$$\mathcal{X}_{12} = \mathcal{X}_{21} = D_{12} \left(\frac{16Hd}{9\pi^2}\right)^2 \frac{1}{\left(\frac{3\pi^2\tau}{2md^2}\right)^2 + 1}.$$

Asymmetric quantum well

A triangular potential well is described by the potential

$$W(z) = \begin{cases} \infty & z < 0\,, \\ wz & z > 0\,. \end{cases}$$

The eigenfunction are Airy functions,

$$\phi_k(z) = c_k \,\mathrm{Ai}\left((2mw)^{1/3} z + a_k\right), \tag{C.17}$$

where the normalisation factor reads $c_k = 1/\mathrm{Ai}'(a_k)$. The a_k are zeros of the Airy function, the first few values being $a_1 \approx -2.34$, $a_2 \approx -4.09$, $a_3 \approx -5.52$, $a_4 \approx -6.79$, and $a_5 \approx -7.94$. The corresponding energies are given as

$$\epsilon_k = -\left(\frac{w^2}{2m}\right)^{1/3} a_k.$$

Thus,

$$A_{kk'} = \frac{H}{\mathrm{Ai}'(a_k)\mathrm{Ai}'(a_{k'})} \int_0^\infty dz\, \mathrm{Ai}\left(\frac{z}{d}+a_k\right)\, z\, \mathrm{Ai}\left(\frac{z}{d}+a_{k'}\right),$$

where $d = (2mw)^{1/3}$ sets the scale for the width of the well.

The relevant values for the case of only two occupied subbands are $A_{11} = 1.56Hd$, $A_{12} = -0.67Hd$, and $A_{22} = 2.73Hd$. (More general: $A_{kk} = -\frac{2}{3}a_k Hd$, roughly.)

D. Zero-modes: Integration volume

The volume of the group $\mathrm{U}(N)$ is given as $\mathcal{V}(\mathrm{U}(N)) \sim 1/\left(\prod_{j=1}^{N-1} j!\right)$. Thus, the volume of the coset space reads

$$\mathcal{V}\left(\frac{\mathrm{U}(N)}{\mathrm{U}(p)\times\mathrm{U}(N-p)}\right) \sim \frac{\prod_{j=1}^{p-1} j!\ \prod_{j=1}^{N-p-1} j!}{\prod_{j=1}^{N-1} j!}. \tag{D.1}$$

Now $\left(\prod_{j=1}^{4-1} j!\right) / \left(\prod_{j=1}^{N-p-1} j!\right) = \prod_{j=1}^{4}(N-p-1+j)! = \prod_{j=1}^{p}(N-j)!$, i.e.

$$\begin{aligned}\mathcal{V} \equiv \mathcal{V}\left(\frac{\mathrm{U}(N)}{\mathrm{U}(p)\times\mathrm{U}(N-p)}\right) &\sim \prod_{j=1}^{p}\frac{(j-1)!}{(N-j)!} = \\ &= \prod_{j=1}^{p}\Gamma(j)/\Gamma(N-j+1).\end{aligned}$$

By means of the identity $\Gamma(z+1)\Gamma(-z) = -\pi/\sin(\pi z)$, one obtains

$$\mathcal{V} \sim -\frac{1}{\pi}\sin^p(\pi N)\prod_{j=1}^{p}(-1)^j\Gamma(j)\Gamma(j-N). \tag{D.2}$$

In this form the replica limit $N \to 0$ may be taken which – for the relevant case $p = 1$ – yields

$$\mathcal{V}\left(\frac{\mathrm{U}(N)}{\mathrm{U}(1)\times\mathrm{U}(N-1)}\right) \xrightarrow[N\to 0]{} \sim N. \tag{D.3}$$

Bibliography

[1] N. G. van Kampen, *Stochastic Processes in Physics and Chemistry* (North-Holland, Amsterdam, 1981).

[2] Y. Imry, in *Directions in Condensed Matter Physics*, edited by G. Grinstein and G. Mazenko (World Scientific, Singapore, 1986).

[3] B. L. Altshuler, P. A. Lee, and R. A. Webb, *Mesoscopic Phenomena in Solids* (North-Holland, Amsterdam, Oxford, New York, Tokio, 1991).

[4] *Mesoscopic Quantum Physics (Les Houches Session LXI)*, edited by E. Akkermans, G. Montambaux, J.-L. Pichard, and J. Zinn-Justin (Elsevier, North-Holland, Amsterdam, 1995).

[5] *Mesoscopic Electron Transport*, Vol. 345 of *NATO Advanced Study Institute, Series E: Applied Sciences*, edited by L. L. Sohn, L. P. Kouwenhoven, and G. Schön (Kluwer, Dordrecht, 1997).

[6] B. D. Simons and A. Altland, in *Theoretical Physics at the End of the XXth Century, Banff, CRM Series in Mathematical Physics* (Springer, New York, 2001), Chap. Mesoscopic Physics.

[7] M. Janßen, Phys. Reports **295**, 1 (1998).

[8] P. W. Anderson, J. Phys. Chem. Sol. **11**, 26 (1959).

[9] H. L. Störmer *et al.*, J. Vac. Sci. and Technol. **16**, 1517 (1979).

[10] A. Palevski *et al.*, Phys. Rev. Lett. **65**, 1929 (1990).

[11] G. S. Boebinger, A. Passner, L. N. Pfeiffer, and K. W. West, Phys. Rev. B **43**, 12673 (1991).

[12] A. Kurobe *et al.*, Phys. Rev. B **50**, 4889 (1994).

[13] Y. Berk *et al.*, Phys. Rev. B **51**, 2604 (1995).

[14] J. P. Eisenstein, L. N. Pfeiffer, and K. W. West, Appl. Phys. Lett. **57**, 2324 (1990).

[15] W. Demmerle *et al.*, Phys. Rev. B **44**, 3090 (1991).

[16] J. A. Simmons *et al.*, Phys. Rev. B **47**, 15741 (1993).

[17] K. M. Brown *et al.*, Appl. Phys. Lett. **64**, 1827 (1994).

[18] J. Smoliner, E. Gornik, and G. Weimann, Appl. Phys. Lett. **52**, 2136 (1988).

[19] J. Smoliner *et al.*, Phys. Rev. Lett. **63**, 2116 (1989).

[20] J. P. Eisenstein, T. J. Gramila, L. N. Pfeiffer, and K. W. West, Phys. Rev. B **44**, 6511 (1991).

[21] L. Zheng and A. H. MacDonald, Phys. Rev. B **47**, 10619 (1993).

[22] S. Q. Murphy, J. P. Eisenstein, L. N. Pfeiffer, and K. W. West, Phys. Rev. B **52**, 14825 (1995).

[23] T. Jungwirth and A. H. MacDonald, Phys. Rev. B **53**, 7403 (1996).

[24] A. Altland, C. H. W. Barnes, F. W. J. Hekking, and A. J. Schofield, Phys. Rev. Lett. **83**, 1203 (1999).

[25] J. S. Meyer, *Tunneling Spectroscopy with Two-Dimensional Electron Gases*, Diplomarbeit, 1999.

[26] J. S. Meyer, A. Altland, and M. Janßen, Ann. Physik **8**, SI-173 (1999).

[27] U. Sivan *et al.*, Europhys. Lett. **25**, 605 (1994).

[28] B. D. Simons and B. L. Altshuler, Phys. Rev. Lett. **70**, 4063 (1993); Phys. Rev. B **48**, 5422 (1993).

[29] L. Zheng and A. H. MacDonald, Phys. Rev. B **48**, 8203 (1993).

[30] A. G. Rojo, J. Phys. Cond. Matt. **11**, R31 (1999).

[31] *Single Charge Tunneling*, edited by H. Grabert, J. M. Martinis, and M. H. Devoret (Plenum Press, New York, 1991).

[32] L. P. Gor'kov, A. I. Larkin, and D. E. Khmel'nitskii, JETP Lett. **30**, 228 (1979).

[33] S. Hikami, A. I. Larkin, and Y. Nagaoka, Prog. Theor. Phys. **63**, 707 (1980).

[34] B. L. Altshuler and A. G. Aronov, JETP Lett. **33**, 499 (1981).

[35] V. K. Dugaev and D. E. Khmel'nitskii, Sov. Phys. JETP **59**, 1038 (1984).

[36] V. I. Fal'ko, J. Phys. Cond. Matt. **2**, 3797 (1990).

[37] M. V. Budantsev, Z. D. Kvon, and A. G. Pogosov, Sov. Phys. Semicond. **26**, 879 (1992).

[38] H. Mathur and H. U. Baranger, preprint cond-mat/0008375.

[39] P. M. Mensz and R. G. Wheeler, Phys. Rev. B **35**, 2844 (1987).

[40] W. R. Anderson, D. R. Lombardi, R. G. Wheeler, and T.-P. Ma, IEEE Electron Dev. Lett. **14**, 351 (1993).

[41] J. Bardeen, L. N. Cooper, and J. R. Schrieffer, Phys. Rev. **108**, 1175 (1957).

[42] A. A. Abrikosov and L. P. Gork'ov, Sov. Phys. JETP **12**, 1243 (1961).

[43] Y. N. Ovchinnikov, Sov. Phys. JETP **29**, 853 (1969).

[44] A. Lamacraft and B. D. Simons, Phys. Rev. Lett. **85**, 4783 (2000).

[45] A. Lamacraft and B. D. Simons, preprint cond-mat/0101080.

[46] W. Meissner and R. Ochsenfeld, Naturwissenschaften **21**, 787 (1933).

[47] M. R. Zirnbauer, J. Math. Phys. **37**, 4986 (1996).

[48] A. A. Abrikosov, *Fundamental Theory of Metals* (North-Holland, Amsterdam, 1988).

[49] A. I. Larkin and Y. N. Ovchinnikov, Sov. Phys. JETP **34**, 1144 (1972).

[50] I. M. Lifshitz, Sov. Phys. Usp. **7**, 549 (1965).

[51] B. I. Halperin and M. Lax, Phys. Rev. **148**, 722 (1966).

[52] J. Zittartz and J. S. Langer, Phys. Rev. **148**, 741 (1966).

[53] I. Affleck, J. Phys. C **17**, 2323 (1984).

[54] K. B. Efetov and V. G. Marikhin, Phys. Rev. B **40**, 12126 (1989).

[55] O. Viehweger and K. B. Efetov, Phys. Rev. B **44**, 1168 (1991).

[56] A. A. Abrikosov, L. P. Gork'ov, and I. E. Dzyaloshinskii, *Methods of Quantum Field Theory in Statistical Physics* (Prentice-Hall, Inc., Englewood Cliffs, N.J., 1963).

[57] G. Rickayzen, *Green's Functions and Condensed Matter* (Academic Press, New York, London, 1980).

[58] A. D. Stone, in *Physics of Nanostructures*, *Scottish Universities Summer Schools in Physics Series*, edited by J. H. Davies and A. R. Long (IOP Publishing, Bristol, 1993).

[59] J. S. Langer and T. Neal, Phys. Rev. Lett. **16**, 984 (1966).

[60] G. Bergmann, Phys. Rep. **107**, 2 (1984).

[61] F. J. Wegner, Z. Phys. B **35**, 207 (1979).

[62] K. B. Efetov, Adv. Phys. **32**, 53 (1983).

[63] K. B. Efetov, *Supersymmetry in Disorder and Chaos* (Cambridge University Press, New York, 1997).

[64] L. V. Keldysh, Sov. Phys. JETP **20**, 1018 (1965).

[65] M. K. Horbach and G. Schön, Ann. Physik **2**, 51 (1993).

[66] A. Kamenev and A. V. Andreev, Phys. Rev. B **60**, 2218 (1999).

[67] J. J. M. Verbaarschot, H. A. Weidenmüller, and M. R. Zirnbauer, Phys. Rep. **129**, 367 (1985).

[68] B. D. Simons, O. Agam, and A. V. Andreev, J. Math. Phys. **38**, 1982 (1997).

[69] J. J. M. Verbaarschot and M. R. Zirnbauer, J. Phys. A **18**, 1093 (1985).

[70] A. Kamenev and M. Mezard, J. Phys. A **32**, 4373 (1999); Phys. Rev. B **60**, 3944 (1999).

[71] I. V. Yurkevich and I. V. Lerner, Phys. Rev. B **60**, 3955 (1999).

[72] E. P. Wigner, Ann. Math. **53**, 36 (1953).

[73] L. P. Gor'kov and G. M. Eliashberg, Sov. Phys. JETP **21**, 940 (1965).

[74] F. J. Dyson, J. Math. Phys. **3**, 140, 157, 166 (1962).

[75] F. J. Dyson and M. L. Mehta, J. Math. Phys. **4**, 701 (1963).

[76] O. Bohigas, M. J. Giannoni, and C. Schmit, Phys. Rev. Lett. **52**, 1 (1984); J. Physique Lett. **45**, L1615 (1984).

[77] C. E. Porter, *Statistical Theory of Spectra: Fluctuations* (Academic Press, New York, 1965).

[78] M. D. Mehta, *Random Matrices* (Academic Press, New York, 1991), 2nd edition.

[79] T. Guhr, A. Müller-Groeling, and H. A. Weidenmüller, Phys. Rep. **299**, 189 (1998).

[80] C. W. J. Beenakker, Rev. Mod. Phys. **69**, 731 (1997).

[81] J. J. M. Verbaarschot, Phys. Rev. Lett. **72**, 2531 (1994).

[82] A. Altland and M. R. Zirnbauer, Phys. Rev. B **55**, 1142 (1997).

[83] M. J. Kelly, *Low-dimensional Semiconductors: Materials, Physics, Technology, Devices* (Clarendon Press, Oxford, 1995).

[84] C. W. J. Beenakker and H. van Houten, in *Solid State Physics*, edited by H. Ehrenreich and D. Turnbull (Academic Press, Inc., San Diego, 1991).

[85] S. Tarucha *et al.*, Phys. Rev. Lett. **77**, 3613 (1996).

[86] L. P. Kouwenhoven *et al.*, Science **278**, 1788 (1997).

[87] B. L. Altshuler and B. I. Shklovskii, Sov. Phys. JETP **64**, 127 (1986).

[88] D. Ullmo and H. U. Baranger, preprint cond-mat/010398.

[89] A. L. Efros and B. I. Shklovskii, J. Phys. C **8**, L49 (1975).

[90] A. L. Efros, J. Phys. C **9**, 2021 (1976).

[91] B. L. Altshuler and A. G. Aronov, Sov. Phys. JETP **50**, 968 (1979); Solid State Commun. **30**, 115 (1979).

[92] B. L. Altshuler, A. G. Aronov, and P. A. Lee, Phys. Rev. Lett. **44**, 1288 (1980).

[93] E. Abrahams, P. W. Anderson, P. A. Lee, and T. V. Ramakrishnan, Phys. Rev. B **24**, 6783 (1982).

[94] A. M. Finkel'stein, Sov. Phys. JETP **57**, 97 (1983); Z. Phys. B **56**, 189 (1984).

[95] C. J. Chen, *Introduction to Scanning Tunneling Microscopy* (Oxford University Press, New York, 1993).

[96] P. W. Anderson, Phys. Rev. Lett. **18**, 1049 (1967).

[97] Y. Oreg and B. I. Halperin, Phys. Rev. B **60**, 5679 (1999).

[98] C. W. H. Barnes, private communication.

[99] M. H. Cohen, L. M. Falicov, and J. C. Phillips, Phys. Rev. Lett. **8**, 316 (1962).

[100] G. D. Mahan, *Many-Particle Physics* (Plenum Press, New York and London, 1981).

[101] *The Quantum Hall Effect*, edited by R. Prange and S. Girvin (Springer, Berlin, 1990).

[102] S. Girvin, in *Topological Aspects of Low Dimensional Systems (Les Houches Session LXIX)*, edited by A. Comtet, T. Jolicoeur, and S. Ouvry (Springer, New York, 1999).

[103] J. P. Eisenstein, L. N. Pfeiffer, and K. W. West, Phys. Rev. Lett. **74**, 1419 (1995).

[104] N. Turner *et al.*, Phys. Rev. B **54**, 10614 (1996).

[105] L. S. Levitov, private communication.

[106] L. S. Levitov and A. V. Shytov, preprint cond-mat/9510006.

[107] I. S. Gradshteyn and I. M. Ryzhik, *Table of Integrals, Series, and Products* (Academic Press, New York and London, 1965).

[108] A. M. Rudin, I. L. Aleiner, and L. I. Glazman, Phys. Rev. B **55**, 9322 (1997).

[109] E. Abrahams, P. W. Anderson, D. C. Licciardello, and T. V. Ramakrishnan, Phys. Rev. Lett. **42**, 673 (1979).

[110] R. Merkt, M. Janßen, and B. Huckestein, Phys. Rev. B **58**, 4394 (1998).

[111] M. Janßen, O. Viehweger, U. Fastenrath, and J. Hajdu, *Introduction to the Theory of the Integer Quantum Hall Effect* (Wiley-VCH, Weinheim, 1994).

[112] M. P. Sarachik and S. V. Kravchenko, Phys. Stat. Sol. B **218**, 237 (2000), and references therein.

[113] J. T. Chalker, Physica A **167**, 253 (1990).

[114] B. Huckestein and M. Backhaus, Phys. Rev. Lett. **82**, 5100 (1999).

[115] A. Wieck, private communication.

[116] A. Altland, S. Iida, and K. B. Efetov, J. Phys. A **26**, 3545 (1993).

[117] N. Taniguchi, A. V. Andreev, and B. L. Altshuler, Europhys. Lett. **29**, 515 (1995).

[118] A. Kamenev and Y. Gefen, preprint cond-mat/9503093; Phys. Rev. B **54**, 5428 (1996).

[119] M. Robnik and M. V. Berry, J. Phys. A **19**, 669 (1986).

[120] B. L. Altshuler, V. E. Kravtsov, and I. V. Lerner, Sov. Phys. JETP **64**, 1352 (1986).

[121] *Superconductivity*, edited by R. D. Parks (Dekker, New York, 1969), Vol. I and II.

[122] P. G. de Gennes, *Superconductivity of Metals and Alloys* (W.A. Benjamin, New York, 1966).

[123] M. Tinkham, *Introduction to Superconductivity* (McGraw-Hill, New York, 1996), 2nd edition.

[124] L. P. Gor'kov, Sov. Phys. JETP **9**, 1364 (1959).

[125] F. B. Silsbee, J. Wash. Acad. Sci. **6**, 597 (1916).

[126] W. S. Corak and C. W. Satterthwaite, Phys. Rev. **99**, 1660 (1954).

[127] W. S. Corak, B. B. Goodman, C. W. Satterthwaite, and A. Wexler, Phys. Rev. **96**, 1442 (1954); **102**, 656 (1956).

[128] L. N. Cooper, Phys. Rev. **104**, 1189 (1956).

[129] E. Maxwell, Phys. Rev. **78**, 477 (1950).

[130] C. A. Reynolds, B. Serin, W. H. Wright, and L. B. Nesbitt, Phys. Rev. **78**, 487 (1950).

[131] H. Fröhlich, Phys. Rev. **79**, 845 (1950).

[132] J. Bardeen, Phys. Rev. **79**, 167; **80**, 567 (1950); **81**, 829, 1070; **82**, 987 (1951).

[133] G. Eilenberger, Z. Phys. **182**, 427 (1965); **214**, 195 (1968).

[134] A. I. Larkin and Y. N. Ovchinnikov, Sov. Phys. JETP **28**, 1200 (1968).

[135] A. L. Shelankov, J. Low Temp. Phys. **60**, 29 (1985).

[136] A. V. Zaitsev, Sov. Phys. JETP **59**, 1015 (1994).

[137] K. D. Usadel, Phys. Rev. Lett. **25**, 507 (1970); Phys. Rev. B **4**, 99 (1971).

[138] A. V. Balatsky and S. A. Trugman, Phys. Rev. Lett. **79**, 3767 (1997).

[139] J. Cardy, J. Phys. C **11**, L321 (1978).

[140] K. B. Efetov, A. I. Larkin, and D. E. Khmel'nitskii, Sov. Phys. JETP **52**, 568 (1980).

[141] A. M. Finkel'stein, Sov. Phys. JETP **57**, 97 (1983).

[142] R. Oppermann, Nucl. Phys. B **280**, 753 (1987).

[143] V. E. Kravtsov and R. Oppermann, Phys. Rev. B **43**, 10865 (1991).

[144] A. M. Finkel'stein, JETP Lett. **45**, 46 (1987); Physica B **197**, 636 (1994).

[145] A. Altland, B. D. Simons, and J. P. D. Taras-Semchuk, JETP Lett. **67**, 22 (1998); Adv. Phys. **49**, 321 (2000).

[146] A. Altland, B. D. Simons, and M. R. Zirnbauer, preprint cond-mat/0006362.

[147] H. Y. Kee, I. L. Aleiner, and B. L. Altshuler, Phys. Rev. B **58**, 5757 (1998).

[148] K. Maki, Prog. Theor. Phys. (Kyoto) **31**, 731 (1964).

[149] S. Coleman, *Aspects of Symmetry* (Cambridge University Press, Cambridge, 1985).

[150] D. S. R. Bundschuh, C. Cassanello and M. R. Zirnbauer, Nucl. Phys. B **532**, 689 (1998).

[151] Y. N. Ovchinnikov, Sov. Phys. JETP **37**, 366 (1973).

[152] M. G. Vavilov, P. W. Brouwer, V. Ambegaokar, and C. W. J. Beenakker, Phys. Rev. Lett. **86**, 874 (2001).

[153] A. I. Larkin and Y. N. Ovchinnikov, J. Low. Temp. Phys. **10**, 407 (1973).

[154] See e.g. Ref. [63], pp. 257/8.

[155] P. M. Ostrovsky, M. A. Skvortsov, and M. V. Feigelmann, preprint cond-mat/0012478.

[156] B. A. Muzykantskii and D. E. Khmel'nitskii, Phys. Rev. B **51**, 5480 (1995).

[157] V. I. Fal'ko and K. B. Efetov, Phys. Rev. B **52**, 17413 (1995); Europhys. Lett. **32**, 627 (1995).

[158] A. Kamenev, Phys. Rev. Lett. **85**, 4160 (2000).

[159] J. W. Negele and H. Orland, *Quantum Many-Particle Systems* (Addison-Wesley, New York, 1988).

[160] N. Taniguchi, B. D. Simons, and B. L. Altshuler, Phys. Rev. B **53**, R7618 (1996).

[161] B. L. Altshuler and B. D. Simons, in Ref. [4], Chap. Universalities: From Anderson Localization to Quantum Chaos.

[162] P. W. Anderson, Phys. Rev. **109**, 1492 (1958).

[163] S. Washburn and R. A. Webb, Rep. Prog. Phys. **55**, 1311 (1992).

Deutsche Zusammenfassung

Die 'mesoskopische Physik' beschäftigt sich mit Quanteninterferenzphänomenen von Elektronen in ungeordneten Systemen. Voraussetzung für die Beobachtung dieser Phänomene ist die Phasenkohärenz über möglichst große Längenskalen. Dies ermöglichte der technische Fortschritt in den letzten Jahrzehnte durch immer sauberere Proben und tiefere Temperaturen. Damit eröffnete sich der Zugang zu einer Vielzahl interessanter Effekte wie z.B. schwache und starke Lokalisierung [32, 162] oder universelle Leitwertfluktuationen [163]. Alle diese Phänomene haben ihren gemeinsamen Ursprung in einem Zusammenspiel von Nicht-Integrabilität der klassischen Dynamik der Ladungsträger und quantenmechanischer Welleninterferenz.

Zweidimensionale Elektronensysteme

Zu den meistuntersuchten Systemen gehören sogenannte zweidimensionale Elektronengase (2DEGs), die sich an Grenzflächen in Halbleiterheterostrukturen bilden. Zu den Gründen für das starke Interesse an 2DEGs zählen die reichhaltige Phänomenologie dieser Systeme und ihre gute experimentelle Handhabbarkeit sowie nicht zuletzt die sich abzeichnenden Möglichkeiten technologischer Nutzung.

Der erste Teil dieser Arbeit beschäftigt sich mit der Untersuchung von Korrelationsfunktionen in solchen 2DEGs. Im Prinzip ist die gesamte Systeminformation in der Ein-Teilchen Greenschen Funktion $G^{\pm}(\mathbf{x}, \mathbf{x}'; \epsilon)$ enthalten. In ungeordneten Systemen jedoch ist die Greensche Funktion eines einzelnen Systems im allgemeinen ein hochkompliziertes Objekt, das zudem von eher geringer Vorhersagekraft ist. Als interessanter erweist es sich, über ein Ensemble von Systemen gemittelte Eigenschaften zu betrachten. Die gemittelten Greenschen Funktionen sind kurzreichweitig und daher insensitiv gegenüber einem Großteil der Interferenzeffekte, die es zu untersuchen gilt. Um Aussagen über diese Phänomene machen zu können zieht man daher Korrelationsfunktionen der Form

$$F(\mathbf{x}_1, \mathbf{x}_2, \mathbf{x}_3, \mathbf{x}_4; \omega) \equiv \langle G^{-}(\mathbf{x}_1, \mathbf{x}_2; \epsilon) G^{+}(\mathbf{x}_3, \mathbf{x}_4; \epsilon + \omega) \rangle$$

heran. Diese Korrelationsfunktionen sind langreichweitig, wenn jeweils zwei ihrer Koordinaten nahe beieinander liegen, d.h. wenn ihr Abstand kleiner ist als die mittlere freie Weglänge, welche die Stärke der Unordnung charakterisiert. Damit erhält man drei verschiedene Korrelatoren:

- Für $\mathbf{x} \equiv \mathbf{x}_1 \approx \mathbf{x}_2$ und $\mathbf{x}' \equiv \mathbf{x}_3 \approx \mathbf{x}_4$ beschreibt $F^{[d]}(\mathbf{x}, \mathbf{x}') \equiv F(\mathbf{x}, \mathbf{x}; \mathbf{x}', \mathbf{x}')$ Dichte-Dichte-Korrelationen oder, mit anderen Worten, Fluktuationen der lokalen Zustandsdichte.
- Klassische Diffusion ist durch $F^{[D]}(\mathbf{x}, \mathbf{x}') \equiv F(\mathbf{x}, \mathbf{x}'; \mathbf{x}', \mathbf{x})$ beschrieben; d.h. $F^{[D]}(\mathbf{x}, \mathbf{x}')$ hat die Bedeutung einer Übergangswahrscheinlichkeit von $\mathbf{x}$ nach $\mathbf{x}'$.
- Die Korrelationsfunktion $F^{[C]}(\mathbf{x}, \mathbf{x}') \equiv F(\mathbf{x}, \mathbf{x}'; \mathbf{x}, \mathbf{x}')$ schließlich – auch Cooperon genannt – ist nur langreichweitig, wenn das System Zeitumkehr-Invarianz besitzt.

Tunnelspektroskopie (Kapitel 4)

Ein wesentlicher Teil der an 2DEGs durchgeführten experimentellen Untersuchungen basiert auf dem Mechanismus quantenmechanischen Tunnelns: Untersucht werden Charakteristika des Tunnelstroms zwischen separierten elektronischen Komponenten, von denen mindestens eine ein 2DEG darstellt. Beispiele für im Rahmen von Tunnelexperimenten gut untersuchbare Fragestellungen sind das Transportverhalten von Randzuständen in Quanten-Hall-Geometrien oder ganz allgemein die Transportphysik halbleitender Quantenpunkte. Qualitativ neuartige Experimente wurden möglich, nachdem es gelang, in sogenannten 'Double-Quantum-Well' Strukturen zueinander parallel orientierte 2DEGs zu präparieren und tunnelspektroskopisch zu untersuchen [20]. Aufgrund der Möglichkeit, Geometrie und makroskopische Systemparameter der beteiligten 2DEGs individuell zu gestalten, eröffnet sich in diesen Architekturen ein Spektrum experimenteller Analysemöglichkeiten, das sich an einzelnen 2DEGs nicht realisieren läßt. Eine weitere – und besonders in Hinblick auf theoretische Gesichtspunkte interessante – Eigenschaft der Tunnelspektroskopie paralleler 2DEGs ist, daß der zwischen den 2DEGs fließende Tunnelstrom weitreichende Informationen über die mikroskopische Struktur der beteiligten Systeme liefert: Speziell läßt sich durch eine Analyse der Parameterabhängigkeit der Strom*fluktuationen* auf die oben eingeführten Korrelationsfunktionen rückschließen

Der Zusammenhang zwischen Unordnung und Tunneln läßt sich dadurch verstehen, daß der Tunnelstrom durch Prozesse bestimmt ist (vgl. Abb. 4.1), bei denen ein Elektron von 2DEG Nr. 1 in 2DEG Nr. 2 tunnelt, dort propagiert und an einer beliebigen anderen Stelle durch Rücktunneln wieder mit dem in 2DEG Nr. 1 zurückgelassenen Loch rekombiniert. Die Propagation von Elektron bzw. Loch innerhalb der Einzelsysteme wird durch die jeweiligen Ein-Teilchen Greenschen Funktionen beschrieben. Das räumliche Verhalten letzterer ist wiederum wesentlich durch die Beschaffenheit der in den 2DEGs vorhandenen Unordnungspotentiale bestimmt. In ausgedehnten Systemen läßt sich mittels eines parallelen magnetischen Feldes die typische Reichweite der zum Strom dominant beitragenden Prozesse und damit die 'Reichweite' der Greenschen Funktionen direkt abtasten [25, 26].

Besonders interessant wird dies in Systemen, deren Leitwert von der Größenordnung $\mathcal{O}(1)$ ist und die daher anomale Diffusion aufweisen [113]. In diesem Bereich sind die Korrelationsfunktionen nicht exakt bekannt, und ihre Form, die durch drei charakteristische Exponenten bestimmt ist, läßt sich nur aus Skalierungsargumenten herleiten. Der vorgeschlagene Aufbau bietet nun eine Möglichkeit, diese Exponenten experimentell zu untersuchen. Allerdings könnten Coulomb-Wechselwirkungseffekte, die im Bereich kleiner Leitwerte *alle* Messungen beeinflussen, diese Untersuchung stören.

Grenzt man nun ein Teilsystem durch 'Gates' zu einem Quantenpunkt ein, so lassen sich hier spektrale sowie parametrische Korrelationen mithilfe des Tunnelstroms auflösen. Ein ähnlicher experimenteller Ansatz wurde bereits von Sivan et al. [27] verwirklicht; allerdings wurde in dieser Arbeit anstelle eines ausgedehnten Systems ein einzelnes Energieniveau als Spektrometer verwendet, womit man sich auf die Untersuchung von $F^{[d]}$ einschränkt. Auch im hier betrachteten Aufbau liefert $F^{[d]}$ die dominanten Beiträge zu den Stromfluktuationen, jedoch lassen sich die Anteile von $F^{[D;C]}$ durch ein paralleles Magnetfeld herausfiltern.

Schwache Lokalisierung im parallelen Magnetfeld (Kapitel 5)

Bei der obigen Analyse wurde von ideal zweidimensionalen Einzelsystemen ausgegangen, die den Einfluß eines parallelen Magnetfelds nicht spüren. Jedoch besitzen reale Systeme immer eine

endliche Dicke.

Im allgemeinen führt Quanteninterferenz zu dem Phänomen der *schwachen Lokalisierung*, welche sich in einer Verminderung der Leitfähigkeit gegenüber ihrem klassischen Wert manifestiert. Die Ursache hierfür ist die konstruktive Interferenz von zeitumgekehrten Pfaden, die auch unter Unordnungsmittelung erhalten bleibt. Das führt dazu, daß sich die Rückkehrwahrscheinlichkeit verdoppelt und dadurch die Propagation erschwert wird.

Diese Lokalisierungseffekte reagieren sensitiv auf äußere Magnetfelder, die die Zeitumkehr($\mathcal{T}$)-Invarianz brechen und damit die konstruktive Interferenz zerstören. Dadurch steigt die Leitfähigkeit wieder auf ihren klassischen Wert an. Die Unterdrückung der schwachen Lokalisierung ist durch eine 'magnetische Dekohärenzzeit' τ_H charakterisiert. Für ein senkrechtes Feld ergibt sich $\tau_{H_\perp} \sim H_\perp^{-1}$ [33]. Komplizierter wird die Bestimmung von τ_H im parallelen Magnetfeld. Aufgrund geometrischer Überlegungen läßt sich $\tau_{H_\parallel} \sim H_\parallel^{-2}$ abschätzen [34, 36], wobei – wie wir gleich sehen werden – hier Details wichtig sind.

In dieser Arbeit untersuchen wir speziell Systeme, die nahezu symmetrisch unter Inversion $\mathcal{P}_z : z \to -z$ sind. Unter diesen Bedingungen tritt der Berry-Robnik Symmetrieeffekt [119] auf: Die zusätzliche Symmetrie kann die Brechung der Zeitumkehr-Invarianz (teilweise) kompensieren.

Ein System endlicher Dicke spaltet durch die Impulsquantisierung in Subbänder auf. Unter der Annahme, daß das Unordnungspotential nicht von der (senkrechten) z-Koordinate abhängt, sind diese Subbänder in Abwesenheit eines Magnetfelds entkoppelt und tragen alle separat zur Leitfähigkeit bei, $\sigma = \sum_{k=0}^{M-1} \sigma_k$. Hierbei ist M die Anzahl der besetzten Subbänder. Schwache Lokalisierungskorrekturen existieren ebenfalls für jedes Subband. Das Magnetfeld hat nun zwei Aufgaben: 1.) bricht es die Zeitumkehr-Invarianz (wie auch ein senkrechtes Feld), und 2.) koppelt es die Subbänder.

Der zweite Effekt führt – unabhängig vom ersten – dazu, daß $M-1$ schwache Lokalisierungskorrekturen durch endliche Dekohärenzraten $1/\tau_H^k \sim H^2 > 0$ unterdrückt werden. Dieses Phänomen ist vergleichbar der Energieaufspaltung, wenn vormals entartete Niveaus in Kontakt gebracht werden. Während für ein perfekt symmetrisches System die verbleibende Dekohärenzrate $1/\tau_H^0$ auch in Anwesenheit des Magnetfelds verschwindet, führen eine Asymmetrie des begrenzenden Potentials oder z-abhängige Streuung zur Unterdrückung aller Beiträge zur schwachen Lokalisierung. Dadurch gibt die Magnetfeldabhängigkeit der Leitfähigkeit Aufschluß sowohl über die Form des begrenzenden Potentials als auch der Unordnungsstreuung.

Ein Sonderfall ist die Situation, in der nur ein Subband besetzt ist, und man zunächst keine Magnetfeldeffekte erwarten würde (hier ist das Vektorpotential eine reine Eichgröße). Wenn das System $\mathcal{P}_z$-symmetrisch ist, trifft dies tatsächlich zu. Im asymmetrischen Fall ergibt sich jedoch durch virtuelle Anregungen in unbesetzte Bänder ein Resteffekt, der proportional zu H^6 ist – im Gegensatz zur üblichen H^2-Abhängigkeit. Diese stellt sich wieder ein, wenn man z-abhängige Streuung erlaubt [36].

Supraleitung ohne Energielücke

Das Energiespektrum konventioneller Supraleiter zeichnet sich durch eine Energielücke E_{gap} von der Größe des Ordnungsparameters Δ sowie durch eine inverse Wurzelsingularität am Rande dieser Energielücke, die sogenannte BCS-Singularität [41], aus – siehe Abb. 1.3. Diese charakteristische Form des Spektrums wird durch schwache nicht-magnetische Unordnung kaum beeinflußt [8] (Anderson-Theorem). Sowohl durch Brechung der Zeitumkehr-Invarianz, was letzt-

endlich zur Zerstörung der Supraleitung führt, als auch durch räumliche Variation des Ordnungsparameters jedoch können drastische Modifikationen auftreten. Überraschenderweise gibt es Situationen, in denen der Ordnungsparameter endlich ist, während die Energielücke verschwindet. Die Systeme sind dann supraleitend und weisen den Meissner Effekt [46] auf, wohingegen sich ihre thermodynamischen Eigenschaften deutlich von denen konventioneller Supraleiter unterscheiden können.

Eine Theorie für die Unterdrückung der Energielücke in der Zustandsdichte konventioneller Supraleiter durch $\mathcal{T}$-brechende Störungen wurde von Abrikosov und Gor'kov [42] aufgestellt. Auch wenn sich die ursprüngliche Arbeit mit dem Einfluß von magnetischen Verunreinigungen befaßte, ist die dabei gefundene Phänomenologie viel allgemeiner gültig. Die Unterdrückung der Energielücke wird durch einen (dimensionslosen) Parameter ζ bestimmt: im Fall von magnetischen Verunreinigungen $\zeta = (|\Delta|\tau_s)^{-1}$, wobei $1/\tau_s$ die mittlere Streurate an den magnetischen Störstellen bezeichnet. Die Energielücke verschwindet nun gerade für $\zeta = 1$. Das entspricht einer magnetischen Streurate von 91% der kritischen Streurate, bei der schließlich die Supraleitung zerstört wird.

Dünne Filme im parallelen Magnetfeld (Kapitel 7)

Ein anderes Beispiel für Supraleitung ohne Energielücke ist das Verhalten von dünnen supraleitenden Filmen im parallelen Magnetfeld. 'Dünn' bedeutet hier, daß die Dicke des Films kleiner ist als a) die Londonsche Eindringtiefe, so daß der Meissner Effekt nicht wirksam werden kann und damit das Magnetfeld nicht abgeschirmt wird, und b) die supraleitende Kohärenzlänge, was dazu führt, daß die Greenschen Funktionen über die Dicke des Films nicht variieren (nachdem man über Oszillationen auf der Skala der Fermiwellenlänge gemittelt hat).

Während die Abrikosov-Gor'kov (AG) 'Mean-Field' Theorie eine Wurzelsingularität am Rand der Energielücke vorhersagt, wurde vor kurzem am Fall von magnetischen Verunreinigungen gezeigt, daß diese Aussage nicht haltbar ist [44, 45]. Optimale Fluktuationen führen dazu, daß gebundene Zustände innerhalb der Lücke auftreten. Diese Zustände bilden 'Droplets', deren Ausdehnung größer als die Kohärenzlänge ist. Die Wahrscheinlichkeit für diese seltenen Konfigurationen ist exponentiell klein. Dadurch entwickelt die Zustandsdichte 'Tails' im Bereich der Energielücke.

Im Rahmen eines feldtheoretischen Zugangs zu diesem Problem zeigt sich, daß diese 'Sub-Gap' Zustände mit inhomogenen Lösungen der Sattelpunktsgleichung des supersymmetrischen nichtlinearen σ-Modells assoziiert sind. Diese sogenannten Instanton-Lösungen sind nicht supersymmetrisch und deshalb mit einer endlichen Wirkung verbunden. Nullmoden im Boson-Fermion Raum stellen die Symmetrie wieder her und garantieren damit die Normalisierung der Zustandssumme. In zwei Dimensionen läßt sich die Sattelpunktsgleichung nicht analytisch lösen, aber dimensionelle Betrachtungen erlauben die Bestimmung ihrer Parameterabhängigkeit.

Wir zeigen hier, daß dieselbe Analyse auch für einen diffusiven Film, dessen Dicke größer als die mittlere freie Weglänge ist, anwendbar ist. Der relevante Parameter für die Unterdrückung der Energielücke ist dabei $\zeta \sim H^2/\Delta$. Die Mean-Field Energielücke ergibt sich dann zu $E_{\rm gap} = \Delta(1-\zeta^{2/3})^{3/2}$ [42]. Für Energien kleiner als $E_{\rm gap}$ erhält man eine lineare Energieabhängigkeit im Exponenten: $\ln \nu \sim -(E_{\rm gap} - \epsilon)/\Delta$. Es läßt sich zeigen, daß dieses Verhalten universell ist [45, 152] und nur durch die Dimensionalität des Systems bestimmt wird.

Zum Vergleich betrachten wir einen Film mit kolumnaren Störstellen. Wie auch bei normalleitenden Systemen (s.o.) spielen hierbei Symmetrieeffekte eine wichtige Rolle. Während die

Sattelpunktslösung nicht von der Symmetrie des Systems abhängt (auch hier findet man eine Unterdrückung der Energielücke gemäß dem AG-Szenario), beeinflußt sie doch die Fluktuationen. Das führt dazu, daß die niederenergetischen Anregungen in der 'lückenlosen' Phase, die wegen des Magnetfelds typischerweise durch die Symmetrieklasse C beschrieben sein müßten, im Falle von $\mathcal{P}_z$-Symmetrie zur höheren Symmetrieklasse CI gehören. Auch hier manifestiert sich der Berry-Robnik Effekt [119], indem das System trotz Anwesenheit des Magnetfelds Anzeichen von $\mathcal{T}$-Invarianz zeigt. Das äußert sich in einer unterschiedlichen Energieabhängigkeit der Zustandsdichte für kleine Energien. Dieser Effekt wird auch in der Numerik deutlich: im ersten Fall (diffusiver Film) verschwindet die Zustandsdichte für $\epsilon \to 0$ quadratisch, während sie im zweiten (kolumnare Störstellen) linear in der Energie ist.

Inhomogene Supraleiter (Kapitel 8)

Noch direkter wird die Energielücke durch räumliche Fluktuationen der BCS-Kopplungskonstante beeinflußt. Diese führen zu Inhomogenitäten des Ordnungsparameters, $\Delta(\mathbf{r}) = \bar{\Delta} + \Delta_1(\mathbf{r})$, und damit zu einer Verschmierung der BCS-Singularität am Rand der Energielücke und zu einer Verminderung dieser. In diesem Fall wurde schon von Larkin und Ovchinnikov [49] festgestellt, daß die harte Energielücke nicht haltbar ist, sondern durch optimale Fluktuationen der Unordnungspotentiale zerstört wird.

Wichtig ist hier die Dimension der Inhomogenitäten. Wenn die Variationsskala r_c der Kopplungskonstante größer als die Kohärenzlänge ξ ist, kann der Ordnungsparameter dieser Variation folgen, und die lokale Zustandsdichte ist durch den lokalen Wert des Ordnungsparameters bestimmt. Interessanter ist der Fall, in dem die Kopplungskonstante auf kürzeren Längenskalen fluktuiert. Hier sind Quantenkohärenzeffekte wichtig, und durch den 'Proximity-Effekt' werden die schnellen Fluktuationen geglättet. Wiederum stellt man in der Mean-Field Näherung eine Unterdrückung der Energielücke nach Abrikosov-Gor'kov fest. Der relevante Parameter hierfür ist durch $\eta \sim (r_c/\xi)^2 \langle \Delta_1^2 \rangle / \bar{\Delta}^2$ gegeben. Unter der Annahme, daß die Kopplungskonstante nicht negativ wird, ist man in diesem Fall jedoch auf den Parameterbereich $\eta \ll 1$ beschränkt.

Das (feldtheoretische) Programm, welches für die Untersuchung magnetischer Verunreinigungen und dünner Filme im Magnetfeld verwendet wurde, läßt sich nicht direkt auf dieses Problem übertragen. Hier ist es wichtig, die Fluktuationen des Ordnungsparameters selbstkonsistent zu berechnen, was die Anwendung einer supersymmetrischen Theorie ausschließt. Stattdessen arbeiten wir mit einem Replica-Modell. Die einzelnen Schritte bleiben jedoch dieselben: Nachdem man die AG-Sattelpunktslösung gefunden hat, sucht man nach inhomogenen Lösungen. Um einen exponentiell kleinen Beitrag zur Zustandsdichte zu ergeben, müssen diese Lösungen die Replica-Symmetrie brechen; verbunden damit ist wiederum eine Nullmode.

Schließlich stellt man fest, daß sich die universellen Eigenschaften der Sub-Gap Zustandsdichte [45, 152] auch hier wiederfinden. Obwohl ein Großteil der Analyse den Vorgaben von Ref. [49] folgt, tritt bei der Energieabhängigkeit der Tails eine Diskrepanz auf. Das läßt sich darauf zurückführen, daß in Ref. [49] ein Lifshitz-Argument [50] – wie es zur Berechnung von 'Band-Tails' eingeführt wurde – verwendet wurde, was hier jedoch keine Gültigkeit besitzt. Im Falle von Band-Tails betrachtet man sich langsam verändernde Wellenfunktionen mit Energien weit entfernt von der Fermienergie. Dagegen sind die hier relevanten Zustände Superpositionen von schnell oszillierenden Wellenfunktionen; d.h. die Sub-Gap Zustände sind quasi-klassischer Natur. Außerdem hängt das Ergebnis, wenn ein Lifshitz-Argument zur Anwendung kommt, sensitiv von der zugrundeliegenden Unordnungsverteilung ab, während hier die Energieabhängigkeit der Zustandsdichte universell ist.

Danksagung

Bei meiner Promotion, die in Bochum, Cambridge und Köln durchgeführt wurde, haben mich zahlreiche Leute unterstützt, denen ich an dieser Stelle dafür danken möchte:

Zuallererst danke ich meinem Betreuer Prof. Dr. Alexander Altland, der mir viele interessante und hilfreiche Anregungen gegeben, mich sehr unterstützt und gefördert hat – und mir dennoch großen Freiraum gelassen – sowie den schnellen Abschluß dieser Arbeit ermöglicht hat.

Desweiteren geht mein Dank an Prof. Dr. Martin Zirnbauer für die Übernahme des Zweitreferats.

Priv.-Doz. Dr. Martin Janßen danke ich für die Zusammenarbeit während des ersten Teils der Arbeit, die Gesprächsbereitschaft bei allen Fragen und die große Geduld beim Schreiben unserer gemeinsamen Veröffentlichungen. Weiterhin danke ich ihm für das kritische Lesen des Manuskripts.

Mein besonderer Dank gilt auch Dr. Ben Simons, mit dem ich ein Jahr in Cambridge zusammen gearbeitet habe. Ich habe von diesem Aufenthalt sehr profitiert, und ich danke für die große Unterstützung sowohl bei fachlichen Fragen als auch organisatorischen Problemen.

Meinen 'Bürokollegen' Rainer Merkt, Alexander Tschersich und Ugur Er in Bochum, Marzena Szymanska und Martin Vogt in Cambridge sowie Corinna Kollath und Burkhard Seif in Köln danke ich für die angenehme Arbeitsatmosphäre.

Für das Korrekturlesen meiner Arbeit und wertvolle Verbesserungsvorschläge bin ich Corinna Kollath, Ludger Santen und Alexander Tschersich sehr dankbar.

Desweiteren danke ich Prof. Boris Altshuler für die Zusammenarbeit an einem Teilprojekt im Rahmen dieser Arbeit. Hilfreich waren dabei auch interessante Diskussionen mit Prof. Vladimir Fal'ko.

Schließlich möchte ich mich auch noch bei meinen Eltern bedanken, die mich immer unterstützt haben – und über die Fertigstellung dieser Arbeit genauso froh sein werden wie ich.

Erklärung

Ich versichere, daß ich die von mir vorgelegte Dissertation selbständig angefertigt, die benutzten Quellen und Hilfsmittel vollständig angegeben und die Stellen der Arbeit – einschließlich Tabellen, Karten und Abbildungen –, die anderen Werken im Wortlaut oder dem Sinn nach entnommen sind, in jedem Einzelfall als Entlehnung kenntlich gemacht habe; daß diese Dissertation noch keiner anderen Fakultät oder Universität zur Prüfung vorgelegen hat; daß sie – abgesehen von unten angegebenen Teilpublikationen – noch nicht veröffentlicht worden ist sowie, daß ich eine solche Veröffentlichung vor Abschluß des Promotionsverfahrens nicht vornehmen werde. Die Bestimmungen dieser Promotionsordnung sind mir bekannt. Die von mir vorgelegte Dissertation ist von Prof. Dr. Alexander Altland betreut worden.

Köln, den 21. Mai 2001

Teilpublikationen:

J. S. Meyer, A. Altland, and M. Janßen, *Tunneling spectroscopy with two-dimensional electron gases*, Ann. Phys. **8**, SI-173 (1999).

J. S. Meyer, A. Altland, and M. Janßen, *Magnetotunneling spectroscopy of mesoscopic correlations in two-dimensional electron systems*, Phys. Rev. B **63**, 245327 (2001).

J. S. Meyer and B. D. Simons, *Gap fluctuations in inhomogeneous superconductors*, Phys. Rev. B **64**, 134516 (2001).

J. S. Meyer, A. Altland, and B. L. Altshuler, *Quantum transport in parallel magnetic fields: A realization of the Berry-Robnik symmetry phenomenon*, preprint cond-mat/0105623, submitted to Phys. Rev. Lett..

J. S. Meyer and B. D. Simons, *Phase coherence phenomena in superconducting films*, preprint cond-mat/0111039, submitted to Phys. Rev. B.

Abstract

Correlation functions are the key elements of theoretical investigations in mesoscopic physics. The first part of this work is concerned with the experimental observation of these correlation functions on the one hand and with the information they contain about microscopic properties of the system on the other hand. A possible method for measuring correlation functions is tunnelling spectroscopy with parallel two-dimensional systems separated by a uniform tunnelling barrier. Here we extend the concept – developed in an earlier work – to extract information on the microscopic properties of a single system from the tunnelling current fluctuations (Chapter 4). The setup allows one to study transport correlations in extended systems as well as spectral and parametric correlations in finite quantum dots. One of the crucial tuning parameters is a parallel or in-plane magnetic field. This field does not influence the transport within an ideal two-dimensional layers. In a quantum well with finite width (Chapter 5), the effect of the field depends sensitively on symmetry properties of the well and the nature of impurity scattering. We find a manifestation of the Berry-Robnik symmetry phenomenon, i.e. the compensation for time-reversal symmetry breaking (due to the magnetic field) by the presence of an additional discrete symmetry.

The influence of parallel fields does not only lead to interesting phenomena in normal $2d$-systems, but also in superconducting films (Chapter 7). There the magnetic field may induce a gapless phase, where the system is still superconducting but does not possess a quasi-particle gap in its spectrum. The phenomenology of gap suppression is contained in the Abrikosov-Gor'kov (AG) theory (formulated for the case of magnetic impurities). Beyond this mean field result, we discuss the existence of tail states within the gap. Using a field theoretic aproach, these 'sub-gap' states are associated with inhomogeneous solutions of the mean-field equation. In the gapless phase, the low-energy physics is again influenced by the Berry-Robnik symmetry phenomenon. A more direct way of influencing the spectral gap are spatial inhomogeneities of the superconducting coupling constant (Chapter 8) which lead to a strikingly similar phenomenology. Gap fluctuations soften the gap edge and, thus, entail sub-gap states. The universality of the results is emphasised.

Kurzzusammenfassung

Die vorliegende Arbeit befaßt sich mit der Untersuchung mesoskopischer Effekte in zweidimensionalen Elektronensystemen und konventionellen Supraleitern. Aus theoretischer Sicht spielen hierbei Korrelationsfunktionen eine zentrale Rolle. Der erste Teil der Arbeit beschäftigt sich mit der experimentellen Meßbarkeit dieser Korrelationsfunktionen mittels Tunnelspektroskopie mit sogenannten 'Double-Well' Strukturen. Aufbauend auf einer früheren Arbeit wird dabei herausgestellt, daß die Fluktuationen des Tunnelstroms zwischen den beiden Schichten weitreichende Informationen über sowohl Transport- als auch spektrale Korrelationen enthalten (Kapitel 4). Ein wichtiges Analyseinstrument ist hierbei ein schwaches paralleles Magnetfeld, welches auf die Dynamik eines zweidimensionalen Systems keine Auswirkung hat. Weitergehend untersuchen wir Magnetfeldeffekte in reellen Systemen mit endlicher Dicke (Kapitel 5). Hierbei findet man, daß das Ergebnis von der Symmetrie des zugrundeliegenden Systems abhängt: eine zusätzliche diskrete Symmetrie kann die Brechung der Zeitumkehrinvarianz durch das Magnetfeld kompensieren; dies ist eine Manifestation des Berry-Robnik Symmetrieeffekts.

Auch in Supraleitern führen parallele Magnetfelder zu interessanten Effekten. Insbesondere läßt sich Supraleitung ohne Energielücke beobachten (Kapitel 7): Bevor die Supraleitung durch das Feld vollständig unterdrückt wird, findet ein Übergang zu einer Phase mit endlichem Ordnungsparameter aber verschwindender Energielücke statt. Außerdem findet man, wie vor kurzem für magnetische Verunreinigungen gezeigt, 'Tails' innerhalb der Energielücke. Im Rahmen einer feldtheoretischen Beschreibung sind diese auf inhomogene Instanton-Lösungen der 'Mean-Field' Gleichungen zurückzuführen. Der oben untersuchte Symmetrieeffekt tritt auch hier auf, wenn man die Niederenergie-Physik in der 'lückenlosen' Phase betrachtet. Noch direkter läßt sich das Energiespektrum durch Fluktuationen der Kopplungskonstante beeinflußen (Kapitel 8). Diese führen zu Fluktuationen des Ordnungsparameters und darüber zu einer Verschmierung der BCS-Singularität. Die Unterdrückung der Energielücke erfolgt analog zum obigen Fall. Die Universalität der Energieabhängigkeit der Tail-Zustände wird herausgestellt.